PB83-223362

Modeling Fine Sediment Transport in Estuaries

Florida Univ., Gainesville. Coll. of Engineering

Prepared for

Environmental Research Lab., Athens, GA

Jun 83

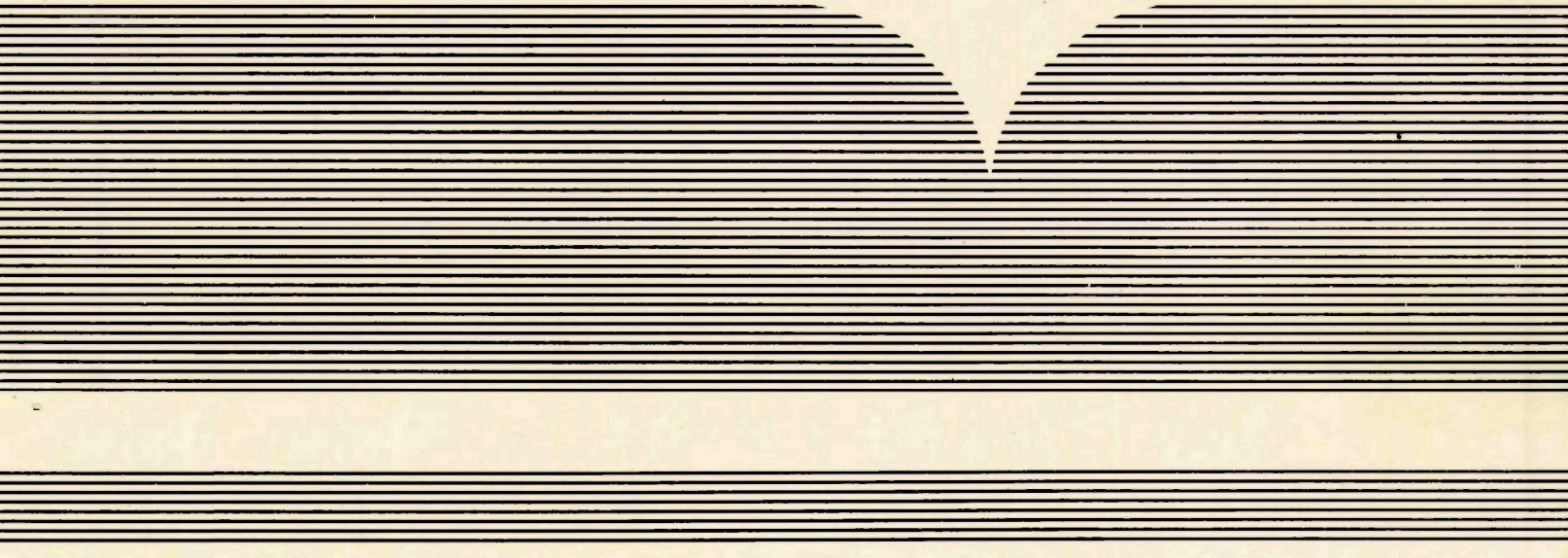

U.S. DEPARTMENT OF COMMERCE
National Technical Information Service
NTIS

EPA-600/3-83-045
June 1983

MODELING FINE SEDIMENT TRANSPORT IN ESTUARIES

by

E. J. Hayter
A. J. Mehta

Coastal and Oceanographic Engineering Department
College of Engineering
University of Florida
Gainesville, Florida 32611

Grant No. R-80668401

Project Officer

Robert B. Ambrose, Jr.
Technology Development and Applications Branch
Environmental Research Laboratory
Athens, Georgia 30613

ENVIRONMENTAL RESEARCH LABORATORY
OFFICE OF RESEARCH AND DEVELOPMENT
U.S. ENVIRONMENTAL PROTECTION AGENCY
ATHENS, GEORGIA 30613

TECHNICAL REPORT DATA
(Please read Instructions on the reverse before completing)

1. REPORT NO.	2.	3. RECIPIENT'S ACCESSION NO.
EPA-600/3-83-045		PB83 223562

4. TITLE AND SUBTITLE	5. REPORT DATE
Modeling Fine Sediment Transport in Estuaries	June 1983
	6. PERFORMING ORGANIZATION CODE
7. AUTHOR(S)	8. PERFORMING ORGANIZATION REPORT NO.
E.J. Hayter and A.J. Mehta	
9. PERFORMING ORGANIZATION NAME AND ADDRESS College of Engineering Coastal and Oceanographic Engineering Department University of Florida Gainesville FL 32611	10. PROGRAM ELEMENT NO. CARB1A 11. CONTRACT/GRANT NO. R806684010
12. SPONSORING AGENCY NAME AND ADDRESS Environmental Research Laboratory--Athens GA Office of Research and Development U.S. Environmental Protection Agency Athens GA 30613	13. TYPE OF REPORT AND PERIOD COVERED Final 14. SPONSORING AGENCY CODE EPA/600/01
15. SUPPLEMENTARY NOTES	

16. ABSTRACT

A sediment transport model (SEDIMENT IIIA) was developed to assist in predicting the fate of chemical pollutants sorbed to cohesive sediments in rivers and estuaries. Laboratory experiments were conducted to upgrade an existing two-dimensional, depth-averaged, finite element, cohesive sediment transport model. The utility of SEDIMENT IIIA was demonstrated by laboratory resuspension and deposition tests and simulations of the sedimentation processes in a hypothetical canal. The effect of salinity in these simulations also was examined. The model should enhance capabilities for predicting water quality impacts and for analyzing sedimentation management issues. The improved transport descriptions should be useful in making more reliable predictions of the fate of dissolved and sorbed pollutants discharged into an estuary or harbor by stormwater runoff or industry releases, thus assisting in the evaluation of water pollution control options. The enhanced descriptions should also be useful in predicting the movement of dredged material released in open marine waters, identifying harbor sites in estuaries and bays where shoaling is minimized, predicting changes in sedimentation that may result from proposed changes or developments of an estuary or harbor, and estimating shoaling rates and maintenance dredging requirements in areas of low flow.

17. KEY WORDS AND DOCUMENT ANALYSIS

a. DESCRIPTORS	b. IDENTIFIERS/OPEN ENDED TERMS	c. COSATI Field/Group

18. DISTRIBUTION STATEMENT	19. SECURITY CLASS *(This Report)*	21. NO. OF PAGES
RELEASE TO PUBLIC	UNCLASSIFIED	
	20. SECURITY CLASS *(This page)*	22. PRICE
	UNCLASSIFIED	

EPA Form 2220-1 (9-73)

NOTICE

THIS DOCUMENT HAS BEEN REPRODUCED FROM THE BEST COPY FURNISHED US BY THE SPONSORING AGENCY. ALTHOUGH IT IS RECOGNIZED THAT CERTAIN PORTIONS ARE ILLEGIBLE, IT IS BEING RELEASED IN THE INTEREST OF MAKING AVAILABLE AS MUCH INFORMATION AS POSSIBLE.

DISCLAIMER

Although the research described in this report has been funded wholly or in part by the United States Environmental Protection Agency through Grant Number R80668401 to the University of Florida, it has not been subjected to the Agency's required peer and policy review and therefore does not necessarily reflect the views of the Agency and no official endorsement should be inferred.

FOREWORD

As environmental controls become more costly to implement and the penalties of judgment errors become more severe, environmental quality management requires more efficient management tools based on greater knowledge of the environmental phenomena to be managed. As part of this Laboratory's research on the occurrence, movement, transformation, impact and control of environmental contaminants, the Technology Development and Applications Branch develops management or engineering tools to help pollution control officials achieve water quality goals through watershed management.

Heavy metals, insecticides, herbicides, and other organic compounds can be transported into natural waters on fine sediment materials. Storage of river waters for agricultural, urban and industrial uses will reduce sediment inflows to estuaries as water resources become scarce. The effects of reduced sediment inflows must be evaluated to ascertain minimum water quality management needs. This report describes an improved transport model for simulating the erosion and deposition of cohesive sediments in estuaries and the effect of salinity on these transport processes. By modeling the movement of fine sediments in a water body of concern, predictions can be made of the fate of sorbed pollutants.

William T. Donaldson
Acting Director
Environmental Research Laboratory
Athens, Georgia

ABSTRACT

Laboratory experiments were carried out to determine: 1) the resuspension characteristics of partially consolidated, flow-deposited cohesive sediment beds under turbulent flows, 2) the effects of salinity on the rates of erosion of these beds, and 3) the effects of salinity on the rates of deposition and the settling velocity of suspended cohesive sediments under turbulent flows. The experimental results together with other available information have been used to upgrade SEDIMENT III, a two-dimensional, depth-averaged finite element cohesive sediment transport model. The purpose of the new model, SEDIMENT IIIA, is to assist in the prediction of the fate of pollutants sorbed to cohesive sediments in rivers and estuaries.

Resuspension tests conducted in a rotating annular flume and in a straight recirculating flume at the University of Florida using kaolinite and a natural mud revealed that flow-deposited beds are stratified with respect to bed shear strength and density and can consist of unconsolidated stationary suspensions, partially consolidated beds and settled, fully consolidated beds. Both the cohesive shear strength and the bed density increase with increasing period of consolidation. When subjected to an excess bed shear stress, stationary suspensions erode almost instantly, while partially and fully consolidated beds undergo surface (aggregate by aggregate) erosion. An empirical expression for the rate of surface erosion of partially consolidated beds, that is analogous to the rate expression which results from a heuristic interpretation of the rate process theory of chemical reactions, was derived. This rate expression indicates that the rate of erosion varies exponentially with the excess bed shear stress. The rate of erosion of settled beds is linearly proportional to the excess shear stress.

A cohesive sediment bed schematization algorithm and an erosion algorithm have been developed. Based on an interpretation of typically observed Eulerian time-concentration records in estuaries, erosion is considered to occur during accelerating flows. Likewise, deposition is considered to occur during decelerating flows. The erosion algorithm simulates mass erosion of stationary suspensions and the surface erosion of partially consolidated and settled beds. The bed schematization includes these three bed sections, and divides each section into discretized layers. The amount of sediment eroded from the bed or deposited onto the bed in each element is determined, and the thickness and the structure of the bed in that element are adjusted accordingly. Consolidation of the bed due to overburden is accounted for by first filling up the top stationary suspension layers and then the partially consolidated layers as deposition occurs.

A deposition algorithm has been developed. This algorithm integrates the concepts proposed by various investigators and represents a unified model of this process. Deposition is predicted to occur when the bed shear stress is less than the maximum depositional shear stress, τ_{bmax}. The rate of deposition is dependent, among other factors, upon the bed shear stress and the settling velocity of the suspended sediment.

The bed shear strength was found to vary with the salinity S of the eroding fluid for salinities less than 2 ppt. The shear strength increased linearly in the range $\sim 0 < S < 2$ ppt. For $S > 2$ ppt, no further increase in the bed shear strength was observed. Consequently, the rate of erosion decreased with increasing salinity up to 2 ppt, where it became practically invariant with respect to salinity.

The rates of deposition of the natural mud were found to increase with increasing salinity. A power relationship between the settling velocity, W_s, and the salinity, of the form $W_s \propto S^{0.13}$, was determined from analysis of deposition tests conducted at salinities ranging from 0 to 35 ppt and under bed shear stresses varying from 0.0 to 0.30 N/m^2.

The utility of the model is shown by simulations of laboratory resuspension and deposition tests and of the sedimentation processes in a 10 km hypothetical canal. The effect of salinity in these simulations has been described.

TABLE OF CONTENTS

	Page
ABSTRACT	iv
LIST OF FIGURES	viii
LIST OF TABLES	xiii
ACKNOWLEDGEMENT	xiv
CHAPTER	
I. INTRODUCTION	1
1.1. Estuarial Fine Sediment Dynamics	1
1.2. Significance of Clays in Pollutant Transport	7
1.3. Purpose of Study	14
1.3.1. Need for Research	14
1.3.2. Predictive Modeling	16
1.3.3. Objectives and Scope of Investigation	21
II. MODELING CONSIDERATIONS	23
2.1. Significance of Important Physical Factors in Estuarial Transport	23
2.2. Governing Equations	34
2.2.1. Convective-Diffusive Transport Equation	34
2.2.2. Initial and Boundary Conditions	38
2.2.3. Solution of Governing Equation	39
2.3. Description of Selected Transport Model	41
2.4. Model Modifications	42
2.5. Fine Sediment Bed	44
2.5.1. Introductory Note	44
2.5.2. Bed Schematization	50
2.6. Erosion of Fine Sediment Bed	54
2.6.1. Introductory Note	54
2.6.2. Erosion Algorithm	68
2.7. Deposition of Fine Sediment	72
2.7.1. Introductory Note	72
2.7.2. Deposition Rates	86
2.7.3. Deposition Algorithm	88

2.8. Influence of Salinity on Estuarial Sediment Processes..... 90
2.8.1. Effect of Salinity of Interparticle Forces.... 90
2.8.2. Effect of Salinity on Bed Structure..... 95
2.8.3. Effect of Salinity on Surface Erosion..... 96
2.8.4. Effect of Salinity on Coagulation..... 106
2.8.5. Effect of Salinity on Deposition..... 113
2.9. Convergence and Stability of the Numerical Scheme..... 124
2.10. Model Limitations..... 125
2.11. Model Applicability..... 126
2.11.1. Water Quality Problems..... 126
2.11.2. Sedimentation Management Problems..... 126
III. SIMULATION OF FINE SEDIMENT TRANSPORT PROCESSES..... 128
3.1. Introductory Note..... 128
3.2. Simulation of Laboratory Erosion Tests..... 128
3.3. Simulation of Laboratory Depositional Tests..... 131
3.4. Simulation of Sedimentation Processes in an Artificial Canal..... 136
IV. SUMMARY, CONCLUSIONS AND RECOMMENDATIONS..... 141
4.1. Summary and Conclusions..... 141
4.2. Recommendations for Future Research..... 145
V. REFERENCES..... 147
APPENDIX
A. Model Flow Chart of SEDIMENT IIIA..... 161
B. User's Manual..... 172
B.1. Data Required for Model Use..... 173
B.2. Description of Field Data Collection Program..... 185
B.3. Description of Laboratory Sediment Testing Program.... 187
C. Characterization of Factors Involved in the Study of Erosion of Fine Sediments..... 190

LIST OF FIGURES

Figure		Page
1.1.	Schematic Representation of Transport and Shoaling Processes in the Mixing Zone of a Stratified Estuary, including Ebb Predominance Factors (after Mehta and Hayter, 1981)	2
1.2.	Longitudinal Salinity and Suspended Sediment Concentrations in the Hooghly River Estuary (India) (after Mehta and Hayter, 1981)	6
1.3.	Time and Depth Variation of Suspended Sediment Concentration in Savannah River Estuary (after Krone, 1972)	8
1.4.	Schematic Representation of the Physical States of Fine Sediment in Estuarial Mixing Zone (after Mehta et al., 1982a)	8
1.5.	Variation of Heavy Metal Concentration with Sediment Particle Size (after Salomons and Mook, 1977)	10
1.6.	Time and Depth Variation of Salinity in Savannah River Estuary (after Krone, 1972)	17
1.7.	Time Variation of Chloride Concentration in a Pacific Ocean Estuary Due to Stormwater Runoff (after Orlob et al., 1967)	17
1.8.	Interactions of Tidal and Estuarial Sediment Transport Processes (after Owen, 1977)	18
2.1.	Monthly Salinity Distributions in the Cumbarjua Canal Goa, India; ——— Ebb; ----- Flood (after Rao et al., 1976)	24
2.2.	Variation of Chloride Concentration in San Francisco Bay and Sacramento-San Joaquin Delta-September 1955 (after Orlob et al., 1967)	25
2.3.	Salinity of the Surface Waters of the Pamlico River Estuary as a Function of the Distance from the Railroad Brodge at Washington, N.C. (after Edzwald et al., 1974)	26
2.4.	Computed Longitudinal Salinity Profile in the Yangtze River Estuary as a Function of the Distance Downstream from Jiang Zhen Dong for Two River Discharges: Q = 33000 cms and 45500 cms (after Huang et al., 1980)	26

2.5. A Plot of Raw Viscometer Data Obtained from the U.S. Army Corps of Engineers Philadelphia District Sample (after Krone, 1963)..... 31
2.6. Coordinate System..... 34
2.7. z/H vs. $\rho/\bar{\rho}$ for Avonmouth, Brisbane and Grangemouth Muds (after Dixit, 1982)..... 47
2.8. z/H versus $\rho/\bar{\rho}$ for Consolidation Periods (a) Less than 48 Hours and (b) Greater than 48 Hours (after Dixit, 1982).. 47
2.9. Bed Shear Strength Observed as a Function of Depth (after Parchure, 1980)..... 48
2.10. Variation of Critical Bed Shear Strength, τ_c, with Depth (after Dixit, 1982)..... 49
2.11. Bed Schematization used in SEDIMENT IIIA..... 51
2.12. Hypothetical Shear Strength Profile Illustrating Determination of Bed Layers Thicknesses..... 51
2.13. Typical Laboratory Determined Relationship between Surface Erosion Rate ε and Time-mean Bed Shear Stress τ (after Mehta, 1981)..... 57
2.14. Example of Relationship between Surface Erosion Rate ε and Bed Shear Stress τ. Data of Christensen and Das (1973) for Grundite (after Mehta, 1981)..... 58
2.15. ε-τ Data of Partheniades (1962), Series I and II (After Mehta, 1981)..... 58
2.16. Dimensionless ε-t Relationship Based on Results of Ariathurai and Arulanandan (1978) (after Mehta, 1981)..... 60
2.17. Relative Suspended Sediment Concentration versus Time for a Stratified Bed at Bed Shear Stress τ_b = 0.207 N/m^2 (after Mehta and Partheniades, 1979)..... 60
2.18. Schematic Representation of the Selected Methodology for the Variation of the Applied Bed Shear Stress During Bed Preparation and Resuspension Tests (after Mehta *et al.*, 1982a)..... 62
2.19. Variation of Suspension Concentration with Time for T_{dc} = 48 Hours (after Dixit, 1982)..... 64
2.20. $C(T_f)$ versus τ_f for Three Values of T_{dc}, using Kaolinite in Salt Water (after Mehta *et al.*, 1982a)..... 65

2.21. Normalized Rate of Erosion, $\varepsilon_i/\varepsilon_{oi}$, versus Normalized Excess Shear Stress, $(\tau_i-\tau_c(z)/\tau_c(z)$, using Kaolinite in Tap Water (after Mehta et al., 1982a)..... 66
2.22. Normalized Rate of Erosion, $\varepsilon_i/\varepsilon_{oi}$, versus Normalized Excess Shear Stress, $(\tau_i-\tau_c(z)/\tau_c(z)$, using Kaolinite in Distilled Water (after Mehta et al., 1982a)..... 67
2.23. Ratio C/C_o versus Time t for Kaolinite in Distilled Water (after Mehta and Partheniades, 1975)..... 75
2.24. Ratio C_{eq}/C_o versus Bed Shear Stress τ_b (after Mehta and Partheniades, 1975)..... 75
2.25. Relative Steady State Concentration C^*_{eq} in Percent Against Bed Shear Stress Parameter τ^*_b-1 (after Mehta and Partheniades, 1975)..... 77
2.26. C^* in Percent versus t/t_{50} for Kaolinite in Distilled Water (after Mehta and Partheniades, 1975)..... 79
2.27. Log t_{50} versus τ^*_b for Kaolinite in Distilled Water (after Mehta and Partheniades, 1975)..... 80
2.28. σ_2 versus τ^*_b for Kaolinite in Distilled Water (after Mehta and Partheniades, 1975)..... 80
2.29. Settling Velocity, W_s, versus Suspended Sediment Concentration, C, for San Francisco Bay Mud (after Krone, 1962)... 82
2.30. Settling Velocity, W_s, versus Suspended Sediment Concentration, C, for Yangtze River Estuary Mud (after Huang et al., 1980)..... 83
2.31. Settling Velocity, W_s, versus Suspended Sediment Concentration, C, for Severn Estuary Mud (after Thorn, 1981)..... 83
2.32. Effect of Size and Settling Velocity of Elementary Particles on the Coagulation Factor of Natural Muds (after Bellessort, 1973)..... 85
2.33. Repulsive and Attractive Energy as a Function of Particle Separation at Three Electrolyte Concentrations (after van Olphen, 1963)..... 92
2.34. Net Interaction Energy as a Function of Particle Separation at High Electrolyte Concentration (after van Olphen, 1963)..... 92

2.35. Net Interaction Energy as a Function of Particle Separation at Intermediate Electrolyte Concentration (after van Olphen, 1963)..... 94
2.36. Net Interaction Energy as a Function of Particle Separation at Low Electrolyte Concentration (after van Olphen, 1963)..... 94
2.37. Critical Shear Stress versus SAR for Montomorillonitic Soil (after Alzadeh, 1974)..... 97
2.38. Dimensionless Bed Density versus Bed Depth Profiles for Salinities of 0, 1, 2, 5 and 10 ppt..... 100
2.39. Bed Shear Strength Profiles as a Function of Salinity..... 101
2.40. Surface Erosion Rate ε versus Normalized Excess Shear Stress $(\tau_b-\bar{\tau}_c)/\bar{\tau}_c$..... 102
2.41. Slope, α, Plotted Against Depth Below Bed Surface, z, as a Function of Salinity..... 103
2.42. Ordinate Intercept, ε_0, Plotted Against Depth Below Bed Surface, z, as a Function of Salinity..... 103
2.43. Variation of SAR with Salinity (Sea Salt Concentration) (after Ariathurai, 1974)..... 107
2.44. Coagulation-Dispersion Boundary Curves for (a) Montmorillonite, (b) Illite and (c) Kaolinite at Three pH Ranges (after Kandiah, 1974)..... 107
2.45. Comparison of the Collision Functions for Brownian, Shear and Differential-Sedimentation Coagulation (after Hunt, 1980)..... 112
2.46. Effect of Salinity on Settling Velocity of San Francisco Bay Mud (after Krone, 1962)..... 112
2.47. Effect of Salinity on Settling Velocity of Avonmouth Mud (after Owen, 1970)..... 115
2.48. Effect of Salinity and Suspension Concentration on Settling Velocity of Avonmouth Mud (after Owen, 1970)..... 116
2.49. Ratio C/C_0 versus Time as a Function of the Bed Shear, τ_b, for Lake Francis Sediment with S = 5 ppt..... 118
2.50. Ratio C_{eq}/C_0 versus τ_b for Deposition Tests with Lake Francis Sediment..... 118

2.51. Effect of Salinity and Bed Shear Stress on Settling Velocity of Lake Francis Sediment..... 120
2.52. Settling Velocity versus Suspension Concentration for Deposition Test with Lake Francis Sediment..... 122
2.53. Variation of C^*_{eq} with Salt Concentration, S, and Bed Shear Stress, τ_b..... 122
3.1. Comparison of Predicted and Measured Suspension Concentrations versus time for a Resuspension Experiment..... 129
3.2. Demonstration of the Effect of Salinity on the Resuspension Rates of a Flow Deposited Kaolinite Bed..... 130
3.3. Comparison of Predicted and Measured Deposition Rates for Lake Francis Sediment at a Salinity of 0.0 ppt, and Demonstration of the Effect of Salinity on the Deposition Rate..... 132
3.4. Comparison of Predicted and Measured Variation of C^* versus $(t/t_{50})^{1/\sigma_2}$ for Kaolinite in Distilled Water with $\tau_b^* = 0.90$..... 133
3.5. Comparison of Predicted and Measured Variation of C^* versus $(t/t_{50})^{1/\sigma_2}$ for Kaolinite in Distilled Water with $\tau_b^* = 1.41$..... 134
3.6. Comparison of Predicted and Measured Variation of C^* versus $(t/t_{50})^{1/\sigma_2}$ for Kaolinite in Distilled Water with $\tau_b^* = 2.70$..... 135
3.7. Plan View of 10 km Hypothetical Canal..... 137
3.8. Predicted Concentration-time Record for Element 4 in 10 km Canal..... 138
3.9. Predicted Concentration-time Record for Element 5 in 10 km Canal..... 139
C.1. Diagramatic Representation of the Steps in the Study of Erosion Rates of Fine Sediments..... 193

LIST OF TABLES

		Page
1.1.	Valence and Atomic Number of Cations in Sediment.....	12
2.1.	Properties of Sediment Aggregates (after Krone, 1963).....	32
2.2.	Principal Factors Controlling Erosion of Saturated Cohesive Sediment Beds.....	55
2.3.	Cation Concentrations in Processed Sodium Chloride and Standard Sea Salt.....	98
A.	Characterization of Sediment.....	194
B.	Characterization of Pore Fluid.....	196
C.	Characterization of Bed Structure.....	198
D.	Characterization of Coagulation and Settling.....	199
E.	Erodibility Index.....	199
F.	Characterization of Bed Shear Stress.....	200
G.	Measure of Erosion.....	201

ACKNOWLEDGEMENT

The authors wish to acknowledge the significant assistance provided by Dr. Ranjan Ariathurai to this investigation. Dr. Ariathurai was a consultant to the project and provided a copy of the SEDIMENT III fine sediment transport model program to the investigators. He also gave invaluable advice regarding the use of SEDIMENT III and related experimental research. Mr. T. M. Parchure, graduate assistant, wrote Appendix C and also contributed to some aspects of Chapters I and II.

The investigation was supported by the U.S. Environmental Protection Agency under Grant Number R806684010. Funds for research work by Messers. J. G. Dixit (M. S. Thesis), S. D. Hunt (M. S. project report) and T. M. Parchure (M. S. Thesis) were partially derived from this grant.

The authors wish to sincerely thank Mr. Robert B. Ambrose (Project Officer) and Dr. James W. Falco of the Environmental Protection Agency for their involvement and guidance during the course of the investigation.

I. INTRODUCTION

1.1. Estuarial Fine Sediment Dynamics

Fine, cohesive sediments in estuaries are comprised largely of terrigenous clay-sized particles plus fine silts. The remainder may include biogenic detritus, algae, organic matter, waste materials and sometimes small quantities of very fine sand. Although in water with a very low salinity (less than about 1 part per thousand) the elementary sediment particles are usually found in a dispersed or "non-salt flocculated" state, small amounts of salts are sufficient to repress the electrochemical surface repulsive forces between the elementary particles, with the result that the particles coagulate to form much larger units known as aggregates. Each aggregate may contain thousands or even millions of elementary particles and have a settling velocity that is much larger than those of the elementary particles. The transport properties of aggregates are affected by the hydrodynamic conditions and by the chemical composition of the suspending fluid. Most estuaries contain abundant quantities of cohesive sediments which usually occur in the coagulated form in various degrees of aggregation. Therefore, an understanding of the transport properties of these sediments in estuaries requires a knowledge of the manner in which the aggregates are transported in these waters.

Fine sediment transport in estuaries is a complex process involving a strong coupling between tides, baroclinic circulation and the coagulated sediment. This process has been described extensively elsewhere (Postma, 1967; Partheniades, 1971; Dyer, 1971; Krone, 1972; Kirby and Parker, 1977; Kranck, 1980). In Fig. 1.1, a schematic description is given. The case considered is one in which the estuary is stratified, and a stationary saline wedge is formed as shown. Various phases of suspended fine sediment transport are shown, assuming a quasi-steady state, i.e. a tidally-averaged situation. In the case of a partially mixed estuary, the description will be modified, but since relatively steep vertical density gradients are usually present even in this case, the sediment transport processes will generally remain qualitatively similar as depicted in Fig. 1.1.

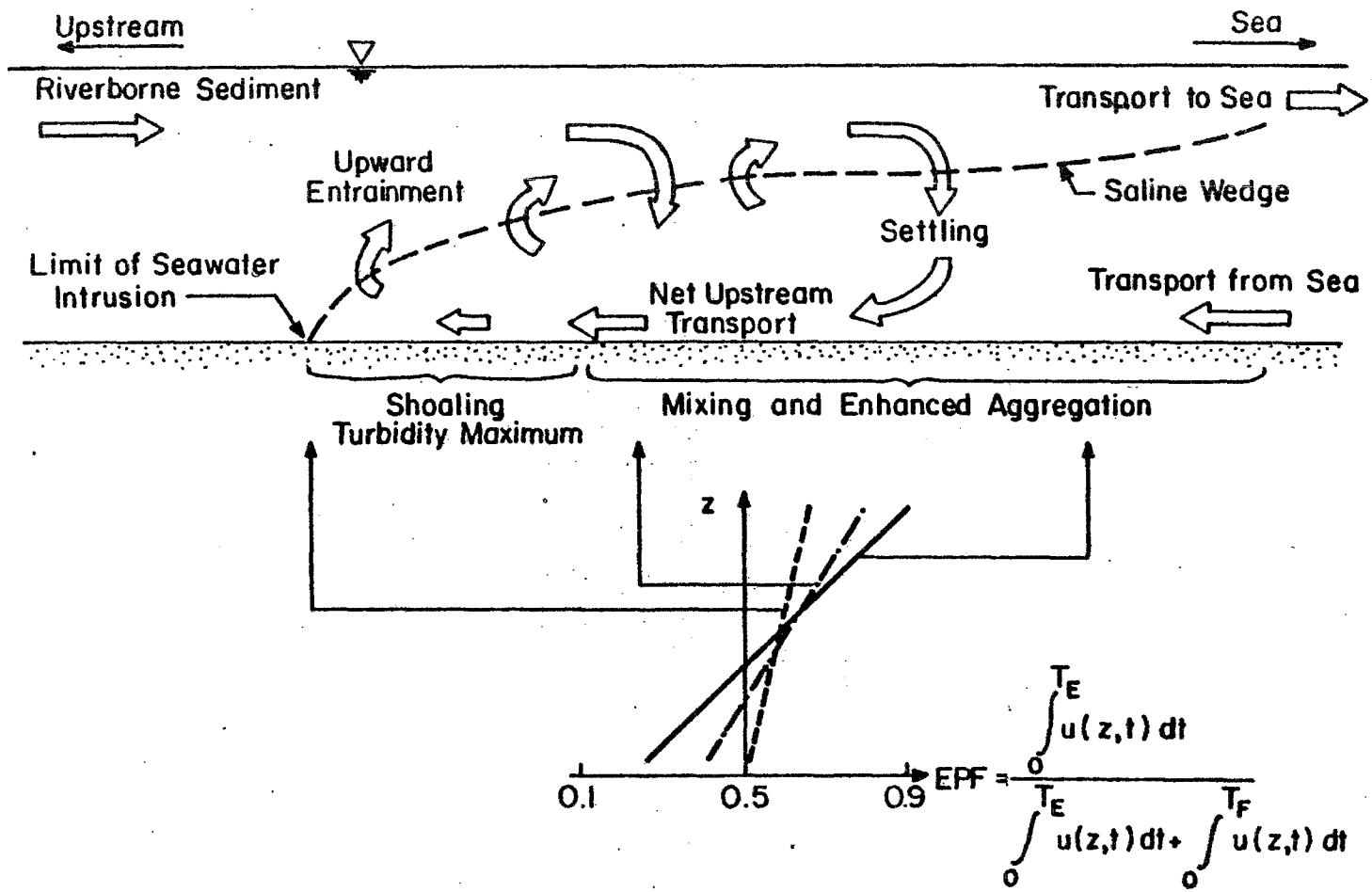

Fig. 1.1 Schematic Representation of Transport and Shoaling Processes in the Mixing Zone of a Stratified Estuary, including Ebb Predominance Factors (after Mehta and Hayter, 1981).

With reference to this figure, the vertical variation of the horizontal flows on a tidally-averaged basis can be conveniently described by computing the ebb predominance factor, EPF, defined as

$$EPF = \frac{\int_0^{T_E} u(z,t)dt}{\int_0^{T_E} u(z,t)dt + \int_0^{T_F} u(z,t)dt} \qquad (1.1)$$

where $u(z,t)$ = instantaneous longitudinal current velocity at an elevation z above the bed, T_E = ebb period, T_F = flood period and $T = T_E + T_F$, where T = tidal period. If the strengths of flood and ebb were the same throughout the water column, EPF would be equal to 0.5 over the entire depth of flow. This is almost never the case; EPF is usually less than 0.5 near the bottom, particularly in the saline wedge, and greater than 0.5 in the upper layers. The net upstream bottom current is due to the characteristic nature of flow circulation induced by the presence of the wedge, which means that the strength of this current will decrease as the limit of seawater intrusion is approached, and is theoretically zero at the limit (node) itself (Keulegan, 1966). Distributions of EPF at three locations - at the mouth, in the wedge and at the node, would qualitatively appear as shown in Fig. 1.1. When interpreted in terms of tidal flows, these distributions correspond to the general observation that in the mixing zone of the estuary (i.e. the region where sea water mixes with fresh water) flood flows landward at the bottom and ebb flows seaward at the surface.

The trends indicated by the EPF distributions suggest the dominating influence of flow hydrodynamics on sediment movement. As noted in Fig. 1.1, riverborne sediments from upstream fresh water sources arrive in the mixing zone of the estuary. The comparatively high degree of turbulence, the associated shearing rates and the increasingly saline waters will cause aggregates to form and grow in size as a result of frequent inter-particle collisions and increased cohesion. The large aggregates will settle to the lower portion of the water column because of their high settling velocities. Results based on laboratory experiments show that aggregate settling velocities can be

up to four orders of magnitude larger than the settling velocities of the elementary particles (Bellessort, 1973). Some of the sediment will deposit and some will be carried upstream near the bottom until periods close to slack water when the bed shear stresses decrease sufficiently to permit deposition. The deposited sediment will start to consolidate due to overburden forces. The depth to which the new deposit scours when the currents increase after slack will depend on the bed shear stresses imposed by the flow and the shear strength of the deposit. If the currents during both flood and ebb are sufficient to scour all of the new deposit, the net movement will be determined approximately by current predominance. However, if the bed shear stress during ebb is less than sufficient to suspend all of the newly deposited material, a portion of the material will remain on the bed during ebb, and will be resuspended and transported during the predominant flood flows, resulting in a net upstream transport. Net deposition, i.e. shoaling, will occur when the bed shear during flood, as well as during ebb, is insufficient to resuspend all of the material deposited during preceding slack periods. Some of the fine material that is resuspended will be re-entrained throughout most of the length of the mixing zone to levels above the salt water-fresh water interface and will be transported downstream to form larger aggregates once again, and these will settle as before. At the seaward end some material may be transported out of the system, a portion or all of which could ultimately return with the net upstream current. Some sediment moving upstream along the bottom may also be derived from oceanic sources, as for example occurs in the channel which connects the Gulf of Venezuela with Lake Maracaibo (Partheniades, 1966). The strength of this upstream current is often enhanced by the inequality between the flood and the ebb flows induced by the usually observed distortion of the tidal wave. Inasmuch as the low water depth is often significantly less than the depth at high water, the speed of the propagating tidal wave, being proportional to the square root of the depth, is higher at high water than at low water. This typically results in a higher peak flood velocity than peak ebb velocity and a shorter flood period than ebb period. Such a situation tends to enhance the strength of the upstream bottom current, and the sediment is sometimes transported to regions upstream of the limit of seawater intrusion.

The shoals formed in the mixing zone may be periodically scoured by high freshwater discharges, and the material will deposit near the mouth of the estuary or in the sea. During periods of low freshwater discharge, the sediment will slowly return to the shoal area with the net upstream current. In a typical estuary the sediment residence time in the mixing zone is large, and the transport rates often are an order of magnitude greater than the rate of inflow of "new" sediment derived from upland or oceanic sources. The estuarial sedimentary regime is characterized by several periodic (or quasi-periodic) macro time-scales. These are:

a) The tidal period (diurnal, semi-diurnal, or mixed),

b) One-half the lunar month (spring to spring or neap to neap),

c) Yearly cycle,

d) Periods greater than a year, e.g. the 19 year metonic cycle.

Of these, the first is of course the most important since it is the fundamental period which characterizes the basic mode of the sediment transport phenomenon in an estuary. The second is important from the point of view of determining net shoaling rates in many cases of engineering interest, and by the same token the third and sometimes the fourth time-scales are involved in considerations of long-term stability and shoaling in estuaries.

As an example of the yearly cycle, Fig. 1.2 shows the depth-averaged distributions of salinity and suspended sediment concentrations in the Hooghly River estuary, India (inset). It is observed that following the freshet season, as the freshwater outflow is reduced, the salinity progresses upstream at a rate of approximately 30 km/month. Thus in November, the penetration is 40-50 km upstream of Gasper Shoals, and in the following April the penetration distance is in excess of 180 km. The mean of these two profiles gives an average for the dry season, as shown. It is observed that the turbidity maximum for the same period occurs at a distance of 90-110 km, which is where the dry season salinity (normalized with respect to seawater salinity) is reduced to approximately one-tenth the seawater value.

From an Eulerian point of view, the super position of oscillating tidal flows on the quasi-steady state transport phenomenon depicted in Fig. 1.1 results in corresponding oscillations of the suspended sediment

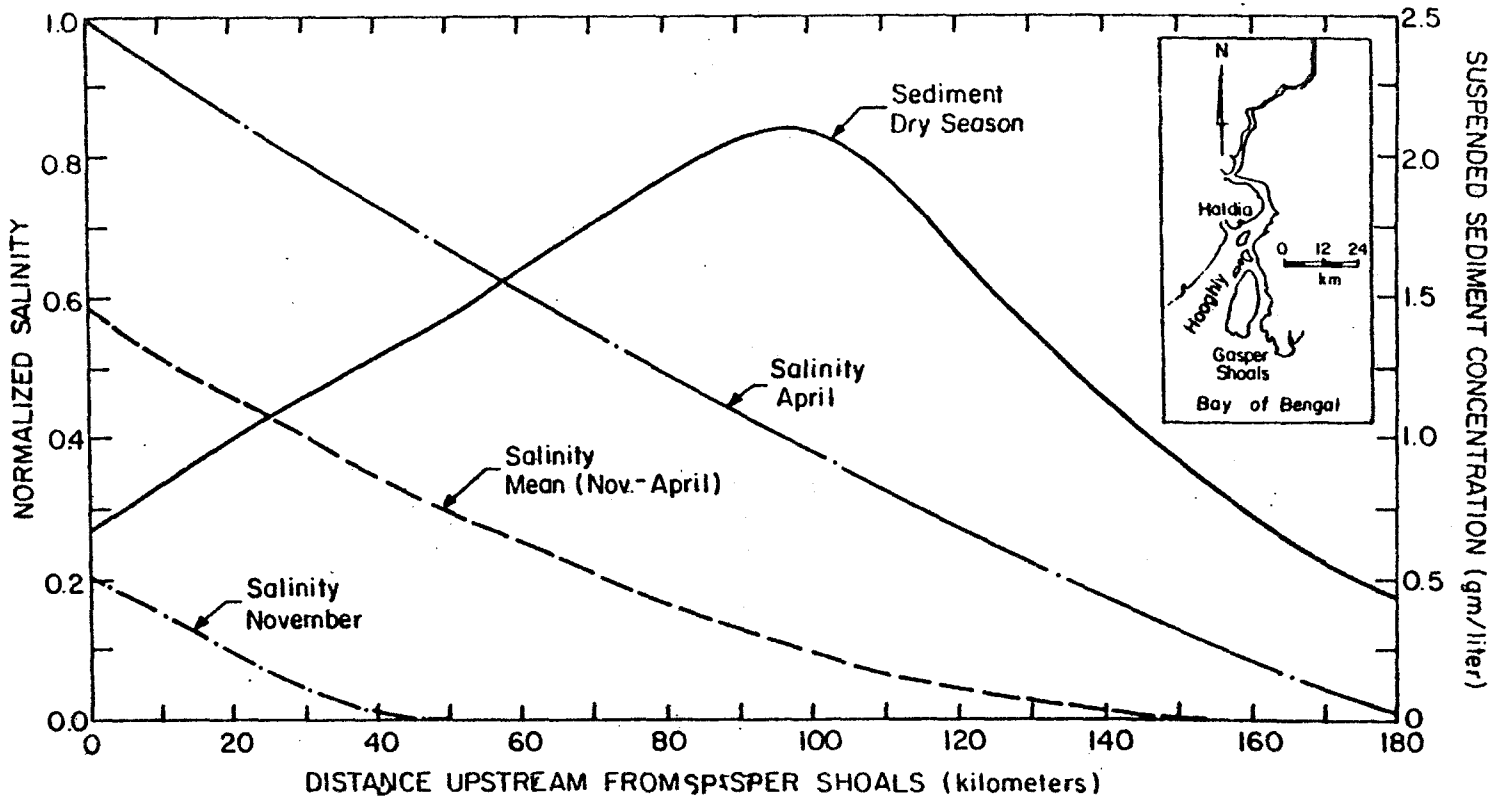

Fig. 1.2 Longitudinal Salinity and Suspended Sediment Concentrations in the Hooghly River Estuary (India) (after Mehta and Hayter, 1981).

concentration with time as shown by the Savannah River data in Fig. 1.3. Such a variation of the suspended load ultimately results from a combination of convective transport, diffusion, erosion and deposition.

Understanding the last two processes is crucially important and is the thrust of most, if not all, current research. Because of the complexity of the erosion-deposition phenomena, more than one interpretation is possible as far as any schematic representation of these phenomena is concerned. One such representation is shown in Fig. 1.4. According to this description, fine sediments can exist in four different physical states in a tidal estuary or sea: as a mobile suspension, a stationary suspension, a consolidating bed and as a settled bed. The last two are formed as a result of consolidation of a stationary suspension. Stationarity here implies little horizontal movement, although consolidation does mean that there is vertical (downward) movement. Beds corresponding to the latter three states may erode if the shear stress exceeds a certain critical value. Erosion of a stationary suspension is referred to as redispersion while erosion of a consolidating as well as a settled bed is termed resuspension.

1.2. Significance of Clays in Pollutant Transport

Substances which are known to cause discomfort, illness or death, and substances which are carcinogenic, mutagenic or harmful to metabolism are usually called pollutants. Thus, radioactive elements, heavy metals, complex organic substances, certain bacteria and viruses, etc. are all considered pollutants in a typical aquatic environment such as an estuary. Substances affecting economic interests are also often catagorized as pollutants. In this section the role of fine, cohesive sediments in pollutant transport is qualitatively discussed.

The importance of considering the transport of cohesive sediments in predicting the fate of pollutants introduced in a water body is pointed out by Kirby and Parker (1973). They state that the bulk of the pollution load is quite often transported sorbed to these sediments rather than in the non-sorbed state. In fact, most pollutants are associated with particulates in one way or another. Their position in the sediment can probably be classified into several groups: sorbed on the mineral, oxide or hydrous oxide surfaces, bonded in humic materials,

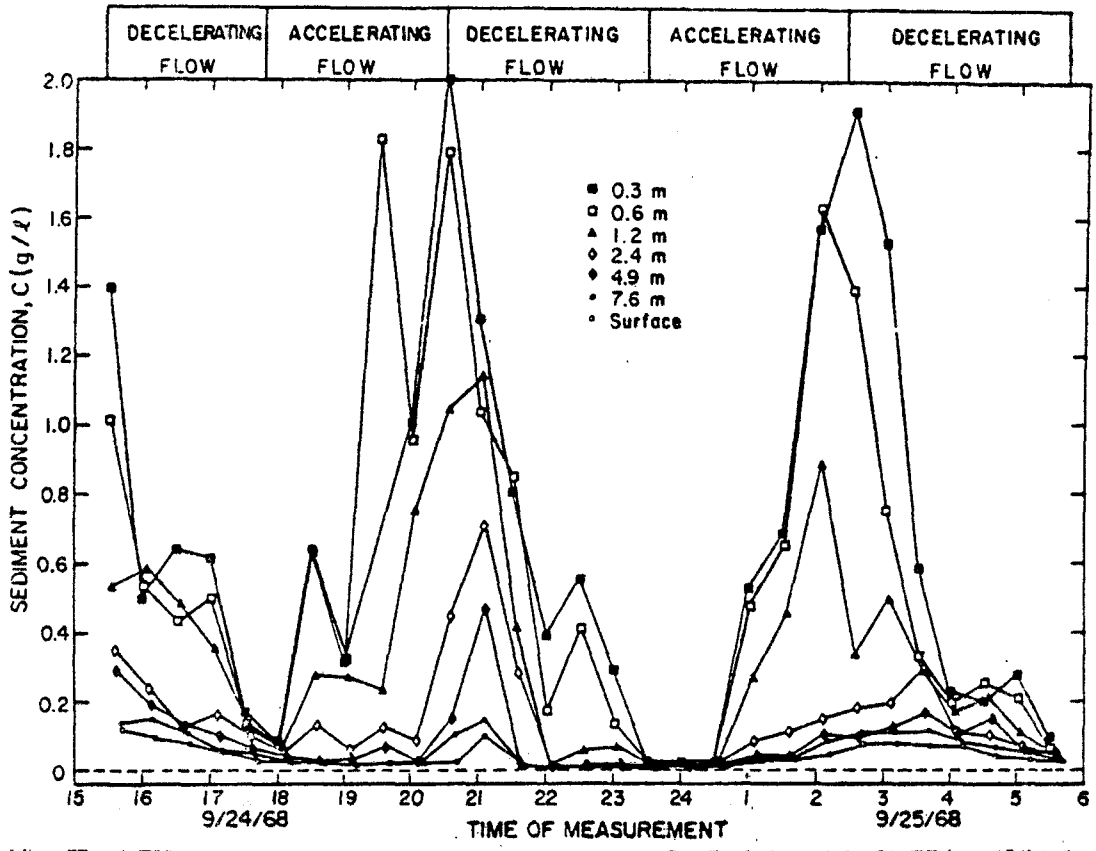

Fig. 1.3 Time and Depth Variation of Suspended Sediment Concentration in Savannah River Estuary (after Krone, 1972).

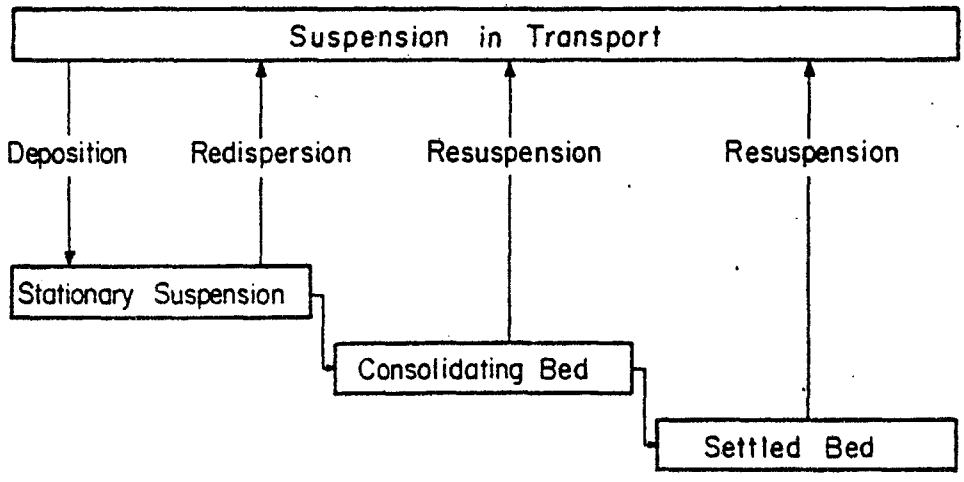

Fig. 1.4. Schematic Representation of the Physical States of Fine Sediment in Estuarial Mixing Zone (after Mehta et al., 1982a).

precipitated as metal sulfides, sorbed on the exchange sites of clay minerals or incorporated in the detrital organic or mineral phase.

Salomons and Mook (1977) studied the concentration of trace metals sorbed to estuarial and marine sediments. The grain size as well as the concentration of trace metals has a considerable variation in natural sediments. However, a positive correlation was seen between the quantity of pollutants, i.e. heavy metals, and the amount of fine-grained particles expressed by the percentage of particles less than 16 μm in diameter. The results, which show an increase in the concentration of heavy metals with decreasing grain size, are shown in Fig. 1.5. Figure 1.5(a) shows the correlation with Al, Fe, P and K. Fig. 1.5(b) shows the correlation with quartz, feldspar, carbonates and organic matter, and Fig. 1.5(c) shows the correlation with Zn, Cr, Pb and Cu. It is observed that the concentration of species increased in the order: Al > Fe > K > P, and Zn > Cr > Pb > Cu. Linear relationships between metal content and percentages of fractions smaller than 16 μm have been reported as well by Veltman (1979).

Hauser and Fauth (1972) verified the presence of high concentrations of barium, calcium, cobalt, copper, lead, mercury, nickel, silver and zinc in sediments. Mercury has received particular attention due to its transformation to the highly toxic methylmercury by benthic organisms (Fagerstrom and Zernelov, 1971). According to Jones (1972), the sources of metallic elements in the sediment are accessory mineral sites, lithic fragments, and surface coatings on grains and clay minerals. Changes in redox potential, pH or composition of solution media probably bring about changes in the availability of trace substances.

The important properties of clays which cause the adsorption of pollutants are the large surface area to volume ratio of clay particles, the presence of net negative electrical charges on their surfaces and their cation exchange capacity. These properties are described below.

When a substance is subdivided into smaller and smaller units, the ratio of surface area to volume, i.e. specific area, becomes larger and larger. For a given particle shape the specific area is inversely proportional to the equivalent spherical particle diameter, or Stokes diameter. When this diameter is reduced to 2 μm or less, the surface

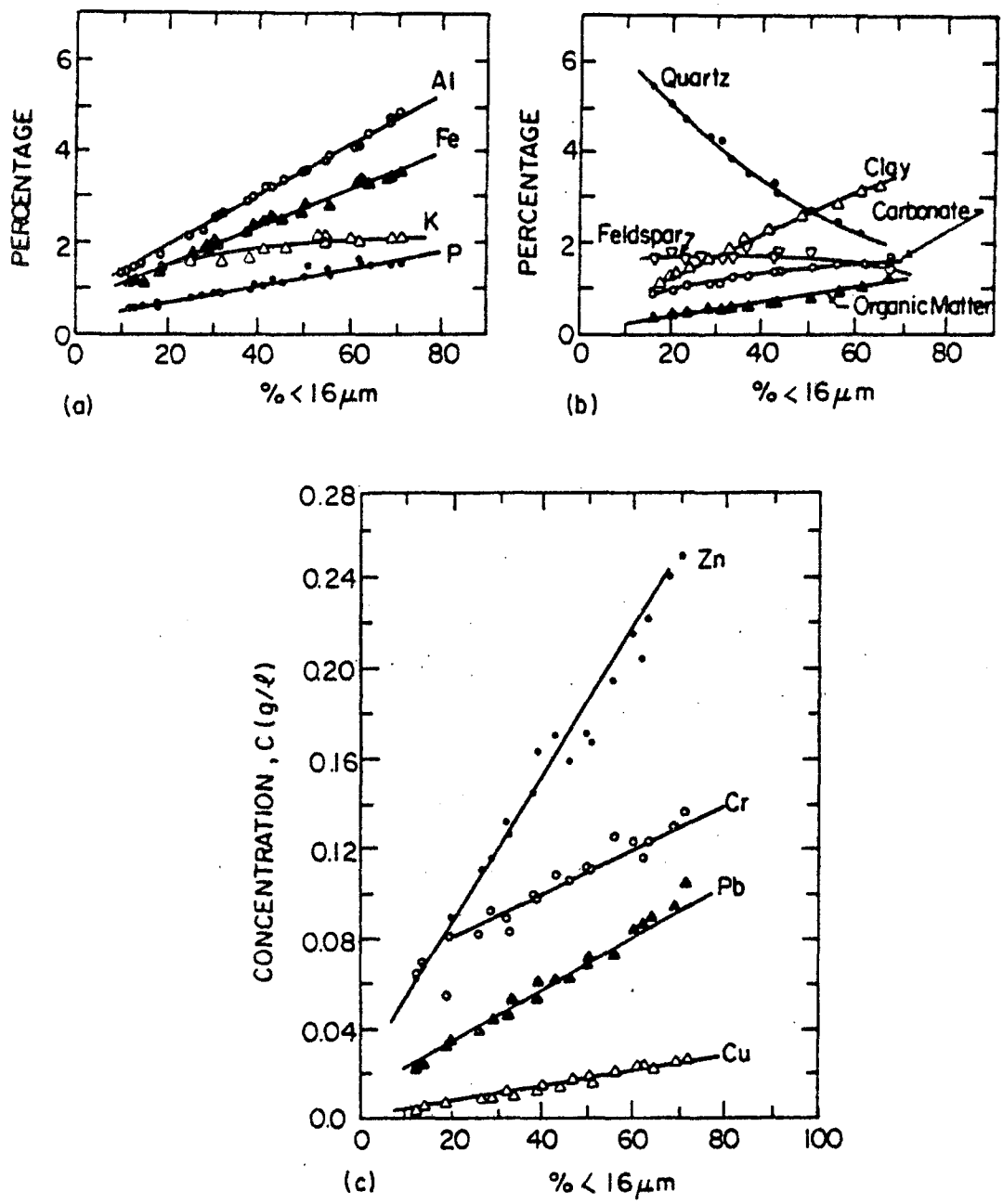

Fig. 1.5 Variation of Heavy Metal Concentration with Sediment Particle Size (after Salomons and Mook, 1977).

physico-chemical forces begin to exert a distinct influence on the behavior of this particle due to the large specific area and the particle is considered to be in the colloidal size range . Most clay particles fall within the colloidal range in terms of both their size and the controlling influence of surface forces on their behavior. In fact, the average surface force on one clay particle is approximately 10^6 times greater than the force due to gravity (Partheniades, 1962). Clays are usually platelet shaped and have a very large surface area to volume ratio. For instance, montmorillonite has a specific surface area of 800 m^2/gram. If all particles contained in about 10 grams of this clay could be spread out side by side, they would cover a football field (Mitchell, 1976). The shape in the form of platelets and the large surface area provide a large potential for different arrangements and trapping dissolved substances in the pore water.

Clays are primarily hydrous aluminum silicates with magnesium or iron occupying all or part of the aluminum positions in some minerals, and with alkalies (e.g. sodium, potassium) or alkaline earths (e.g. calcium, magnesium) also present as essential constituents in some of them (Grim, 1968). Substitution of ions of one kind by ions of another kind, with the same or different valence, but with retention of the same crystal structure is termed isomorphous substitution. This process does not necessarily involve replacement. In reality, the "replaced" cations are never there and the mineral is formed with its existing proportions of different cations in the structure. The tetrahedral and octahedral positions in the crystal lattice can be occupied by cations other than those in the ideal structure. Common examples are aluminum and ferrous iron (Fe^{+2}) for magnesium. The tetrahedral and octahedral cation distributions develop during initial formation of the mineral, and not by later substitution (Mitchell, 1976). However, the isomorphous substitution in all the clay minerals, except for kaolinite, gives clay minerals a net negative charge which is of great significance in coagulation of clays and in adsorption of pollutants.

The cation exchange capacity (CEC) is an important property of clay minerals by which they sorb certain cations and anions in exchange for those already present and retain them in an exchangeable state. The CEC of different clays varies from 3-15 meq/100 gm for kaolinite to 100-150

meq/100 gm for vermiculite. Higher CEC indicates greater capacity to adsorb other cations. The negative charge caused by isomorphous substitution is neutralized by attracting and holding cations on the surfaces and edges of a clay particle. These cations remain in an exchangeable position and may in turn be replaced by other cations.

The following factors are the causes of cation exchange: 1) substitution within the lattice structure results in unbalanced charges in the structural units of some clay minerals, and 2) broken bonds around the edges of the silica-alumina units give rise to unsatisfied charges. In both cases the unbalanced charges are balanced by the adsorbed cations. The number of broken bonds and hence the CEC increases with decreasing particle size. Lattice distortion would tend as well to increase the number of broken bonds. Also, the exchange capacity increases with decreased degree of crystallinity.

The ability to replace exchangeable cations depends on the following factors: 1) concentration: increased concentration of a replacing cation causes greater exchange by that cation. 2) population of exchange positions: the ease of release of an ion depends not only on the nature of the ion itself, but also upon the nature of the complementary ions filling the remainder of the exchange positions and on the degree to which the replaced ion saturates the exchange sites. 3) nature of anions in the replacing solution. 4) nature of the cation: higher the valence of the cation, the greater is its replacing power and the more difficult it is to displace when already present on the clay. Some of the predominantly occurring cations in sediments are listed in Table 1.1 in the order of their valence and atomic number. In the case of metals having the same valence, the metal with the higher atomic number replaces the one with the lower atomic number.

Table 1.1. Valence and Atomic Number of Cations in Sediments

Cation	Na	K	Ca	Cd	Zn	Hg	Cu	Pb	Al	Cr
Valence	1	1	2	2	2	2	2	2,4	3	2,3,6
Cation	Na	Al	K	Ca	Cr	Cu	Zn	Cd	Hg	Pb
Atomic No.	11	13	19	20	24	29	30	48	80	82

Chemicals are sorbed on the sediments or are released from them depending upon the conditions favorable for the corresponding process. Quantities in excess of the adsorption capacity may be found in the pore water surrounding the sediment. Some soluble substances such as phosphates sorb strongly on calcium carbonate, which explains why calcium carbonate-rich sediments contain low concentrations of dissolved phosphates in their pore water. There are several factors which affect the adsorption/desorption and hence the exchange rate of chemicals with sediments. For instance, the adsorption isotherm of PO_4^{-3}-Fe^{+3} system is controlled by the phosphate-iron ratio, the age of the complex formed, and pH.

Schindler et al. (1980) studied the effect of pH (acidity) on the mobilization of heavy metals from the sediments. They found that aluminum, zinc, manganese and iron were released from lake sediments at pH 5 and 6. Concentrations of zinc in the overlying water column exceeded 300 µg/l.

Soule and Oguri (1974) have mentioned that an understanding of the sorption and release mechanism of trace substances can only be achieved by considering the sediment as a dynamic system where the composition and geochemistry of the bulk materials vary through the following processes:

a) Diffusion of ions within the sediment
b) Reactions occurring in the interstitial water
c) Humic binding forces
d) Organic/inorganic complexes
e) Nutrient mobilization
f) Reactions at the sediment-water interface

Molecular diffusion plays a dominant role in describing the transport of dissolved substances especially below the zone of bioturbation. Molecular diffusion is assumed to follow Fick's Law and is expressed in terms of a diffusion coefficient, D_s. Despite the importance of diffusion in diagenetic models, there have been very few measurements of D_s for various chemical species in anoxic pore waters. To quote Krom and Berner (1980), "we know of only three direct determinations of the diffusion coefficient of sulfate in marine sediments and none at all of the diffusion coefficients of ammonia and

phosphate in such sediments." Krom and Berner (1980) determined the diffusion coefficient of phosphate to be $D_s = 3.7 \times 10^{-6}$ cm^2/sec by laboratory experiments using homogenized anoxic mud.

Mathematical models have been developed and used: 1) to describe and predict the concentration profiles of dissolved sulfate, ammonia, silica, phosphate, etc. in the pore waters of anoxic sediments (e.g. Berner, 1974; Lasage and Holland, 1976; Vanderborght et al., 1977; Murray et al., 1978) and 2) to describe the chemical composition of organic matter undergoing decomposition (e.g. Sholkovitz, 1973; Hartmann et al., 1973; Berner, 1977).

Mortimer (1971) showed the effect of aerobic and anaerobic status of soil on the chemical exchange of phosphorus, manganese and iron. With a progressive decline of O_2 concentration from 2 mg/l to analytical zero at the sediment-water interface, first manganese and later iron was solubilized from sediment and transferred to the water. Patrick and Khalid (1974) studied release and sorption of phosphate by soils and sediments under aerobic and anaerobic conditions. They found that anaerobic soils released more phosphate to soil solutions low in soluble phosphate and sorbed more phosphate from soil solutions high in soluble phosphate than did aerobic soils. The difference in behavior was attributed to the change brought about in ferric oxyhydroxide by soil reduction.

1.3. Purpose of Study

1.3.1. Need for Research

The necessity of better understanding fine, cohesive sediment transport in estuaries is demonstrated by examining the following two sediment related problems.

The first pertains to water quality effects on biota. The effects of sediments on water quality for biota include limitation of the penetration of sunlight and the sorption of toxic compounds from solution. The concentrations of nutrients for algae in some estuaries are often sufficient to cause excessive algae blooms. The rate of multiplication of algae in such estuarial waters is limited by a reduced light supply resulting from high turbidity caused by suspended sediment particles. Estuarial waters are often used by industries as convenient

dump sites for waste products. As discussed in the previous section, pollutants such as heavy metals, pesticides, herbicides, and organics are often found sorbed onto sediment materials with equilibrium between dissolved and sorbed materials frequently favoring the sorbed phase (Ariathurai et al., 1977). Due to their property of cohesion, these sediments provide a large assimilative capacity as well as the transporting mechanism for such toxic compounds. For example, in an investigation of the bottom sediments from several coastal marinas in Florida, two interesting observations were made (Weckmann, 1979; Bauer, 1981). First, when comparing sediment particle size inside the basin with that obtained immediately outside in the main body of water, it was found that in the majority of the marinas investigated, the sediment inside was measurably finer than that outside. Second, a similar comparison in terms of heavy metal (e.g. Cu, Pb, Ni, Cd and Zn) content within the basin and without indicated measurably higher concentrations inside the basin. These two observations when correlated exemplify the role of fine sediments in accumulating pollutant levels in estuarial depositional environments such as marina basins.

Storage of river waters upstream and their diversion for agricultural, urban and industrial uses will sharply reduce sediment inflows as water resources become scarce. Therefore, it will be necessary to predict the effects of reduced sediment inflows to ascertain the minimum waste water management needed to achieve and maintain desirable water quality. Several aspects of water quality problems related to sediment contamination have been discussed in a series of papers edited by Baker (1980).

The second problem concerns the maintenance of navigable waterways. Under low flow velocities, sometimes coupled with turbulent conditions which favor the formation of large aggregates, cohesive sediments have a tendency to deposit in areas such as dredged cuts and navigation channels, in basins such as harbors and marinas, and behind pilings placed in water (Einstein and Krone, 1962). In addition, as noted previously, the mixing zone between upland fresh water and sea water in estuaries is a favorable site for bottom sediment accumulation. Inasmuch as estuaries are often used as commerce routes to the sea, it is desirable to be able to accurately estimate the amount of dredging

required to maintain navigable depths in these water bodies, and also to predict the effect of new estuarial development projects such as the construction of a port facility or dredging of additional navigation channels.

The influence of salinity on fine sediment erosion, deposition and transport (e.g. as shown in Fig. 1.4), must be considered for the following reason: the structure of aggregates has been found to be dependent on the salinity for salinities lower than about 10 ppt (Krone, 1962; 1978). In the upper reaches of estuaries, where the salinities are typically less than 10 ppt for at least the latter stages of ebb flow and first part of flood, and in situations where high stormwater runoff significantly lowers the salinity over the entire water depth, the aggregate structure, and hence the transport processes become dependent upon the salinity level. Figure 1.6 shows the variation in the vertical salinity profile with time measured in the upper reaches of the Savannah River estuary at the same station as the suspended sediment concentration-time profile shown in Fig. 1.3. As shown, the salinities are less than 10 ppt for the entire measurement period. The effect of stormwater runoff from a short duration, high intensity storm on the salinity (chloride concentration) at the mouth of a Pacific ocean estuary is observed in Fig. 1.7, which shows field measurements as well as predictions from a water quality model developed by Orlob et al. (1967). It is apparent that the effects of salinity variation must be taken into account when the sedimentary regime in any estuary is being investigated.

1.3.2. Predictive Modeling

Prediction of the fate of sorbed pollutants or the frequency and quantity of dredging required to maintain navigable depths in a channel or harbor can be accomplished by modeling the movement of fine sediments in the water body of concern. It becomes necessary to simulate the various transport processes, i.e. erosion, convective and diffusive transport, deposition and consolidation, and the physical factors, e.g. movement of water and dissolved salt, that govern these processes. The movement of suspended sediment, water and salt are highly interrelated, as is evident upon examination of Fig. 1.8 which defines possible

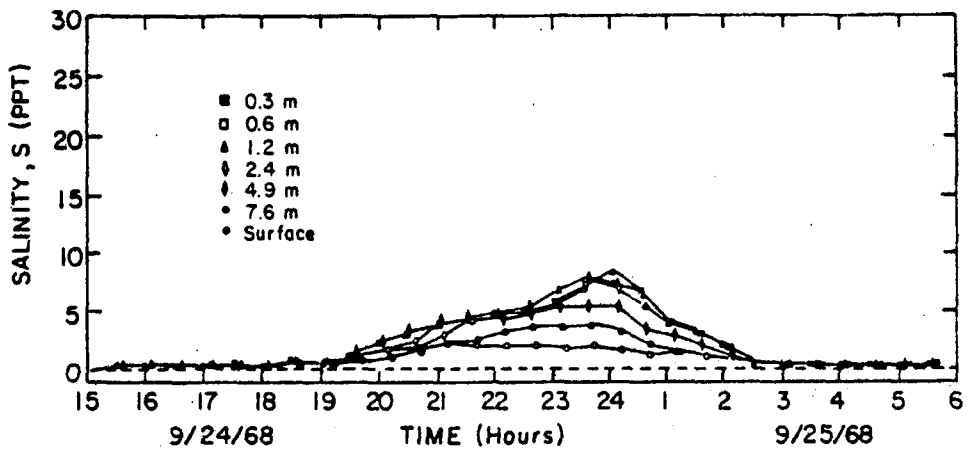

Fig. 1.6 Time and Depth Variation of Salinity in Savannah River Estuary (after Krone, 1972).

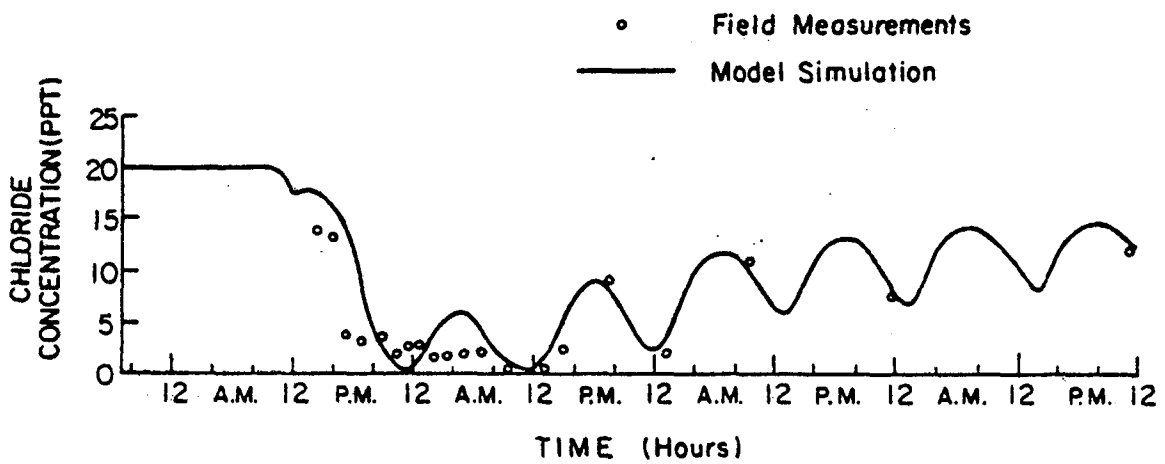

Fig. 1.7 Time Variation of Chloride Concentration in a Pacific Ocean Estuary Due to Stormwater Runoff (after Orlob et al., 1967).

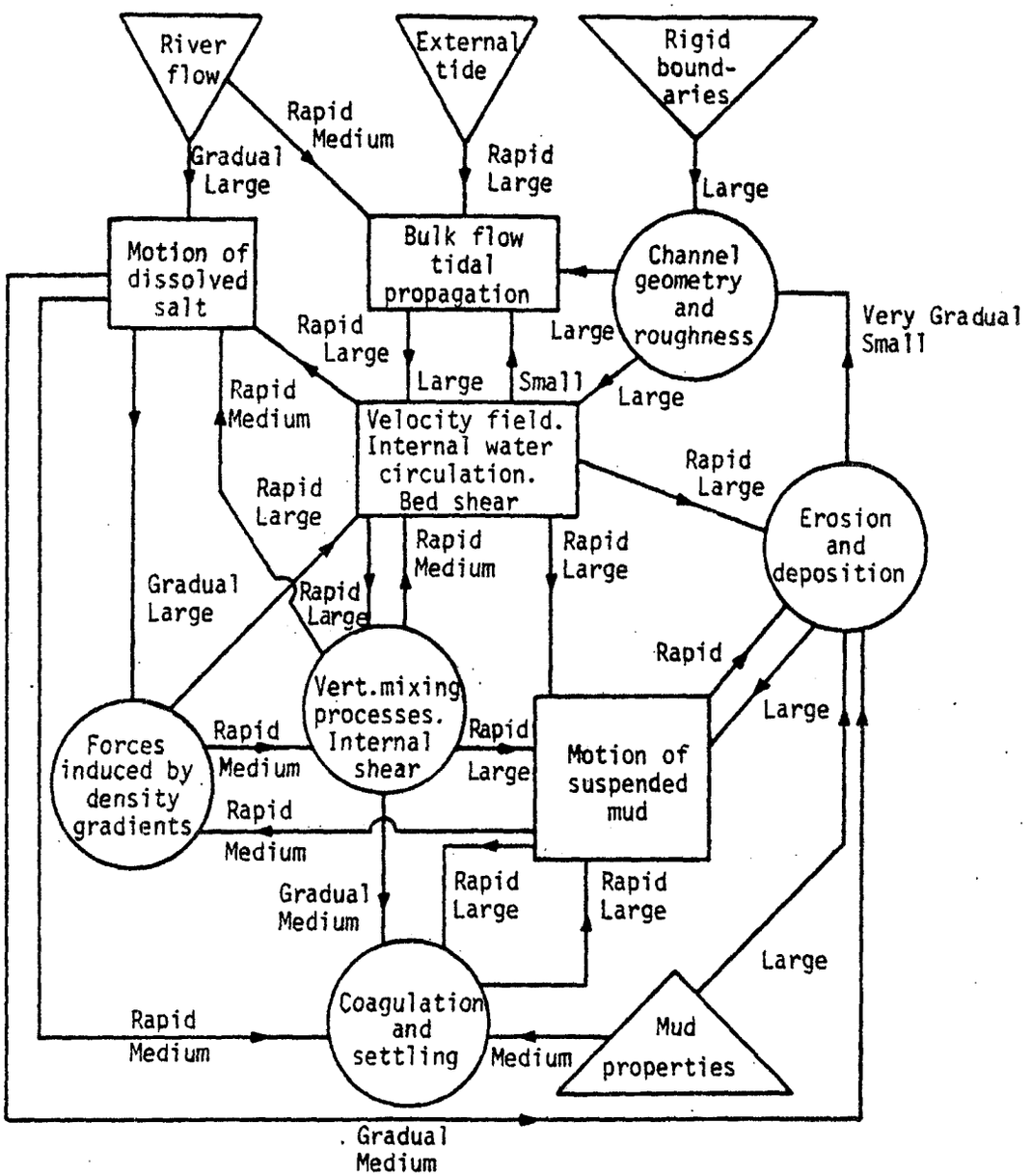

Fig. 1.8 Interactions of Tidal and Estuarial Sediment Transport Processes (after Owen, 1977).

interactions between these constituents in an estuary. The forces which control tidal motions are given in triangles, the movements of the water, salt and sediment are depicted in rectangles, and secondary processes and factors which influence the movements of water, salt and sediment are given in circles. Two scales are given between each of the interacting processes. The top one indicates the speed, i.e. time-scale, of the interaction, while the bottom one indicates the magnitude of the interaction. Not surprisingly, theoretical descriptions of the major processes and interactions involved in the motion of water, sediment and salt are still far from complete.

Physical and mathematical models or combinations ("hybrid approach") of these two types are the types of models available for use in predicting cohesive sediment movement in a water body. Physical scale models have been only partially successful due to lack of an appropriate model sediment as well as due to poor model reproduction of estuarial mixing processes and internal shear stresses (Owen, 1977). Mathematical models, however, have been generally more successful in reproducing, with some degree of accuracy, the movement of cohesive sediments in estuarial waters. The modeling philosophy is delineated below.

To mathematically model the motion of the three main constituents in an estuarine environment the three-dimensional forms of the conservation of momentum and mass equations for the water and the conservation of mass equations for the dissolved salt, suspended sediment and pollutant, if present, must be solved numerically. However, due to the current high cost of solving such three-dimensional, coupled, partial differential equations, only a few three-dimensional models exist (Liu and Leendertse, 1978). The common procedure has been to spatially integrate these equations, laterally and/or vertically, in order to reduce them to their two- or one-dimensional forms. Two-dimensional vertical (i.e. laterally integrated) fine sediment transport models have been developed by O'Connor (1971), Odd and Owen (1972), Ariathurai et al. (1977) and others. Two-dimensional horizontal (i.e. vertically integrated) models have been developed by among others April and Brett (1975) and Ariathurai et al. (1977). The horizontal length scales relative to the transport of estuarial sediment typically are one

to three orders of magnitude greater than the vertical length scales. As a consequence, and because horizontal transport distances are usually of primary interest in ascertaining the magnitude of sedimentation or the fate of sorbed pollutants, it is in most cases not unreasonable to use vertically integrated transport equations for modeling purposes. However, even using the two-dimensional forms of the governing equations, some eight to ten coupled equations must be solved to completely model the depth-averaged motion of water, sediment and salt. As a result, the modeling of water and salt movement is commonly performed separately from the sediment transport modeling. For example, a two-dimensional hydrodynamic model, which solves the coupled momentum and (water and dissolved salt) continuity equations, would be used to model the movement of water and salt. Then a two-dimensional fine sediment transport model would be used to predict the motion of sediment using the results from the hydrodynamic model. This is the modeling approach that has been used in this study, with all research and development concerned with the two-dimensional vertically integrated modeling of fine sediment transport.

None of the fine sediment transport models listed above has the capability of determining the effect of salinity variation (e.g. in the mixing zone between fresh and sea water in estuaries) on the processes of erosion and deposition of cohesive sediments in a turbulent flow field, since the empirical laws used in the models for these transport processes were derived using empirical evidence from laboratory experiments conducted in natural or artificial sea water. In addition, the empirical laws of erosion and deposition cannot be considered to be "the state-of-the-art" even for sea water, as a considerable number of laboratory experimental tests conducted since these laws were proposed, including some during this study, have revealed new evidence on the erosional and depositional behavior of cohesive sediments.

1.3.3. Objectives and Scope of Investigation

The study described herein had the following five main objectives:

1) Conduct a comprehensive review of the existing laws on the erosion and deposition of fine, cohesive sediments.

2) Determine the effects of salinity on the rates of erosion of flow-deposited cohesive sediment beds under turbulent flows.
3) Determine the effects of salinity on the deposition rates under turbulent flows.
4) Upgrade an existing "state-of-the-art" two-dimensional, vertically integrated mathematical model of cohesive sediment transport by improving upon this model's capability of predicting the erosion and deposition of cohesive sediments in estuaries.
5) Demonstrate the utility of the improved transport model in simulating the erosion and deposition of cohesive sediments and the effect of salinity on these transport processes.

Research conducted to accomplish these objectives was directed towards obtaining an improved understanding and quantitative description of the erosion (resuspension) and deposition of fine sediments under turbulent flows. This was achieved by experimental investigations on: 1) the erosive behavior of flow-deposited (i.e. stratified) cohesive sediment beds, and 2) the effect of salinity on the rates of erosion and deposition. The results from these investigations, in the form of empirical erosion and deposition functions and an improved schematization of flow-deposited beds, were incorporated into the selected cohesive sediment transport model. The fifth objective given above was accomplished by using the modified model to: 1) simulate laboratory erosion and deposition experiments, and 2) demonstrate the effect of salinity on the rates of erosion and deposition of cohesive sediments in both laboratory experiments and in a 10 km long hypothetical canal. The following format is used to present the results.

In Chapter II, the improved cohesive sediment transport model is described in detail. First, the governing equations for sediment transport in an estuarial environment are developed in Section 2.1. In Section 2.2, the numerical technique for solving the governing equations is described. A description of the selected transport model and the modifications made to this model are given in Sections 2.3 and 2.4, respectively. The new bed schematization and new erosion and deposition algorithms developed and incorporated into the transport model are described in detail in Sections 2.5, 2.6 and 2.7, respectively. In Section 2.8, the effects of salinity on the physico-chemical properties

and estuarial transport processes of cohesive sediments are discussed. Also presented in this section are the results from laboratory erosion and deposition experiments, in which the effects of salinity on these two processes were studied, and a description of the method used to incorporate these effects into the transport model. The stability characteristics of the improved model are discussed in Section 2.9, and the limitations of the modeling approach used are discussed in Section 2.10. Lastly, possible applications of the improved model to water quality and sedimentation management problems are given in Section 2.11.

In Chapter III, the results from the simulations of laboratory erosion and deposition experiments using the improved model are presented. The effects of salinity on selected laboratory experiments and on the transport processes in the hypothetical canal are as well demonstrated and presented therein.

In Chapter IV, important conclusions from this study and recommendations for future research are stated.

In Appendix A, a flow chart of the model is presented. In Appendix B, a user's manual for the model is given. Lastly, in Appendix C, a discussion of the various physico-chemical factors that should be characterized in any study of the erosive behavior of cohesive sediments is given.

II. MODELING CONSIDERATIONS

2.1. Significance of Important Physical Factors in Estuarial Transport

Prior to discussing the governing equations for the convective and diffusive transport of suspended fine sediments, the significance of the important factors controlling the hydrodynamic and sedimentary regimes in an estuary is discussed.

As implied in Section 1.1, the hydrodynamic regime in an estuary is governed by the interaction between the following seven factors: fresh water flow, astronomical tides, wind-generated surface waves, surface (i.e. wind) stresses, Coriolis force, the geometry of the water body and the roughness characteristics of the sedimentary material composing the bed (Dyer, 1973). Incorporated in geometry is the shape and the bathymetry of the estuary. The geometry and bed roughness interact with the driving forces - the first five factors - to control the pattern of water motion (in particular the shear stress and turbulence structure near the bed), frictional resistance, tidal damping and the degree of tidal reflections (Ippen, 1966).

The magnitude of the tidal flow relative to the fresh water inflow governs, to a large extent, the intensity of vertical mixing of the lower high density layer with the upper less dense layer. There exists in all estuaries a horizontal, i.e. longitudinal, salinity profile which decreases from the mouth to the upper reaches of the estuary. Such profiles have been measured in numerous estuaries world-wide. A few examples are: Cumbarjua Canal, Goa, India during the dry season, i.e. October through June (Fig. 2.1); the San Francisco Bay and Sacramento-San Joaquin Delta (Fig. 2.2); the Pamlico River estuary, North Carolina (Fig. 2.3); and the Yangtze River Estuary, China (Fig. 2.4). As noted in Section 1.1, the existence of a longitudinal salinity gradient, or baroclinic force, implies that there could be a gravity driven upstream transport of a high density sediment suspension in the lower portion of the water column (Officer, 1981; Mehta and Hayter, 1981).

Winds affect the hydrodynamic regime and mixing in an estuary by generating a surface shear stress and waves. The surface stress is capable of generating a surface current (whose magnitude will be approximately three percent of the wind speed at 9.1 m elevation

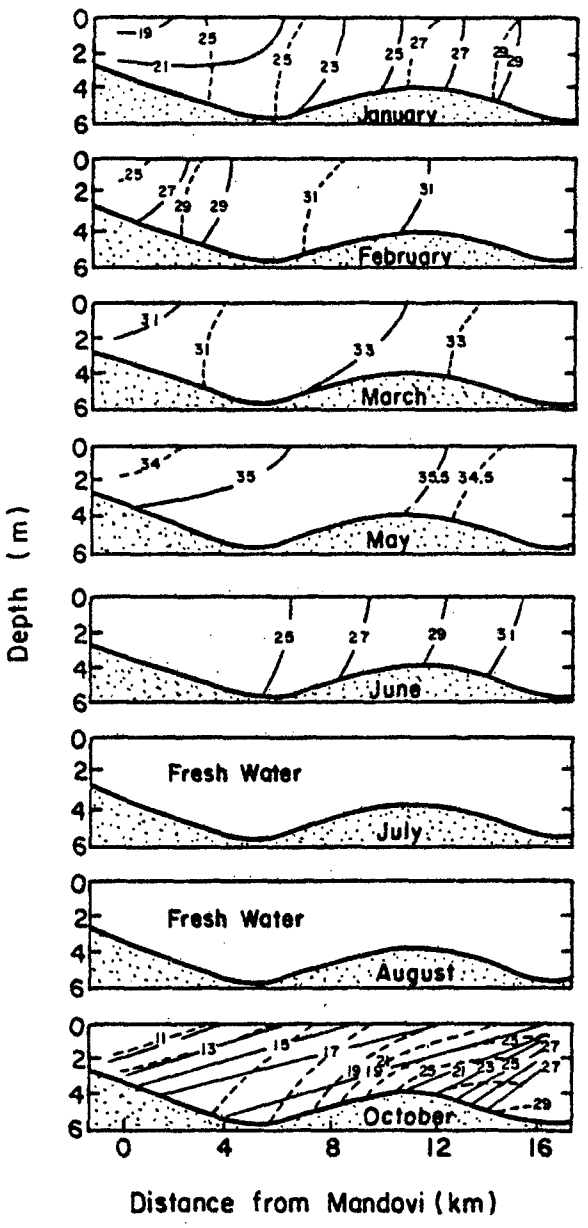

Fig. 2.1 Monthly Salinity Distributions in the Cumbarjua Canal, Goa, India; —— Ebb; ---- Flood (after Rao et al., 1976).

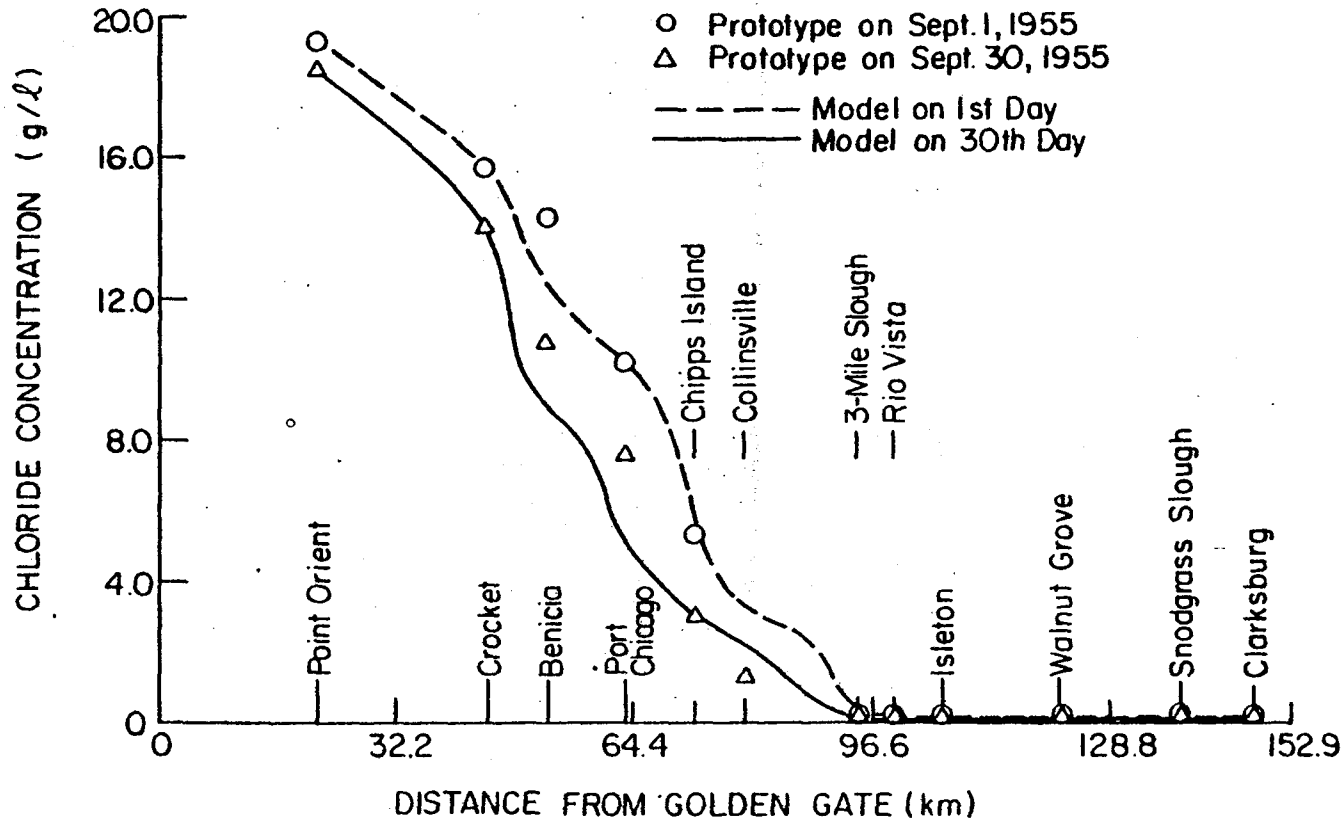

Fig. 2.2 Variation in Chloride Concentration in San Francisco Bay and Sacramento-San Joaquin Delta-September 1955 (after Orlob et al., 1967).

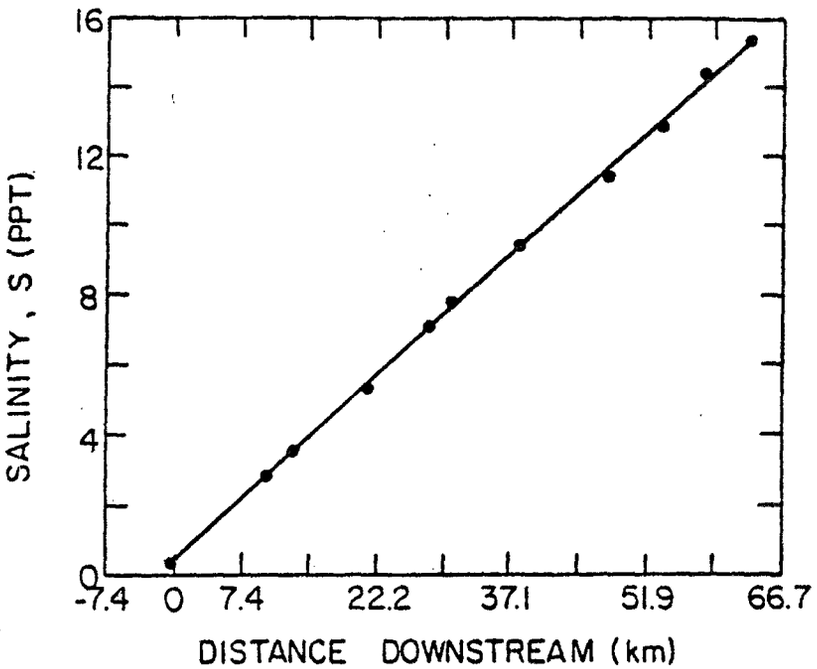

Fig. 2.3 Salinity of the Surface Waters of the Pamlico River Estuary as a Function of the Distance from the Railroad Bridge at Washington, N.C. (after Edzwald et al.,1974).

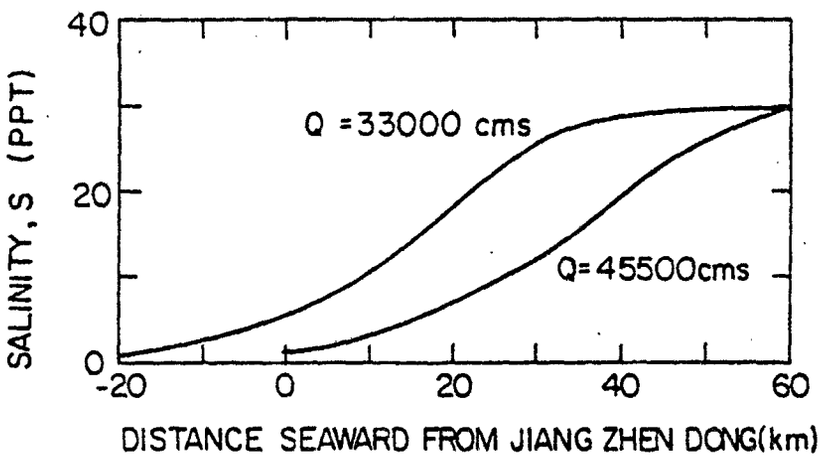

Fig. 2.4 Computed Longitudinal Salinity Profile in the Yangtze River Estuary as a Function of the Distance Downstream from Jiang Zhen Dong for Two River Discharges: Q = 33000 cms and 45500 cms (after Huang et al., 1980).

(Hughes, 1956)) and a superelevation of the water surface along a land boundary located at the downwind end of the estuary (Ippen, 1966). The latter effect causes a vertical circulation cell, with landward flow at the surface and a reversed seaward flow along the bottom. This phenomenon as well increases the degree of vertical mixing.

Along the banks and in shallow areas, surface gravity waves induced by the wind are capable of eroding bottom sediments. Since a tidal current of sufficient strength to transport (but not necessarily to erode the sediment by itself) suspended sediment is generally present, this material is convected and dispersed both longitudinally with the main tidal flow and sometimes laterally with secondary currents towards the deeper sections of the estuary. Wave action and in particular wave breaking substantially increase the intensity of surficial turbulence and mixing.

The Coriolis force, caused by the earth's rotation, has both a radial (horizontal) and a tangential (vertical) component. The latter is generally negligible as it is linearly proportional to the vertical component of the flow velocity, which is typically an order of magnitude smaller than the horizontal velocity components. The magnitude of the radial component depends upon the size of the water body. Most extra-tropical estuaries are relatively large and therefore the effect of this force on the hydrodynamic regime is measurable. Estuarial hydrodynamics are described in extensive detail in such texts as Ippen (1966), Barnes and Green (1971), Dyer (1973), Officer (1976) and Fischer et al. (1979).

As noted in Section 1.1, the sedimentary regime in an estuary is controlled by the hydrodynamics, the chemical composition of the fluid and the physico-chemical properties of the cohesive sediment. These factors affect the following processes which cohesive sediments typically are subjected to in such a water body: erosion, convection, diffusion, coagulation, aggregation, settling, deposition and consolidation of the deposited bed. These processes are briefly described below, following a definition of a clay suspension.

A "solution" of clay in a medium consists of a homogeneous dispersion of very small kinetic units, i.e. particles (van Olphen, 1963). When the Stokes diameter of the clay solution is less than 2 μm, the clay dispersion is usually referred to as a sol. The Stokes

diameter of an arbitrarily shaped particle is determined by equating the particle's settling velocity with Stokes law for spherical particles and solving for the "equivalent spherical diameter" (Stokes diameter). When this diameter is greater that 2 μm, the dispersion is called a suspension. However, through use, the term suspension has become synonymous with dispersion, and thus a clay suspension refers to both sol and suspension.

Erosion of cohesive soils occurs whenever the shear stress induced by fluid flow over the bed is great enough to break the electro-chemical inter-particle bonds (Partheniades, 1965; Paaswell, 1973). When this happens, erosion takes place by the removal of individual sediment particles and/or flocs. This type of erosion is time dependent and is defined as surface erosion or resuspension. In contrast, another type of erosion occurs more or less instantaneously by the removal or entrainment of relatively large pieces of soil. This process is referred to as mass erosion or redispersion and occurs when the flow-induced shear stresses on the bed exceed the soil bulk strength along some deep seated plane.

Once eroded from the bed, the sediment is transported entirely as suspended load (not as bed load) by the estuarial flow. Such transport is the result of three processes: 1) convection - the sediment is assumed to be transported at the speed of the local mean flow, 2) turbulent diffusion - driven by spatial suspended sediment concentration gradients; the material is diffused laterally across the width of the flow channel, vertically over the depth of flow and longitudinally in the direction of the transport, and 3) longitudinal dispersion - the suspended sediment is as well dispersed in the flow direction by spatial velocity gradients (Ippen, 1966).

Coagulation of suspended particles depends upon inter-particle collision and inter-particle cohesion after collision. The former process occurs by: 1) Brownian motion of the suspended particles, 2) effects of internal shear or velocity gradients within the fluid, and 3) differential settling of the suspended particles or flocs (Edzward et al., 1974; Krone, 1978; Hunt, 1980). A description of these collision mechanisms is given in Section 2.8.4. Cohesion or particle destabilization of cohesive sediments occurs in an estuary because of

the altered chemical environment found there. In fresh water, most clay particles are in a stabilized or dispersed state because the repulsive electro-chemical surface forces between the particles prevent them from adhering to one another upon collision. In the increasingly saline conditions encountered moving seaward in estuaries, the repulsive forces are suppressed and clay particles coagulate to form flocs. A systematic "build up" of flocs as occurs in estuaries is defined as aggregation. An aggregate is considered to be the structural unit formed by the joining of flocs. The rate and degree of aggregation are two important factors which govern the transport of fine sediments in estuaries. Factors, besides the water chemistry and the magnitude of the surface forces, known to govern coagulation and aggregation include sediment size grading, mineralogical composition, particle density, organic content and the suspended sediment concentration (i.e. availability) of the sedimentary material, the water temperature, height through which the flocs have settled, and the turbulence intensity of the suspending flow (Owen, 1971).

Given the mechanisms which influence the rate of aggregation in an estuary, the order of aggregation, which characterizes the packing arrangement, density and shear strength of aggregates, is determined by the following factors: 1) sediment type, 2) fluid composition, 3) local shear field, and 4) concentration of particles or flocs available for aggregation.

Primary or 0-order flocs are highly packed arrangements of elementary particles, with each floc consisting of perhaps as many as a million particles. Typical values of the void ratio (volume of pore water divided by volume of solids) have been estimated to be on the order of 1.2. This is equivalent to a porosity of 0.55, which is a more "open" structure than commonly occurs in cohesionless sediments (Krone, 1963). Continued aggregation under favorable shear gradients can result in the formation of first or higher order aggregates composed of loosely packed arrays of 0-order flocs. Each succeeding order consists of aggregates of lower density and lower shear strength. Experimental observations (Krone, 1963; 1978) tend to indicate the following approximate relationship between the aggregate shear strength, τ_s, and aggregate density, ρ_a, for many (although not all) sediments

$$\tau_s = \alpha(\rho_a - 1)^{\beta} \qquad (2.1)$$

where α and β are coefficients which must be determined experimentally for each sediment. Inasmuch as the shear field in an estuary exhibits significant spatial and temporal variations, a range of aggregates of different shear strengths and densities are formed, with the highest order determined by the prevailing shearing rate, du/dz, provided that: 1) the sediment and the fluid composition remain invariant, and 2) sufficient number of suspended particles are available for promoting coagulation and aggregation.

The determination of τ_s and ρ_a corresponding to each sediment-fluid mixture can be carried out through rheological diagrams of applied shear stress against the shearing rate. Such plots were developed by Krone (1963; 1978) with the help of a specially designed annular viscometer. An example of such a diagram is presented in Fig. 2.5, with the shear stress proportional to the dial reading on the viscometer and the shearing rate proportional to the rotation rate of the outer cylinder of the viscometer. Each order of aggregation corresponds to a given volume fraction of the aggregates (volume occupied by the aggregates divided by the total volume of the suspension) which in turn can be shown to be related to the relative differential viscosity (the viscosity of the suspension divided by the viscosity of the suspending medium). Given the viscosity of the suspending medium, the relative differential viscosity is determined from the slope of the rheological diagram, and hence the volume fraction can be calculated. The density is then computed from the volume fraction. The intercept on the applied shear stress axis of the diagram corresponds to τ_s; in Fig. 2.5 the ordinate intercept is proportional to τ_s. Table 2.1 gives the orders of aggregation, cation exchange capacity (CEC), densities and shear strengths of sediment samples from five different sources. As observed in this table, the first four sediment samples are characterized by three orders of aggregation while the sediment from San Francisco Bay is characterized by six orders. The number of aggregation orders possible for a suspension of a given sediment is equal to the number of linear segments on the rheological diagram with different slopes. Thus, in

Fig. 2.5, the sediment sample has two possible orders of aggregation. Krone (1963) postulated that each segment is related to a particular volume fraction and therefore to a different manner in which the same sediment can aggregate, i.e. different order of aggregation. Thus, for the suspensions of the first four sediments listed in Table 2.1, three different linear segments were obtained on the rheological diagrams, while for Bay mud, six segments, and therefore six orders of aggregation were found. This indicates that Bay mud can aggregate in three more ways than the other four sediments, and further suggests that the Bay sediment is more cohesive than the others. Also observed in this table is the very rapid decrease in the shear strengths and somewhat less rapid decrease in densities with increasing order of aggregation. These trends indicate that as the order of aggregation increases, the inter-aggregate pore volume increases and the strength of these aggregates decreases because of limited bonding area between the lower order aggregates (Krone, 1978).

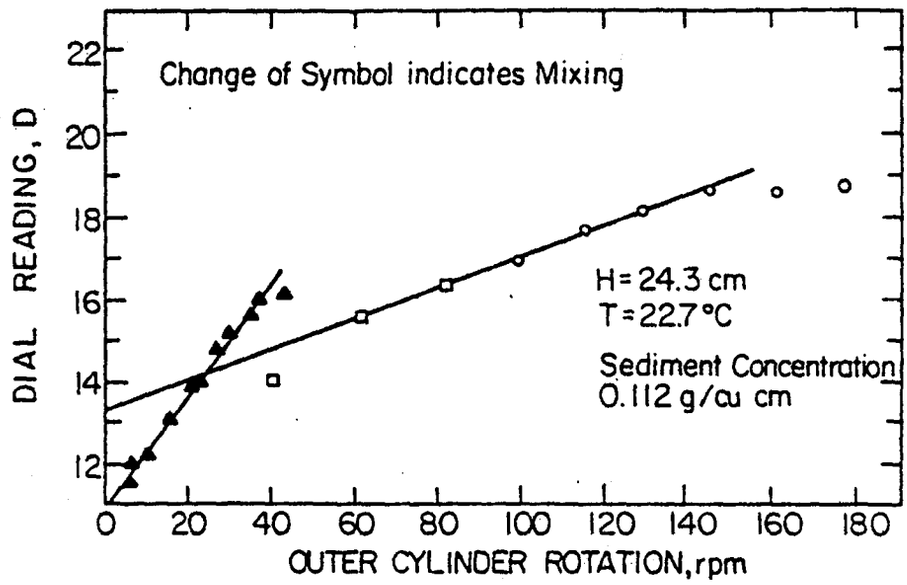

Fig. 2.5 A Plot of Raw Viscometer Data Obtained from the U.S. Army Corps of Engineers Philadelphia District Sample (after Krone, 1963).

Table 2.1

Properties of Sediment Aggregates (after Krone, 1963)

Sediment Sample	Order of Aggregation	CEC (meq/100 gm)	Density ρ_a(Kg/m^3)	Shear Strength τ_s(N/m^2)
Brunswick Harbor	0	38	1164	3.40
	1		1090	0.41
	2		1067	0.12
	3		1056	0.062
Wilmington District	0	32	1250	2.10
	1		1132	0.94
	2		1093	0.26
	3		1074	0.12
Gulfport Channel	0	49	1205	4.60
	1		1106	0.69
	2		1078	0.47
	3		1065	0.18
White River (salt)	0	60	1212	4.90
	1		1109	0.68
	2		1079	0.47
	3		1065	0.19
San Francisco Bay	0	34	1269	2.20
	1		1179	0.39
	2		1137	0.14
	3		1113	0.14
	4		1098	0.082
	5		1087	0.036
	6		1079	0.020

The settling rate of coagulated sediment particles depends on, in part, the size and the density of the aggregates and as such is a function of the process of coagulation and aggregation (Owen, 1970). Therefore the factors which govern these two processes also effect the settling rate of the resulting aggregates. As noted in Section 1.1, the settling velocities of aggregates can be several orders of magnitude larger than those of individual clay particles (Bellessort, 1973).

Deposition of aggregates occurs relatively quickly during slack water. Deposition also occurs in slowly moving and/or decelerating flows, as was observed (see Fig. 1.3) in the Savannah River estuary during the second half of flood and ebb flows (Krone, 1972). Under such conditions only those aggregates with shear strengths of sufficient magnitude to withstand the highly disruptive shear stresses in the near bed region will actually deposit and adhere to the bed. Thus, deposition is governed by the bed shear stresses, turbulence structure above the bed, type of sediment, depth of flow, suspension concentration and the ionic constitution of the suspending fluid (Mehta and Partheniades, 1973). An important conclusion derived from laboratory erosion and deposition experiments using a wide range of cohesive sediments under steady flow conditions was that under these conditions the two processes do not occur simultaneously as they do in cohesionless sediment transport (Mehta and Partheniades, 1975; 1979).

A flow-deposited bed of cohesive sediment aggregates possesses a vertical bulk density and shear (i.e. yield) strength profile which changes in time primarily due to consolidation. Secondary causes are thixotropy (see Section 2.5.1) and associated physico-chemical changes affecting inter-particle forces. Consolidation, caused by the gravitational force (overburden) of overlying deposited aggregates which crushes and thereby decreases the order of aggregation of underlying sediment, is known to occur in three phases (Migniot, 1968). During the first phase the bed consolidates quickly as the water in the bed moves upward through the interstices of the bed material. This phase has been found to last up to approximately 10 hours for cohesive sediments (Owen, 1977). During the second phase, which can last up to about 500 hours, water is expelled from the bed by percolation. The rate of consolidation during the third phase is even slower and the length of

time it takes for a cohesive sediment bed to reach its final, fully consolidated state depends upon the nature of the sedimentary material comprising the bed and the chemical composition (i.e. ionic concentrations) of the bed pore water (Owen, 1977). The average values of the bed bulk density and shear strength increase and their vertical profiles change during each of these three phases. Consideration of the consolidation process is essential in modeling the erosive behavior of such beds because of the following two factors: 1) the susceptibility to erosion of a consolidating bed decreases with time due to the continual increase in shear strength, and 2) the vertical profile of the shear strength determines the level to which a bed will erode when subjected to excess shear, i.e. an applied bed shear stress in excess of the shear strength of the bed surface.

2.2. Governing Equations

2.2.1. Convection-Diffusion Transport Equation

A right-handed Cartesian coordinate system is used (Fig. 2.6). The positive x-axis is coincident with the longitudinal axis of the estuary and points downstream. The coordinate system origin is located at some datum below the bed level. The positive z-axis is the vertical dimension and points upward. The y-axis defines lateral distances and points from right to left.

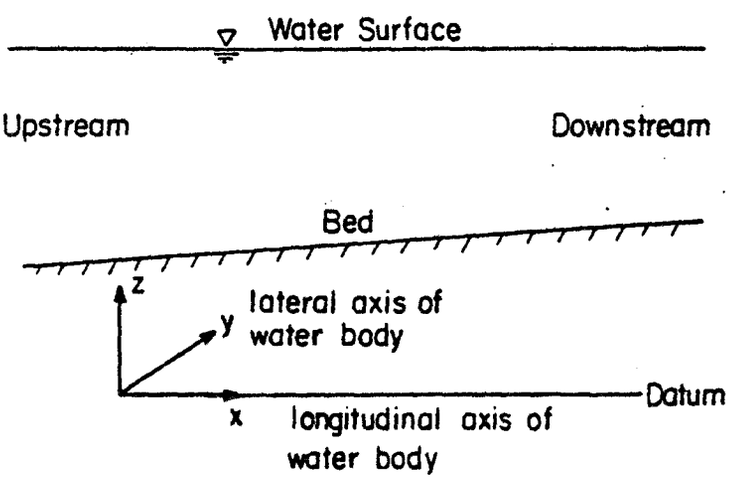

Fig. 2.6 Coordinate System.

The principle of conservation of mass describes the convective and diffusive transport of suspended sediment in a turbulent flow field. In this law the time-rate of change of mass of sediment in a stationary control volume is equated to the spatial rate of change of mass due to convection by an external flow field plus the spatial rate of change of mass due to diffusion. Specifically for a binary sediment-water system the Eulerian law of mass conservation is given as

$$\frac{\partial C}{\partial t} + \nabla\cdot(C\vec{V}) + \nabla\cdot\vec{f} = S \qquad (2.2)$$

where

C = mass concentration of suspended sediment

$\rightarrow$ $\equiv$ vector notation

$\nabla \equiv \text{del} \equiv \hat{i}\frac{\partial}{\partial x} + \hat{j}\frac{\partial}{\partial y} + \hat{k}\frac{\partial}{\partial z}$

$\vec{V}$ = sediment velocity

$\vec{f}$ = diffusive flux

S = source/sink term to account for erosion/deposition of sediment.

The velocity of suspended sediment, $\vec{V}$, is given by

$$\vec{V} = u\hat{i} + v\hat{j} + (w + W_s)\hat{k} \qquad (2.3)$$

where

$\hat{i}$, $\hat{j}$ and $\hat{k}$ = unit vectors in the x-, y- and z-directions, respectively,

u, v and w = local instantaneous water velocity components in the x-, y- and z-directions, respectively,

W_s = terminal settling velocity of the suspended sediment particles or aggregates.

Implicit in Eq. 2.3 is the assumption that the suspended material is convected in the x- and y-directions at the respective water velocity components. This assumption is reasonable for sediment that is not transported as bed load since rolling and saltation of the sediment, which occurs during bed load transport, can cause a significant difference between the water and sediment velocities. Of course, the vertical transport velocity is given by the vector sum of the vertical water velocity and the settling velocity.

The diffusive flux term in Eq. 2.2 is that due to molecular diffusion, which by Fick's law is

$$\vec{f} = - \rho E_M \nabla \left(\frac{C}{\rho}\right) \tag{2.4}$$

where E_M = coefficient of molecular diffusion, and ρ = density of the sediment-water system. For low suspension concentrations the density may be assumed to be spatially and temporally invariant. Substituting Eqs. 2.3 and 2.4, including the constant density assumption, into Eq. 2.2 yields

$$\frac{\partial C}{\partial t} + \nabla \cdot C[u\hat{i} + v\hat{j} + (w + W_s)\hat{k}] - \nabla \cdot E_M \nabla C = S \tag{2.5}$$

Expressing the instantaneous velocities and concentration in Eq. 2.5 in terms of a time-averaged term (e.g. $\bar{u}$) and a fluctuating component (e.g. u'), and time-averaging the entire equation over some period T gives

$$\frac{\partial \bar{C}}{\partial t} + \bar{u}\frac{\partial \bar{C}}{\partial x} + \bar{v}\frac{\partial \bar{C}}{\partial y} + (\bar{w} + W_s)\frac{\partial \bar{C}}{\partial z} + \bar{C}\frac{\partial W_s}{\partial z} + \frac{\partial}{\partial x}(\overline{u'c'}) +$$

$$\frac{\partial}{\partial y}(\overline{v'c'}) + \frac{\partial}{\partial z}(\overline{w'c'}) - \frac{\partial}{\partial x}\left(E_M \frac{\partial \bar{C}}{\partial x}\right) - \frac{\partial}{\partial y}\left(E_M \frac{\partial \bar{C}}{\partial y}\right) - \frac{\partial}{\partial z}\left(E_M \frac{\partial \bar{C}}{\partial z}\right) = S \tag{2.6}$$

in which the continuity equation $\left(\frac{\partial \bar{u}}{\partial x} + \frac{\partial \bar{v}}{\partial y} + \frac{\partial \bar{w}}{\partial z} = 0\right)$ for an incompressible fluid has been applied. The period T must satisfy the following criteria: 1) it must be large enough so that the time averages of u', v', w' and c' over T are approximately zero, and 2) it must be small enough that the variations of $\bar{u}$, $\bar{v}$, $\bar{w}$ and $\bar{c}$ are changed with respect to time (MacArthur, 1979).

The Reynolds analogy is used to relate the turbulent diffusive flux terms such as $\overline{u'c'}$ to the mean concentration gradients, e.g. $\partial\bar{C}/\partial x$, as follows:

$$\overline{u'c'} = -E_x \frac{\partial \bar{C}}{\partial x}$$

$$\overline{v'c'} = -E_y \frac{\partial \bar{C}}{\partial y} \qquad (2.7)$$

$$\overline{w'c'} = -E_z \frac{\partial \bar{C}}{\partial z}$$

where E_x, E_y and E_z are the turbulent diffusion coefficients in the x-, y- and z-directions, respectively. Substituting Eq. 2.7 into Eq. 2.6 gives

$$\frac{\partial C}{\partial t} + u \frac{\partial C}{\partial x} + v \frac{\partial C}{\partial y} + w \frac{\partial C}{\partial z} + C \frac{\partial W_s}{\partial z} + W_s \frac{\partial C}{\partial z} - \frac{\partial}{\partial x}\left(E_x \frac{\partial C}{\partial x}\right) -$$

$$\frac{\partial}{\partial y}\left(E_y \frac{\partial C}{\partial y}\right) - \frac{\partial}{\partial z}\left(E_z \frac{\partial C}{\partial z}\right) - \frac{\partial}{\partial x}\left(E_M \frac{\partial C}{\partial y}\right) - \frac{\partial}{\partial y}\left(E_M \frac{\partial C}{\partial y}\right) - \frac{\partial}{\partial z}\left(E_M \frac{\partial C}{\partial z}\right) = S \qquad (2.8)$$

where the bars over the mean components have been dropped for convenience.

In turbulent flows, molecular diffusion processes are generally insignificant compared to the processes of turbulent diffusion, so that

$$E_x, E_y, E_z \gg E_M$$

and (2.9)

$$E + E_M \approx E(x,y,z)$$

where E is the turbulent diffusion tensor with the off-diagonal terms equal to zero (Aris, 1962). As indicated above, E is a function of position. Combining Eqs. 2.8 and 2.9 yields

$$\frac{\partial C}{\partial t} + u \frac{\partial C}{\partial x} + v \frac{\partial C}{\partial y} + w \frac{\partial C}{\partial z} + \frac{\partial}{\partial z}(W_s C) - \frac{\partial}{\partial x}\left(E_x \frac{\partial C}{\partial x}\right) -$$

$$\frac{\partial}{\partial y}\left(E_y \frac{\partial C}{\partial y}\right) - \frac{\partial}{\partial z}\left(E_z \frac{\partial C}{\partial z}\right) = S \qquad (2.10)$$

This is the three-dimensional form of the convection-diffusion equation for suspended sediment transport in an incompressible, fully developed turbulent flow field. The desired two-dimensional form of Eq. 2.10 is obtained by integrating this equation over the depth of flow. Performing this integration and assuming that: 1) W_s is constant

over the depth (i.e. $\partial W_s/\partial z = 0$), 2) the fluid mass density is constant and 3) the concentration flux $\overline{u''c''}$ (where u" and c" are the deviations of u and C over the depth of flow about their respective depth-averaged values, $\bar{u}$ and $\bar{c}$) is equal to $-K_x \partial\bar{C}/\partial x$ by the Reynolds analogy, gives the following form of the depth-averaged convection-diffusion equation for sediment transport:

$$\frac{\partial C}{\partial t} + u\frac{\partial C}{\partial x} + v\frac{\partial C}{\partial y} = \frac{\partial}{\partial x}(D_x\frac{\partial C}{\partial x}) + \frac{\partial}{\partial y}(D_y\frac{\partial C}{\partial y}) + S \qquad (2.11)$$

where $D = E + K$ is the effective turbulent diffusion tensor with K a dispersion tensor introduced through use of the Reynolds analogy in the third assumption above. The tensor D, with components D_x and D_y, accounts for both turbulent diffusion and dispersion due to spatial velocity gradients. The source/sink term in this equation can be expressed as

$$S = \left.\frac{dC}{dt}\right|_e + \left.\frac{dC}{dt}\right|_d \qquad (2.12)$$

where $\left.\frac{dC}{dt}\right|_e$ is the rate of sediment addition (i.e. source) due to erosion from the bed, and $\left.\frac{dC}{dt}\right|_d$ is the rate of sediment removal (i.e. sink) due to deposition of sediment. Expressions for $\left.\frac{dC}{dt}\right|_e$ and $\left.\frac{dC}{dt}\right|_d$ are given respectively in Sections 2.6 and 2.7.

2.2.2. Initial and Boundary Conditions

In order to solve Eq. 2.11 for the depth-averaged suspended sediment concentrations at specified points in the flow field the following boundary and initial conditions are required:

1. Free surface boundary condition: There can be no net rate of transport across the free surface. This condition may be expressed mathematically as

$$\{uC - D_x\frac{\partial C}{\partial x}\}n_x + \{vC - D_y\frac{\partial C}{\partial y}\}n_y = 0 \qquad (2.13)$$

where n_x and n_y are the x and y components, respectively, of the unit normal vector to the free surface.

2. Bottom boundary condition: Eroded sediment material is transported in the vertical direction away from the bed by turbulent diffusion. Deposited sediment becomes part of the bed. This condition is expressed by Eq. 2.12.
3. Boundary condition at solid boundaries: At all solid boundaries of the water body being modeled the normal transport flux is equal to zero, i.e.

$$D_x \frac{\partial C}{\partial x} n_x + D_y \frac{\partial C}{\partial y} n_y = 0 \qquad (2.14)$$

where, in this case, n_x and n_y are the x and y components, respectively, of the unit normal vector to the solid boundary.

4. Boundary condition at water boundaries: At each external water boundary (EWB) either the depth-averaged suspended sediment concentration must be a known function of time, F(t), for the time period being modeled, i.e.

$$C(t)\Big|_{EWB} = F(t) \qquad (2.15)$$

or the zero normal flux condition (Eq. 2.14) must be used as the boundary condition.

5. Initial condition: The initial (i.e. at the start of the model simulation) value of the suspension concentration at each node must be known.

In addition, the flow depth and the two horizontal velocity components must be specified at each node for the time period of model simulation.

2.2.3. Solution of Governing Equation

The finite element method has been used to solve the governing equation (Eq. 2.11). This method is a numerical analysis technique for obtaining approximate solutions of differential equations. The discretization procedures used reduce the equation to be solved to one with a finite number of dependent variables by dividing the solution domain into a number of elements and by expressing the dependent variable in terms of approximating interpolation (i.e. shape) functions within each element. The values of the dependent variable at node

points are used to define the interpolation functions. Node points are usually located on the boundaries of elements and are used to define the connection between adjacent elements. The number and location of the node points must be chosen such that continuity of the dependent variable across common boundaries of adjacent elements is achieved (Zienkiewicz, 1971). The behavior of the dependent variable within each element is defined by the values of the dependent variable at the nodes and the interpolating function. A detailed description of the method is presented by Zienkiewicz (1971).

This method is preferred over the finite difference method because derivative boundary conditions do not require special treatment in the finite element method as they do in the former. In addition, the finite element method is generally more numerically stable than the finite difference method. It is a particularly advantageous method to use in estuarial transport problems because of the ability to use arbitrarily shaped elements.

Isoparametric quadrilateral and/or triangular elements may be used in which a quadratic functional approximation is used to describe both the intra-element spatial variation of the geometry and suspended sediment concentration. Therefore, the elements may have curved sides.

The Galerkin weighted residual method is used to solve Eq. 2.11 for the nodal sediment concentrations. As described earlier, the dependent variable, C, is approximated as the following function of the unknown nodal point values, C_i:

$$\hat{C}_j = \sum_{i=1}^{i=n} N_i C_i \tag{2.16}$$

where $\hat{C}_j$ = approximate sediment concentration at any location inside the jth element, N_i = quadratic shape function at the ith node, and n = number of nodes forming the jth element. The value of n is equal to 8 and 6, respectively, for isoparametric quadrilateral and triangular elements. Substituting the approximate concentration $\hat{C}$ into Eq. 2.11 gives

$$\frac{\partial \hat{C}}{\partial t} + u \frac{\partial \hat{C}}{\partial x} + v \frac{\partial \hat{C}}{\partial y} - \frac{\partial}{\partial x}\left(D_x \frac{\partial \hat{C}}{\partial x}\right) - \frac{\partial}{\partial y}\left(D_y \frac{\partial \hat{C}}{\partial y}\right) - S = r(x,y) \tag{2.17}$$

where r(x,y) = residual resulting from the use of $\hat{C}$.

In order for $\hat{C}$ to satisfy all the stipulated boundary conditions, the sum of the normal concentration fluxes from adjacent elements and any source or sink must be equal to zero on all internal and external boundaries in the solution domain. This condition may be expressed mathematically as (Ariathurai and Krone, 1976):

$$q_i^+ + q_i^- + q_i^s = 0 \qquad i = 1,\ldots,NL \tag{2.18}$$

where

q_i^+ = outward normal flux from one element

q_i^- = inward normal flux from adjacent element

q_i^s = normal flux from source/sink on the ith boundary

NL = number of element interfaces and external boundaries

Application of the Galerkin weighted residual method to Eq. 2.17 and the residual which results from the use of $\hat{C}$ in Eq. 2.18 requires that the summation of the weighted residuals over the solution domain vanish when the weighting factors are the nodal interpolation functions. This procedure results in a set of simultaneous equations. The necessary boundary conditions are included and the equation set is solved for the nodal values of the suspended sediment concentrations. The transient problem is solved using the Crank-Nicholson scheme. Details of the solution technique for solving Eq. 2.11 are given by Ariathurai (1974) and Ariathurai et al. (1977).

2.3. Description of Selected Transport Model

The fine sediment transport model selected for use and modification, i.e. incorporation of the results from this study is SEDIMENT III developed by Ariathurai et al. (1977). This model was selected because at the beginning of this study it was a "state-of-the-art" mathematical model of estuarial fine sediment transport. SEDIMENT III is a time varying two-dimensional finite element model that is capable of predicting the horizontal and temporal variations in the depth-averaged suspended concentrations of cohesive sediments and bed surface elevations in an estuary, coastal waterway or river. In addition, it can be used to predict the steady-state or unsteady transport of any conservative substance (e.g. salt) or non-conservative

constituent if the reaction rates are known. The model describes the convective and diffusive transport of suspended or dissolved constituents, the settling, deposition (i.e. sink) and erosion (i.e. source) of cohesive sediments to and from the bed respectively, and consolidation of the bed due to continuing deposition.

The model uses experimentally developed empirical expressions for: 1) rates of surface and mass erosion, 2) rate of deposition and 3) settling velocities of coagulated particles as a function of the suspended sediment concentration, thus accounting for the time-varying coagulation and aggregation of fine sediment particles. The effective turbulent diffusion coefficients in the two horizontal dimensions are required input in order to predict the diffusive transport of the constituent being modeled. The sediment bed is considered to be composed of a specified number of layers, each of which is characterized by an experimentally determined thickness, average bulk density, average shear strength, and average erodibility rate constant. The consolidation of the bed due to crushing of underlying sediment by new sediment deposits, i.e. increased overburden pressures, is accounted for by increasing the average bulk density and shear stength of each bed layer.

At each time-step the average bed shear stress induced by the turbulent flow velocity of the suspending fluid is calculated for each grid element. Then the amount of fine sediment either deposited onto or resuspended from the bed in each element during the previous time-step is determined. The concentrations of suspended fine sediment at the next time-step are then computed for every node point. The new bed elevation at each element is determined by adding or subtracting the thickness of sediment deposited to or resuspended from, respectively, the bed profile that existed during the previous time-step. Lastly, consolidation of the previous bed profile is simulated using the method described above.

2.4. Model Modifications

Newly developed bed schematization model as well as mass erosion, surface erosion and deposition algorithms and the effect of salinity on the rates of surface erosion and deposition, described in Sections 2.5,

2.6, 2.7 and 2.8, respectively, were coded in FORTRAN and integrated into SEDIMENT III. The modified version of the model is referred to as SEDIMENT IIIA. Each of these algorithms was thoroughly tested to insure that no errors occur in the operation of the program.

In addition to these algorithms, the following additions and/or modifications were made to SEDIMENT III:

1) The mean water temperature is read in and the kinematic viscosity, ν (in m^2/s) is calculated using the following equation:

$$\nu = 1.701721 \times 10^{-6} \cdot \exp(-0.025109 \cdot T_w) \qquad (2.19)$$

where T_w is the water temperature in degrees Celcius. This equation was determined, with data obtained from Bolz and Tuve (1976), using least squares linear regression analysis, with the coefficient of determination $r^2 = 0.9935$. This coefficient indicates how closely Eq. 2.19 fits the actual data. The value of r^2 can vary between 0 and 1, and the closer r^2 is to 1, the better the fit. As indicated by the given r^2 value, a good agreement was obtained.

2) The salinity field is read in to the model as nodal values (i.e. the value of the suspending fluid salinity at each node is read in at every designated time-step). The nodal salinity values are used in evaluating the settling velocity and the deposition rate at every node. Elemental average salinity values are calculated and then used to adjust the bed shear strength of the top new deposit layer (if such exists) and in calculating the total dry mass of sediment deposited per element for the time-steps and elements at which deposition occurs.

3) The density of the suspending fluid (in kg/m^3) is calculated at each node as a function of the mean water temperature and nodal salinity value using the following equation (Wilson and Bradley, 1968):

$$\rho_w = 1000.0 \cdot (0.702 + 100.0 \cdot (17.5273 + 0.1101 \cdot T_w - 0.000639 \cdot T_w^2$$

$$-0.039986 \cdot S - 0.000107 \cdot T \cdot S)(5881.913 + 37.592 \cdot T_w$$

$$-0.34395 \cdot T_w^2 + 2.2524 \cdot S)^{-1}) \qquad (2.20)$$

Incorporating, in addition, the effect of the suspended sediment on the local fluid density gives (MacArthur, 1979)

$$\rho_{eff,w} = \rho_w + \frac{C}{\rho_s} (\rho_s - \rho_w) \qquad (2.21)$$

where $\rho_{eff,w}$ = effective local fluid density = f(T,S,C), and ρ_w is given by Eq. 2.20. At each time-step where nodal salinity values change, new nodal values of ρ_w and $\rho_{eff,w}$ are calculated. At each time-step where nodal concentrations change, new nodal values of $\rho_{eff,w}$ are determined. The values of $\rho_{eff,w}$ are used to calculate the nodal values of the bed shear stress τ_b, while the values of ρ_w are used in determining the nodal values of the dry bed density, ρ_d, which are used in the erosion and deposition algorithms.

In the following section, the fine sediment bed schematization developed during the course of this study is described. This description is preceded by a general discussion on the nature (i.e. structure) of these beds as revealed in several laboratory investigations.

2.5. Fine Sediment Bed

2.5.1. Introductory Note

As noted in Section 1.1, surficial layers of estuarial beds, typically composed of flow-deposited fine, cohesive sediments, occur in three different states: stationary suspensions, partially consolidated (or consolidating) beds and settled (or fully consolidated) beds. Stationary suspensions, also referred to as new deposits, are defined by Parker and Lee (1979) as assemblages of high concentrations of sediment particles that are supported jointly by the water and the developing skeletal soil framework. These suspensions, which result from the settling of suspended aggregates during periods of deposition (e.g. the period immediately preceding as well as during slack water) and adhesion to the existing bed surface, tend to have a high water content (therefore low bulk density) and a very low, but measureable, shear strength, τ_c, that must be at least as high as the bed shear, τ_b, which existed during the deposition period (Mehta et al., 1982a). Thus, they exhibit a definite non-Newtonian rheology. Krone (1963) found that, in

addition to the bed shear, the structure (or framework) of these suspensions depends on the aggregate order in the following manner: if the aggregates settle onto the bed without being broken up by the bed shear, the surficial layers of these new deposits will be composed of an aggregate network whose order is one higher than that of the individual settling aggregates; therefore, these layers will have lower bulk densities and shear strengths than those of the aggregates which form them.

Whether or not entrainment of these deposits, also referred to as redispersion (Parker and Kirby, 1977) and mass erosion (Paaswell, 1973), occurs during periods of erosion (e.g. typically the period following slack water) depends upon the mechanical shear strength (i.e. stability) of this aggregate network. That portion which remains on the bed undergoes: 1) consolidation, due to overburden pressure resulting from the weight of the overlying sediment which crushes the aggregate network below, and 2) thixotropic effects, defined as the slow rearrangement of deposited aggregates attributed to internal energy and unbalanced internal stresses (Mitchell, 1961), both of which reduce the order of aggregation of the sub-surface bed layers. This implies that the bed becomes stratified with respect to bulk density and shear strength, with both properties typically increasing monotonically with depth, at least under laboratory conditions (Mehta et al., 1982a). Differential settling caused by sorting processes is another cause of stratified bed formation.

Continued consolidation results in the formation of settled mud, defined by Parker and Lee (1979) as "assemblages of particles predominantly supported by the effective contact stresses between particles as well as any excess pore water pressure." This portion of the bed has a lower water content, a lower order of aggregation, and a higher shear strength and therefore is better able to resist high bed shear stresses.

In this study the primary characteristic used to distinguish between a stationary suspension and a partially consolidated or settled bed is the mode of failure that occurs when the bed surface is subjected to an excess shear stress (i.e. $\tau_b > \tau_c$). As stated previously, stationary suspensions undergo redispersion while partially consolidated

and/or settled beds undergo resuspension (Parker and Kirby, 1977) or surface erosion (Paaswell, 1973). Both erosion processes are discussed in Section 2.6.1.

The nature of the bulk density and shear strength profiles typically found in flow-deposited cohesive sediment beds has been revealed in laboratory tests, among others, by Richards et al. (1974), Owen (1975), Thorn and Parsons (1980), Parchure (1980), Bain (1981) and Dixit (1982). A review of this subject has been made by Parchure (1980) and Dixit (1982); only a synopsis is given here.

Figure 2.7 shows the dimensionless relationship found using reanalyzed data of Owen (1975) and Thorn and Parsons (1980) for consolidation periods, t_{dc}, greater than 48 hours between the bed bulk density, ρ_B, and the depth below the bed surface, z, for four natural muds. This relationship between ρ_B and z can be expressed as

$$\frac{\rho_B(z)}{\bar{\rho}_B} = \zeta \left[\frac{z'}{H}\right]^{-\xi} \qquad (2.22)$$

where $\bar{\rho}_B$ = depth-averaged bulk density, H = bed thickness, $z' = H - z$, $\zeta = 0.660$ and $\xi = 0.347$. This equation is in agreement with results obtained by Dixit (1982) for $t_{dc} > 48$ hours (Fig. 2.8a) which gave $\zeta = 0.794$ and $\xi = 0.288$. However, the data for $t_{dc} < 48$ hours (Fig. 2.8b) did not follow the relationship given by Eq. 2.22.

Parchure (1980) made the following observation with regard to shear strength profiles, $\tau_c(z)$, in flow-deposited cohesive sediment beds: $\tau_c(z)$ increases rapidly with distance below the water-sediment interface for $z < z_{ch}$, at which $\tau_c = \tau_{ch}$, where τ_{ch} is a characteristic value of τ_c. For $z > z_{ch}$, $\tau_c(z)$ continues to increase but at a greatly decreased rate (Fig. 2.9). The influence of such a $\tau_c(z)$ profile on the erosion rate is discussed in the following section. Figure 2.10 shows a $\tau_c(z)$ profile found by Dixit (1982). From the tests conducted by Dixit, the following two observations may be made: 1) such a $\tau_c(z)$ profile was not found in five out of nine experiments, and 2) the sediment beds used by Dixit were up to six times thicker than those used by Parchure. Therefore, the $\tau_c(z)$ profiles measured by Dixit are naturally more representative of estuarine beds, and as such it is believed that until further studies are conducted, no definitive statement regarding the precise nature of $\tau_c(z)$ profiles in cohesive sediment beds can be made.

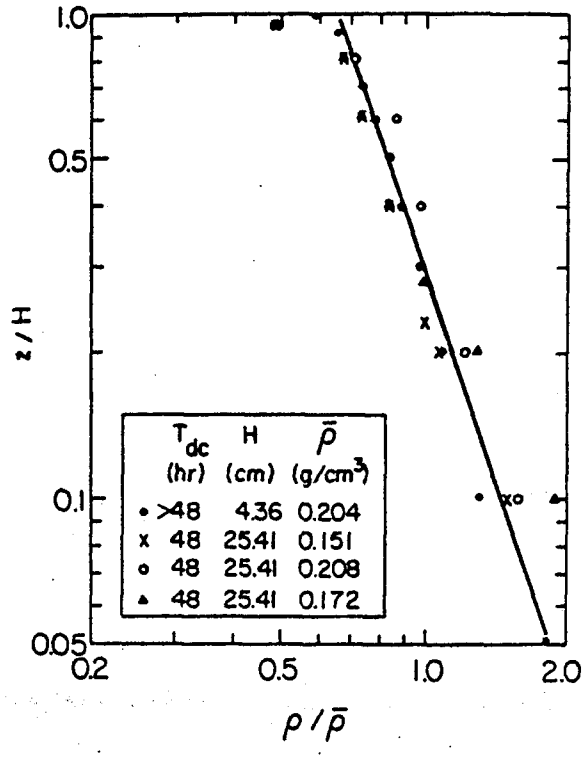

Fig. 2.7 z/H vs. $\rho/\bar{\rho}$ for Avonmouth, Brisbane and Grangemouth Muds (after Dixit, 1982).

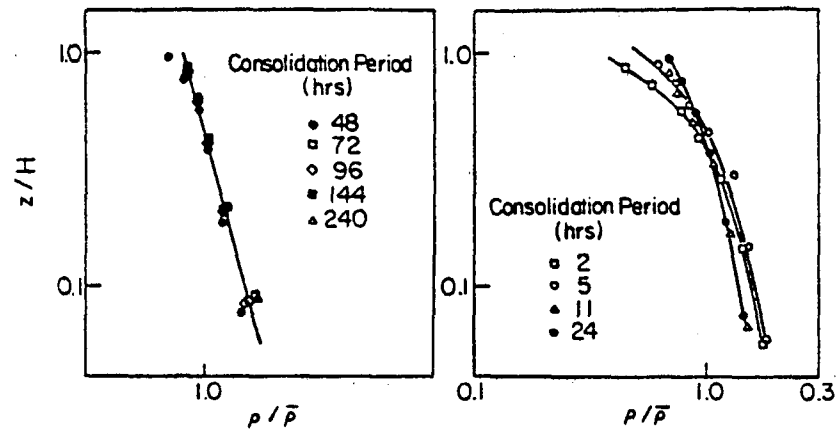

Fig. 2.8 z/H vs. $\rho/\bar{\rho}$ for Consolidation Periods (a) Less than 48 Hours and (b) Greater than 48 Hours (after Dixit, 1982).

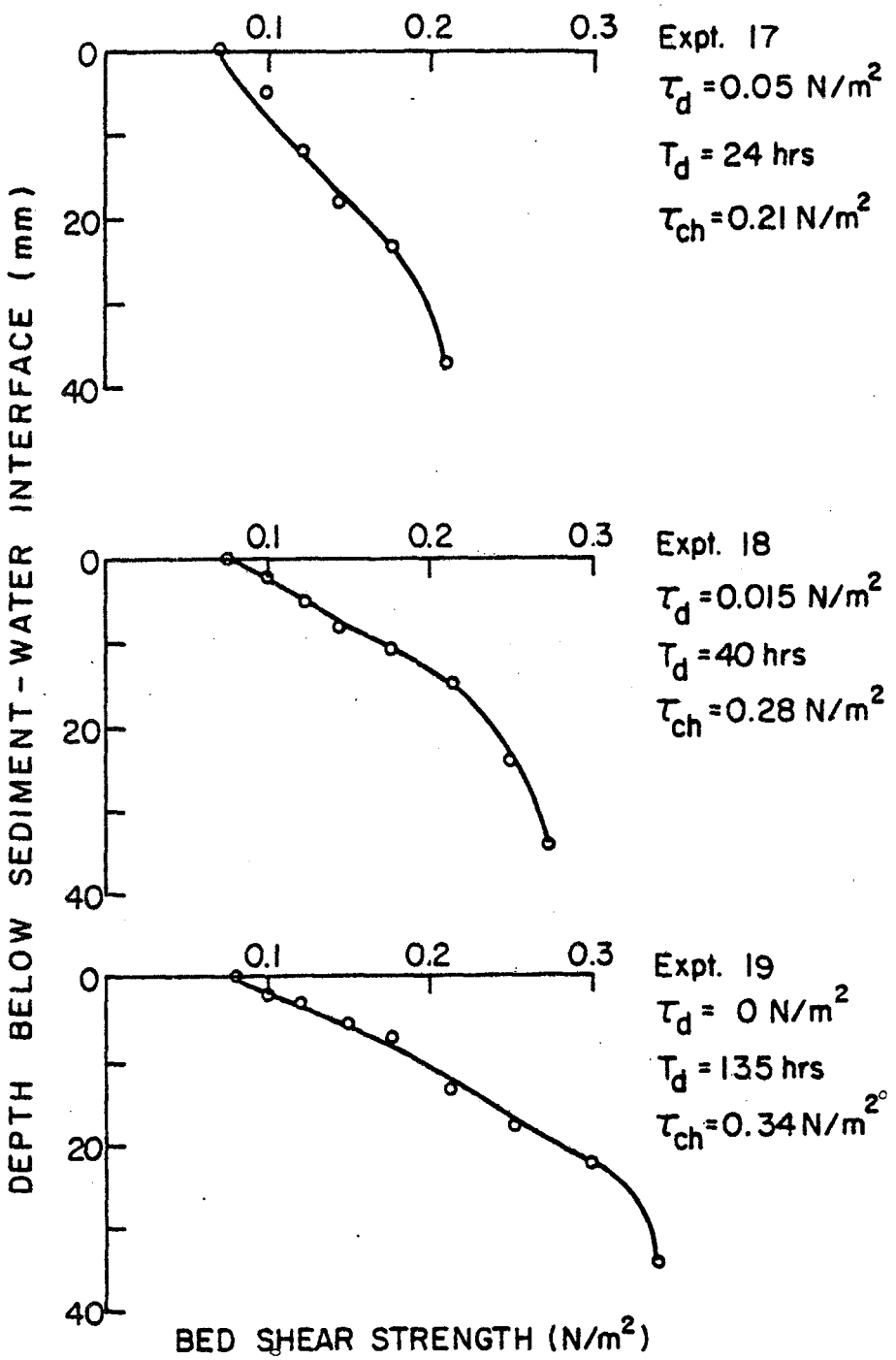

Fig. 2.9 Bed Shear Strength Observed as a Function of Depth (after Parchure, 1980).

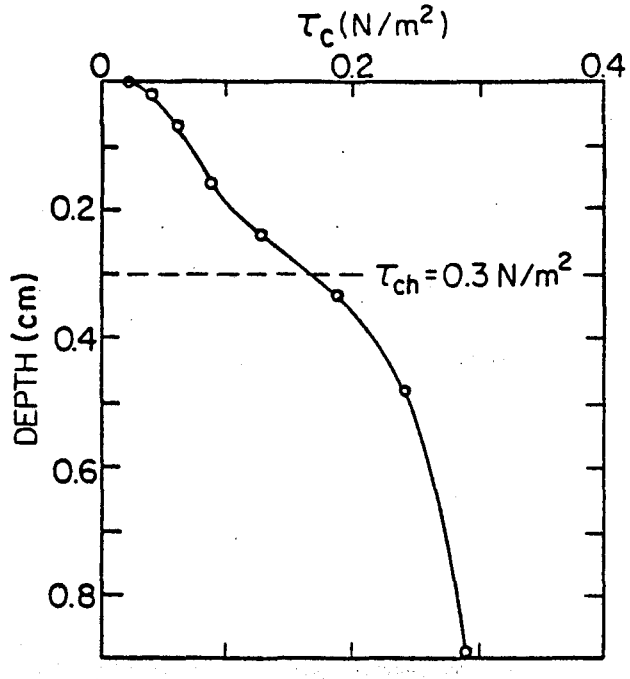

Fig. 2.10 Variation of Critical Bed Shear Strength, τ_c, with Depth (after Dixit, 1982).

Thorn and Parsons (1980) found the following relationship between τ_c and ρ_s, the dry sediment density at the bed surface, for three different natural muds:

$$\tau_c = \alpha_1 \rho_s^{\beta_1} \tag{2.23}$$

where $\alpha_1 = 5.42 \times 10^{-6}$ and $\beta_1 = 2.28$, provided the units of τ_c are N/m^2 and the units of ρ_s are kg/m^3. In an earlier study, however, these researchers observed no strong correlation between τ_c and ρ_s for Grangemouth mud (Thorn and Parsons, 1977). Dixit (1982) concurred with their earlier findings as he observed no relationship between these two soil properties for at least the upper bed layers. However, for the lower bed layers, where τ_c does not increase as rapidly, there may be a higher degree of correlation, as suggested by the following. Bain (1981) found a relationship between the bed voids ratio (which is

related to the bed density) and τ_c at relatively high shear stress (τ_b > 0.5 N/m^2) for Mersey and Grangemouth muds. The high shear stresses used by Bain suggests that this relationship was for lower, more consolidated bed layers, where such high τ_c values exist.

In addition to being formed by deposition from flowing water, sediment beds may be formed artificially, i.e. placed beds. Such beds include those that are remolded and/or compacted after placement in a test apparatus (Mehta and Partheniades, 1979). A basic difference between these two types of beds is their stress history (i.e. the conditions under which they are formed and the time allowed for consolidation). The stress history of a bed largely dictates the degree and the rate of failure that will occur when subjected to an excess shear stress. In these beds, the shear strength and bulk density profiles show much less significant stratification over the depth of the bed than in flow-deposited beds (Mehta et al., 1982a).

2.5.2. Bed Schematization

To facilitate the modeling of changes in the bed surface elevation due to erosion and deposition processes, the bed is treated in the following manner: 1) it is discretized into a number of layers, or strata, and 2) the bed properties, e.g. thickness, are assumed to be spatially (in the x-y plane) invariant within each element, but not so from element to element, in order to account for inter-element spatial variances in shoaling and/or scouring patterns. These two factors are expounded upon below.

The bed in each element is considered to be composed of the following two sections: 1) the original, settled (consolidated) bed that is present at the start of the modeling, and 2) new deposits located on top of the original bed, that result from deposition during the modeling. Each of these two sections is divided into a number of layers in order to specify the actual shear strength and bulk density profiles in the model. The new deposit bed section is subdivided into two sub-sections, the top referred to as unconsolidated new deposit (UND) layers and the bottom as partially consolidated new deposit (CND) layers (Fig. 2.11). The former sub-section, i.e. the one corresponding to a stationary suspension, is considered to undergo mass erosion while the

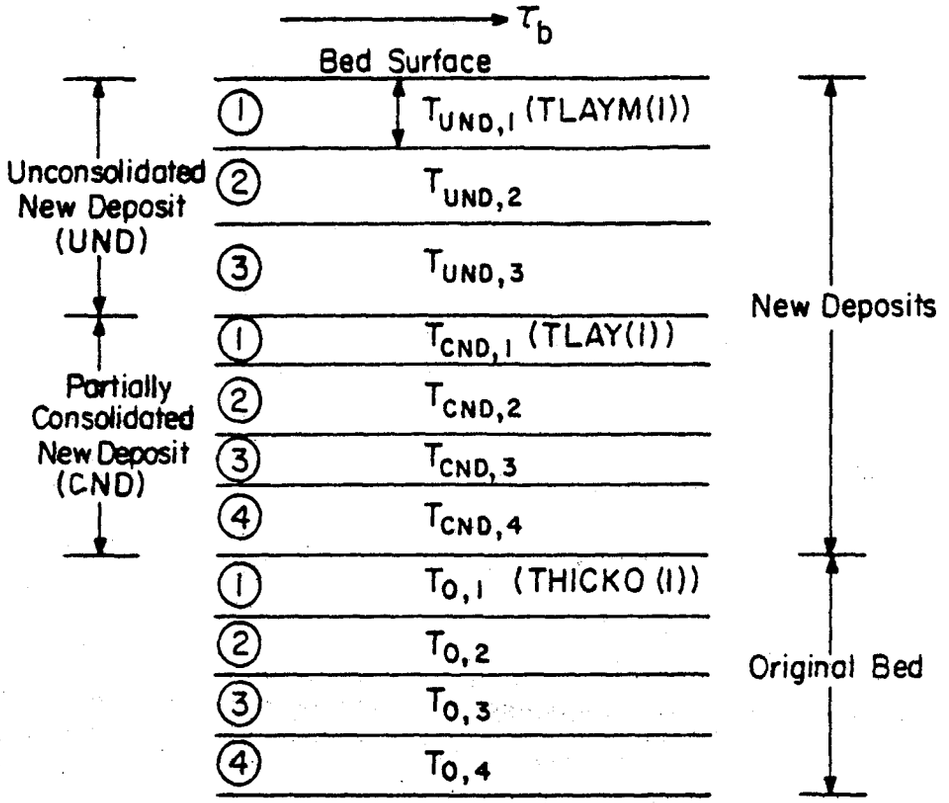

Fig. 2.11 Bed Schematization used in SEDIMENT IIIA.

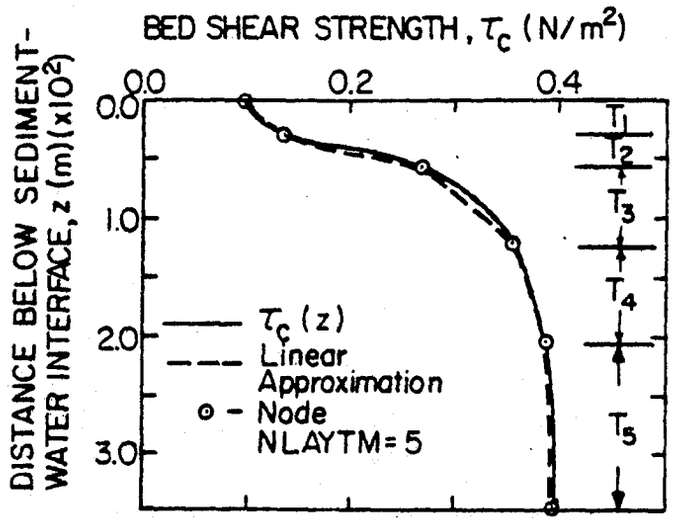

Fig. 2.12 Hypothetical Shear Strength Profile Illustrating Determination of Bed Layers Thicknesses.

latter, i.e. the partially consolidated bed, undergoes surface erosion when subjected to an excess shear stress. The original bed as well undergoes surface erosion. The number of layers indicated in Fig. 2.11 for each of the three bed sections are not fixed, as each section can be assigned any given number of layers. The following bed-related model input parameters are required:

1) The bed shear strength profile in the UND. This can be ascertained from laboratory erosion tests using samples of the sediment from the water body being modeled (see Appendix B, Section B.3).
2) The number of UND layers (NLAYTM) and the thickness of each layer (TLAYM(I), I=1,NLAYTM) . These parameters must be determined using the shear strength profile. For example, Fig. 2.12 shows a hypothetical $\tau_c(z)$ profile and illustrates that this bed section must be divided such that the variation of τ_c within each layer is approximately linear. The τ_c values at the NLAYTM+1 nodes need to be read into the model.
3) The bulk density values at the NLAYTM+1 nodes as well need to be determined. The $\rho_B(z)$ profile may be determined using a laboratory freeze-drying method (appropriately modified for field samples, where necessary) described by Parchure (1980), the pumping method described by Thorn and Parsons (1977) or through use of a gamma-ray nuclear transmission densitometer (Whitmarsh, 1971).
4) The same parameters for the CND layers and the original, settled bed layers must be read, with the original bed parameters read in for each element (where an original bed exists). The parameters read in for the UND and CND layers are assumed to be constants for all elements.
5) A stationary suspension present on top of the original bed at the start of the modeling is simulated in the model by reading in the dry mass per unit bed area of stationary suspension samples obtained from every element (where such exists).

Included in Appendix B is a brief description of how these various bed properties can be determined through the use of a field data collection program and a laboratory testing program. Other parameters characterizing the rate of surface erosion that each layer undergoes when subjected to an excess shear must be evaluated as well; these are discussed in Section 2.7.2.

The following procedure was developed for forming the new deposit bed layer(s) which result from stationary suspensions initially present on top of the original bed and/or formed during the modeling.

The dry sediment mass per unit bed area per element, M_D, read in initially if a stationary suspension exists in any given element, or formed during modeling (as determined by the deposition algorithm) is used in conjunction with the UND and CND properties to solve iteratively for the thickness of bed formed by M_D for each element where $M_D > 0$. This thickness, ΔT, depends on the bulk density profile, $\rho_B(z)$, for the UND and CND layers. The bulk density profile is converted to the dry sediment density profile, $\rho_D(z)$, using the following formula:

$$\rho_D(z) = \frac{\rho_B(z) - \rho_w}{\rho_s - \rho_w} \cdot \rho_s \qquad (2.24)$$

As in the case of the ρ_B profile, the ρ_D profile is discretized, and the variation between the nodal values (i.e. within each layer) is assumed to be linear. The thickness ΔT is determined using the following relationship:

$$\Delta T = \frac{\int_0^{\phi} \rho_D(z) \cdot z dz}{M_D} \qquad (2.25)$$

where $\phi = \Delta T \pm 0.02\Delta T$. If ΔT is greater than TLAYM(1) (see Fig. 2.11) then more than one layer of UND is added. The assumed linear variation of ρ_D within each layer is used in the above equation. When or if the UND layers are filled, the same procedure is used to fill up the CND layers below the UND layers. The bottom CND layer can never fill up; therefore, continuing deposition is accounted for by increasing the thickness of this layer, while the thicknesses of the overlying UND and CND layers remain the same. As a result, the thickness of the bottom CND layer, i.e. TLAY(NLAYT) is not specified in the input data. This particular filling sequence was used in order to account for the consolidation of the sediment bed due to overburden pressure by virtue of the increasing τ_c and ρ_B values with bed depth.

In the next section, a discussion on the erosive behavior of fine sediment beds is given, followed by a description of the erosion algorithm.

2.6. Erosion of Fine Sediment Beds

2.6.1. Introductory Note

Of interest in this study are the erosion (resuspension) characteristics of saturated, flow-deposited fine sediment beds. A number of laboratory investigations were carried out in the sixties and early seventies in order to determine the rate of resuspension, ε, defined as the mass of sediment eroded per unit surface area unit time, as a function of the bed shear stress in steady, turbulent flows. An important conclusion from these tests was that the usual soil indices such as liquid or plastic limit do not adequately describe the erosive behavior of these soils (Mehta, 1981). For example, Partheniades (1962) concluded that the bed shear strength as measured by standard tests, e.g. the direct-shear test (Terzaghi and Peck, 1960), has no direct relationship with the soil's resistance to erosion, which is essentially governed by the strength of the inter-particle and inter-aggregate bonds between the deposited sediment material. Shown in Table 2.2 are the various physico-chemical factors known to govern the erosive properties of these beds. These factors must be specified to properly characterize the erosive behavior. The hydrodynamic factors define the erosive forces while the bed and fluid physico-chemical properties determine the resistivity of the bed to erosion.

The erosive forces, characterized by the flow-induced instantaneous bed shear stress, are determined by the flow characteristics and the surface roughness of the fluid-bed interface. The sediment composition, pore and eroding fluid compositions and the structure of the flow-deposited bed at the onset of erosion must be determined in order to properly define the erosion resistance of the bed. Sediment composition is specified by the grain size distribution of the bed material (i.e. weight fraction of clays, silts), the type of clay minerals present, and the amount and type of organic matter. The CEC can be used to characterize the clay mineral type. Arulanandan et al. (1973) and Alizadeh (1974) have attempted to characterize clay composition using the apparent dielectric constant measured at selected frequencies. Each clay tested appeared to have a characteristic value of a "dielectric dispersion" parameter determined from these measurements. The

Table 2.2

Principal Factors Controlling Erosion of
Saturated Cohesive Sediment Beds

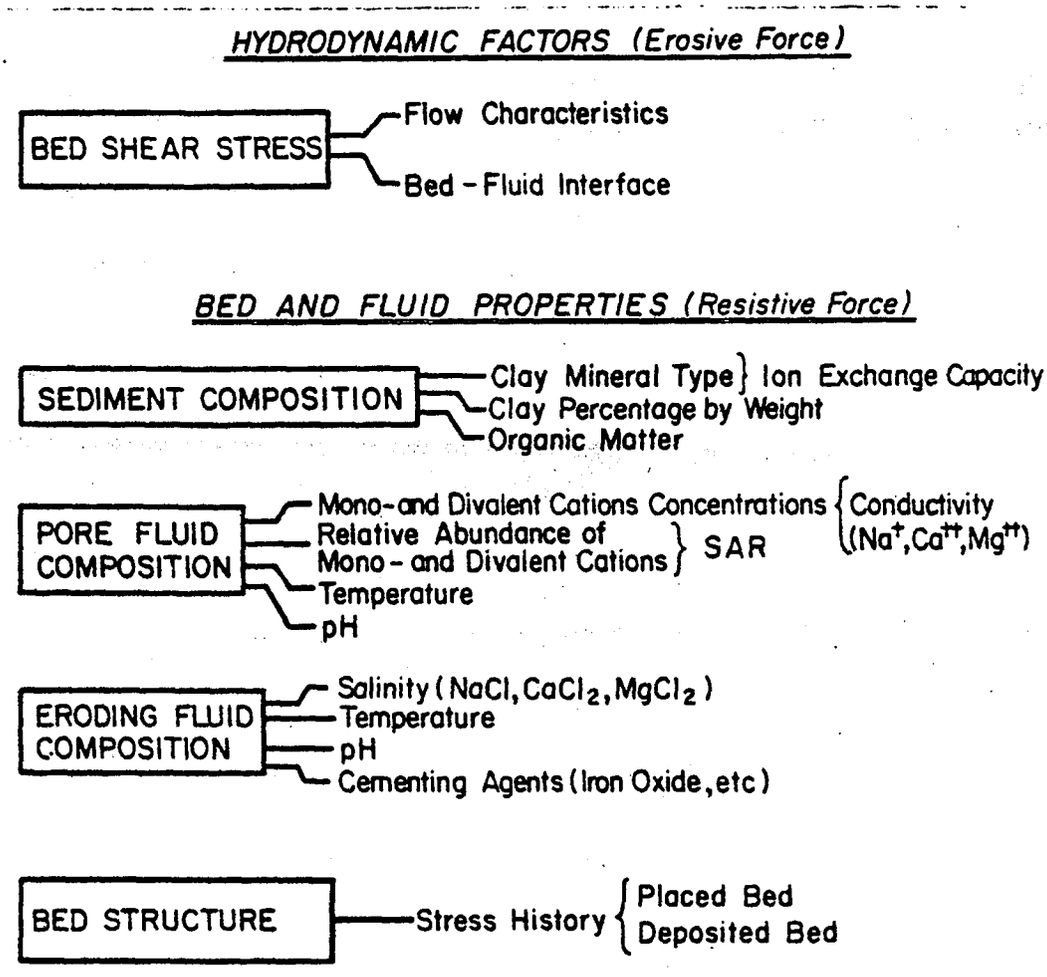

dielectric dispersion has been defined as the amount of decrease in the apparent dielectric constant with frequency (Alizadeh, 1974).

The composition of the pore and eroding fluid are specified by the temperature, pH, total amount of salts and the type and abundance of ions present, principally Cl^-, Na^+, Ca^{+2} and Mg^{+2}. Cementing agents such as iron oxide can significantly increase the resistance of a sediment bed to erosion. Measurement of the electrical conductivity is used to determine the total salt concentration, whereas the concentration of Na^+ relative to that of $Ca^{+2} + Mg^{+2}$ is characterized by the sodium adsorption ratio (SAR), defined as:

$$SAR = \frac{Na^+}{\left[\frac{1}{2}\left(Ca^{+2} + Mg^{+2}\right)\right]^{1/2}} \tag{2.26}$$

where the cation concentrations are in milliequivalents per liter (Arulanandan, 1975). The effect of SAR on the rate of erosion is discussed in Section 2.8.3. The physico-chemical aspects pertaining to the aforementioned factors have been summarized by Sargunam et al. (1973), Kandiah (1974), Arulanandan et al. (1975) and Ariathurai and Arulanandan (1978). The effect of the bed structure, specifically the vertical bulk density and shear strength profiles, on the rate of erosion is discussed by Lambermont and Lebon (1978) and Mehta et al. (1982a).

Several different types of relationships between the rate of erosion, ε, and the time-mean value of the flow-induced bed shear stress, τ_b, have been reported for non-stratified beds. These include statistical-mechanical models (Partheniades, 1965; Christensen, 1965), a rate process model (Paaswell, 1973; Kelly and Gularte, 1981) and empirical relationships (Ariathurai and Arulanandan, 1978). These relationships typically have the following general form (Mehta, 1981):

$$\varepsilon = \varepsilon(\tau_b, \eta_1, \eta_2, \ldots \eta_i) \tag{2.27}$$

where $\eta_1, \eta_2, \ldots, \eta_i$ are parameters that specify the bed resistivity.

The surface erosion rate, ε, is related to the time-rate of change of the suspension concentration, dC/dt, and to the time-rate of change of the depth of erosion, z, with respect to the original bed surface elevation, by the following expressions:

$$\varepsilon = d\frac{dC}{dt} \tag{2.28}$$

$$\frac{dC}{dt} = \frac{1}{d}\cdot\rho_D(z)\cdot\frac{dz}{dt} \tag{2.29}$$

where d = flow depth and $\rho_D(z)$ = dry bed density profile.

Figure 2.13 shows the general nature of laboratory determined relationships, found by, among others, Partheniades (1962) and Christensen and Das (1973) for placed beds. Shown in Figs. 2.14 and 2.15 are examples of this relationship, which may be expressed as

$$\varepsilon = M(\tau_b - \tau_{ch}) + \varepsilon_{ch} \tag{2.30}$$

where M = slope, and the subscript ch refers to a "characteristic" value (Mehta, 1981; Hunt, 1981). For $\tau_b < \tau_{ch}$, $M = M_1$ and for $\tau > \tau_{ch}$, $M = M_2$. Thus, Eq. 2.30 has the general form $\varepsilon = \varepsilon(\tau_b, \tau_{ch}, \varepsilon_{ch}, M_1, M_2)$ as in Eq. 2.27. The parameter τ_{cr}, determined by extrapolation of the M_2 line to the $\varepsilon = 0$ axis, has been interpreted to be the critical shear stress for erosion (Partheniades, 1962; Gularte, 1978). Values of ε_{ch}, τ_{ch}, M_1 and M_2 are largely determined by the physico-chemical factors given in Table 2.2.

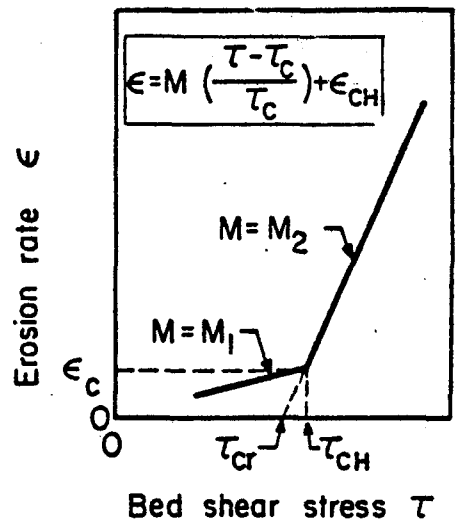

Fig. 2.13 Typical Laboratory Determined Relationship between Surface Erosion Rate ε and Time-mean Bed Shear Stress τ (after Mehta, 1981).

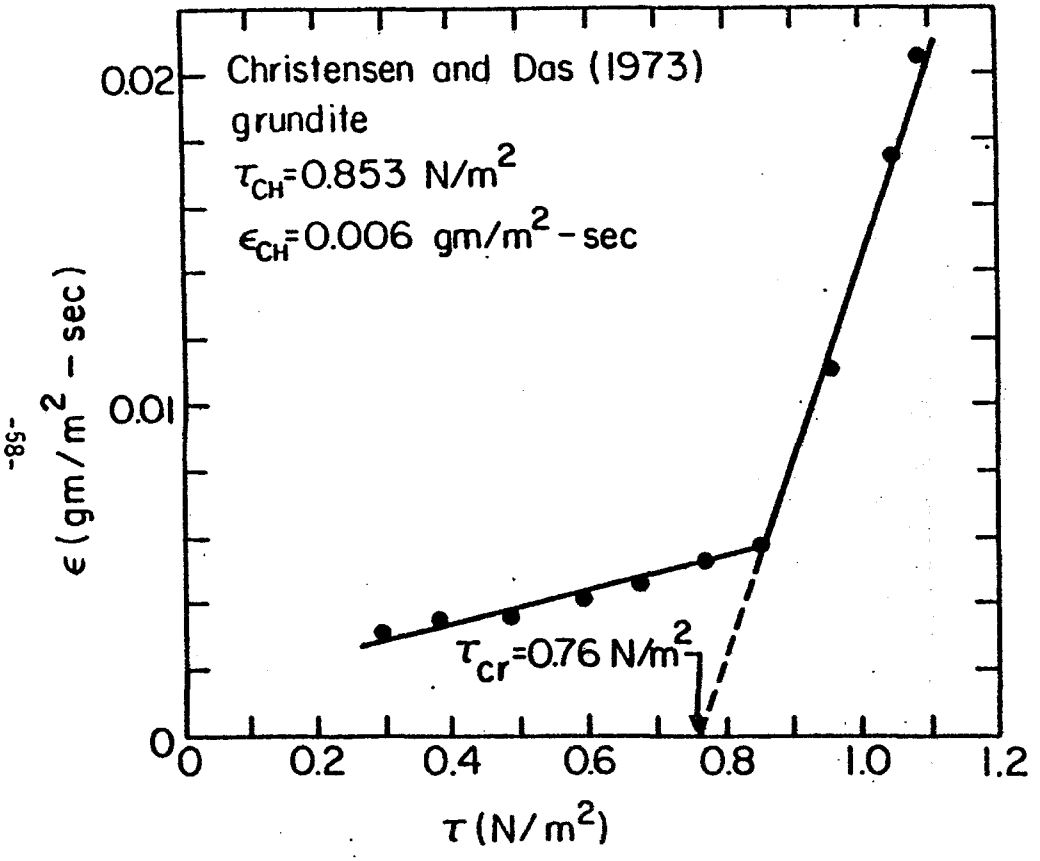

Fig. 2.14 Example of Relationship between Surface Erosion Rate ϵ and Bed Shear Stress τ. Data of Christensen and Das (1973) for Grundite (after Mehta, 1981).

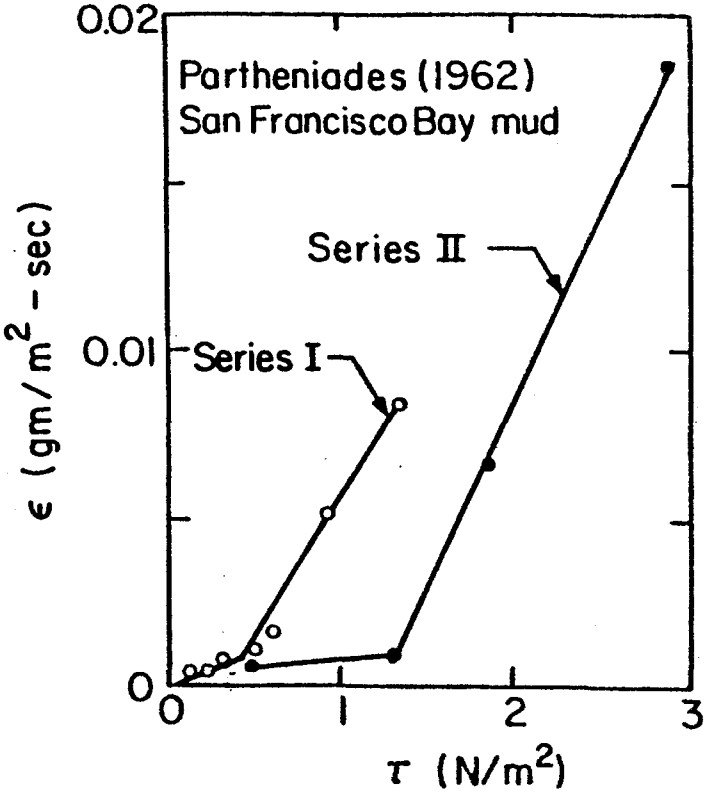

Fig. 2.15 ϵ-τ Data of Partheniades (1962), Series I and II (after Mehta, 1981).

Ariathurai and Arulanandan (1978) found the same general relationship for remolded beds as given in Eq. 2.30, but with M1 = M2. Thus, Eq. 2.30 becomes

$$\varepsilon = M'\left(\frac{\tau_b - \tau_{cr}}{\tau_{cr}}\right) \tag{2.31}$$

where $M' = M \cdot \tau_{cr}$. Figure 2.16 gives an example of this relationship, with $\alpha' = 1/M'$.

Figure 2.17 shows the measured variation of C with time typically found by several investigators (Partheniades, 1962, Mehta and Partheniades, 1979; Mehta et al., 1982a) in laboratory resuspension tests with flow-deposited (stratified) beds under a constant applied τ_b. As observed, dC/dt is high initially, decreases monotonically with time and appears to approach zero. The value of τ_c at the depth of erosion at which dC/dt, and therefore ε becomes essentially zero has been interpreted to be equal to τ_b (Mehta et al., 1982a). This interpretation is based on the hypothesis that erosion continues as long as $\tau_b > \tau_c$, i.e. the excess shear stress $\tau_b - \tau_c > 0$. Erosion is arrested at the bed level at which $\tau_b - \tau_c = 0$. This interpretation, coupled with measurement of $\rho_D(z)$ and the variation of C with t can result in an empirical relationship for the rate of erosion of stratified beds.

Resuspension experiments with deposited (stratified) beds were performed by Parchure (1980) in a rotating annular flume and by Dixit (1982) in a recirculating straight flume. The objective of these experiments was to determine the effect of varying bed shear strength with depth below the initial bed surface on the rate of surface erosion under a flow-induced shear stress. A description of the experimental procedures and results from these experiments has been given by Parchure (1980), Dixit (1982) and Mehta et al. (1982a). A synopsis is given here.

The annular flume used in these experiments had the following dimensions: 0.20 m wide, 0.46 m deep and 0.76 m mean radius. The flume consisted of three main components: 1) a rotating circular channel which held the sediment-water mixture, 2) an annular ring with the same mean radius as the channel, and 3) a steel frame and electric motors. The ring, positioned in contact with the water surface, and channel could be

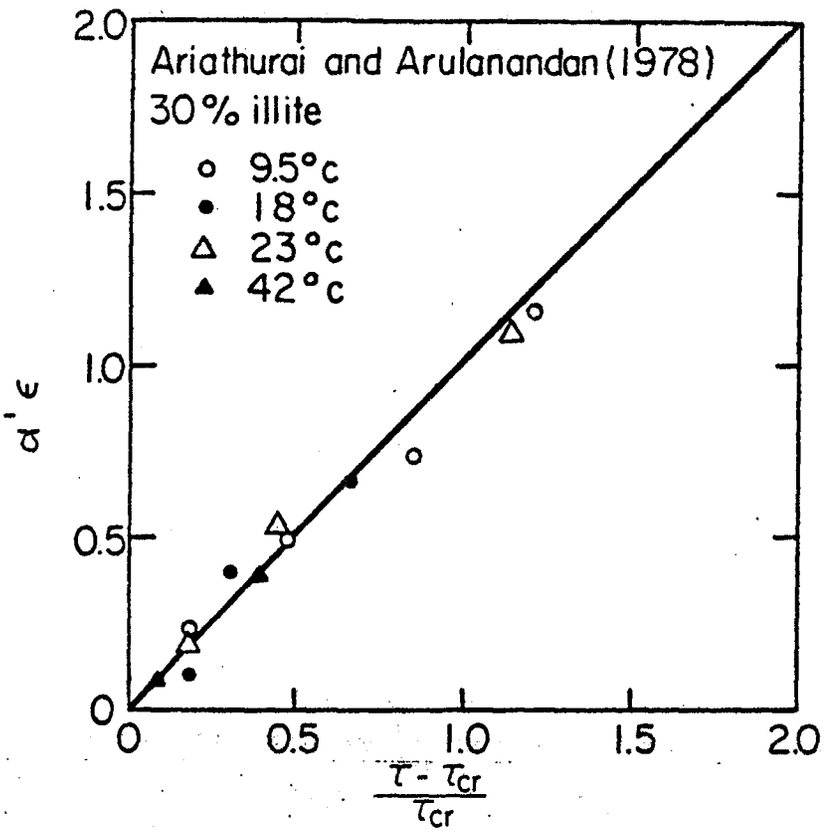

Fig. 2.16 Dimensionless ε-τ Relationship Based on Results of Ariathurai and Arulanandan (1978) (after Mehta, 1981).

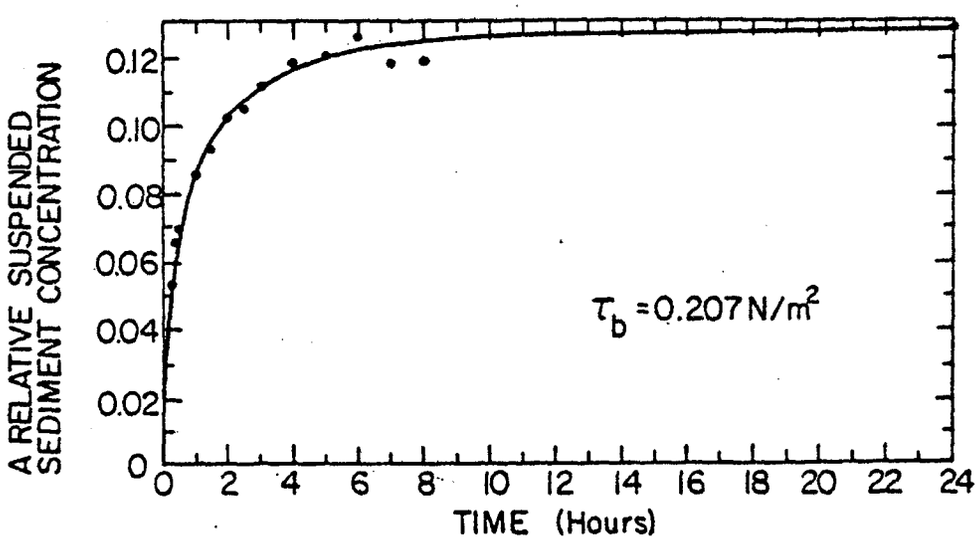

Fig. 2.17 Relative Suspended Sediment Concentration versus Time for a Stratified Bed at Bed Shear Stress τ_b=0.207 N/m^2 (after Mehta and Partheniades, 1979).

rotated simultaneously in opposite directions in order to achieve a uniform turbulent shear field in the channel, and to minimize the effects of rotation-induced radial secondary currents. This design and operational procedure eliminated the presence of aggregate-disrupting elements such as circulatory pump blades. The required bed shear stress was attained by adjustment of the rotational speeds of the channel and the ring. Four taps, located on the outer channel wall, were used to obtain suspended sediment samples from the channel.

The recirculating flume was 18 m long, 0.6 m wide and 0.9 m deep with an underflow-type control gate at the downstream end. One side of the flume was made of glass panels to allow visual observations. The diameter of the return pipe was 0.2 m.

A commercial grade kaolinite with a CEC of approximately 9 meq/100 gm was used in these experiments. Tap water, with a total salt concentration of 0.28 ppt, pH = 8.5 and SAR = 0.012, was used in the recirculating flume, while tap water plus commercially available sodium chloride at 35 ppt concentration, pH = 8.1 and SAR = 12.0 was used in the annular flume. The kaolinite was equilibrated with the fluid used for at least two weeks prior to the tests. The equilibration time is an important factor that can affect the rate of erosion due to the possibility of concentration gradients of ionic constituents between the solid and the liquid phases, or between the pore fluid and the eroding fluid, in the sediment-water system if the time allowed for equilibration is insufficient (Mehta, 1981).

The resuspension test methodology is depicted in Fig. 2.18. Specifically, this figure shows how the bed shear was varied over the course of each experiment. In Phase I the sediment-water mixture with sediment concentration C_o was mixed at a high shear stress, τ_m, for a period T_m. The shear stress τ_m must be greater than $\tau_{b_{max}}$, the maximum bed shear stress at which deposition of suspended sediment occurs. In Phase II the bed shear was lowered in steps, to τ_{d_1} for T_{d_1}, then to τ_{d_2} for T_{d_2} and finally to zero shear stress for a period T_{dc}. During this phase the sediment settled out of suspension, forming a bed which began to consolidate. As indicated in Fig. 2.18, the first two phases define the pre-erosion stress history of the bed. In Phase III, the shear stress was increased as shown in discretized (one-hour) steps,

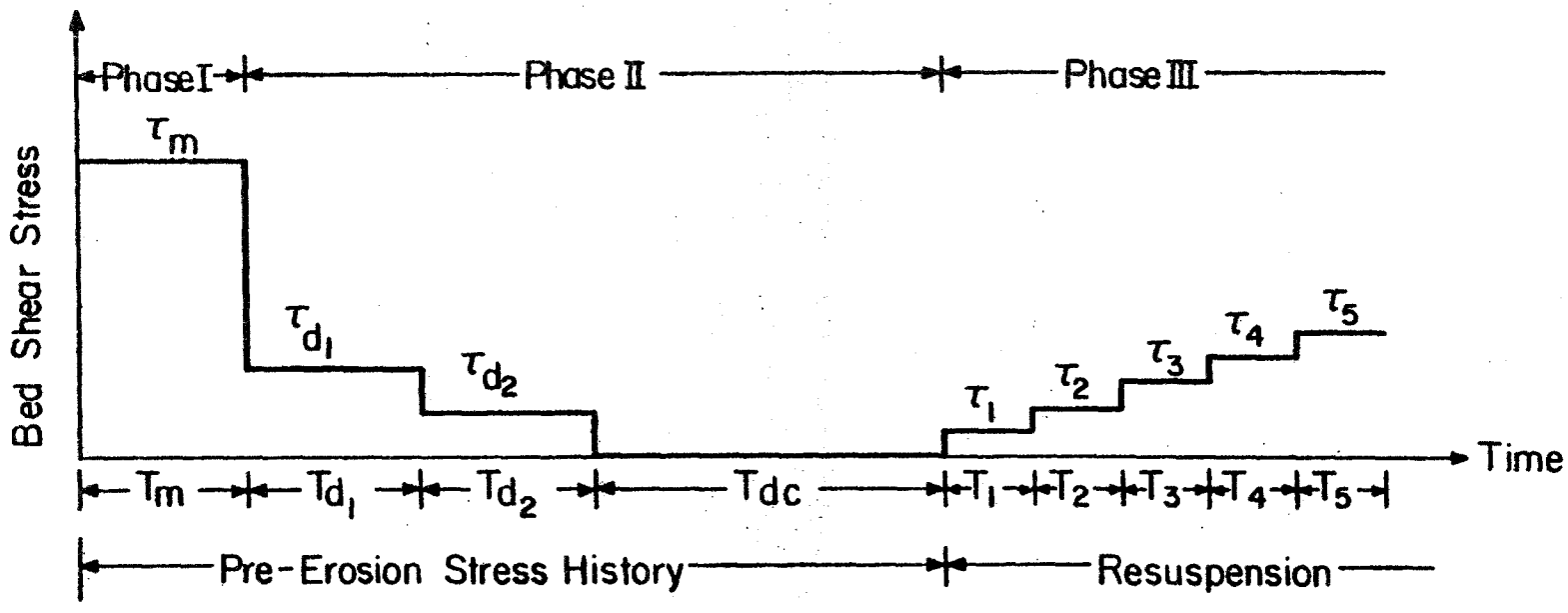

Fig. 2.18 Schematic Representation of the Selected Methodology for the Variation of the Applied Bed Shear Stress During Bed Preparation and Resuspension Tests (after Mehta et al., 1982).

i.e. $T_1 = T_2 = \ldots T_i$ (= 1 hour), and resuspension of the deposited material occurred.

The following parameters were held constant in most of the experiments in each flume: C_o, τ_m, T_m, τ_{d_1}, T_{d_1}, τ_{d_2}, T_{d_2} and T_i. Shown in Fig. 2.19 are typical values for these parameters and the measured variation of suspended sediment concentration with time for a test in tap water. The parameter $\Delta\tilde{\tau}_i$, which may be referred to as the normalized incremental bed shear stress, is defined as $(\tau_{i+1}-\tau_i)/\tau_i$ where τ_i is the bed shear stress, τ_b, during ith time-step.

In steps i = 1,...,5 in this figure it is apparent that the suspension concentration approaches a constant value during the latter stages of each time-step, i.e. $dC/dt \to 0$, while for steps i = 6 and 7 no appreciable decrease in dC/dt occurs over the one hour periods. This difference in the concentration-time profiles is represented in a different manner in Fig. 2.20, which shows the suspension concentration at the end of step i, $C(T_i)$, plotted against τ_i for three different tests in the recirculating flume. The value of τ_{ch}, a characteristic shear stress (similar to one defined previously for tests with placed beds) is determined as shown for each test. It is apparent that $dC(T_i)/dt$ is higher for $\tau_i > \tau_{ch}$ than for $\tau_i < \tau_{ch}$. The significance of this observation is better appreciated when it is realized that ε is proportional to the excess shear stress, $\tau_i - \tau_c$, and that τ_c increases more rapidly with depth, z, for $z < z_{ch}$ than for $z > z_{ch}$, where z_{ch} is the depth below the initial bed surface at which $\tau_c = \tau_{ch}$ (Mehta et al., 1982a).

The following empirical relationship between ε_i and $\tau_i - \tau_c(z)$ was derived from these experiments

$$\varepsilon_i = \varepsilon_{o_i} \exp\left[\alpha_i \frac{(\tau_i - \tau_c(z))}{\tau_c(z)}\right] \qquad (2.32)$$

where ε_{o_i} and α_i are empirical coefficients. Figures 2.21 and 2.22 show this relationship for tests in tap water and salt water respectively. This relationship is analogous to the rate expression which results from a heuristic interpretation of the rate process theory for chemical reactions (Mehta et al., 1982a). Christensen and [illegible] (1973), Paaswell (1973) and Kelly and Gularte (1981) have used rate process theory in

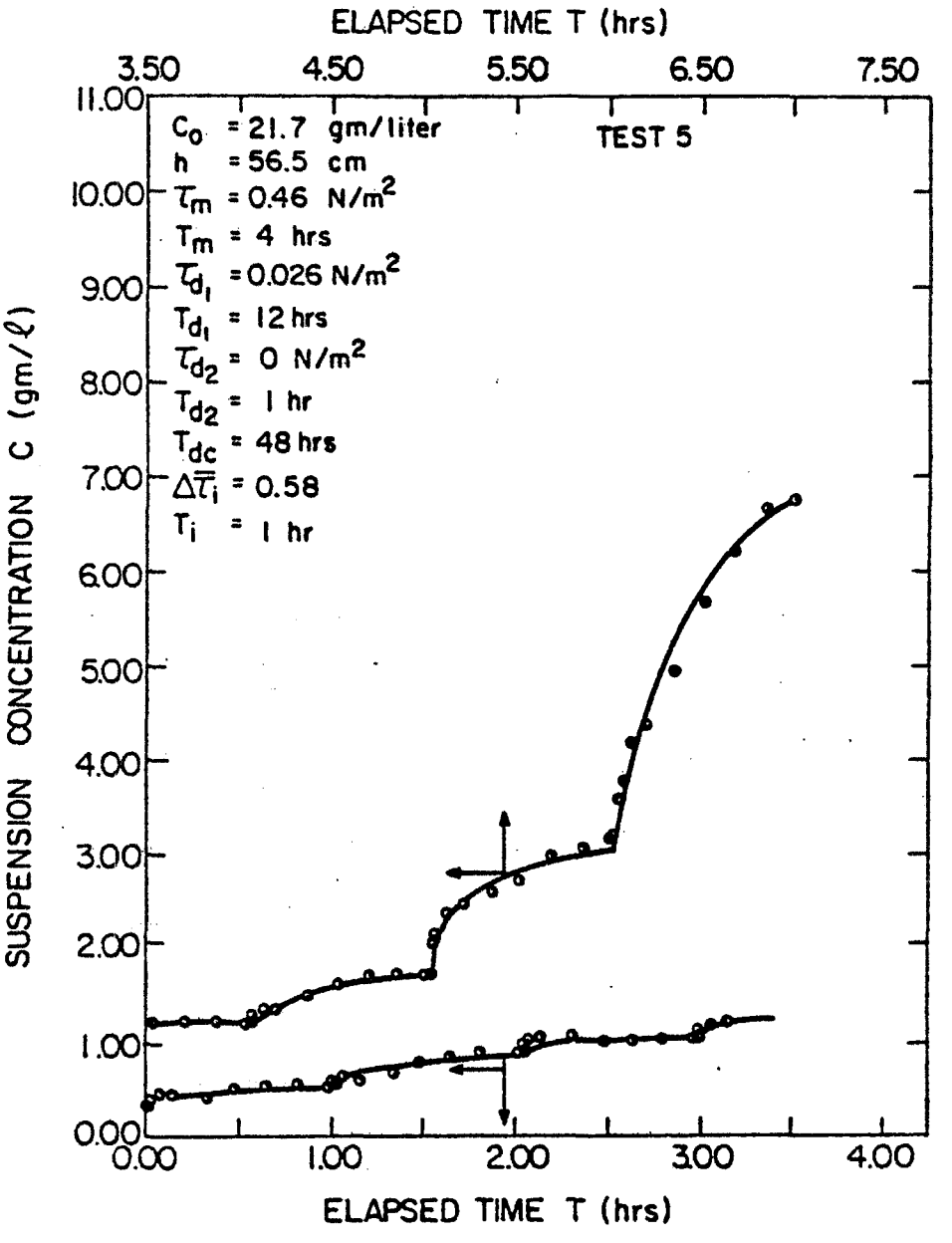

Fig. 2.19 Variation of Suspension Concentration with Time for T_{dc}=48 Hours (after Dixit, 1982).

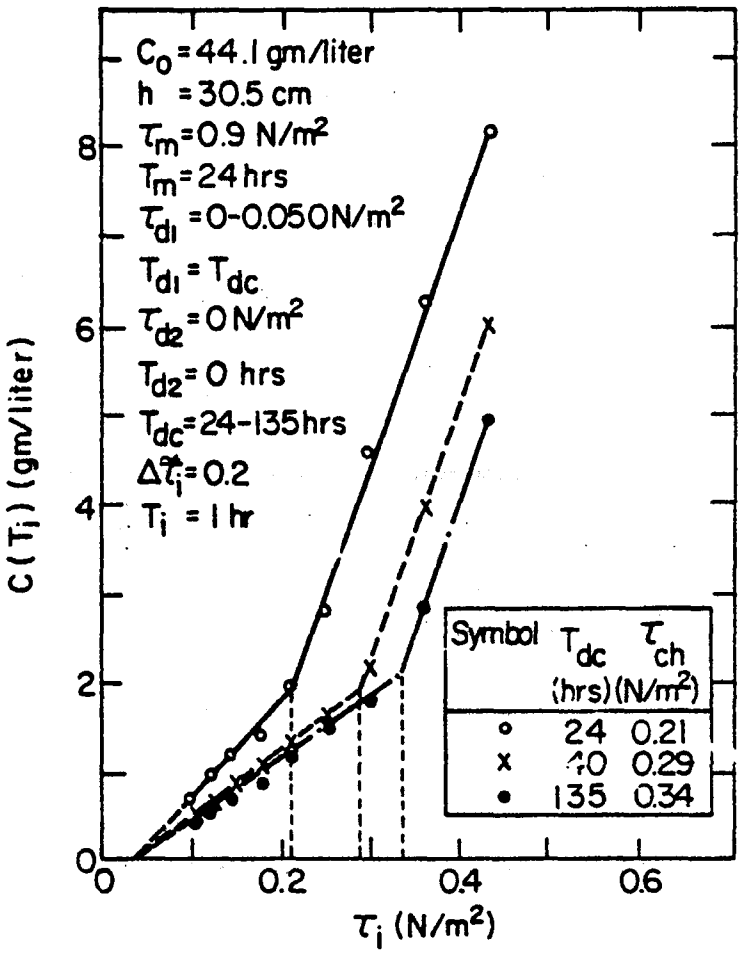

Fig. 2.20 $C(T_j)$ versus τ_j for Three Values of T_{dc}, Using Kaolinite in Salt Water (after Mehta et al., 1982a).

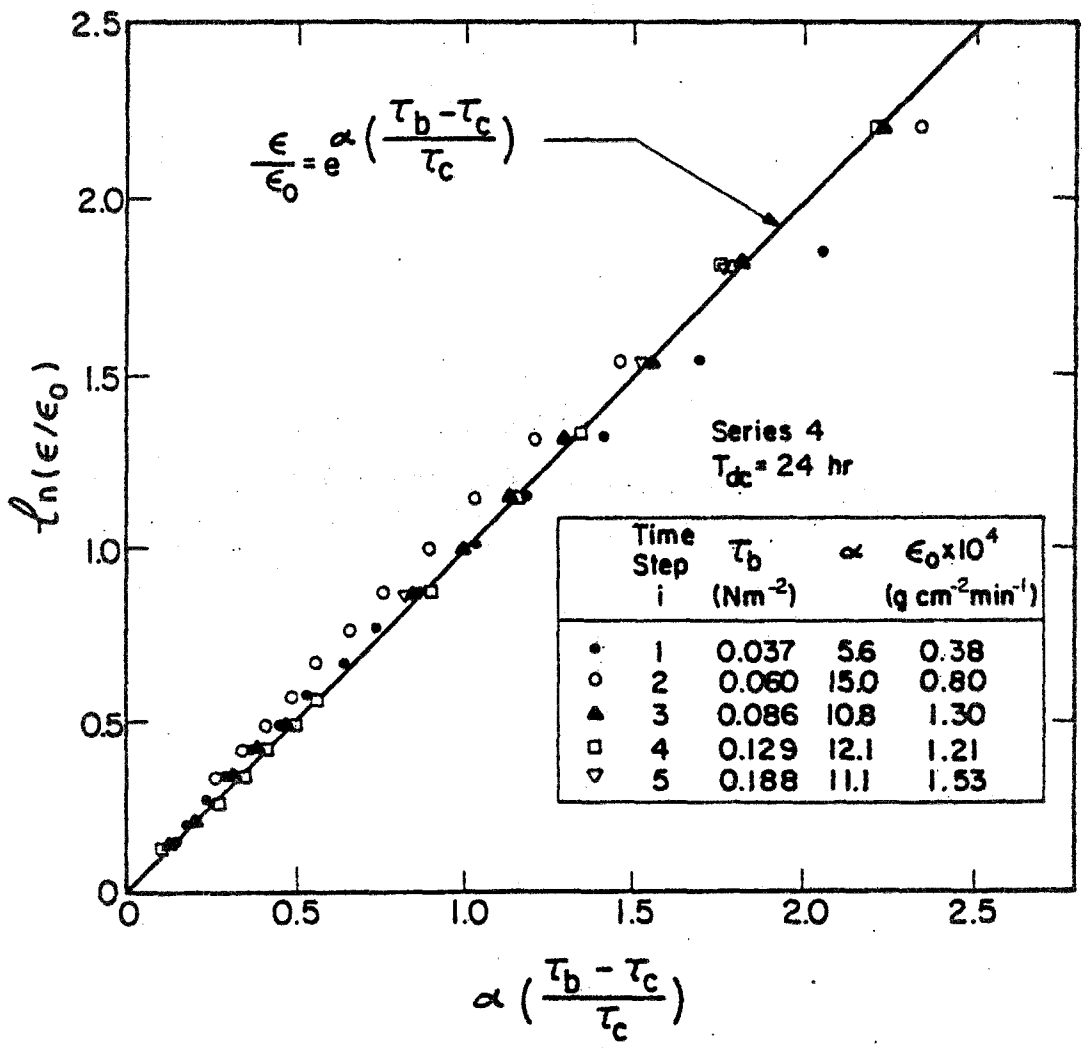

Fig. 2.21 Normalized Rate of Erosion, ϵ_j/ϵ_{0j}, versus Normalized Excess Shear Stress, $(\tau_j - \tau_c(z))/\tau_c(z)$, Using Kaolinite in Tap Water (after Mehta et al., 1982).

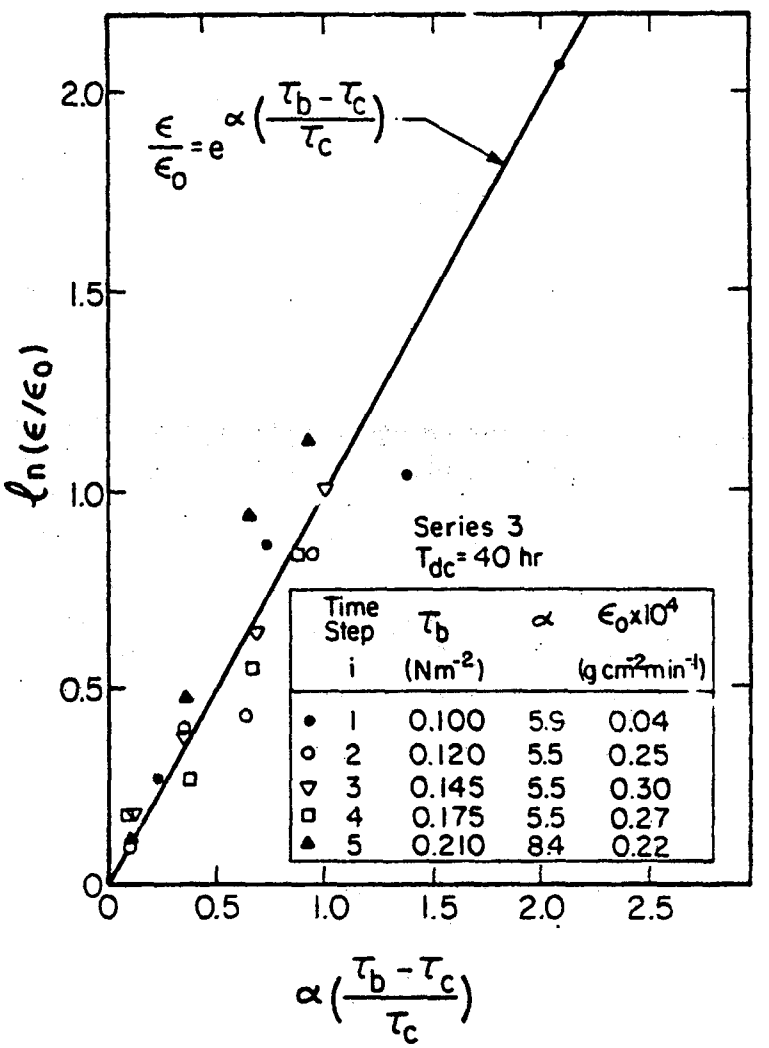

Fig. 2.22 Normalized Rate of Erosion, ϵ_i/ϵ_{0i}, versus Normalized Excess Shear Stress, $(\tau_b/\tau_c(z))/\tau_c(z)$, Using Kaolinite in Salt Water (after Mehta et al., 1982).

explaining the erosional behavior of cohesive sediment beds. By analogy, ε_i is a quantitative measure of the work done by τ_i on the system, i.e. the bed, and ε_{0i} and $\alpha_i/\tau_c(z)$ are measures of the system's internal energy, i.e. bed resistance to an applied external force.

An important conclusion reached from the above experiments was that new deposits should be treated separately from settled, consolidated beds (Mehta et al., 1982a). The rate of surface erosion of new deposits may be evaluated using Eq. 2.32, while the erosion rate for settled beds may be suitably determined using Eq. 2.31, in which ε varies linearly with the normalized excess shear stress. The reasons for this differentiation in determining ε are twofold: 1) typical τ_c and ρ_B profiles in settled beds vary less significantly with depth than in new deposits, and may even be nearly invariant. Therefore, the value of $(\tau_b/\tau_c) - 1 = \tilde{\Delta\tau_b}$ will be relatively small. For small values of $\tilde{\Delta\tau_b}$, the exponential function in Eq. 2.32 can be approximated by $\alpha\cdot(1 + \tilde{\Delta\tau_b})$, which represents the first two terms in the Taylor series expansion of $\exp(\alpha(\tilde{\Delta\tau_b}))$. For small values of $\tilde{\Delta\tau_b}$, i.e. $\tilde{\Delta\tau_b} << 1$, both expressions for ε vary linearly with $\tilde{\Delta\tau_b}$. Thus, the variation of ε with depth in settled beds can be just as accurately and more simply determined using Eq. 2.31. 2) the laboratory resuspension tests (briefly described in Appendix B) required to evaluate the coefficients ε_0 and α for each CND layer can not be practically or easily performed using vertical sections of the original settled bed (obtained from cores). A simpler laboratory test has been described by Ariathurai and Arunlanandan (1978) to evaluate the variability of M with depth. This procedure is briefly noted in Appendix B.

2.6.2. Erosion Algorithm

A description of the mass erosion algorithm, contained in Subroutine MASERO in SEDIMENT IIIA, followed by that for the surface erosion algorithm, contained in Subroutine SURERO, are given below. In both algorithms, the rate of erosion is calculated on an element by element basis.

A portion of the unconsolidated new deposit (UND), when present, will mass erode (redisperse) when τ_b is greater than the surface shear strength of the UND, i.e. $\tau_c(z=0)$. The thickness of the UND that fails

totally and is instantly redispersed is equal to z_*, where z_* = bed depth at which $\tau_c(z) = \tau_b$. The value of z_* is determined from the linearly varying $\tau_c(z)$ profile in each UND layer. The value of z_* may be greater than the thickness of the top layer, TLAYM(1), in which case more than one layer is redispersed. The dry mass of sediment that is redispersed, M_D, is calculated according to

$$M_D = \int_0^{z_*} \rho_D(z)dz \qquad (2.33)$$

where M_D has units of Kg/m^2 and is considered to be the mass eroded over one time-step Δt. The contribution to the source term in the governing equation (Eq. 2.11) caused by mass erosion is given by Eq. 2.33 divided by the product of the average element water depth and the time-step Δt. New UND layer(s) thicknesses and $\tau_c(z)$, $\rho_B(z)$ and $\rho_D(z)$ profiles are calculated at each time-step when mass erosion occurs by subtracting z_* and resetting $\tau_c(z=0)$, $\rho_B(z=0)$ and $\rho_D(z=0)$ equal to the respective initial values at $z = z_*$. If z_* is calculated to be greater than the thickness of the entire UND, then all of this sediment is redispersed.

For both the mass and surface erosion algorithms, erosion is considered to occur only during accelerating flows, i.e. $\tau_b(t+\Delta t) > \tau_b(t)$. Thus, $\tau_b(t+\Delta t)$ may be greater than $\tau_c(z=0)$, no erosion will occur if $\tau_b(t) > \tau_b(t+\Delta t)$. This stipulation for the occurrence of erosion, and an analogous one for deposition as will be discussed in the following section, is based on an interpretation of the typically observed Eulerian time-concentration variation in an estuarial environment. For example, Fig. 1.3 shows a time-concentration profile from the Savannah River estuary (Krone, 1972). Also indicated is the observed correlation between accelerating flows and increasing suspension concentration and between decelerating flows and decreasing suspension concentration. Laboratory evidence (Mehta and Partheniades, 1975; Partheniades, 1977; Mehta et al., 1982a) suggests that under accelerating flows, erosion occurs without redeposition of the eroded sediment. Likewise, during decelerating flows, sediment deposits without reentrainment of the deposit. During periods of steady flows, erosion or deposition may occur. These two processes will not, however, occur simultaneously even in this case. The initial condition at the

inception of the steady flow period will determine whether erosion or deposition will occur. If the antecedent phase was one of deceleration, deposition will continue under the steady flow condition. If the antecedent phase was one of acceleration, the sediment will continue to erode under the steady flow condition. In both cases, however, relatively short transient periods of simultaneous erosion and deposition sometimes do tend to occur (Yeh, 1979). For estuarial modeling purposes, however, these periods may be ignored without introducing any significant errors.

Surface erosion of consolidating new deposits (CND) occurs when: 1) the entire UND has been redispersed, 2) $\tau_b(t+\Delta t) > \tau_b(t)$ and 3) $\tau_b(t+\Delta t) > \tau_c(z=0)$, where z=0 is now at the fluid-CND interface. The surface erosion rate expression (Eq. 2.32) found by Mehta et al. (1982a) is used to determine the thickness of the CND, z_*, that is resuspended during a time-step, Δt. The following iterative procedure is used to calculate z_* during any given time-step.

The average erosion rate, $\bar{\varepsilon}$, for the period Δt is calculated as:

$$\bar{\varepsilon}(t+\Delta t) = \frac{1}{2}\left(\varepsilon(t) + \varepsilon(t+\Delta t)\right) \tag{2.34}$$

in which

$$\varepsilon(t+\Delta t) = \varepsilon_0(1)\exp\left[\alpha(1)\left(\frac{\tau_b(t+\Delta t)}{\bar{\tau}_c} - 1\right)\right] \tag{2.35}$$

where $\varepsilon_0(1)$ and $\alpha(1)$ are the average empirical coefficients for the first (i.e. top) CND layer, and

$$\bar{\tau}_c = \frac{1}{2}\left[\tau_c(z=0) + \frac{1}{z_*}\int_0^{z_*}\tau_c(z)dz\right] \tag{2.36}$$

As a first guess, z_* is set equal to TLAY(1) = z_{*_1} (see Fig. 2.11). A new value of z_*, designated z_{*_2}, is calculated according to:

$$z_{*_2} = \bar{\varepsilon}\cdot\Delta t\cdot\frac{d_e}{\bar{\rho}_D} \tag{2.37}$$

where d_e is the elemental average flow depth, and $\bar{\rho}_D$ is the average dry bed density over the first bed depth z_{*_1}. Then the following parameter is evaluated:

$$\Delta\lambda = \frac{\bar{\rho}_D \cdot z_{*_2}}{\bar{\varepsilon} \cdot \Delta t \cdot d_e} - 1 = |\lambda - 1| \qquad (2.38)$$

If $\Delta\lambda < 0.02$, then z_{*_2} is taken to be the depth of bed eroded during this time-step. If $\Delta\lambda > 0.02$, then yet another new value of z_*, designated z_{*_3}, is calculated using the following equation:

$$z_{*_3} = z_{*_2} + \frac{(z_{*_2} - z_{*_1})|\lambda - 1|}{\lambda_1 - \lambda} \qquad (2.39)$$

where $\lambda_1 = \bar{\rho}_D \cdot z_{*_1} / (\bar{\varepsilon} \cdot \Delta t \cdot d_e)$, with $\bar{\rho}_D$ and $\bar{\varepsilon}$ determined using $z_* = z_{*_1}$. Using z_{*_3}, the entire procedure, i.e. Eqs. 2.34 through 2.39, is repeated until the chosen error criterion, i.e. $\Delta\lambda < 0.02$, is satisfied. As in the mass erosion routine, new CND layer thickness(es) and $\tau_c(z)$, $\rho_B(z)$ and $\rho_D(z)$ profiles are determined. As before, z_* may be greater than the thickness of the top layer. Laboratory tests required to evaluate $\tau_c(z)$, $\rho_B(z)$, and the average values of ε_0 and α for each CND layer are described in Appendix B.

Once the entire new deposit bed section has been eroded, the original consolidated bed, if any exists, will undergo surface erosion when the following two conditions exist: 1) $\tau_b(t+\Delta t) > \tau_b(t)$ and 2) $\tau_b(t+\Delta t) > \tau_c(z=0)$, where $z=0$ is now at the top of the original bed. The surface erosion rate expression (Eq. 2.31) given by Ariathurai and Arulanandan (1978) is used to evaluate the thickness, z_*, of the original bed that is eroded each time-step. The iterative procedure used for the CND is again used to solve for z_*, with only the expression for ε being different. Equation 2.34 becomes

$$\varepsilon(t+\Delta t) = M(1)\left(\frac{\tau_b(t+\Delta t)}{\bar{\tau}_c} - 1\right) \qquad (2.40)$$

where M(1) is the erodibility constant for the first layer.

The contribution to the source term in Eq. 2.11 caused by surface erosion is given by Eq. 2.34, with Eq. 2.35 used for the consolidating bed section and Eq. 2.40 used for the original consolidated bed section, divided by the average element water depth.

In the following section, the depositional behavior of cohesive sediments is summarized, followed by a description of the deposition algorithm.

2.7. Deposition of Fine Sediment

2.7.1. Introductory Note

Deposition has been defined to occur when τ_b is not high enough to resuspend sediment material that settles onto and bonds with the bed surface. This process, therefore, involves two other processes, settling and bonding, i.e. cohesion. Laboratory studies on the depositional behavior of cohesive sediment in steady turbulent flows have been conducted by, among others, Krone (1962), Rosillon and Volkenborn (1964), Partheniades (1965), Partheniades et al. (1966), Migniot (1968), Lee (1974), Mehta and Partheniades (1975) and Mehta et al. (1982b). The results from these and other studies on the settling rates of cohesive sediments pertinent to the deposition model described in Section 2.7.2. are summarized below.

In laboratory flumes, the depositional behavior is usually investigated by allowing sediment suspended in a flume at a high shear stress to deposit by reducing the shear stress. Since the sediment concentration gradient in the direction of flow is usually small, the observed time-rate of change of the depth-averaged concentration, C, is due to the deposition of suspended material. The conservation of sediment mass can be expressed as

$$\frac{dC}{dt} = - \frac{p_d W_s(C) C}{d} \qquad (2.41)$$

where t = time, d = flow depth, $W_s(C)$ = sediment settling velocity as a function of C, and p_d = probability of deposition, or the probability of a sediment particle or floc bonding to the bed and not being instantly resuspended.

Krone (1962) conducted a series of depositional tests in a 31 m long and 0.90 m wide recirculating flume using mud from San Francisco Bay which contained approximately equal proportions of clay and silt. Krone postulated that p_d increases linearly with a decrease in τ_b according to

$$p_d = 1 - \frac{\tau_b}{\tau_{cd}} \qquad (2.42)$$

where τ_{cd} = critical shear stress for deposition, above which no deposition occurs. Therefore, p_d decreases linearly from a value of 1.0 at $\tau_b = 0$ to 0 for $\tau_b > \tau_{cd}$. The value of τ_{cd} was found to be equal to 0.06 N/m^2 for the Bay mud with C < 0.3 g/l. Krone found that when C < 0.3 g/l, W_s was independent of C. In this case, integration of Eq. 2.41 gives:

$$\frac{C}{C_o} = \exp\left[-\frac{p_d W_s}{d} t\right] \qquad (2.43)$$

where C_o is the initial suspended sediment concentration. Thus, according to this equation all the suspended sediment will eventually deposit when $\tau_b < \tau_{cd}$.

For 0.3 g/l < C < 10 g/l and for C > 10 g/l, logarithmic laws of the following form were derived:

$$\log C \quad -K \cdot \log(t) + \text{Constant} \qquad (2.44)$$

where K was found to be a function of d and p_d. Krone attributed the variation of the depositional properties with suspension concentration to different forms of settling. Various forms of settling of coagulated fine sediment are discussed later in this section.

Partheniades (1965) conducted deposition tests in an open, flow recirculating flume using Bay mud. He noted that for flows above a certain critical bed shear, the suspended sediment concentration, after an initial period of rapid deposition, approached a constant value, which he referred to as an equilibrium concentration, C_{eq}. The ratio $C_{eq}/C_o = C^*_{eq}$ was found to be a constant for given flow conditions, regardless of the value of C_o. Whereas for flow velocities even slightly less than this critical value, all the sediment eventually deposited.

Partheniades *et al.* (1966) conducted deposition experiments in a rotating annular flume (similar to the one at the University of Florida, but with mean diameter of 0.82 m and 0.19 m wide) at the Massachusetts

Institute of Technology using a commercial grade kaolinite. Based upon these experiments it was concluded the C_{eq} represents the amount of sediment that, having settled to the near bed region, cannot withstand the high shear stresses present there (due to insufficiently strong inter-particle bonds) and are broken up and resuspended. In addition, C_{eq} in the fine sediment deposition tests appears not to be the result of an interchange between suspended and bed material as it is for cohesionless sediment, because, if such were the case, C_{eq} would not be dependent on C_o. Therefore, it follows that C_{eq} does not represent the maximum sediment carrying capacity of the flow, as it does in the case of cohesionless sediment, but instead may be considered to be the steady state concentration (Mehta and Partheniades, 1973).

As noted by Mehta and Partheniades (1975), Krone did not observe C_{eq} in his tests because most of them were conducted at $\tau_b < \tau_{cd}$, wherein C_{eq} would be expected to be equal to zero. It is apparent that the definition of p_d must be extended to include bed shear stresses greater than τ_{cd}.

Mehta and Partheniades (1975) investigated the depositional properties of a commercial grade kaolinite in distilled water and in salt water at seawater salinity (35 ppt) in the rotating annular flume facility at the University of Florida. Figure 2.23 shows typical suspended sediment concentration-time plots found in these tests. It is evident that a steady state concentration was reached in each test and that for bed shears above approximately 0.16 N/m^2, the value of C_{eq} was greater than zero and in fact increased monotonically with increasing τ_b.

Figure 2.24 shows the ratio $C^*_{eq} = C_{eq}/C_o$ plotted against τ_b for all the tests with kaolinite in distilled water. Two important conclusions are obtained from this figure: 1) C^*_{eq} is a constant for a given τ_b (and type of sediment) and is not a function of depth, d, or C_o, and 2) for $\tau_b < \tau_{b_{min}}$, $C^*_{eq} = 0$. The first conclusion is based on the observation that the data points for all the different flow conditions are almost randomly scattered about a "best fit" line. The minimum bed shear, $\tau_{b_{min}}$, observed in Fig. 2.24 is the same as the τ_{cd} value defined by Krone (1962), and the critical bed shear obtained by Partheniades (1965). As observed in this figure, $\tau_{b_{min}}$ was found to be approximately 0.18 N/m^2 for kaolinite in distilled water.

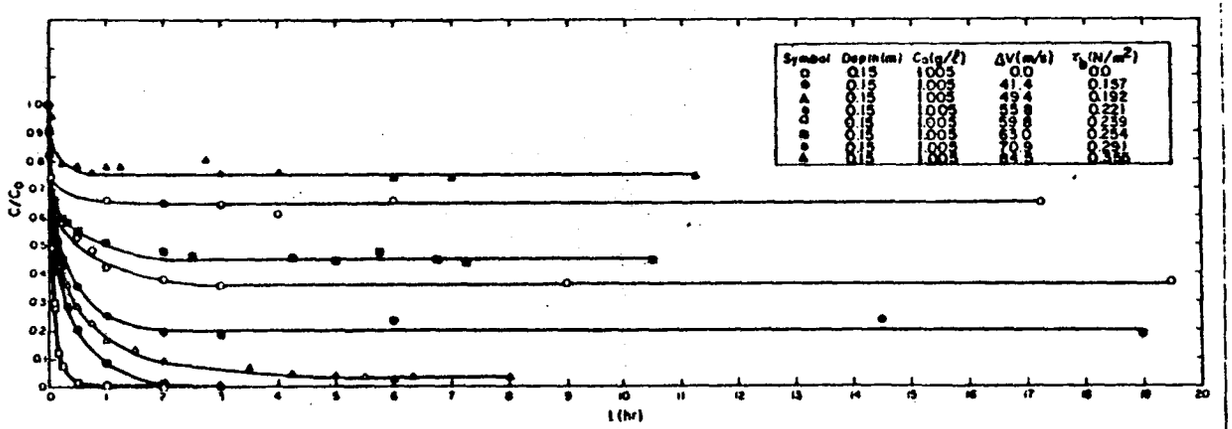

Fig. 2.23 Ratio C/C_o versus Time t for Kaolinite in Distilled Water (after Mehta and Partheniades, 1975).

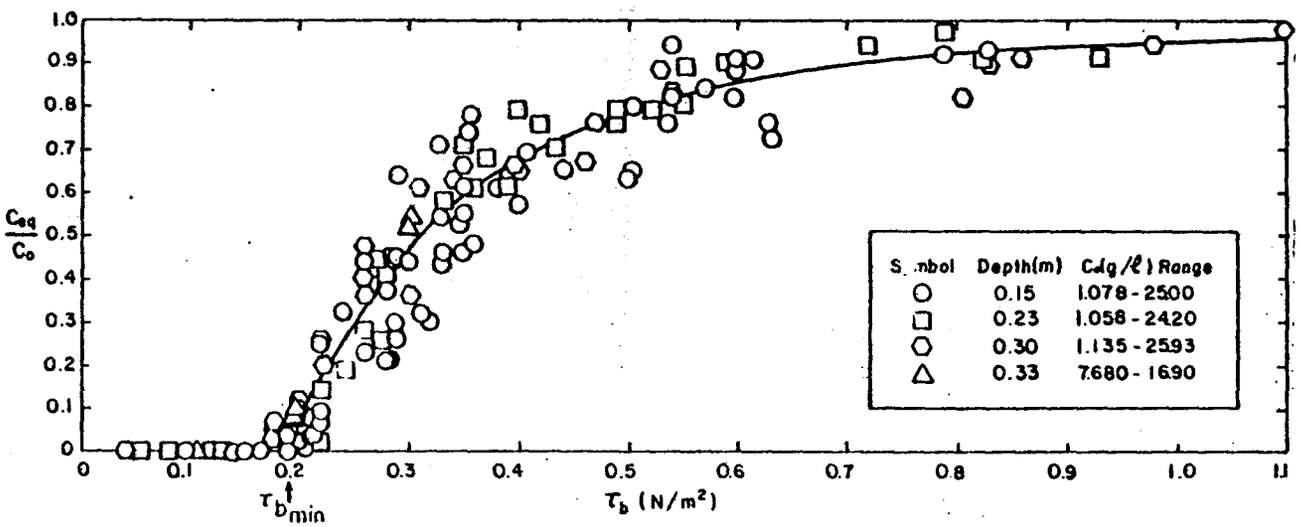

Fig. 2.24 Ratio C_{eq}/C_o versus Bed Shear Stress τ_b (after Mehta and Partheniades, 1975).

In Fig. 2.25 the data of Fig. 2.24 are plotted on log-normal coordinates as C^*_{eq} in percent against τ^*_b-1, where $\tau^*_b = \tau_b/\tau_{b_{min}}$. The straight line through the data points gives the following relationship between these two dimensionless parameters:

$$C^*_{eq} = \frac{1}{2}\left(1 + \text{erf}\left(\frac{y_a}{\sqrt{2}}\right)\right) \tag{2.45}$$

with

$$y_a = \log_{10}\left[\frac{(\tau^*_b-1)}{(\tau^*_b-1)_{50}}\right]^{1/\sigma_1} \tag{2.46}$$

where σ_1 is the standard deviation, $(\tau^*_b-1)_{50}$ is the geometric mean of the log-normal relationship given by Eq. 2.45, and erf is the error function (Mehta and Partheniades, 1975).

It was found that for all tests with kaolinite in both distilled and salt water, with a 50/50 mixture of kaolinite and San Francisco Bay mud in salt water, and with only Bay mud in salt water, and for the reanalyzed deposition tests of Rosillon and Volkenborn (1964), Partheniades (1965) and Partheniades et al. (1968), the value of σ_1 was 0.49. Therefore, as noted from Eq. 2.46, C^*_{eq} is dependent solely on the value of the ratio $(\tau^*_b-1)/(\tau^*_b-1)_{50}$. Mehta and Partheniades (1973) found for deposition tests in salt water the following relationship between $\tau_{b_{min}}$ and $(\tau^*_b-1)_{50}$:

$$(\tau^*_b-1)_{50} = 4\exp(-1.27\cdot\tau_{b_{min}}) \tag{2.47}$$

Mehta and Partheniades (1975) found the following dimensionless log-normal relationship for the variation, i.e. decrease, of the suspended sediment concentration with time:

$$C^* = \frac{1}{2}\left(1 + \text{erf}\left(\frac{T}{\sqrt{2}}\right)\right) \tag{2.48}$$

where

$$T = \log_{10}(t/t_{50})^{1/\sigma_2} \tag{2.49}$$

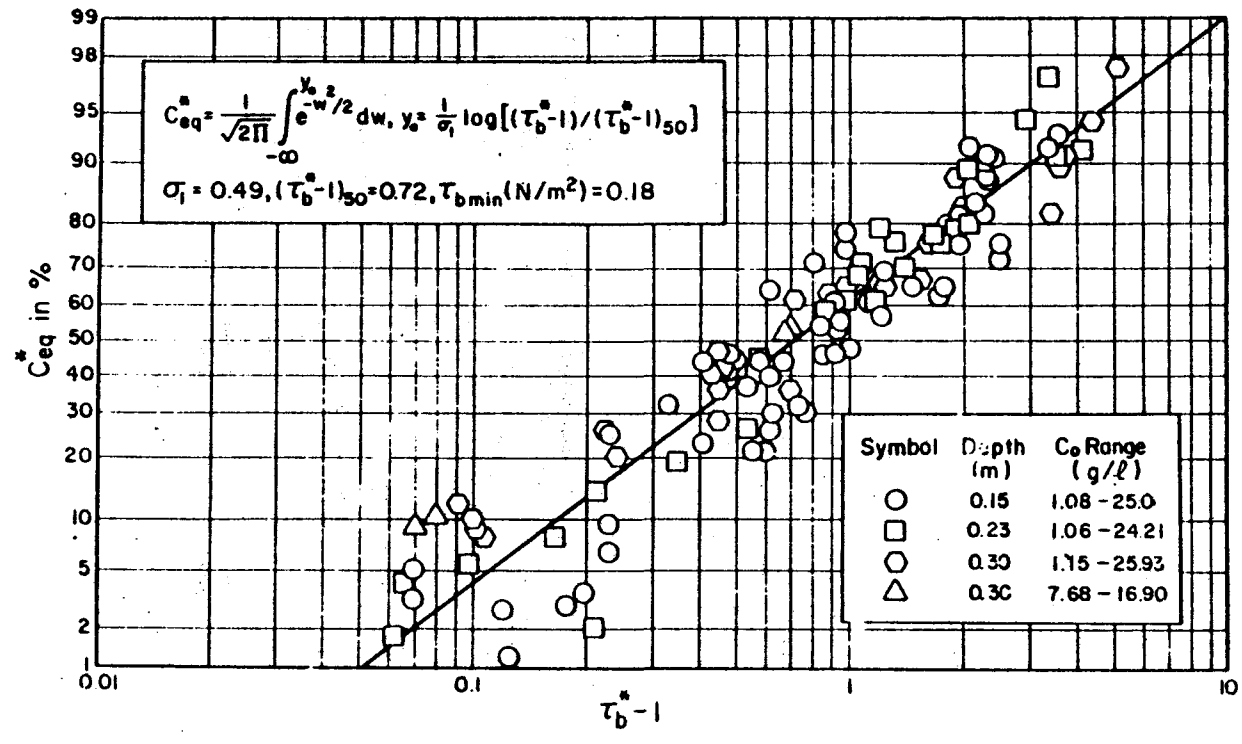

Fig. 2.25 Relative Steady State Concentration C^*_{eq} in Percent Against Bed Shear Stress Parameter τ_b^*-1 (after Mehta and Partheniades, 1975).

and where $C^* = (C_o-C)/(C_o-C_{eq})$ represents the fraction of the depositable sediment, C_o-C_{eq}, deposited at any given time t, σ_2 is the standard deviation of the log-normal relationship, and t_{50} is the geometric mean (i.e. the time at which $C^* = 50\%$). Figure 2.26 shows a comparison between some typical depositional data for kaolinite in distilled water and the log-normal relationship given by Eq. 2.48. This relationship was found to hold for all values of $\tau_b^*(= \tau_b/\tau_{b_{min}})$ greater than approximately 0.25, with the exception that for very high C_o values (around 20-25 g/l) with $\tau_b^* < 1$, an acceptable agreement with the measured data was not obtained. Good agreement was as well obtained between Eq. 2.48 and the data sets mentioned previously in this section.

Taking the derivative of Eq. 2.48 with respect to time gives the following expression for the rate of change of C^* with time:

$$\frac{dC^*}{dt} = \frac{0.434}{\sqrt{2\pi}\,\sigma_2}\,\frac{\exp(-T^2/2)}{t} \qquad (2.50)$$

The standard deviation, σ_2, and the geometric mean, t_{50}, were found to be functions of τ_b^*, d, and C_o. Shown in Figs. 2.27 and 2.28 are examples of the relationship found between these parameters. The following conclusions were arrived at from these and other similar plots given by Mehta (1973): 1) for a specific value of τ_b^*, the deposition rate was minimum. This τ_b^* value was found to vary between 1 and 2 for kaolinite in distilled water. The rate of deposition increased for τ_b^* values both less than and higher than this specific value, but not as significantly for higher values as for the lower values. However, for $\tau_b > \tau_{b_{max}}$, no deposition of suspended sediment occured. For Bay mud in sea water, $\tau_{b_{max}}$ was determined to be 1.69 N/m^2. 2) for $\tau_b^* < 1$, the rate of deposition increased with an increase in d, while for $\tau_b^* > 1$, the effect of d on the deposition rate was minimal. 3) the deposition rate decreased with an increase in C_o. A possible explanation for this last result is that C_o was in the hindered settling range (explained below) where the settling velocity of suspended sediment decreases with increasing concentation (Owen, 1970; Huang et al., 1980; Thorn, 1981).

As noted, the settling velocity of suspended fine sediment particles has been found to be a function of, among other parameters,

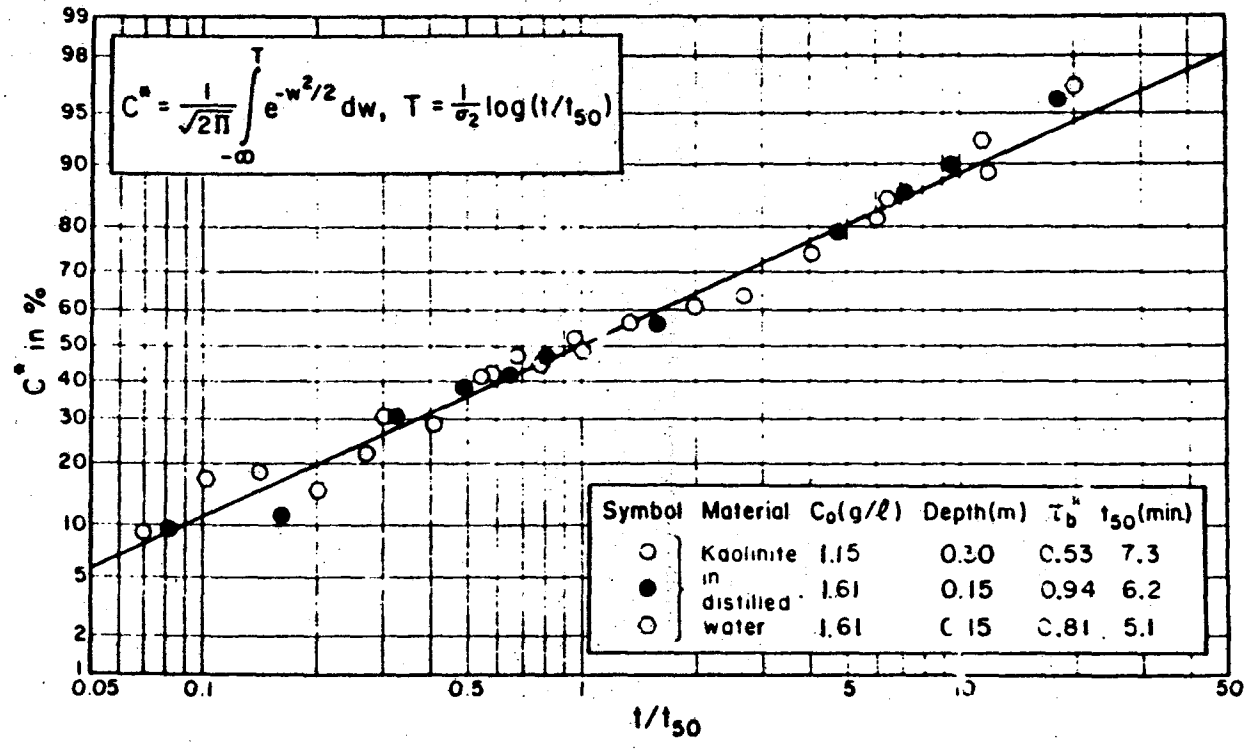

Fig. 2.26 C^* in Percent versus t/t_{50} for Kaolinite in Distilled Water (after Mehta and Partheniades, 1975).

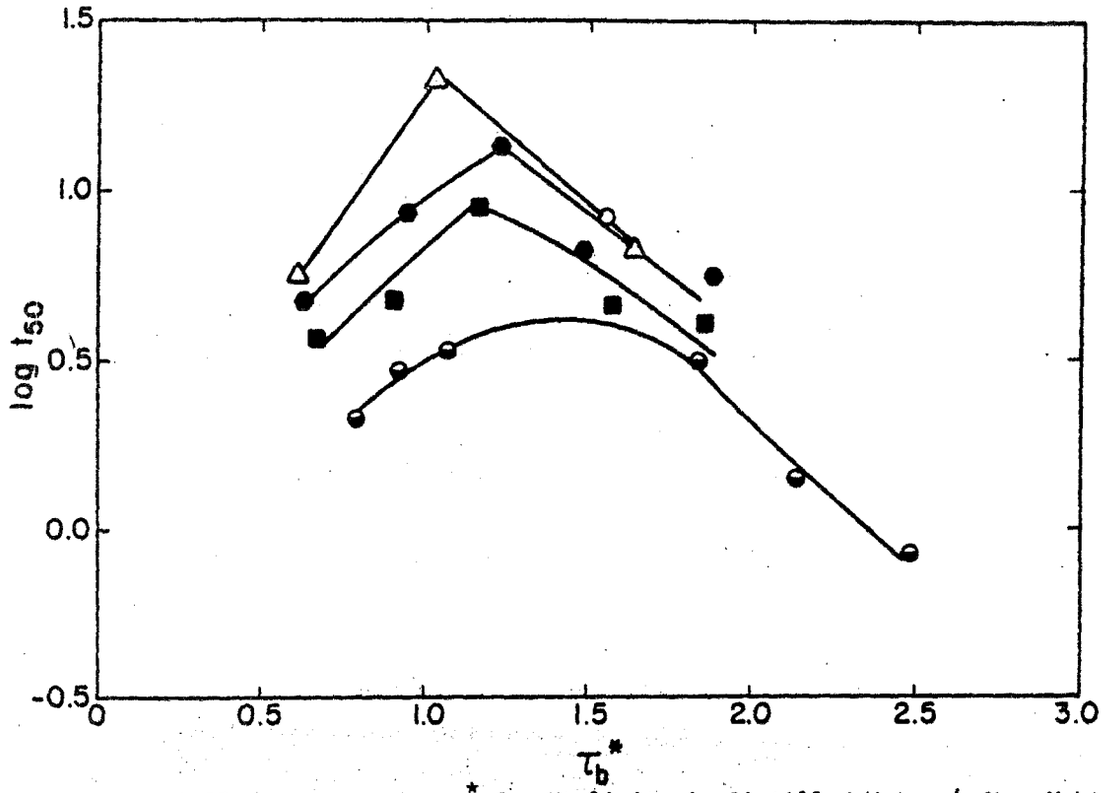

Fig. 2.27 Log t_{50} versus τ_b^* for Kaolinite in Distilled Water (after Mehta and Partheniades, 1975).

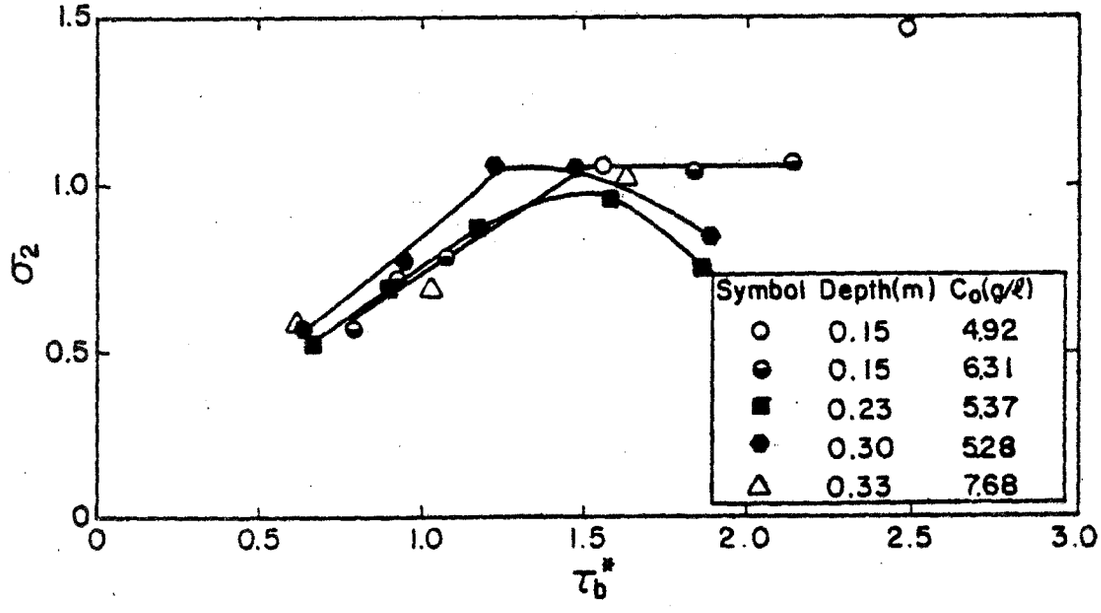

Fig. 2.28 σ_2 versus τ_b^* for Kaolinite in Distilled Water (after Mehta and Partheniades, 1975).

the suspension concentration (Krone, 1962). There appears to be at least three types of settling: 1) no mutual interference, 2) mutual interference and 3) hindered settling. For very low suspension concentrations, on the order of 0.1-0.7 g/l, the aggregates or elementary particles settle independently without much mutual interference, and therefore the settling velocity is independent of C. For concentrations between approximately 0.3 g/l and 10-15 g/l, the settling velocity increases with increasing concentration due to the accompanying increase in inter-particle (floc) collisions, and therefore increased mutual interference (Fig. 2.29). For concentrations higher than 10-15 g/l, the settling velocity actually decreases with increasing concentration (Figs. 2.30 and 2.31). At such high concentrations the sediment suspension, referred to as fluid mud or mud cake (Bellessort, 1973), hinders the upward flux of water expelled by consolidation of the lower suspension (Krone, 1962).

In the mutual interference range, Krone (1962) and Owen (1971) have found the following empirical relationship between the median settling velocity, W_s, and C:

$$W_s = KC^n \tag{2.51}$$

where K and n are empirical constants that depend on the sediment type and the turbulence intensity of the suspending fluid. Krone found n to be equal to 1.33 for Bay mud in laboratory experiments (see Fig. 2.29).

Owen (1971) studied the effect of turbulence on the settling velocities of natural mud. No description of the sediment was reported, except that it was collected in the River Thames near Dagenham, England. A specially designed sampling instrument was used to collect sediment samples during both a spring tide and a neap tide. This tube collected undisturbed samples of suspended sediment in an estuarine environment, and immediately thereafter the median settling velocity of "natural aggregates" could be determined using the bottom withdrawal method described by Owen (1970). The value of n determined using this method was 1.1 and 2.2 for sediment collected during a spring and a neap tide, respectively. The turbulence intensity during a spring tide is greater than that during a neap tide. Owen therefore postulated that n

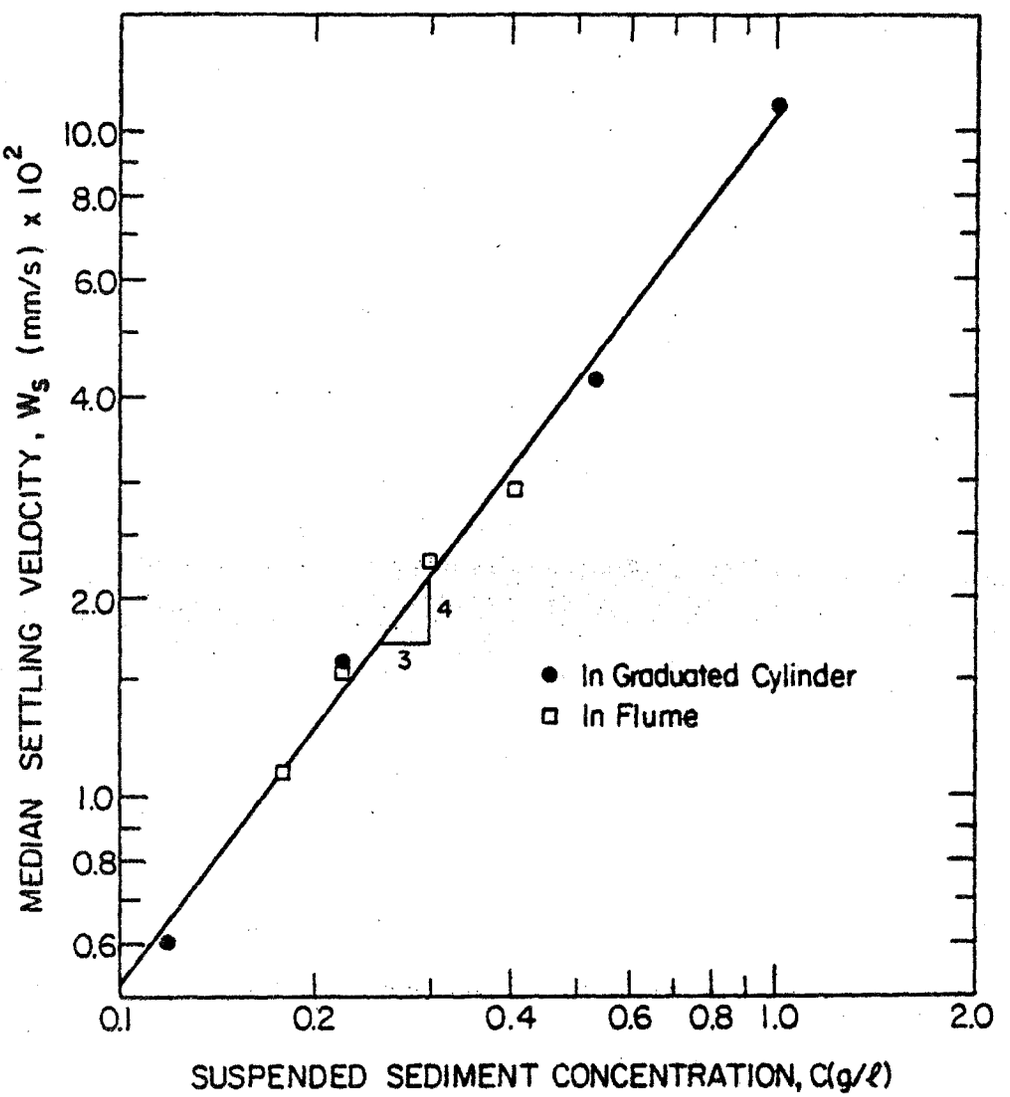

Fig. 2.29 Settling Velocity, W_S, versus Suspended Sediment Concentration, C, for San Francisco Bay Mud (after Krone, 1962).

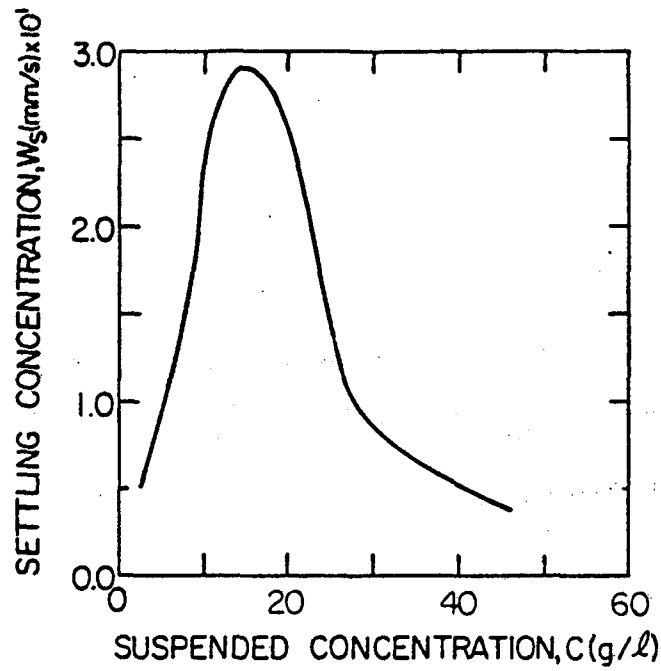

Fig. 2.30 Settling Velocity, W_s, versus Suspended Sediment Concentration, C, for Yangtze River Estuary Mud (after Huang et al., 1980).

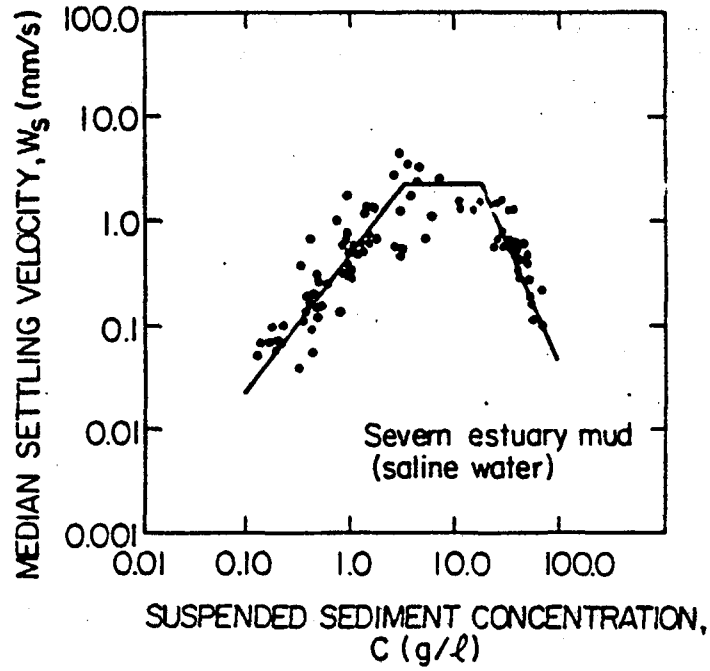

Fig. 2.31 Settling Velocity, W_s, versus Suspended Sediment Concentration, C, for Severn Estuary Mud (after Thorn, 1981).

was greater (and therefore W_s as well was greater) during the neap tide because the lower level of turbulence did not cause significant breakage of the aggregates; thus relatively large aggregates with higher settling velocities were formed. During the spring tide the higher degree of turbulence, and therefore greater internal shearing rates, did result in breakage of a significant proportion of the aggregates. Thus, small aggregates with lower settling rates, and therefore lower value of n, were formed. Owen believed that the inter-particle collision rate was significantly high during both tides and therefore did not consider it very probable that the aggregate size would have been affected (i.e. limited) by this factor. Owen also performed standard settling tests in a one meter high bottom withdrawal tube using the same sediment samples as above, and found that W_s varied linearly with C (i.e. n=1.0) for both spring and neap tide samples and that the values of W_s were approximately one order of magnitude smaller than the W_s values determined with the aggregate collection tube. The latter result is very significant in that it reveals the following apparent effect of turbulence on the behavior (e.g. settling velocities) of sediment aggregates: larger, stronger aggregates with corresponding higher settling velocities are formed in a turbulent flow field than under quiescent conditions primarily because of increased collision rates due to high internal shearing rates (see also Section 2.8.4).

Migniot (1968) defined a "flocculation factor" F, given below, in order to quantify the effect of the aggregation intensity on W_s:

$$F = \frac{W_{s_A}}{W_{s_p}} \tag{2.52}$$

where W_{s_A} is the median settling velocity of the aggregates and W_{sp} is the median settling velocity of the elementary sediment particles. Bellessort (1973) reported that F varies with the grain size of the elementary (i.e. deflocculated) particles according to

$$F = \alpha_3 \cdot D^{-2\beta_3} = W_{sp}^{-\beta_3} \tag{2.53}$$

where D is the mean diameter of the particles in microns (10^{-6}m), α_3 = 250 and β_3 = 0.9, provided W_s is measured in mm/s. Figure 2.32 shows

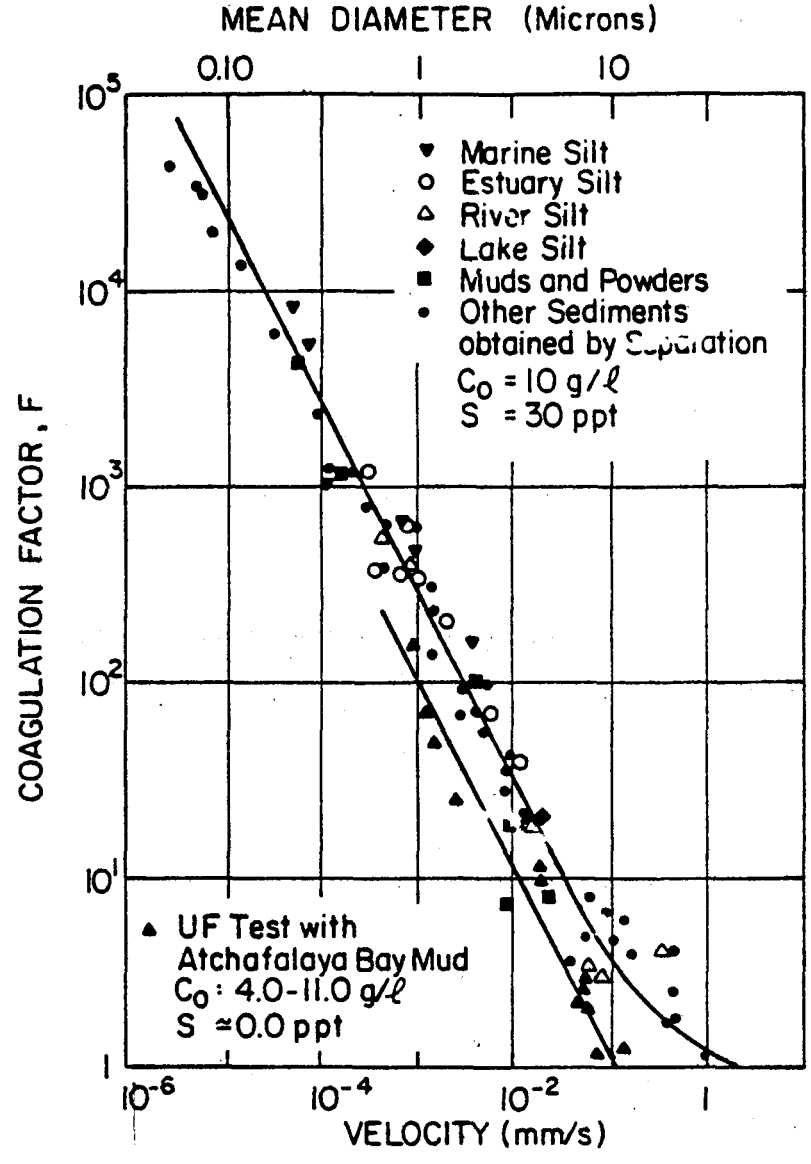

Fig. 2.32 Effect of Size and Settling Velocity of Elementary Particles on the Coagulation Factor of Natural Muds (after Bellessort, 1973).

this effect of the particle size on F and W_{s_A} for numerous sediment samples at C_o = 10 g/l and salinity S = 30 ppt. Also plotted in this figure is the variation of F with D found by Dixit et al. (1982) using mud from Atchafalaya Bay, Louisiana. However, in these data C_o varied from 1.2 to 11 g/l as indicated and S=0.0 ppt. Another important difference between the two data sets is that Bellessort measured W_{s_A} under quiescent conditions, while Dixit et al. measured this settling velocity under turbulent flow in a flume. As observed, these data have the same slope between F and D as given by Bellessort. This suggests that, in general, F may be proportional to $D^{-1.8}$, albeit with different intercept values, for at least suspension concentrations with C_o = 1.2-11 g/l and $0<S<30$ ppt.

2.7.2. Deposition Rates

The product $p_d \cdot W_s$ in Eq. 2.41 defines an effective settling velocity, W_s', which, in general, is smaller in magnitude than W_s since the range of p_d is between 0 and 1. The rate of deposition given by Eq. 2.41 may therefore be written as

$$\frac{dC}{dt} = -\frac{W_s' C}{d} \tag{2.54}$$

where W_s' is hereafter defined as the effective median settling velocity for a given sediment. For the dimensionless bed shear stress τ_b^* less than a certain characteristic value, $\tau_{b,c}^*$, with the range $0<\tau_b^*<\tau_{b,c}^*<1$ designated as Range I, and for the concentration range $C<C_1$ for all values of τ_b^* the following empirical relationships for W_s' are assumed:

$$W_s' = \begin{cases} p_d W_{s,1} & \text{for } C < C_1 \qquad (2.55) \\ p_d K C^n & \text{for } C_1 < C < C_2 \qquad (2.56) \\ \left(\frac{250}{D^{1.8}}\right) \frac{gD^2\left(\frac{\rho_s}{\rho_w}-1\right)p_d}{18\nu} \left(\frac{C}{C_2}-1\right)^{\ell} & \text{for } C > C_2 \qquad (2.57) \end{cases}$$

where $gD^2(\rho_s/\rho_w-1)/(18\nu) = W_{sp}$ and p_d is defined by Eq. 2.42. Therefore, depending upon the value of C, the rate of deposition in

Range I is given by Eqs. 2.54 - 2.57. These three expressions for W_s' are based upon the experiment results of Krone (1962), Bellessort (1973) and Owen (1971). Typical values for C_1 and C_2 are 0.1-0.7 g/l and 10-15 g/l respectively. The value of ℓ was found to be approximately -0.6 using the settling velocities measured by Owen (1970), Huang et al. (1980) and Thorn (1981). The values $W_{s,1}$, K, n and C_1 can vary widely, depending, among other factors, upon the particle diameter, D, the type of sediment and the salinity. These parameters must be determined in laboratory settling tests using a sample of the sediment from the water body being modeled (further discussion of this aspect is given in Appendix B, Section B.3).

For the intersection of $\tau_{b,c}^* \leq \tau_b^* < \tau_{b_{max}}^*$ (where $\tau_{b_{max}}^* = \tau_{b_{max}}/\tau_{b_{min}}$), designated as Range II, and the concentration range $C > C_1$ the rate of deposition is determined using the log-normal relationship (Mehta and Partheniades, 1975):

$$\frac{dC}{dt} = \frac{-0.434}{2\sqrt{2\pi}\,\sigma_2}\,\frac{\exp(-T^2/2)}{t}\,C_0\left(1-\operatorname{erf}\left(\frac{1}{\sqrt{2\pi}}\log_{10}\left[\frac{(\tau_b^*-1)}{4\exp(-1.27\tau_{b_{min}})}\right]^{2.04}\right)\right) \quad (2.58)$$

where $\sigma_1 = 0.49$, Eqs. 2.45 - 2.47 and $C^* = (C_0-C)/(C_0-C_{eq})$ have been substituted into Eq. 2.50. The following expression for W_s' in Range II was determined by equating Eqs. 2.54 and 2.58:

$$W_s' = \frac{k_2 d\,\exp(-T^2/2)}{\sigma_2 t}\,\frac{C_0}{C}\left(1-\operatorname{erf}\left(\frac{1}{\sqrt{2\pi}}\log_{10}\left[\frac{(\tau_b^*-1)}{4\exp(-1.27\tau_{b_{min}})}\right]^{2.04}\right)\right) \quad (2.59)$$

where $k_2 = 0.434/(2\sqrt{2\pi})$. For $\tau_b^* \leq 1$, the argument of the error function is set equal to zero. This expression for W_s', and therefore Eq. 2.58 as well, is assumed to be valid for $C > C_1$ for the following reason: the phenomenon of hindered settling was not observed in the steady-state deposition tests under turbulent flows performed by Mehta (1973) for concentrations up to about 20 g/l. Evidently, the higher τ_b^* values that Mehta used in his tests prevented the occurrence of this mode of settling, inasmuch as Krone (1962) did observe hindered settling in his tests which, in general, were conducted at lower values of τ_b^*. Deposition tests with $0.25 < \tau_b^* < 1$ using San Francisco Bay mud in sea

water and kaolinite in distilled water revealed that for suspension concentrations less than C_1= 0.1-0.7 g/l, the exponential law given by Eq. 2.54 was valid. Therefore, for $C < C_1$ in Range II, the rate of deposition is given by Eqs. 2.54 and 2.55 with p_d equal to the following approximate expression:

$$p_d = \begin{cases} 1 - \tau_b^* & \text{for } \tau_{b,c}^* < \tau_b^* < 0.95 \quad (2.60) \\ 0.05 & \text{for } \tau_b^* > 0.95 \quad (2.61) \end{cases}$$

The lower limit of 0.05 was chosen for p_d when $\tau_b^* > 0.95$ and $C < C_1$ in Range II so that deposition would be predicted to occur under these conditions. Assuming that p_d is a function of only τ_b^* for $C>C_1$ in Range II as has been assumed for Range I and for $C < C_1$ in Range II, it is apparent that p_d is incorporated in the argument of the error function in Eq. 2.58 which gives the rate of deposition for $C>C_1$ in Range II.

The parameter $\tau_{b,c}^*$ is defined to be the value of τ_b^* at which the expression for $W_s'(C)$ in Range I is equal to the same in Range II. Thus, W_s' (and therefore dC/dt) is a continuous function of the entire deposition range ($\tau_{b_{max}}^* < 1$). It is apparent that $\tau_{b,c}^*$ is not a constant, as it is a function of the depth-averaged concentration, C. Solving for $\tau_{b,c}^*$ gives

$$\tau_{b,c}^* = 1 - \frac{W_s'(\tau_{b,c}^* < \tau_b^* < \tau_{b_{max}}^*, C)}{W_s'(0 < \tau_b^* < \tau_{b,c}^*, C)} \quad (2.62)$$

2.7.3. Deposition Algorithm

In SEDIMENT IIIA, deposition of suspended sediment occurs when, 1) the flow is decelerating, i.e. $\tau_b(t+\Delta t) < \tau_b(t)$, and 2) when $\tau_b(t+\Delta t) < \tau_{b_{max}}$. When these two conditions are met at any node, the rate of deposition is calculated as follows. The value of $\tau_{b,c}^*$ is evaluated using Eq. 2.62. Inasmuch as the log-normal relationship was found not to be suitable for $\tau_b^* < 0.25$, the minimum $\tau_{b,c}^*$ value is set equal to 0.25. Therefore, Eqs. 2.54 - 2.57 are always used to calculate the value of dC/dt for $\tau_b^* < 0.25 < \tau_{b,c}^*$ (Range I) while Eqs. 2.54-2.57 and

2.60-2.61 are used for $\tau_b^* > \tau_{b,c}^*$ with $C<C_1$. The maximum allowable value for $\tau_{b,c}^*$ is 0.95; therefore, Eq. 2.58 is used to determine dC/dt for $0.95 > \tau_{b,c}^* < \tau_b^* < \tau_{b_{max}}^*$ (Range II) with $C>C_1$.

The amount of dry mass of sediment deposited per time-step per element, M_D, is determined according to

$$M_D = \overline{\frac{dC}{dt}} \cdot \Delta t \cdot \bar{d}_e \tag{2.63}$$

where $\bar{d}_e = \frac{1}{2}\left(d_e(t) + d_e(t+\Delta t)\right)$ and $\overline{dC/dt}$ is given by

$$\frac{1}{2}\left(\frac{dC}{dt}_t + \frac{dC}{dt}_{t+\Delta t}\right) \tag{2.64}$$

in Range I

$$\frac{\bar{C}}{4\Delta t}\left(1 + \text{erf}\left(\frac{1}{\sqrt{2\pi}}\log\left(\frac{\tau_b^*-1}{4\exp(-1.27\cdot\tau_{b_{min}})}\right)^{2.04}\right)\right)\left[\text{erf}\left(\ln\left(\frac{\Delta t}{t_{50}}\right)\frac{0.434}{\sqrt{2\pi}\,\bar{\sigma}_2}\right) + 1\right] \tag{2.65}$$

in Range II.

In. Eq. 2.65, $\bar{\theta} = \frac{1}{2}\left(\theta(t) + \theta(t+\Delta t)\right)$, where $\theta = C$, t_{50}, τ_b^* and σ_2. Equation 2.65 was obtained by integration of Eq. 2.58 from t=0 to $t=\Delta t$. The thickness of the bed formed by M_D is calculated in Subroutine NEWBED using the procedure described in Section 2.5.2. The sink term in the governing equation (Eq. 2.11) is given by Eq. 2.64 in Range I and for $C < C_1$ in Range II, and by Eq. 2.65 for $C > C_1$ in Range II.

For unsteady flows, as occur in estuaries, the value of C_{eq}, which is the steady state value of the suspended sediment concentration found in laboratory tests under steady flows, is assumed to be zero. Nevertheless, the laboratory determined log-normal relationship for dC/dt, as given by Eq. 2.65, is used for Range II in the deposition algorithm for the following reasons. The time-step, Δt, used in estuarial sediment transport problems is typically of the order

$0.1t_{50} < \Delta t < 10t_{50}$. Therefore, dC/dt (given by Eq. 2.65) is significantly greater than zero at time Δt. This implies that after any time interval Δt, the suspended sediment concentration, $C(t+\Delta t)$, does not approach C_{eq}, but is assumed to be equal to the following:

$$C(t+\Delta t) = C(t) + \frac{\overline{dC}}{dt} \cdot \Delta t \qquad (2.66)$$

where $\overline{dC}/dt$ is given by Eq. (2.65). Thus, for unsteady flow conditions, the rate of deposition is considered to be a function of C_{eq} (given by Eqs. 2.45 - 2.47). Such a consideration is required for a realistic interpretation of laboratory deposition test results for the purpose of ascertaining the depositional rates in the unsteady estuarial environment.

In the next section, the influence of salinity on estuarial sediment transport processes is described and incorporated into SEDIMENT IIIA.

2.8. Influence of Salinity on Transport Processes

In this section a qualitative discussion of the effect of salinity on the inter-particle forces between cohesive sediment (predominantly clay) particles, the bed structure, and the rates of surface erosion, coagulation and deposition is given. Results from laboratory erosion and deposition tests are also presented and interpreted. Salinity is the mass in grams of the dissolved inorganic material in one kilogram of seawater after: 1) the bromide and iodide are replaced by the equivalent amount of chloride, and 2) the carbonate is converted to oxide (Lasater, 1975). Thus, salinity includes the effect of all the dissolved salts in sea water and hence the effect of cations (e.g. Na^{+}, Mg^{+2}, Ca^{+2}, etc.) as well as anions (e.g. Cl^{-}, SO_4^{-2}, etc.).

2.8.1. Effect of Salinity on Interparticle Forces

The relationship between clay particles and water molecules is governed by the inter-particle electro-chemical forces. Clay particles are structurally complex, and have several different configurations and groupings as well as electric charges, all of which affect their association with water molecules (Grimshaw, 1971). Water molecules possess a permanent electrical inbalance or dipole moment which results

from the molecular arrangement of the oxygen and hydrogen atoms. According to Grim (1962), the electrostatic field emanating from the surface of a clay particle orients the polar water molecules in the pores separating adjacent particles.

As noted in Section 2.1, inter-particle forces consist of both attractive and repulsive forces. The attractive forces present are the London-van der Waals, and are due to the nearly instantaneous fluctuation of the dipoles which result from the electrostatic attraction of the nucleus of one atom for the electron cloud of a neighboring atom (Grimshaw, 1971). These electrical attractive forces are weak, and are only significant when the interacting atoms are very close together. However, they are strong enough to cause structural build-up as they are additive between pairs of atoms. Thus, the total attractive force between two clay particles is equal to the sum of the attraction between all the atoms comprising both particles. This additive effect results in a larger attractive force and to a smaller decrease in this force with increasing particle separation. Figure 2.33 shows qualitatively the relationship between the attractive energy V_a and the particle separation distance. V_a is inversely proportional to the sixth power of the separation distance for two atoms and to the second power for two spherical particles. The magnitude of V_a decreases with increasing temperature and is dependent upon the geometry and the size of adjacent clay particles. V_a has been found to be only slightly dependent upon the salt concentration (i.e. salinity) of the medium (van Olphen, 1963).

The repulsive forces in cohesive sediments are due to the repulsive forces of the nuclei of adjacent atoms. The repulsion potential increases in an exponential fashion with decreasing particle separation. The magnitude of these forces is dependent upon the salinity, decreasing with increasing salinity as shown in Fig. 2.33, where V_r is the repulsive energy. This dependence of V_r on the salinity can best be explained using the concept of the electrical double layer and the surrounding diffuse layer. van Olphen (1963) states that the double layer is composed of the net electrical charge of the elementary clay particle and an equal quantity of ionic charge of opposite sign located in the medium near the particle surface. Thus, the net electrical

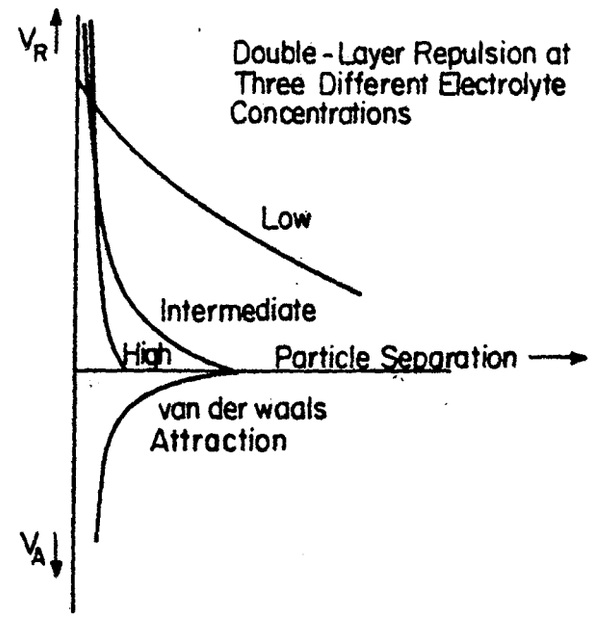

Fig. 2.33 Repulsive and Attractive Energy as a Function of Particle Separation at three Electrolyte Concentrations (after van Olphen, 1963).

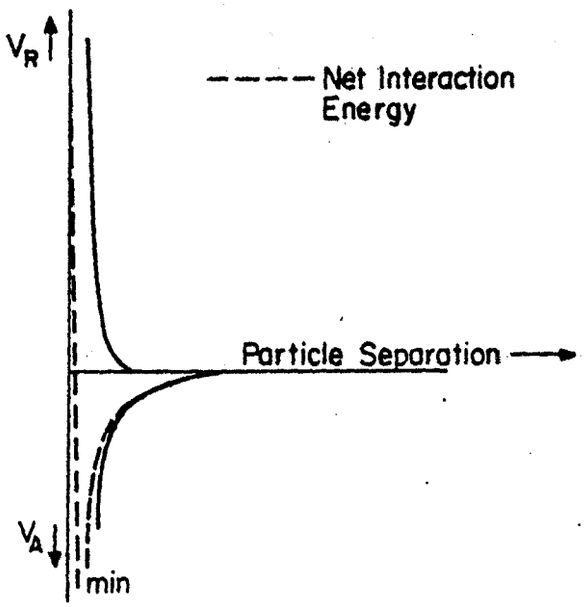

Fig. 2.34 Net Interaction Energy as a Function of Particle Separation at High Electrolyte Concentration (after van Olphen, 1963).

charge is balanced in the surrounding medium. The ions of opposite charge are called the counter-ions, i.e. cations. The counter-ion concentration increases with decreasing distance from the particle surface. This layer of counter-ions is referred to as the diffuse layer. A clay particle and the associated double layer is referred to as a clay micelle (Partheniades, 1971). When the salinity is increased, the diffuse layer is compressed toward the particle surface (van Olphen, 1963). The higher the salinity, and as well the higher the valence of the cations which compose the diffuse layer, the more this layer is compressed and the greater the repulsive force is decreased.

With a high salinity, corresponding to a value approximately that of seawater (35 ppt), the attractive forces become predominant at all but extremely small particle separation distances. The interaction potential, determined by summing V_a and V_r, reflects this dominance, and shows the highest attractive potential (primary minimum) at separation distances on the order of 1 nm (10^{-9}m) (Parker, 1980). At distances less than this the short range repulsive forces are predominant (van Olphen, 1963). Figure 2.34 shows this net interaction potential as a function of particle separation for high salinity. Thus, two clay particles will adhere when they reach the separation distance at which the primary minimum occurs. Destabilization occurs at a maximum rate due to the presence of attractive forces even at relatively great distances.

For medium and low salinities, on the order of 10-15 ppt and 1-2 ppt respectively (Parker, 1980), repulsive forces are predominant at separation distances of approximately 10 nm where a local repulsive potential maximum occurs (Figs. 2.35 and 2.36). At distances closer than this, these interaction potentials are similar to that for high salinity. As indicated by these figures, the destabilization of two or more particles would be expected to decrease for decreasing salinities as a result of net repulsive forces existing at increasingly larger distances (van Olphen, 1963). Nevertheless, clay particles are known to become cohesive at salinities between 0.6 and 2.4 ppt (Ariathurai, 1974).

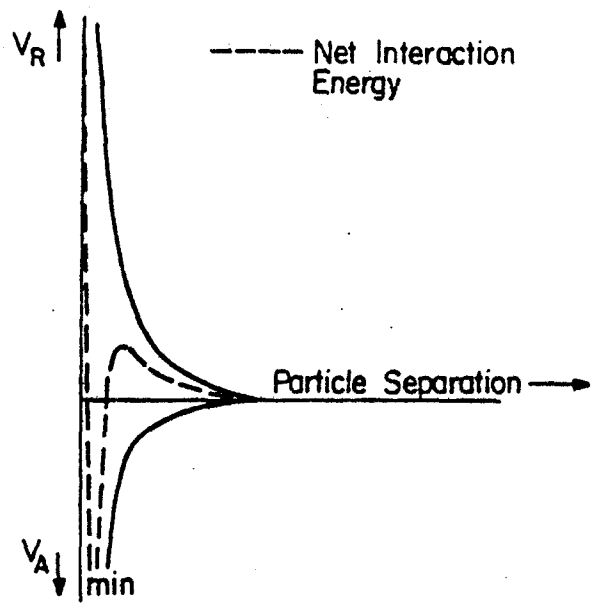

Fig. 2.35 Net Interaction Energy as a Function of Particle Separation at Intermediate Electrolyte Concentration (after van Olphen, 1963).

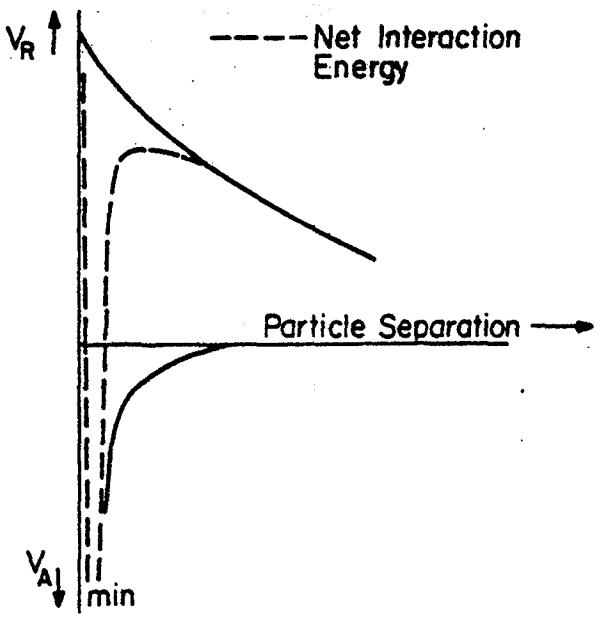

Fig. 2.36 Net Interaction Energy as a Function of Particle Separation at Low Electrolyte Concentration (after van Olphen, 1963).

2.8.2. Effect of Salinity on Bed Structure

For most cohesive soils the inter-particle and inter-floc contact is considered to be the only significant region between particles where normal stresses and shear stresses can be transmitted (Mitchell et al., 1969). In particular, it seems very likely that the primary role of the double-layer interaction and other physico-chemical forces is to control the structure of the soil and to alter the transmitted stresses from what they would be due to the applied flow-induced shear and overburden normal stresses alone. Two factors that effect the structure of a cohesive soil, swelling and permeability, and the effect salinity has on these factors are discussed next.

The degree of swelling which occurs when a cohesive soil is immersed in a fluid is influenced by factors such as the amount of clay, shape and size of the soil particles, the salinity and the sodium adsorption ratio (SAR) of the eroding and pore fluid, and the presence of an imposed load on the swelling areas (Grimshaw, 1971). Sargunam et al. (1973) state that as the salinity of the eroding fluid decreases or the SAR increases, the more surface clay particles will swell. This swelling causes a weakening of the inter-particle attractive forces and thus increases the susceptibility of the soil to erosion. Increasing the salinity of the eroding fluid causes a greater compression of the diffuse layer, thereby reducing the repulsive forces of soil particles which serves to limit the amount of swelling.

Sargunam et al. (1973) found that when the salinity of the eroding fluid is greater than that of the pore fluid the yield strength of the soil is greater and therefore the erosion potential is decreased. In this case the osmotic pressure gradient across the fluid-bed interface may result in deswelling, or consolidation of the bed sediment particles, which would cause an increase in the inter-particle bonding forces and therefore lessen the susceptibility to erosion.

It is believed that while this phenomenon of swelling influences to some degree the structure and hence the erosion potential of a cohesive bed, it is not nearly as significant as the upward flux of pore water due to gravitational forces in a consolidating mud.

Quirk and Schofield (1955) found that the degree of permeability of clay soils depends upon the nature and the concentration of the cations

present in both the eroding and pore fluids. In particular they found that the permeability increased with an increase in the salinity of the eroding fluid. Swelling and stabilization (i.e. decoagulation) are generally considered to be the main reasons for changes in the permeability. The former can cause either partial or total blockage of soil pores which would result in a decrease in permeability. Stabilization essentially occurs during swelling when the clay particles have separated to the extent that the inter-particle repulsive forces are dominant over the attractive forces. Since an increase in the salinity of the eroding fluid serves to limit the amount of swelling which occurs and thus restricts the amount of stabilization as well, an increase in salinity would result in increased permeability. The converse was found to occur as well since, as stated previously, a decrease in the salinity of the eroding fluid causes an increase in the degree of swelling and stabilization.

2.8.3. Effect of Salinity on Surface Erosion

Sherard et al. (1972) have shown that the susceptibility of a cohesive sediment bed to erosion depends on two factors: 1) the pore fluid composition, as characterized by the SAR, and 2) the salinity of the eroding fluid. It was found that as the eroding fluid salinity decreases, soil resistivity to surface erosion decreases as well. These results were verified by Arulanandan et al. (1975). In addition, Sherard et al. (1972) found that the erosion resistance decreased by either the exchange of cations or a reduction of the valence of the cations in the pore fluid. Kandiah (1974) and Arulanandan et al. (1975) confirmed these findings by showing that the erosion resistance decreased and the rate of surface erosion increased with increasing SAR (and therefore decreasing valency of the cations) of the pore fluid. Figure 2.37 shows such a relationship between the SAR and the critical shear stress for erosion, which is a measure of soil resistance to erosion (Alizadeh, 1974).

Experiments were conducted during this study to determine the effect of the eroding fluid salinity on the rate of surface erosion. The experiments were performed in the rotating annular flume described previously using bottom sediment from Lake Francis, Nebraska. The

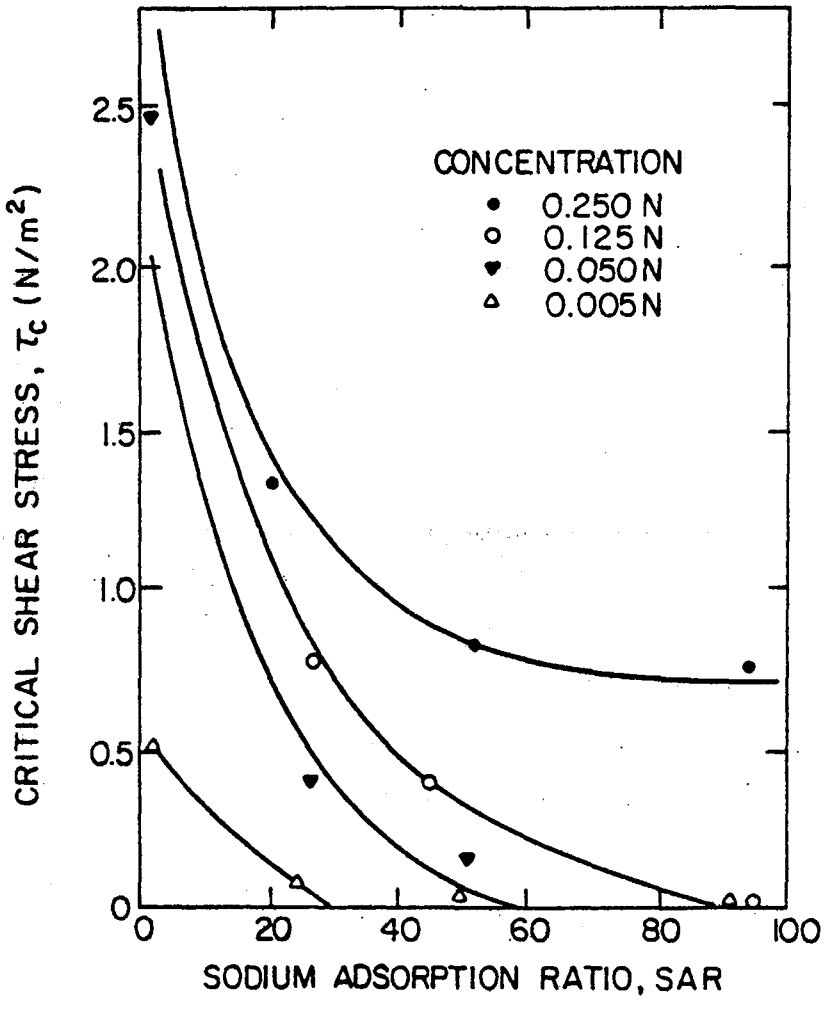

Fig. 2.37 Critical Shear Stress versus SAR for Montmorillonitic Soil (after Alizadeh, 1974).

particle size distribution of this sediment, determined using a standard hydrometer analysis (described in Appendix B), indicated that 50% of the material was finer than 2μm (clay-sized particles) and 90% finer than 20μm. The organic content of the sediment was approximately 1.5%. X-ray diffraction analysis showed that the sediment was predominantly composed of smectite, illite, kaolinite and quartz. The cation exchange capacity (CEC) of the sediment was found to be about 100 meq./100 gm, which indicates a higher percentage of smectite than the other two clay minerals. Analysis of water from the lake indicated the presence of Na^{+}, K^{+}, Ca^{+2}, Mg^{+2}, Al^{+3}, Fe^{+3}, Cl^{-}, SO_4^{-2}. These above cations and anions would be expected to be present in the sediment as well. The average pH of the lake water was 8.6. The sediment was repeatedly washed in an attempt to remove these free salts so that their effect on the sediment properties was minimized. The washing was performed by immersing the sediment in deionized water, vigorously stirring the sediment and water, allowing time for the sediment to settle out of suspension by gravity, and then siphoning off the clear supernatant water. This procedure was repeated at least three times.

Commercial grade sodium chloride dissolved in different proportions in tap water constituted the eroding fluid in these experiments. The manufacturers of the sodium chloride supplied the data given in Table 2.3 regarding the contents of the processed sodium chloride. The cation concentrations in sea salt, also included in this table, were obtained from Bolz and Tuve (1976).

Table 2.3

Cation Concentrations in Processed
Sodium Chloride and Standard Sea Salt

Cation	NaCl	Sea Salt
Sodium	357460.ppm	301720.ppm
Calcium, Magnesium	50.	47770.
Potassium	10.	10860.
Phosphate	1.0	-
Iron	0.5	-

Tests were conducted for the following five salt concentrations: 0, 1, 2, 5 and 10 ppt by weight. However, as the concentrations of the three most abundant cations, Na^{+}, Ca^{+2} and Mg^{+2}, in the manufactured salt were different from those in standard sea salt (see Table 2.3), the five different eroding fluids used in these experiments were not exactly equivalent to sea water at the various salinities. In spite of this, useful qualitative and quantitative information was obtained regarding the effect of varying dissolved salt (i.e. electrolyte) concentrations on the erosive characteristic of the mud.

The experimental procedures used in these tests has been described in Section 2.6.1. Suspended sediment concentration as a function of time as well as the bed bulk density profile were measured. The values of τ_m, T_m and T_d were 0.9 N/m^2, 24 hours and 40 hours respectively (see Fig. 2.18). The bed shear stress during resuspension ranged from 0.14 to 0.52 N/m^2.

Figure 2.38 shows the bed bulk density profiles in a non-dimensional form for each salt concentration. The bulk density generally increases with increasing salinity. These profiles were used in conjunction with the concentration-time profiles for computing the depths of erosion resulting from the different bed shears stresses.

Using the method described in Mehta et al. (1982a) the bed shear strength (or the critical shear stress for erosion), τ_c, as a function of depth below the initial bed surface was determined for each salinity (Fig. 2.39). Two trends are observed in this graph. First, τ_c increased with depth in the upper part of the bed for all salinities (no definite data could be obtained for the lower part of the bed, i.e. for $z > 0.5$ cm, inasmuch as this portion of the bed did not erode during these experiments). Second, τ_c increased with increasing salinity from 0 to 2 ppt; thereafter, for salinities up to 10 ppt, no measurable increase in τ_c occurred.

Rates of surface erosion, ε, were calculated from the concentration-time profiles in the following manner. Smooth curves were drawn through the data points and values of concentration were read off these curves at 0, 5, 15, 30 and 60 minutes after each change in the bed shear stress. Values of dC/dt were determined using a backward difference differentiating scheme. Values of ε were calculated using Eq. 2.32.

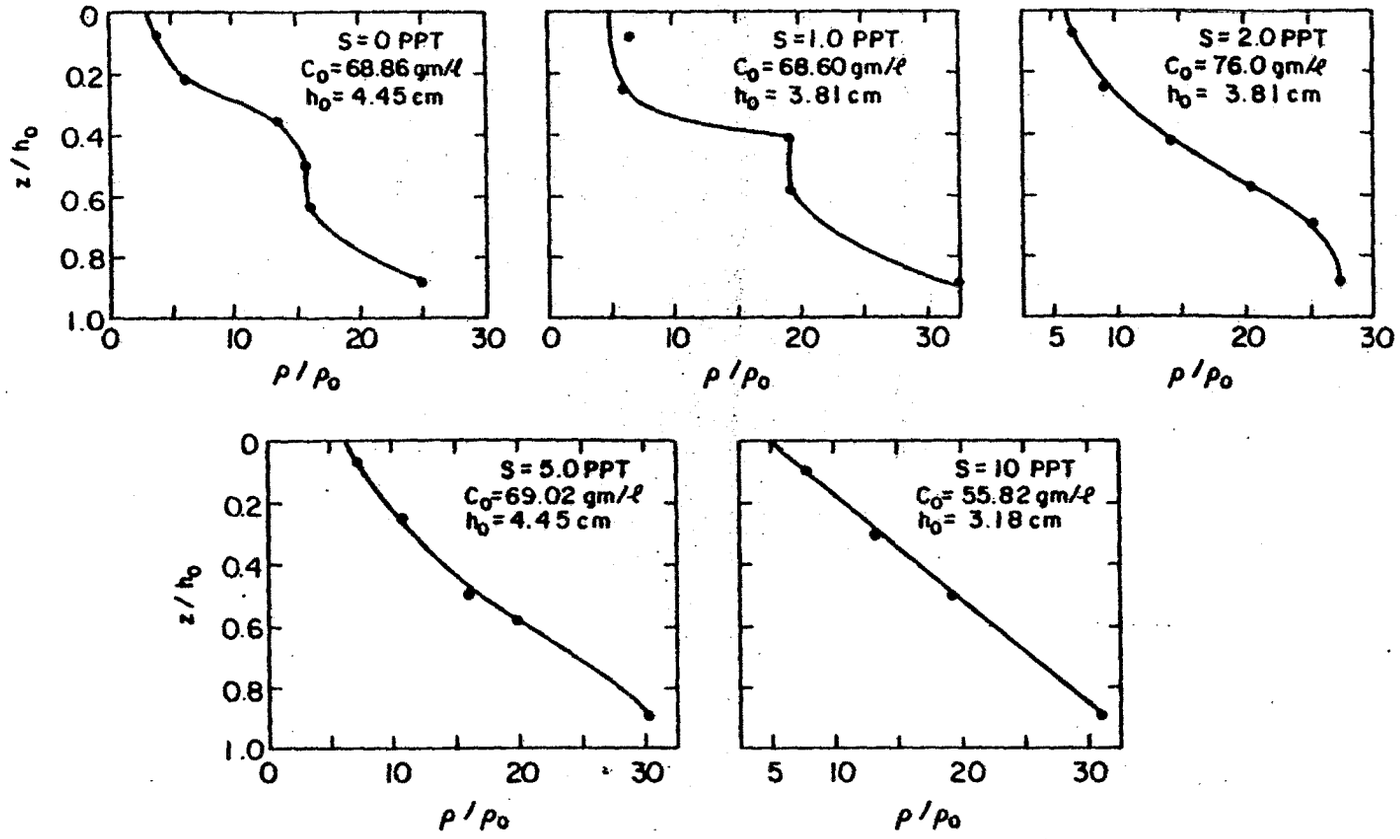

Fig. 2.38 Dimensionless Bed Density versus Bed Depth Profiles for Salinities of 0, 1, 2, 5 and 10 ppt.

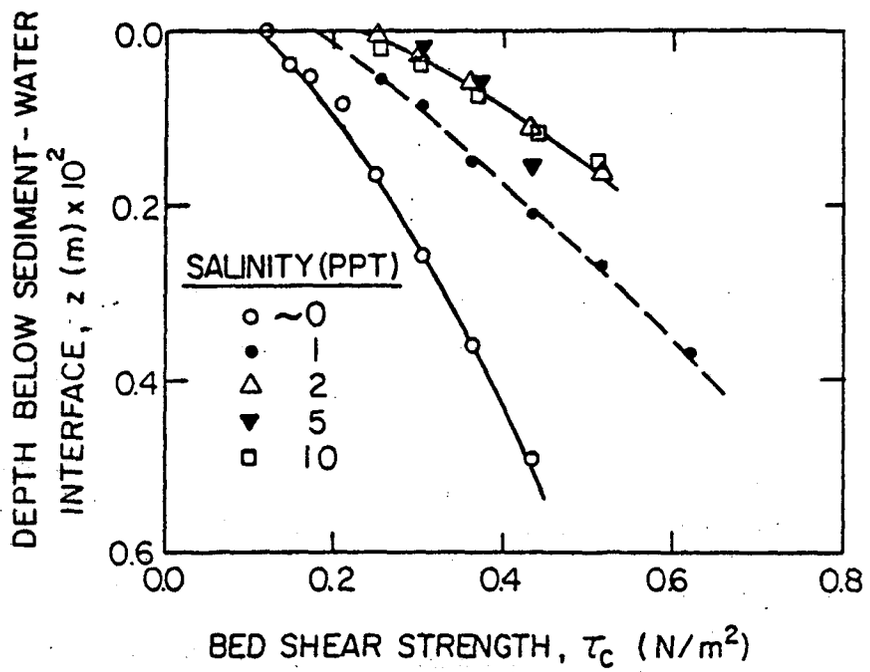

Fig. 2.39 Bed Shear Strength Profiles as a Function of Salinity.

The logarithm of the erosion rate was plotted against the average normalized excess shear stress, i.e. $(\tau_b - \bar{\tau}_c)/\bar{\tau}_c$, where $\bar{\tau}_c$ is the average shear strength of the bed layer that was eroded by the bed shear stress τ_b. Figure 2.40 shows these plots for the 1 ppt salinity test. The slope of each line, α, and the ordinate intercept, ε_o, were determined from each graph. The values of α and ε_o plotted as a function of depth for each salt concentration are given in Figs. 2.41 and 2.42 respectively.

Before evaluating these results it is appropriate to discuss the parameters other than the salt concentration that varied from test to test, in order to examine the possible significance of their variance on the rate of erosion. The other uncontrolled parameters were the temperature, pH and the SAR of the eroding fluid. The rotating annular flume does not have the facility to maintain a constant water temperature during the course of an experiment. As a result the temperature typically varied 3° to 5°C over the seven to eight hour duration. A temperature variation of this magnitude has been found to

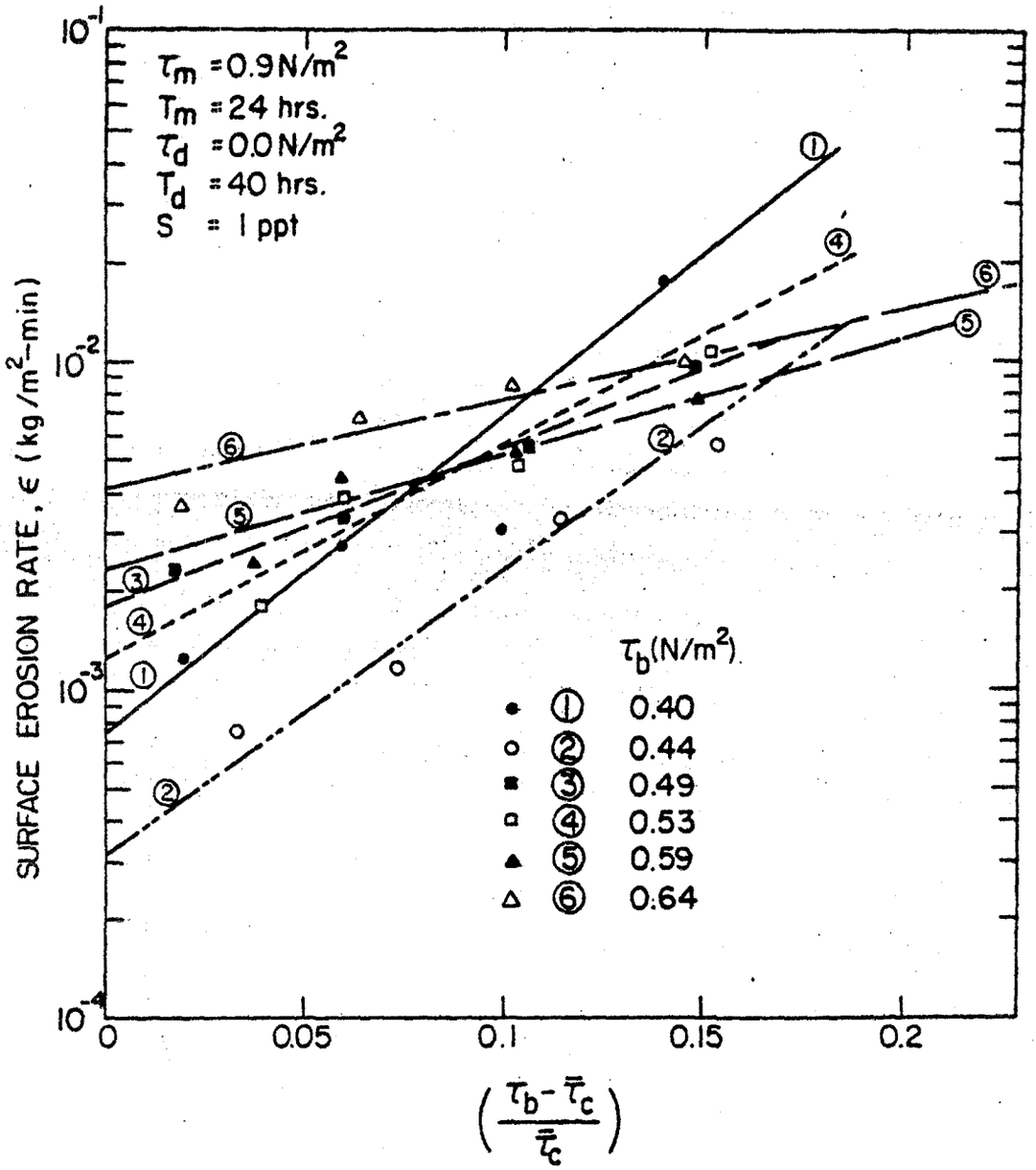

Fig. 2.40 Surface Erosion Rate ε versus Normalized Excess Shear Stress $(\tau_b - \bar{\tau}_c)/\bar{\tau}_c$.

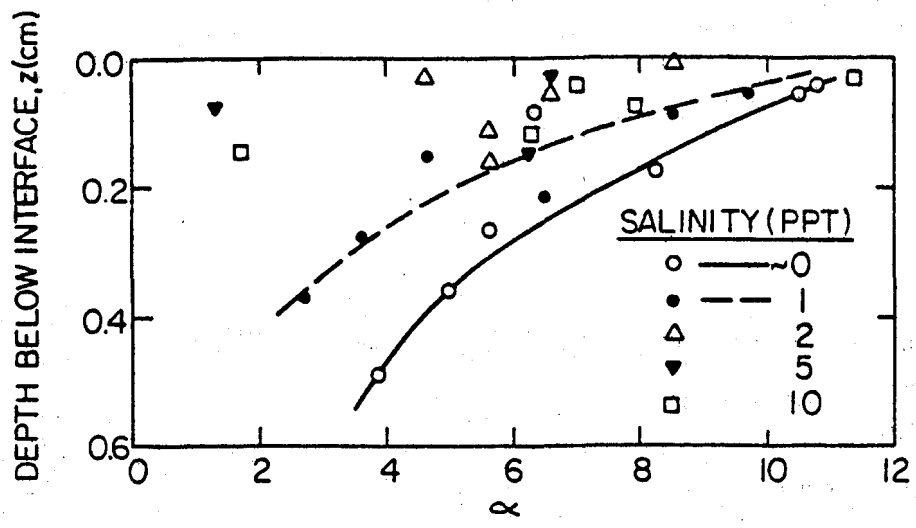

Fig. 2.41 Slope, α, Plotted Against Depth Below Bed Surface, z, as a Function of Salinity.

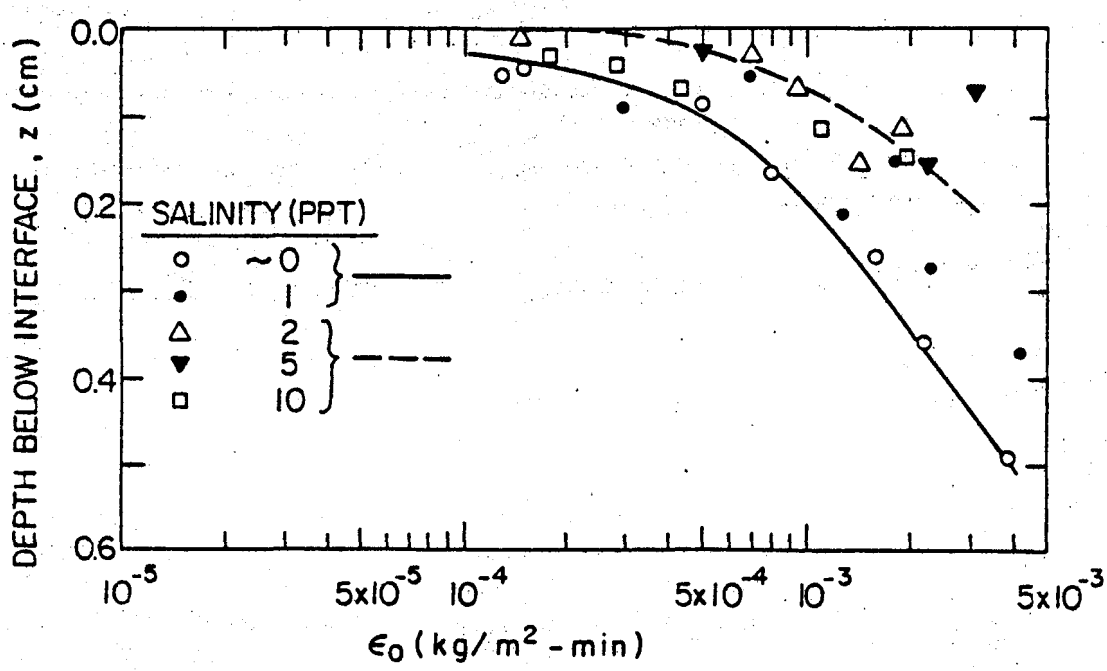

Fig. 2.42 Ordinate Intercept, ϵ_0, Plotted Against Depth Below Bed Surface, z, as a Function of Salinity.

result in less than a 3% decrease in the bed shear strength (Kelly and Gularte, 1981) and is considered to be insignificant. Likewise, over the one per-cent salt concentration range used in these experiments the variation in pH is considered to be not significant. However, due to the relatively small quantitites of Ca^{+2} and Mg^{+2} compared to that of Na^{+}, the SAR values were rather large and increased significantly with increasing salt concentration. For example, the SAR values varied from 110 to 349 as the salinity increased from 1 to 10 ppt. Alizadeh (1974) showed that both the concentration of the electrolyte and the SAR are important controlling factors in the process of coagulation. Specifically he found that the effect of salt concentration gradually decreases with increasing SAR. Thus, the varying SAR values are considered to have had some, albeit unmeasured, effect on these experiments.

Analysis of the variation in the bed density profiles with salinity, shown in Fig. 2.38, revealed no discernable relationship. It is felt that further investigations are necessary to determine if any relationship exists between ρ_B and the salt concentration of the eroding fluid for a stratified fine sediment bed.

The bed shear strength profiles, shown in Fig. 2.39, were analyzed by determining the weighted depth-averaged value (weighted with respect to spacing, i.e. depth, between adjacent data points) of τ_c at the five different salt concentrations, S. The following relationship was found:

$$\begin{aligned} \tau_c(S) &= \tau_c(S=0)\cdot\left(\frac{1}{2}\cdot S + 1\right) \quad \text{for } 0 < S < 2 \\ \tau_c(S) &= 2\cdot\tau_c(S=0) \qquad\qquad\quad \text{for } S > 2 \end{aligned} \tag{2.67}$$

where S is in ppt. This relationship was incorporated into Subroutine NEWBED algorithm in the following manner. The discretized value of τ_c at the top of the uppermost new deposit bed layer is changed instantaneously, i.e. during the same time-step, at every element where the elemental average salinity value changes. For the second bed layer the discretized τ_c value is not changed during the first time-step during which the average value of salinity changes; it is changed at the time-step during which the salinity changes for the second time.

However, for this bed layer the new τ_c value is determined using Eq. 2.67 and the second preceding value of the salinity at that element. This procedure is similarly repeated for the remaining new deposit bed layers. This method of incorporating the effect of the salinity of the eroding fluid on the bed shear strength profile was used in order to account, at least partially, for the finite amount of time it takes for denser (i.e. higher salinity) eroding fluid to diffuse downward into the bed or for denser pore fluid to diffuse upward into the overlying eroding fluid. The diffusion coefficients of Cl^- and Na^+ in Pacific red clay and Lake Ontario sediment were experimentally determined to be of the order of 10^{-5} - 10^{-6} cm^2/sec at a temperature of 24°C (Li and Gregory, 1974; Lerman and Weiler, 1970). These extremely small diffusion coefficients indicate that rates of diffusion in unconsolidated sediments are generally from one half to one twentieth of the diffusion rates in the eroding fluid (Manheim, 1970).

For the first time-step the initial salinity value at each element is used to determine the τ_c values in both the unconsolidated and the partially consolidated bed layers, while the salinity of the pore water in the consolidated original bed layers, an input parameter in SEDIMENT IIIA, is used to evaluate the τ_c values in this bed section. The τ_c values of the fully consolidated bed layers are thereafter assumed to be invariant with respect to the salinity of the eroding fluid. The justification for this assumption is based on the observation that dissolved silica concentrations in pore waters of Lakes Ontario, Erie and Superior sediments were, in general, invariant with respect to depth after the first 20 cm below the water-mud interface (Nriagu, 1978). Therefore, the salinity of the eroding fluid would not be expected to influence that of the pore fluid below the top 20 cm of the bed, which clearly encompasses the consolidated bed section.

The values of α and ε_0 are seen in Figs. 2.41 and 2.42, to decrease and increase, respectively, with increasing salinity. However, inasmuch as these parameters are considered to be characteristic properties of the sediment bed and as the effect of salinity on another bed property, τ_c, which is as well estimated indirectly from measured data, has already been incorporated into the model, it was not necessary to consider the variation of α and ε_0 with salinity in the erosion algorithm.

2.8.4. Effect of Salinity on Coagulation

As noted in Section 2.1, when salt is added to water containing suspended particles in the clay size range, and to a lesser degree in the silt range, the coagulation characteristics of the sediment particles are affected. This effect can be explained by briefly reviewing the theory of coagulation.

In order for dispersed colloidal particles to coagulate and possibly form comparatively large aggregates, two separate processes must occur first; repeated collisions of the particles and cohesion of the colliding particles. The size, strength and the density of the resultant aggregates play an important role in characterizing the transport of cohesive sediments under tidal conditions. Cohesion and collision, discussed in detail by among others Kruyt (1952), Einstein and Krone (1962), Krone (1962), Partheniades (1964), O'Melia (1972) and Hunt (1980) are reviewed here.

As discussed in Section 2.8.1, cohesion of colloidal particles is caused by the presence of net attractive electro-chemical surface forces on the particles. The latter condition is promoted by increased concentration of dissolved ions and/or increased ratio of multivalent to monovalent ions, both of which serve to depress the double layer around micelles and thus allow the attractive London-van der Waals and coulombic forces to predominate (Krone, 1962). Since sea salt is a mixture of salts, with monovalent sodium ions and divalent calcium and magnesium ions prevalent in natural electrolytes, the effect of these salts on cohesion is determined by the relative abundances of mainly these three ions (see Table 2.3), the latter being indicated by the SAR value. The relationship between the SAR and salinity is seen in Fig. 2.43. As noted in Section 2.1, the cation exchange capacity (CEC), along with the salt concentration and SAR all serve to determine the net inter-particle force and thus the potential for micelles to become cohesive (Ariathurai, 1974).

Kandiah (1974) found that the boundary between the dispersed and coagulated states for the three main clay groups, kaolinite, illite and montmorillonite, varied with the SAR, total salt concentration and pH of the solution (see Figs. 2.44a, b, and c). The dashed lines in these figures represent interpolated boundary curves for a pH range of 7.5 to

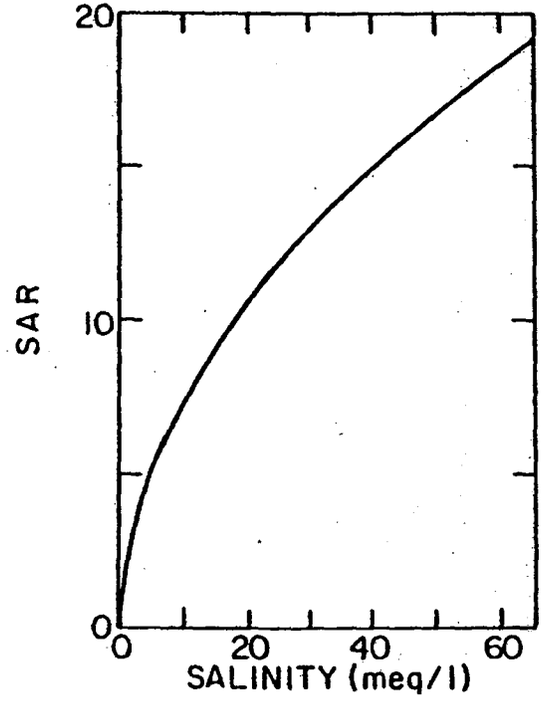

Fig. 2.43 Variation of SAR with Salinity (Sea Salt Concentration)(after Ariathurai, 1974).

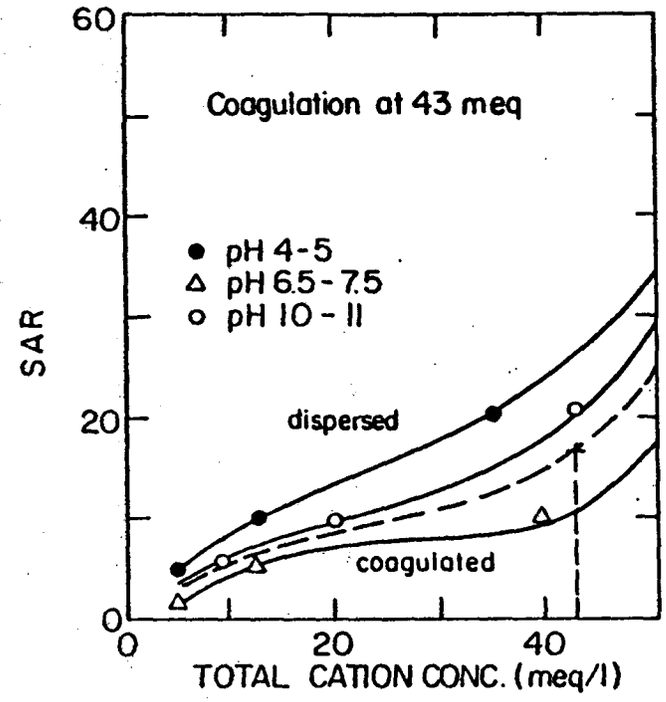

Fig. 2.44a Coagulation-Dispersion Boundary Curves for Montmorillonite at three pH Ranges (after Kandiah, 1974).

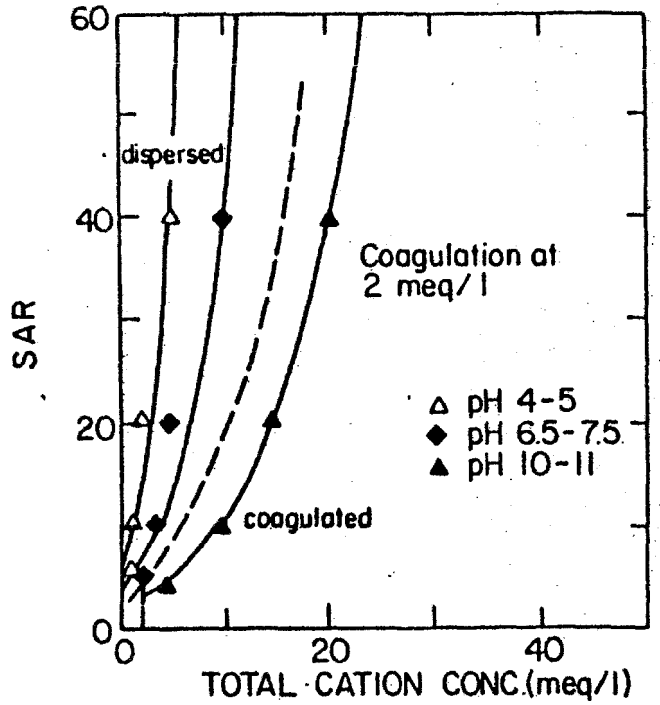

Fig. 2.44b Coagulation-Dispersion Boundary Curves for Illite at three pH Ranges (after Kandiah, 1974).

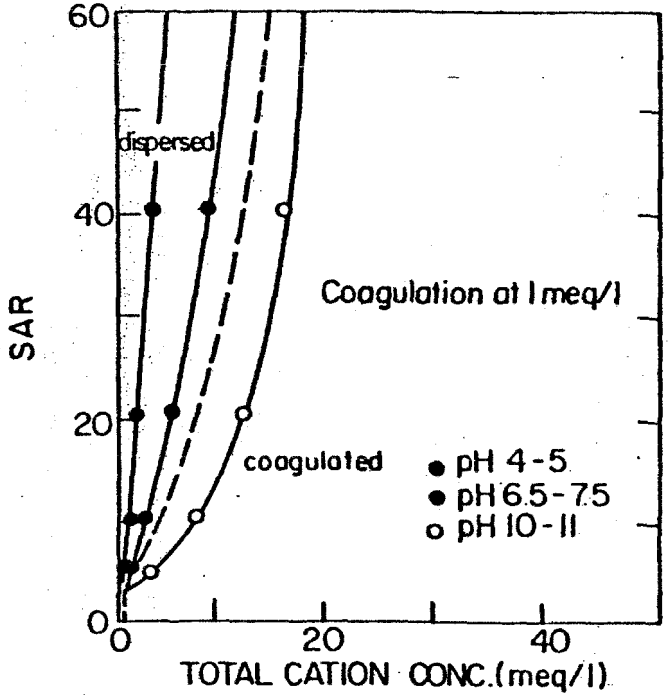

Fig. 2.44c Coagulation-Dispersion Boundary Curves for Kaolinite at three pH Ranges (after Kandiah,1974).

8.5, which is the range found in sea water at all salinities. It is evident that the boundary between the dispersed and coagulated states for these three clays are different. Kaolinite becomes cohesive at a salinity of 0.6 ppt, illite at 1.1 ppt and montmorillonite at 2.4 ppt (Ariathurai, 1974). Whitehouse et al. (1960) and Edzwald et al. (1974) reported that the cohesiveness of these micelles develops quickly at the given salt concentrations, and that little increase in coagulation occurs at higher concentrations, which implies that the micelles must have attained the maximum degree of cohesion. The rapid development of cohesion and the low salt concentrations at which the main clay types become cohesive indicates that cohesion is primarily affected by salinity variations near the landward end of an estuary where salinities are less than about 3 ppt.

The above cohesion mechanism is referred to as salt flocculation. There is another cohesion mechanism that operates in water between micelles in the absence of salt, and hence it is termed non-salt flocculation. However, in an estuary the conditions are conducive for destabilization to be caused by salt flocculation (i.e. depression of the diffuse double layer). Both types of destabilizing mechanisms are reported in detail by Lambe (1953).

The collision frequency, I, for suspended sediment particles of effective diameters d_i and d_j is given by (Hunt, 1980):

$$I = \beta(d_i, d_j) \cdot dN_i \cdot dN_j \tag{2.68}$$

where $\beta(d_i, d_j)$ = collision function determined by the type mechanism (discussed below), which has units of fluid volume per unit time, and dN_i = number of particles with sizes between d_i and $d_i + d(d_i)$ per unit volume of the fluid.

There are three principal mechanisms of inter-particle collision in suspension, and these influence the rate at which elementary sediment particles coagulate. The first is due to Brownian motion resulting from thermal motions of molecules of the suspending ambient medium. The collision function corresponding to this mechanism is given by (Hunt, 1980):

$$\beta_b(d_i, d_j) = \frac{2}{3} \frac{kT_k}{\mu} \frac{(d_i + d_j)^2}{d_i d_j} \tag{2.69}$$

where k = Boltzmann constant, T_k = absolute temperature and μ = dynamic viscosity of the fluid. Generally, coagulation rates by this mechanism are too slow to be significant in estuaries unless the suspended sediment concentration exceeds 10 g/l. Aggregates formed by this mechanism are weak, with a lace-like structure, and are easily fractured by shearing in the flow or are crushed easily when deposited (Krone, 1962).

The second mechanism is that due to internal shearing produced by local velocity gradients in the fluid. Collision will occur if the paths of the particle centers in the velocity gradient are displaced by a distance which is less than the sum of their radii (referred to as the collision radius, R_{ij}, between the d_i and d_j size particles). The collision function is given as

$$\beta_{sh}(d_i,d_j) = \frac{G}{6} R_{ij}^3 \tag{2.70}$$

where G is the local shearing rate and $R_{ij} = d_i+d_j$. Aggregates produced by this mechanism tend to be spherical, and are relatively dense and strong because only those bonds that are strong enough to resist the internal shearing due to local velocity gradients can survive. The frequency of collision is especially high in an estuarial mixing region where a large number of suspended particles are found.

The third mechanism, differential sedimentation, results from the fact that particles of different sizes have different settling velocities. Thus a larger particle, due to its higher settling velocity, will collide with smaller, more slowly settling particles along its path and will have a tendency to "pick up" these particles on its way down. The collision function is expressed as

$$\beta_{ds}(d_i,d_j) = \frac{\pi g}{72\nu} \left(\frac{\rho_s-\rho_w}{\rho_w}\right)(d_i+d_i)^2|d_i^2 - d_j^2| \tag{2.71}$$

where ν = kinematic viscosity of the fluid, ρ_s = floc density and ρ_w = fluid density. This mechanism produces relatively weak aggregates and contributes to the often observed rapid clarification of estuarial waters at slack.

All three mechanisms operate in an estuary, with internal shearing and differential sedimentation generally being predominant in the water column, excluding perhaps the high density near-bed layer, where Brownian motion is likely to contribute significantly as a collision mechanism. Then again, internal shearing is probably more important than differential sedimentation during times excluding those near slack water, when collision and coherence due to differential settling would be expected to be the main mechanism controlling the rate of coagulation.

Hunt (1980) compared the values of the three collision functions (Eqs. 2.69 - 2.71) for collision of a d_i=1 μm size particle with varying sizes, d_j, of the colliding particle under the following conditions: temperature 14°C, shearing rate G = 3 sec^{-1}, and $(\rho_s-\rho_w)/\rho_w$ = 0.02. The comparison is shown in Fig. 2.45 and reveals that each collision mechanism is dominant over a certain particle size range. In this example, Brownian motion is the dominant mechanism for particles less than 1 μm, internal shearing is dominant for particles between 1 and 100 μm, and differential sedimentation is dominant for particles greater than 100 μm. Hunt states that the same ordering of the dominant collision mechanisms with increasing d_j would be achieved for collisions with other d_i sizes. Thus, the collision frequency is controlled not only by the prevailing flow conditions and local suspension concentration, but by the size of the colliding particles and/or flocs as well.

In summary, it is apparent that fine sediment transport in estuaries is strongly influenced by the coagulation behavior of dispersed sediment particles and by the properties (e.g. shear strength, density and size) of the resulting flocs and aggregates, which in turn are controlled by the salinity field, velocity gradients and the concentration of suspended sediments. In particular, the salinity of the suspending fluid effects the process of coagulation in two ways: 1) elementary clay particles become cohesive when the salinity is equal to or greater than 1-3 ppt, and 2) the presence of high velocity gradients in the estuarine mixing zone increase the collision frequency between dispersed particles and/or aggregates.

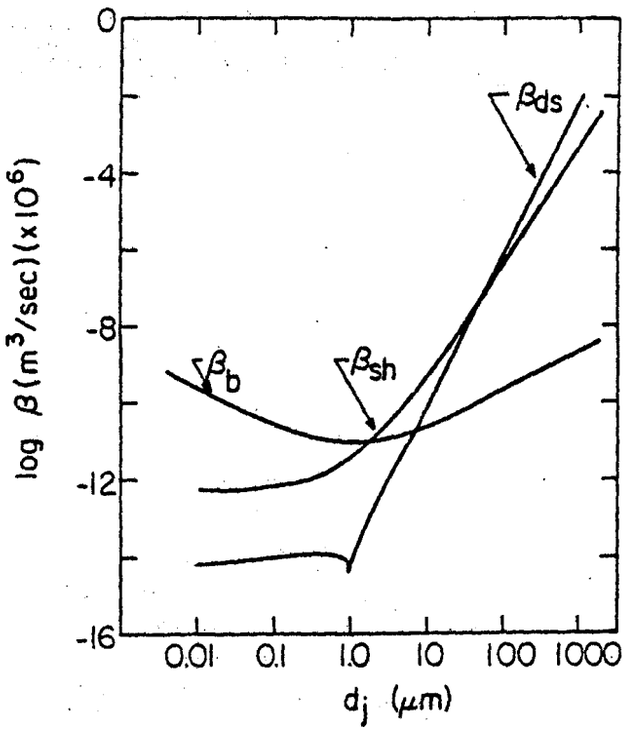

Fig. 2.45 Comparison of the Collision Functions for Brownian, Shear and Differential-Sedimentation Coagulation (after Hunt, 1980).

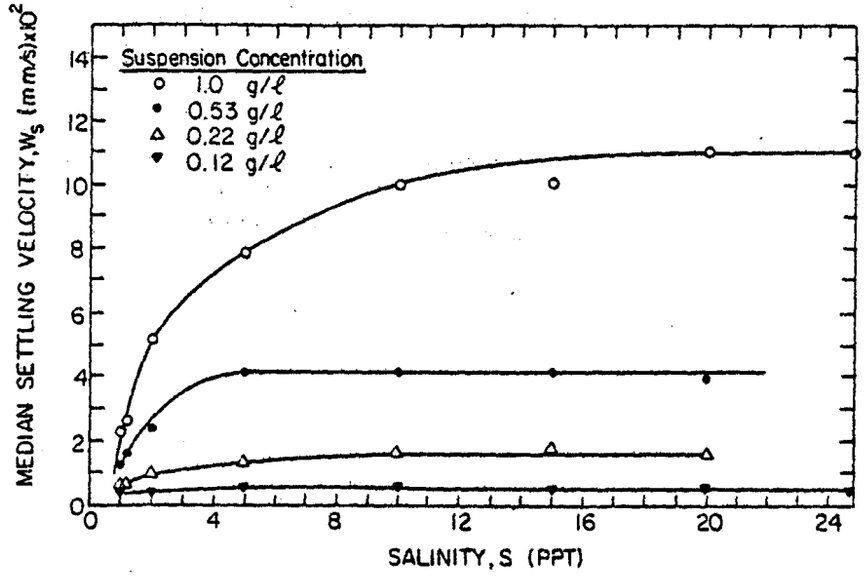

Fig. 2.46 Effect of Salinity on Settling Velocity of San Francisco Bay Mud (after Krone, 1962).

2.8.5. Effect of Salinity on Deposition

The larger, stronger aggregates of natural muds formed in a saline medium have been found to result in higher settling velocities (Krone, 1962; Owen, 1970) which, as apparent in Eq. 2.54, in turn result in higher rates of deposition. Thus, the effect of salinity on the deposition of fine sediments may be quantified in terms of a relationship between salinity and the median settling velocity, W_s, of a particular sediment.

Krone (1962) studied the effect of salinity and suspended sediment concentration on W_s of fine sediment from Mare Island Strait in San Francisco Bay. Hydrometer analysis showed that 60% by weight of this sediment was in the clay size range (i.e. < 2μm), with the remaining in the silt size range. X-ray diffraction and differential thermal analyses of the clay fraction revealed a large content of illite, montmorillonite and kaolinite clay groups along with small quantities of chlorite and quartz. The results from settling tests performed under quiescent conditions in one-liter cylinders showed the effect of both salinity and suspension concentration on W_s (Fig. 2.46). The influence of salinity on W_s is especially significant in the range 0-2 ppt, particularly for the 1.0 and 0.53 g/l suspension concentrations. This result is expected considering the discussion presented in Section 2.8.4. One possible explanation for the apparent increasing influence of salinity on W_s with increasing suspension concentration, as shown in this figure, is the following. As the suspension concentration increases, the number of collisions (by Brownian motion and differential settling mechanisms in such an experiment) would likewise increase and therefore promote the formation of larger aggregates with higher settling velocities. The lowest order aggregate that could be formed would be limited by the suspension concentration, so that even with an increase in salinity (and therefore a corresponding increase in cohesive forces), lower order aggregates with typically higher settling velocities could not form due to the insufficient concentration of suspended particles.

Owen (1970) studied the variation of W_s of a natural mud with salinity and suspension concentration. Approximately 55% of the mud was in the clay size range, with the remainder in the silt range. It was

revealed that the clay fraction was composed of, in order of abundance, illite, kaolinite, montmorillonite and chlorite. These settling tests were conducted in a two meter high bottom withdrawal settling tube.

The results of Owen's tests are shown in Figs. 2.47 and 2.48. These figures show that, in general, as the salinity and suspension concentrations are increased, increased cohesion and inter-particle collision result in higher coagulation rates with accompanying higher settling velocities. This trend corroborates that found by Krone (1962), except that no "leveling off" of W_s above a certain salinity value was found in these tests. The decrease in W_s above a given salinity and concentration, as observed in both figures, usually represents the onset of hindered settling. The effect of salinity on W_s is seen to be diminished at suspension concentrations in the hindered settling range.

Owen (1971) found a negligible effect of salinity on the settling velocity of natural aggregates at two different locations in the Thames River estuary. The salinities at the two sampling stations varied between 6-10 ppt and 21-26 ppt, respectively. Evidently, the effect of salinity on W_s at these salinities in a turbulent flow field was much less than that under quiescent conditions (see Fig. 2.47). This implies that the increased cohesion caused by the higher salinities was counter-balanced by the high internal shear rates which cause the aggregates to be broken apart.

Deposition tests were conducted at the University of Florida during the reported study in order to further investigate the effect of both salinity and bed shear stress on the settling rates of a natural mud. The mud used in these tests was sediment from Lake Francis, Nebraska (see Section 2.6.1 for a description of this sediment). The following salt concentrations were utilized in these tests: 0, 1, 2, 5 10, 20 and 35 ppt. The tests were conducted in the previously described rotating annular flume with a water depth of 0.31 m at values of the bed shear stress, τ_b, during deposition equal to: 0.0, 0.015, 0.10, 0.20 and 0.30 N/m^2. The initial concentration for these tests varied between 3.7 and 4.7 g/l. Before the start of each test, the sediment and water were mixed for two hours at a shear stress of 0.90 N/m^2. The shear stress was then reduced to the appropriate τ_b value and samples of the

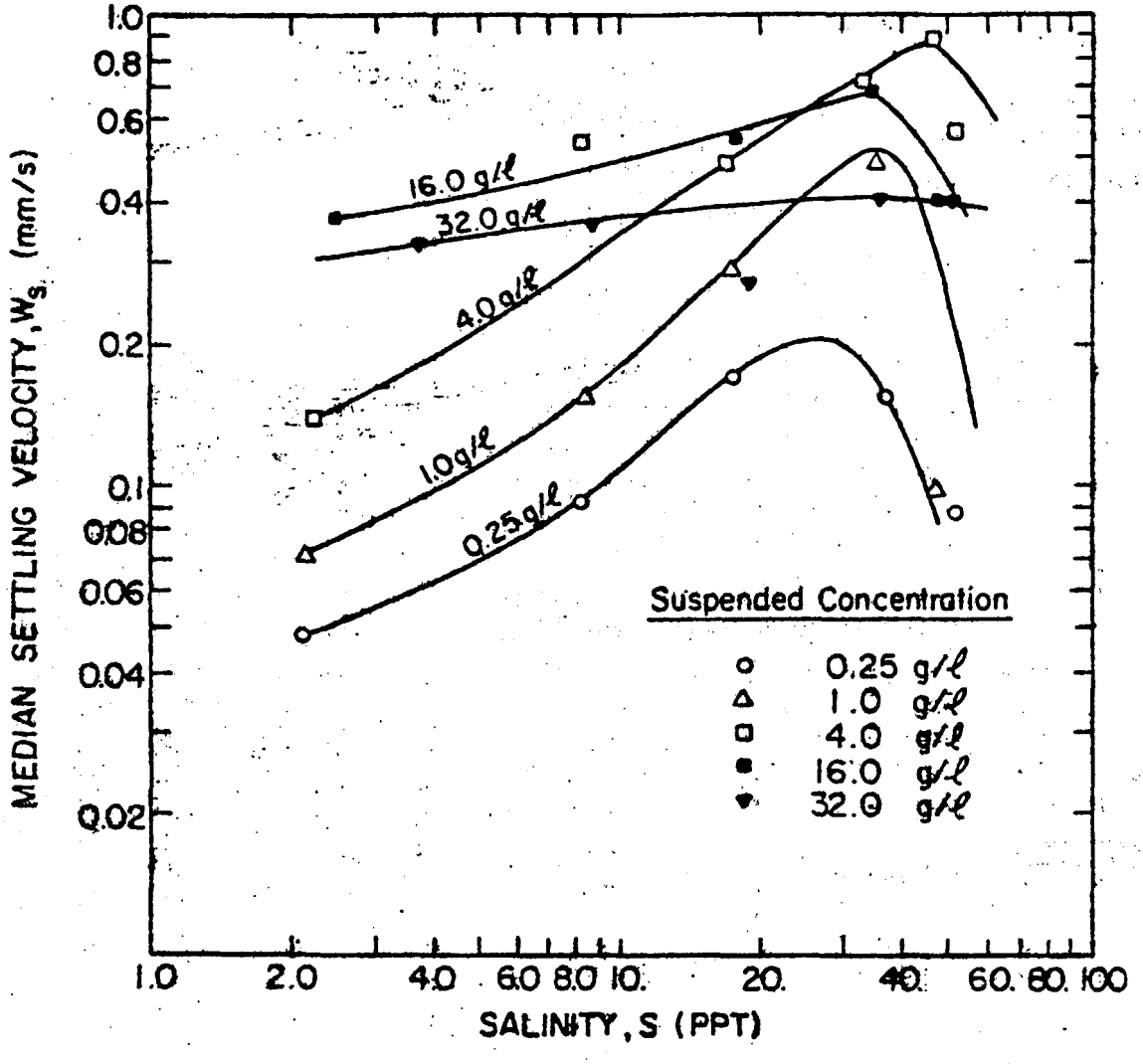

Fig. 2.47 Effect of Salinity on Settling Velocity of Avonmouth Mud (after Owen, 1970).

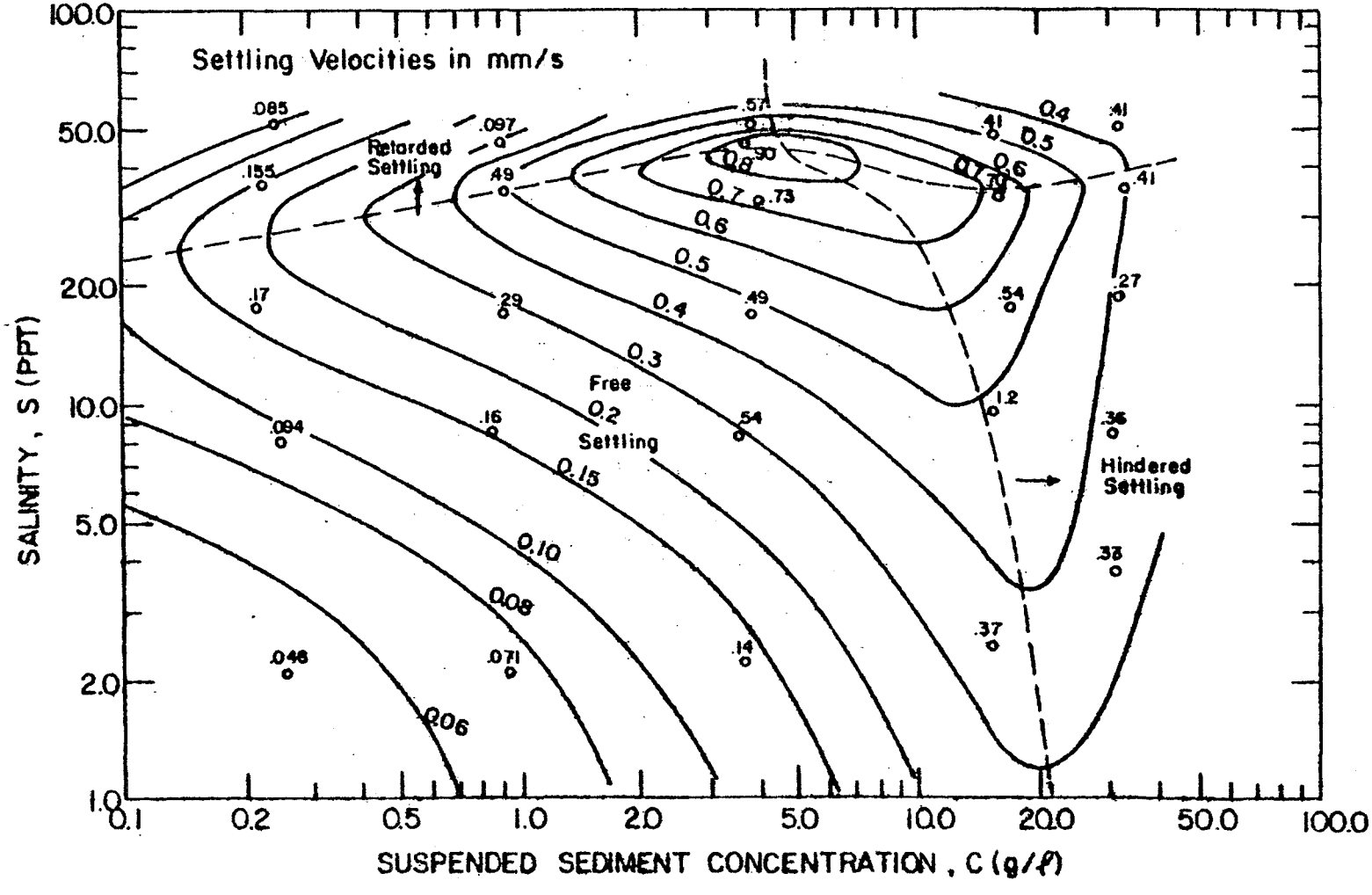

Fig. 2.48 Effects of Salinity and Suspension Concentration on Settling Velocity of Avonmouth Mud (after Owen, 1970).

suspended sediment were collected from a tap located on the outer wall of the flume at 0, 1, 2, 5, 10, 15, 20, 30 and 60 minutes after the shear stress was reduced to τ_b. Subsequent samples were collected with lower frequency. Each experiment was conducted for a period of 21 hours.

The measured suspension concentrations were plotted against time for each experiment. Plots of C/C_0 versus time for each τ_b value at a salt concentration of 5 ppt are shown in Fig. 2.49. The steady state concentration, C_{eq}, for each deposition test was determined from a curve drawn to represent the mean variation of the concentration with time, as seen in this figure. The following observations were made: 1) for the two lowest values of τ_b, i.e. τ_b = 0.0, and 0.015 N/m^2, the concentration decreased over the duration of the experiment for all salt concentration values, indicating that C_{eq} for these τ_b values would have been equal to zero if the experiment had been of longer duration. 2) for τ_b = 0.05, 0.1, 0.2 and 0.3 N/m^2 the concentration decreased rapidly during the first hour and C_{eq} was reached more rapidly as the value of τ_b increased. 3) at the four lowest values of τ_b the effect of the salt concentration on the deposition rate (i.e. concentration variation with time) was appreciable. For the two highest τ_b values the salt effect was much less discernible. These results seem to indicate that at relatively low values of τ_b cohesive forces are predominant whereas at higher values the hydrodynamic forces (i.e. disruptive internal shears) are also significant. This explanation follows from the results obtained by Owen (1970; 1971) and by Mehta and Partheniades (1975).

The ratio C_{eq}/C_0 was plotted against τ_b values for all salt concentrations (Fig. 2.50). Interpolation of the resulting plot yields $\tau_{b_{min}} \approx 0.035$ N/m^2. It is believed that even though additional data, i.e. C_{eq}/C_0 against τ_b values, might result in a different value of $\tau_{b_{min}}$, the two values would be reasonably close (probably within ± 25%).

The settling velocity at the time when 50% of the depositable sediment had deposited, i.e. t_{50}, was determined for each experiment in Range I in order to quantitatively evaluate the effect of salt concentration, and possibly the bed shear stress, on the rate of deposition. This particular value of the settling velocity, designated

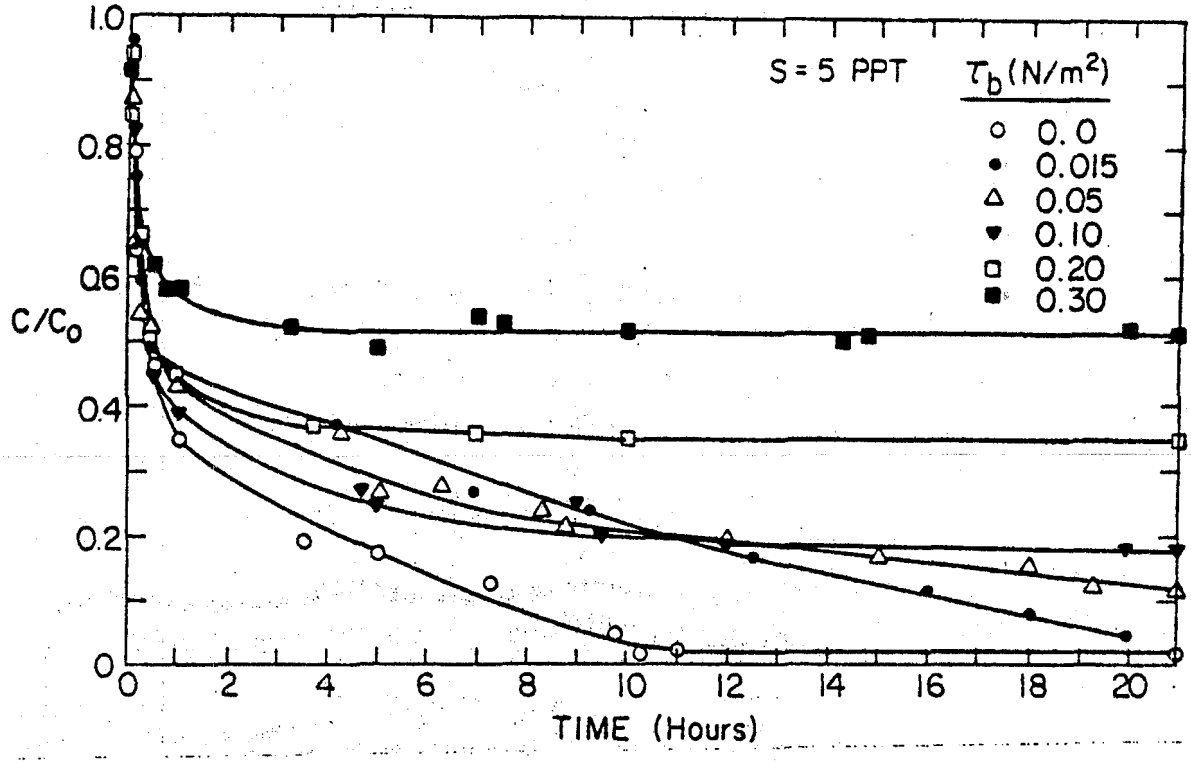

Fig. 2.49 Ratio C/C_o versus Time as a Function of the Bed Shear, τ_b, for Lake Francis Sediment with S=5 ppt.

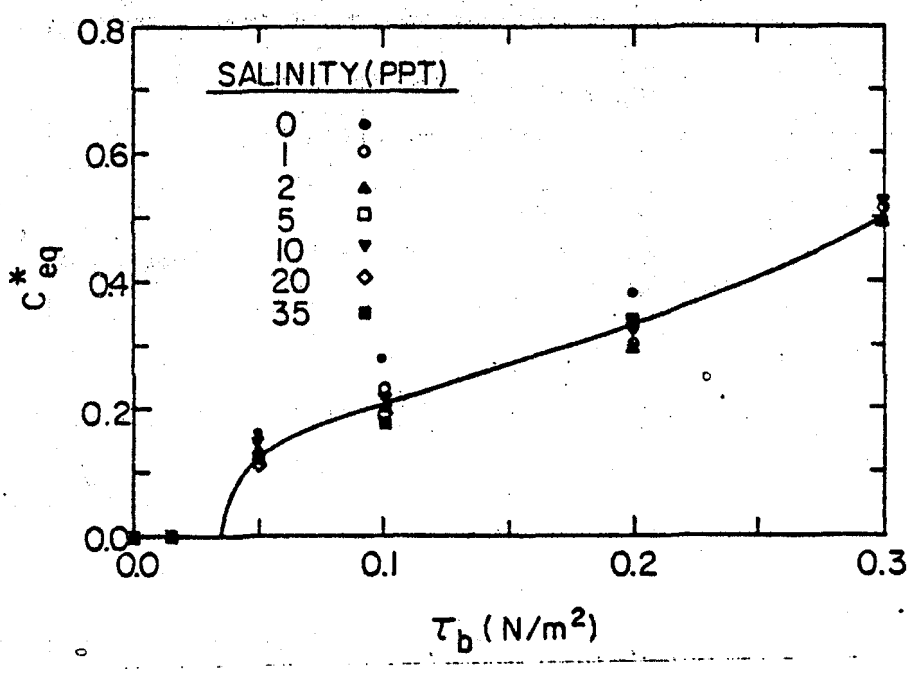

Fig. 2.50 Ratio C_{eq}/C_o versus τ_b for Deposition Tests with Lake Francis Sediment.

as W_{s50}, was chosen for this analysis because it can be shown to be more representative of the deposition rates in the time interval of interest in numerical simulation (see Section 2.7.3 for discussion of this aspect) than either the mean or the median value. The analysis was performed in the following manner for the experiments in Range I (i.e. τ_b = 0.0 and 0.015 N/m^2). Equation 2.41 was integrated and rearranged to yield the given expression for W_{s50}:

$$W_{s50} = \frac{-d}{\rho_d t_{50}} \ln\left(\frac{C_o - C_{50}}{C_o - C_{eq}}\right) \tag{2.72}$$

where C_{50} = suspension concentration at time t_{50}. Values of W_{s50} computed from Eq. 2.72 are shown in Fig. 2.51 superposed on Fig. 2.47, with lines of equal shear stress drawn as indicated. The average value of the initial concentration, C_o, in these experiments was 4.2 g/l. No consistent trend between τ_b and W_{s50} (e.g. increasing W_{s50} values with increasing τ_b values for all salt concentrations) is apparent in Fig. 2.51. This observation suggests that W_{s50} is invariant with respect to τ_b in Range I.

Due to the limited data obtained, as well as the noted invariance of W_{s50} with respect to τ_b for Range I, the values of W_{s50} for the two τ_b values were averaged for each salt concentration. These average values, $\bar{W}_{s50}$, are as well plotted against salt concentration in Fig. 2.51. Such an averaging procedure was performed in order to further investigate the effect of salt concentration on W_{s50}.

A power curve relationship between $\bar{W}_{s50}$ and the salinity, S, of the following form was desired:

$$\bar{W}_{s50}(S,C) = A \cdot \bar{W}_{s50}(35,C) \cdot S^m \tag{2.73}$$

where $\bar{W}_{s50}(35,C) = KC^n$ (K and n are defined in Section 2.7.1) and A and m are empirical constants. It was proposed that when S was less than 0.1 ppt, its value would be set equal to 0.1, so that $\bar{W}_{s50}(S<0.1,C)$ would be greater than zero and in fact $\bar{W}_{s50}(S<0.1,C) = \bar{W}_{s50}(S=0.1,C)$. The value of $\bar{W}_{s50}$ at S = 35 ppt was utilized as the $\bar{W}_{s50}(35,C)$ value. Least squares linear regression analysis was used to determine if the averaged settling velocities followed such a power curve. This analysis

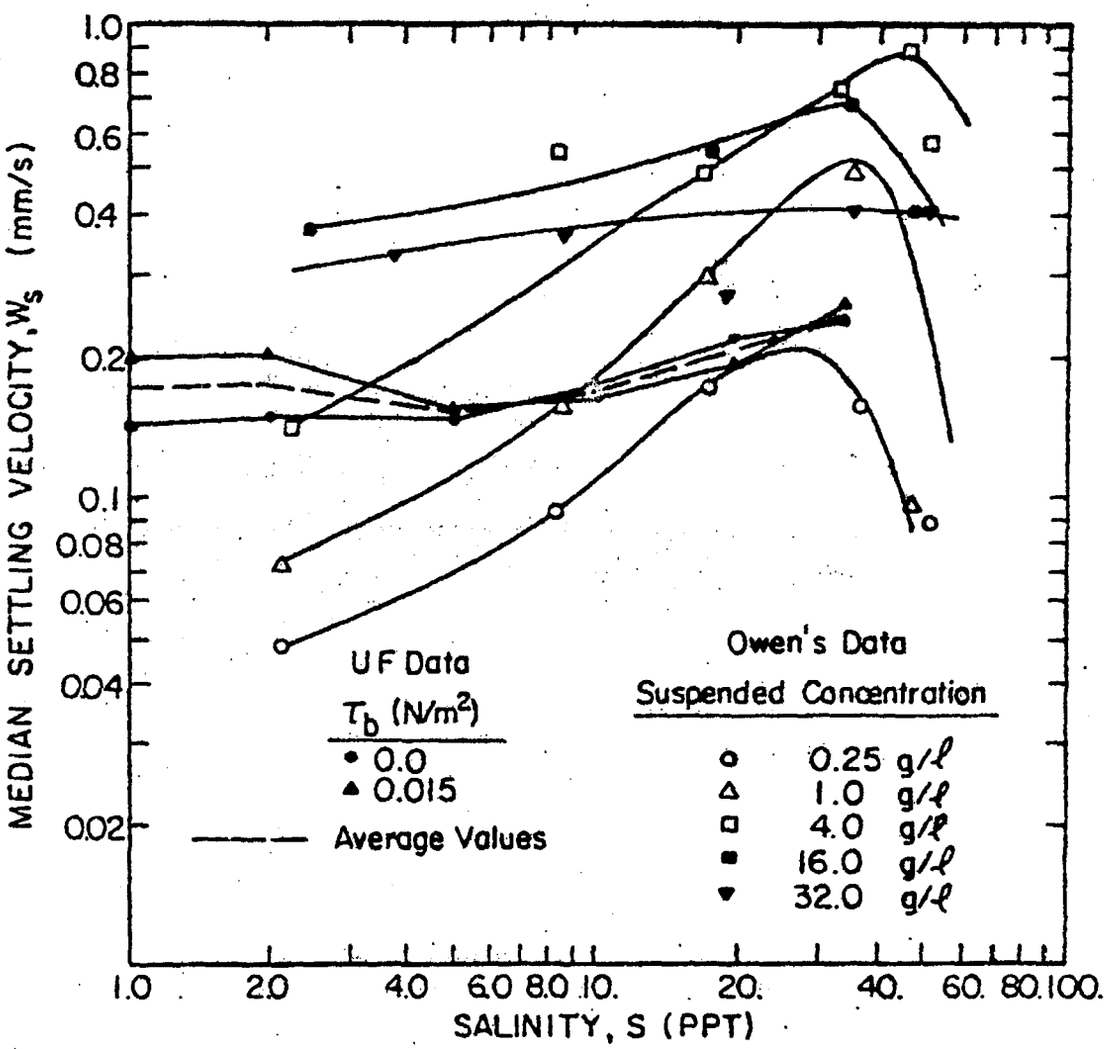

Fig. 2.51 Effect of Salinity and Bed Shear Stress on Settling Velocity of Lake Francis Sediment.

gave the following values for A and m and the coefficient of determination, r^2: A = 0.57, m = 0.13 and r^2 = 0.96. As indicated by this r^2 value, a good agreement was obtained between Eq. 2.73 and the data. This confirms that, at least for these experiments and the analysis method employed, the effect of salt concentration on W_{s50} in Range I can be expressed by a power relationship of the form given in Eq. 2.73.

The function given in Eq. 2.73 is incorporated into the deposition rate expressions for Range I and for $C < C_1$ (which is the concentration below which mutual interference is negligible) in Range II as follows: Equation 2.73 is used to evaluate the settling velocity as a function of the concentration of dissolved salt and suspended sediment. Based on the variety of relationships found between W_{s50} and C for several of these experiments, the following general expressions for W_{s50} in Range I and for $C < C_1$ in Range II have been incorporated into SEDIMENT IIIA:

$$W_{s50} = A_1 \cdot W_{s_1} \cdot S^{m_1} \quad \text{for} \quad C < C_1 \tag{2.74a}$$

$$W_{s50} = K'_1 \cdot C^{n_1} \cdot S^{m_1} \quad \text{for} \quad C_1 < C < C_2 \tag{2.74b}$$

$$W_{s50} = K'_2 \cdot C^{n_2} \cdot S^{m_2} \quad \text{for} \quad C_2 < C < C_3 \tag{2.74c}$$

$$W_{s50} = \left(\frac{250}{D^{1.8}}\right) \frac{A_3 g D^2 \left(\frac{s}{\rho_w} - 1\right)}{18\nu} \left(\frac{C}{C_3} - 1\right)^{\ell} \cdot S^{m_3} \quad \text{for} \quad C > C_3 \tag{2.74d}$$

where $K'_i = A_i K_i$ for i=1,2, and W_{s_1} is the constant settling velocity for $C < C_1$. For concentrations greater than C_1 and less than C_3, where hindered settling begins, two different expressions of the form $W_{s50} = K' C^n S^m$ can be used to express the variation of W_{s50} with C and S. Two relationships were revealed in this concentration range in several of the deposition tests (e.g. see Fig. 2.52). These relationships are permissible in the new deposition/settling algorithm. If only one relationship is revealed from a log-log plot of W_{s50} against C, C_3 must be set equal to C_2. The values of A_1 and m_1 apply for $C < C_2$, while A_2

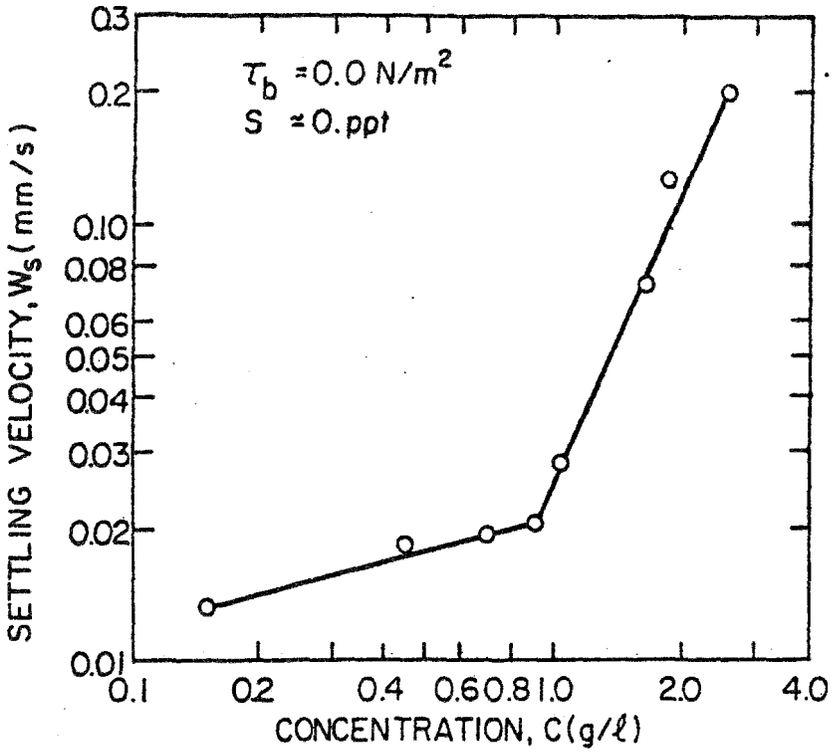

Fig. 2.52 Settling Velocity versus Suspension Concentration for Deposition Test with Lake Francis Sediment.

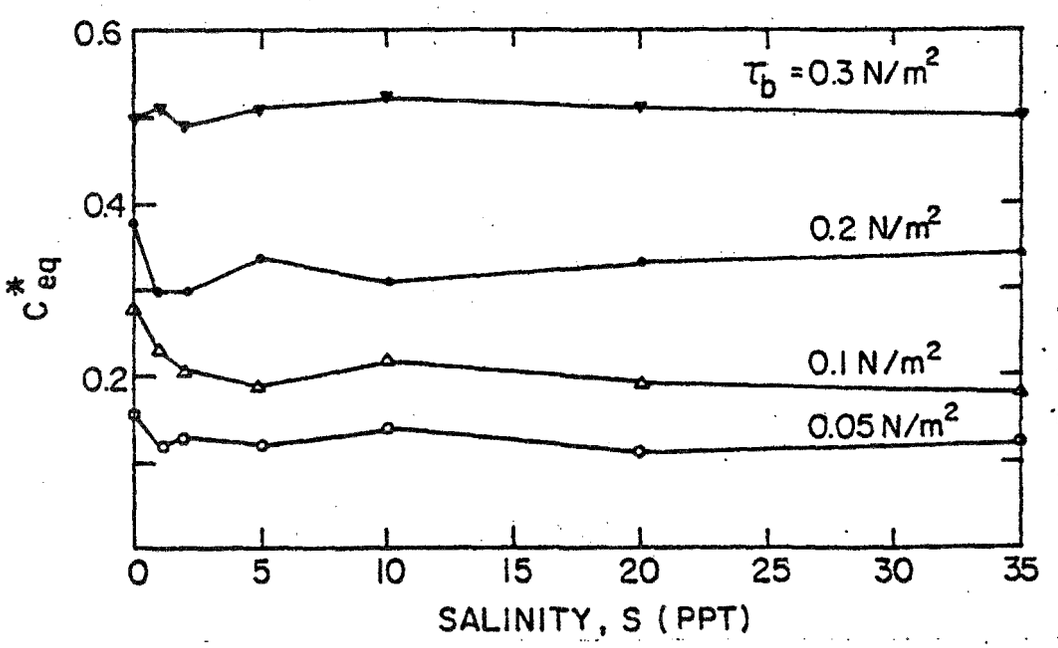

Fig. 2.53 Variation of C^*_{eq} with Salt Concentration, S, and Bed Shear Stress, τ_b.

and m_2 are for $C_2 < C < C_3$ and A_3 and m_3 apply for $C > C_3$; if $C_2 = C_3$, then $A_2 = A_1$ and $m_2 = m_1$. The values of K_1 and n_1 apply for $C_1 < C < C_2$, while K_2 and n_2 are for $C_2 < C < C_3$; if $C_2 = C_3$, then $K_1 = K_2$ and $n_1 = n_2$. The values of K_3 and n_3 apply for $C > C_3$.

For the experiments in Range II (i.e. τ_b = 0.05, 0.1, 0.2, and 0.3 N/m^2) the following analysis was performed. Figure 2.53 shows the relationship found between C^*_{eq} and the salt concentration for the values of $\tau_b > \tau_{b_{min}}$ where $C^*_{eq} > 0$. Based on the nature of the equal τ_b curves in this figure and taking into consideration the limited number of deposition tests performed at $\tau_b > \tau_{b_{min}}$, C^*_{eq} is assumed to be invariant with respect to the salt concentration.

In Range II, the effect of salt concentration of the deposition rate was evaluated in the following manner. The value of dC/dt at $t=t_{50}$ was determined for each experiment. Substituting $t=t_{50}$ into Eq. 2.50 gives the following expression for the rate of deposition at t_{50}:

$$\left.\frac{dC}{dt}\right|_{50} = \frac{-0.434\ C_o(1-C^*_{eq})}{\sqrt{2\pi}\ \sigma_2\ t_{50}} \qquad (2.75)$$

The value of t_{50} for each experiment was determined from the log-normal plot of C^* versus t, and the value of σ_2 was evaluated according to (Aitchison and Brown, 1957):

$$\sigma_2 = \log_{10}\left[\frac{1}{2}\left(\frac{t_{50}}{t_{16}} + \frac{t_{84}}{t_{50}}\right)\right] \qquad (2.76)$$

where t_{16} and t_{84} are the times at which C^* = 16% and 84%, respectively, and likewise were determined from the log-normal plot. Due to the limited data and observed invariance of $\left.(dC/dt)\right|_{50}$ with respect to τ_b, the values of $\left.(dC/dt)\right|_{50}$ were averaged for each salt concentration. The following functional relationship between T (given by Eq. 2.49) and the salt concentation, S, was obtained using a linear regression analysis:

$$T = \log_{10}\left[\left(\frac{t}{t_{50}}\right)BS^f\right]^{1/\sigma_2} \qquad (2.77)$$

where B = 10.78, f = -0.33 and r^2 = 0.93 when S < 0.1 ppt, its value is set equal to 0.1 ppt.

The effect of salinity on the deposition rate expression for $C \geq C_1$ in Range II was incorporated by substituting Eq. 2.77 into Eq. 2.50. The resulting value of the time-rate of change of concentration, dC/dt, will decrease monotonically at any given time with decreasing salt concentration, while at the same time, the expression for C^* given by Eq. 2.48 still approaches 0 as $t \to \infty$. This methodology of incorporating the effect of salinity requires that the values of t_{50} and σ_2, used in Eq. 2.50, be evaluated at a salinity of 35 ppt.

2.9. Convergence and Stability of the Numerical Scheme

The accuracy of the numerical scheme used in SEDIMENT IIIA, which is the same as that used in SEDIMENT III, has been investigated in detail by Ariathurai (1974) and Ariathurai et al. (1977). These authors reported that rapid convergence to the exact analytical solutions was achieved for the numerical formulation for the one-dimensional, transient heat conduction problem with and without radiation, the one-dimensional, for the steady-state and transient convection-diffusion problem, and for the two-dimensional Laplace equation.

The results from these convergence tests also indicated that the combination of the unconditionally stable finite element formulation used to solve the spatial problem and the unconditionally stable Crank-Nicholson finite difference formulation used to solve the temporal problem is as well unconditionally stable. However, these tests revealed that instabilities might still occur when the Peclet numbers (ratio of convection to diffusion, i.e. uL/D_x, where u = flow velocity, D_x = diffusion coefficient and L = system longitudinal dimension) become either too large (greater than ≈ 100) or too small (less than $\approx 10^{-3}$). For too large Peclet numbers, smaller time-steps must be used to improve the accuracy of the numerical scheme (Ariathurai et al., 1977). Too small Peclet numbers rarely ever occur for typical flow conditions in estuaries, and therefore associated roundoff errors, which can lead to instabilities, should never be a problem in modeling such systems. However, spurious results caused by roundoff errors were encountered in simulating laboratory depositional experiments with SEDIMENT IIIA. This

problem was eliminated by using double precision arithmetic in the model. No instability problems were encountered in modeling a prototype system using single precision arithmetic.

2.10. Model Limitations

A two-dimensional, vertically integrated model such as SEDIMENT IIIA can strictly be applied to only estuaries, harbors and basins (such as marinas) where the horizontal dimensions of the water body are at least one order of magnitude greater than the vertical dimension. Applications to partially mixed water bodies or especially to highly stratified water bodies should be made when only rough estimates of some sedimentary process (e.g. shoaling rate) are required.

Currently the model has the capability of simulating the movement of only one constituent (e.g. cohesive sediment, water temperature, or algae, provided the source/sink expressions for a nonconservative constituent are known). It is possible, however, to modify the model so that any number of constituents may be incorporated.

Probably the main "limitation" of a model arises from three sources: 1) insufficient data, 2) poor quality of data and 3) limitations of the hydrodynamic modeling. The first two sources are attributable to the fact that, owing mainly to time and cost considerations, all the bathymetric, hydraulic and sedimentary data required for use in such a model are rarely, if ever, measured and/or collected in the body of water being modeled. In addition, the quality of the data is often questionable. Data requirements and the field collection and laboratory testing programs required to obtain these data are briefly described in Appendix B.

The third source is itself often the result of the first two, inasmuch as progress has been achieved in the past two decades in modeling estuarial hydrodynamics (Leendertse, et al., 1967; King et al., 1973; Liu and Leendertse, 1978).

The importance of experience in effectively using the model cannot be over emphasized. Experience gained through knowledge of the physical systems being modeled and repeated applications of the model will enhance the user's ability to choose the proper values of the various parameters, e.g. time-step size and diffusion coefficients. The user

will also gain the ability to anticipate the effect of changing the value of a particular parameter by a certain percentage on the model solution (i.e. model sensitivity).

2.11. Model Applicability

2.11.1. Water Quality Problems

The model can be used to assist in the performance of the following water quality related computational tasks:

1.) Assessment of the disposition of dissolved and sorbed pollutants, possibly either transported to an estuary or harbor by stormwater runoff or released into these water bodies by nearby industries, and their effect on the receiving waters and the aquatic ecosystem therein, when linked with a particulate contaminant transport model that contains a sorption submodel (Onishi and Wise, 1979).

2.) Prediction of the effect of reduced sediment inflows to estuaries, caused by upstream water storage and subsequent use, to ascertain the degree of waste water management required to control estuarial water pollution.

3.) Prediction of the limitation of sunlight penetration in estuarial waters resulting from high turbidity levels which, in turn, are caused by high concentrations of suspended sediment. This reduced light penetration can cause the algae multiplication rate to decrease significantly, and thus effect the entire aquatic ecosystem.

2.11.2 Sedimentation Management Problems

The model can be used as a tool to help solve the following sedimentation problems:

1.) Prediction of the movement of dredged material released in open waters in order to estimate the effect of the disposal at a given location in the water body on the shoaling rates elsewhere, and in particular in the dredged area.

2.) Selection of harbor sites in estuaries and bays where shoaling is minimized.

3.) Prediction of changes in the sedimentary regime that may occur as a result of a proposed change or development of an estuary or

harbor, such as the dredging of new navigation channels and the possible change in the salinity field (e.g. further inland intrusion) caused by the proposed change.

4.) Estimation of shoaling rates and maintenance dredging requirements in areas of very low flow such as marinas, harbors and docks, and recommendation of means by which shoaling rates might be minimized in these areas.

5.) Prediction of the spatial (primarily longitudinal) variance in the shoaling and/or scouring rates, caused by varying flow conditions and salinities, along the entire reach of an estuary.

III. SIMULATION OF FINE SEDIMENT TRANSPORT PROCESSES

3.1. Introductory Note

In this chapter the results of model simulations of laboratory erosion and deposition tests and sediment transport in a hypothetical prototype canal are presented. The purpose is two-fold: 1) to show the capability of the model in predicting cohesive sediment transport processes by comparing measured and predicted results, and 2) to show the effect salinity has on these same processes.

3.2. Simulation of Laboratory Erosion Test

A resuspension test (Expt. 17) performed by Parchure (1980) in the previously described annular flume was simulated. The result is shown in Fig. 3.1. Good agreement is observed between measurement and prediction for the first six hours of the experiment. The deviation at 6.5, 7.5 and 8.5 hours is attributable to the fact that the results for the last three hours in this experiment did not conform precisely to the empirical surface erosion rate expression given by Eq. 2.32. The sediment and suspending fluid used in the resuspension test were, respectively, kaolinite and water with a 35 ppt concentration of commercial grade sodium chloride (see Section 2.8.4 for a description of this artificial sea water). The bed shear strength profile for Expt. 17, shown in Fig. 2.9, was used in this simulation. The initial, i.e. background, concentration at the start of the test was 0.32 g/l. The rapid increase in suspension concentration (up to 0.60 g/l) at the start of the test was simulated as mass erosion. The remainder of the bed was simulated to undergo surface erosion, with the rate of erosion determined using Eq. 2.32.

The effect of salinity on the bed shear strength (described in Section 2.8.4) and hence on the rate of surface erosion, is shown in Fig. 3.2. In this figure, the results of simulations of the same resuspension test at salinities of 0 and 1 ppt have been superposed on the simulation at a salinity of 35 ppt. The suspension concentration became a constant (8.2 g/l) for the S = ~0 and 1 ppt simulations when the entire bed was resuspended. As indicated by Eq. 2.67, the effect of salinity on the bed shear strength was found to be invariant above a

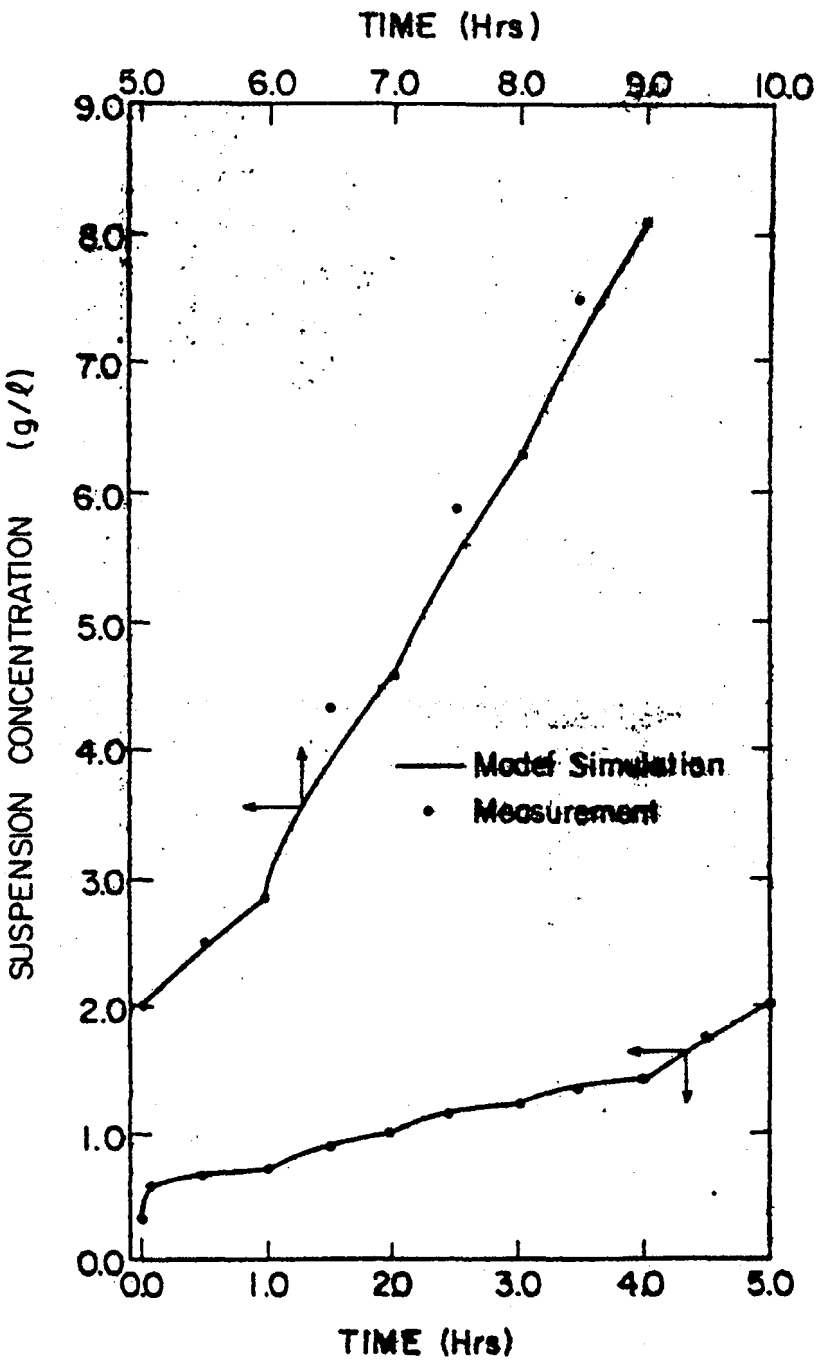

Fig. 3.1 Comparison of Predicted and Measured Suspension Concentrations versus time for a Resuspension Experiment.

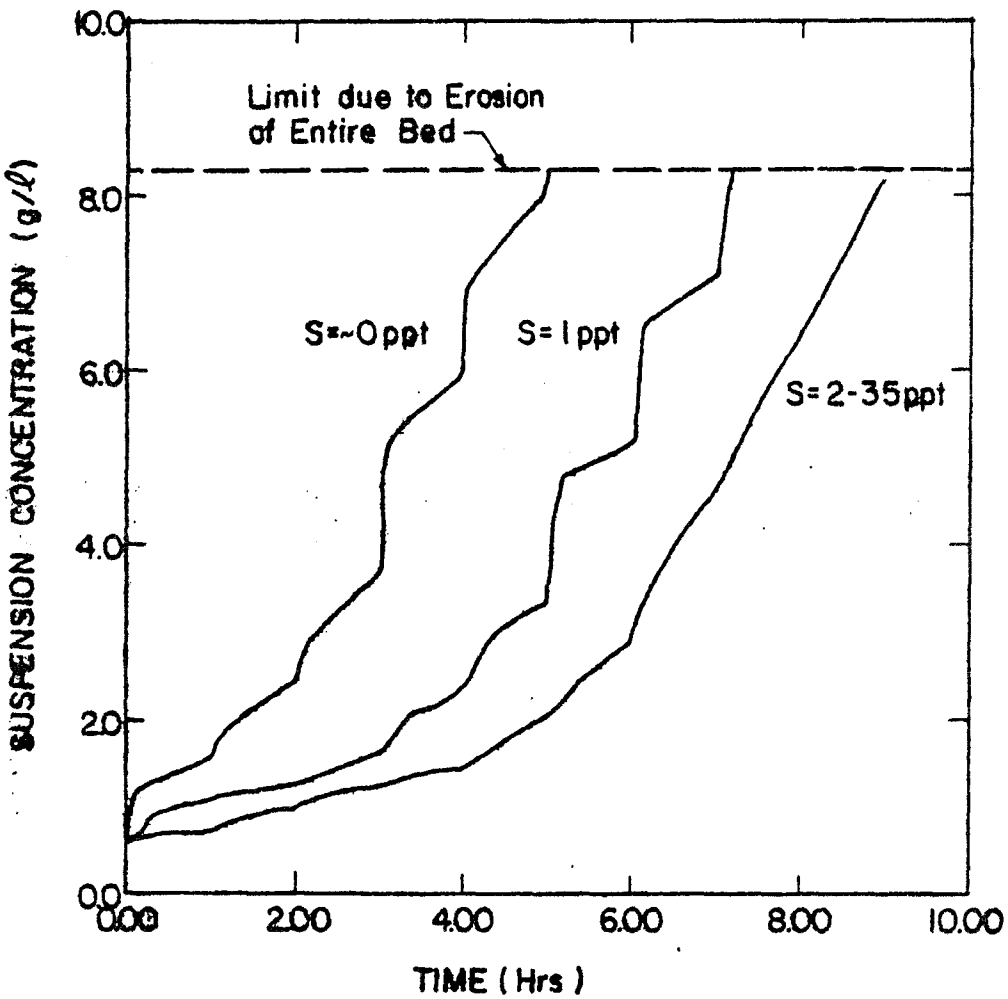

Fig. 3.2 Demonstration of the Effect of Salinity on the Resuspension Rates of a Flow-Deposited Kaolinite Bed.

salinity of 2 ppt. The increase in suspension concentration at a given time with decreasing salinity (below 2 ppt) is a result of the decreasing bed shear strength and therefore increasing rate of surface erosion. Therefore, in the upper-most reaches of an estuary, where salinities are typically less than 2 ppt during at least the latter stages of an ebb tide and the first stages of the subsequent flood tide, the sediment bed would be simulated to undergo a higher rate of surface erosion when subjected to an excess bed shear stress in an accelerating flow in comparison with a bed in the middle and lower reaches where the salinities are generally higher than 2 ppt. In regions where the salinity is in excess of 2 ppt, the influence of salinity upon erosion appears to be negligible.

3.3. Simulation of Laboratory Deposition Tests

Three laboratory deposition tests performed by Mehta (1973) and one performed during the course of this study were simulated. Figures 3.3 - 3.6 show that good agreement was obtained between the measurement and prediction. The sediment used in the deposition test shown in Fig. 3.3 was Lake Francis, Nebraska, sediment in tap water, while the sediment in the other three tests was kaolinite in distilled water. The hydraulic and sedimentary conditions for each test are specified in these figures. The values of τ_b^* in these four tests, i.e. $\tau_b^* = 0.0, 0.9, 1.41$ and 2.70, cover both depositional ranges (i.e. Range I and II, defined in Section 2.7.2).

The effect of salinity on the deposition rates for the $\tau_b^* = 0.0$ test with Lake Francis sediment is shown in Fig. 3.3. The rate of deposition, as reflected by the decrease in suspension concentration with time, increases slightly with increasing salinity of the suspending fluid (see Section 2.8.5 for discussion and development of the quantitative effect of salinity on deposition rates of natural muds). Based on these results alone, a higher shoaling rate may be expected near the mouth of an estuary where, typically, salinities close to that of the sea (i.e. 30 - 35 ppt) occur. Likewise, lower shoaling rates may be expected near the upland end of the estuary where salinities less than 10 ppt are common over an entire tidal cycle (see Fig. 1.6). However, the effect of turbulent shearing rates in the fluid on the

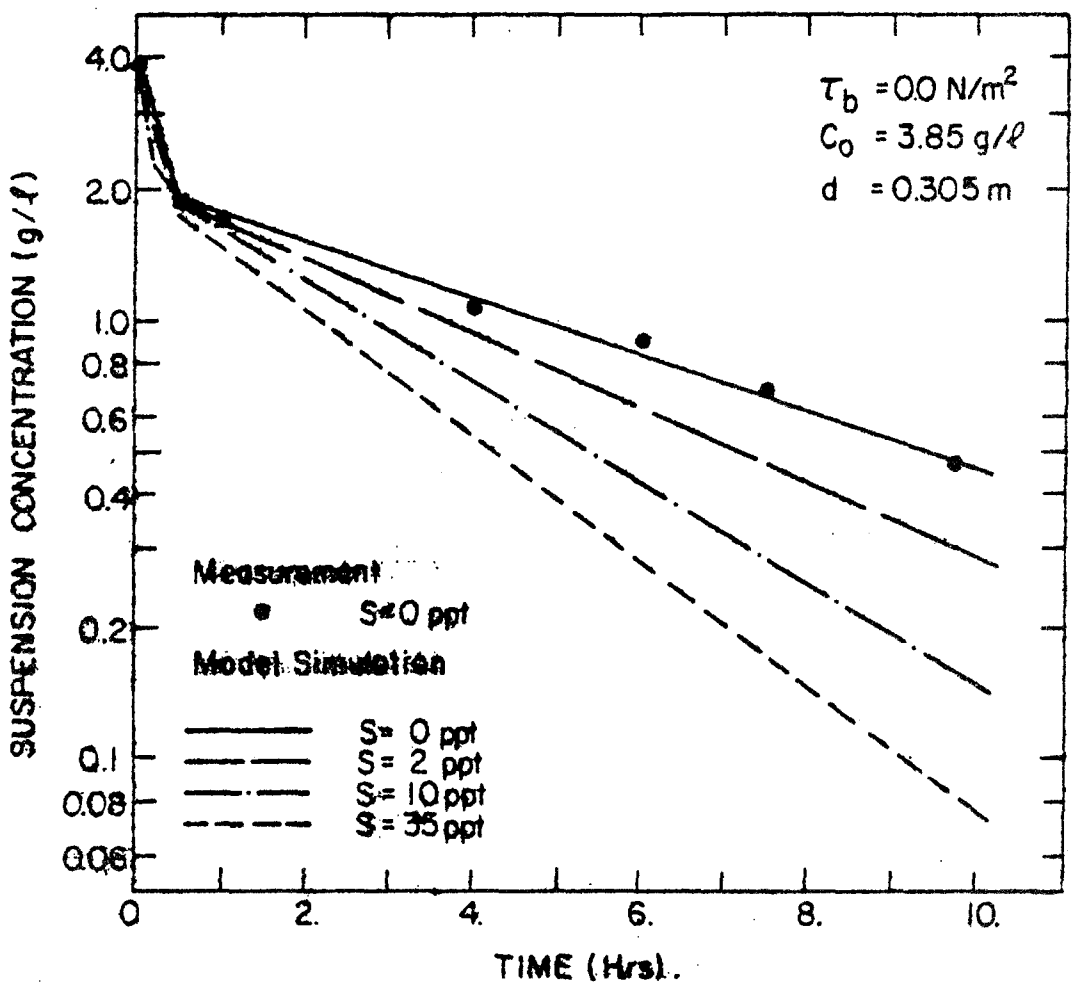

Fig. 3.3 Comparison of Predicted and Measured Deposition Rates for Lake Francis Sediment at a Salinity of 0.0 ppt, and Demonstration of the Effect of Salinity on the Deposition Rate.

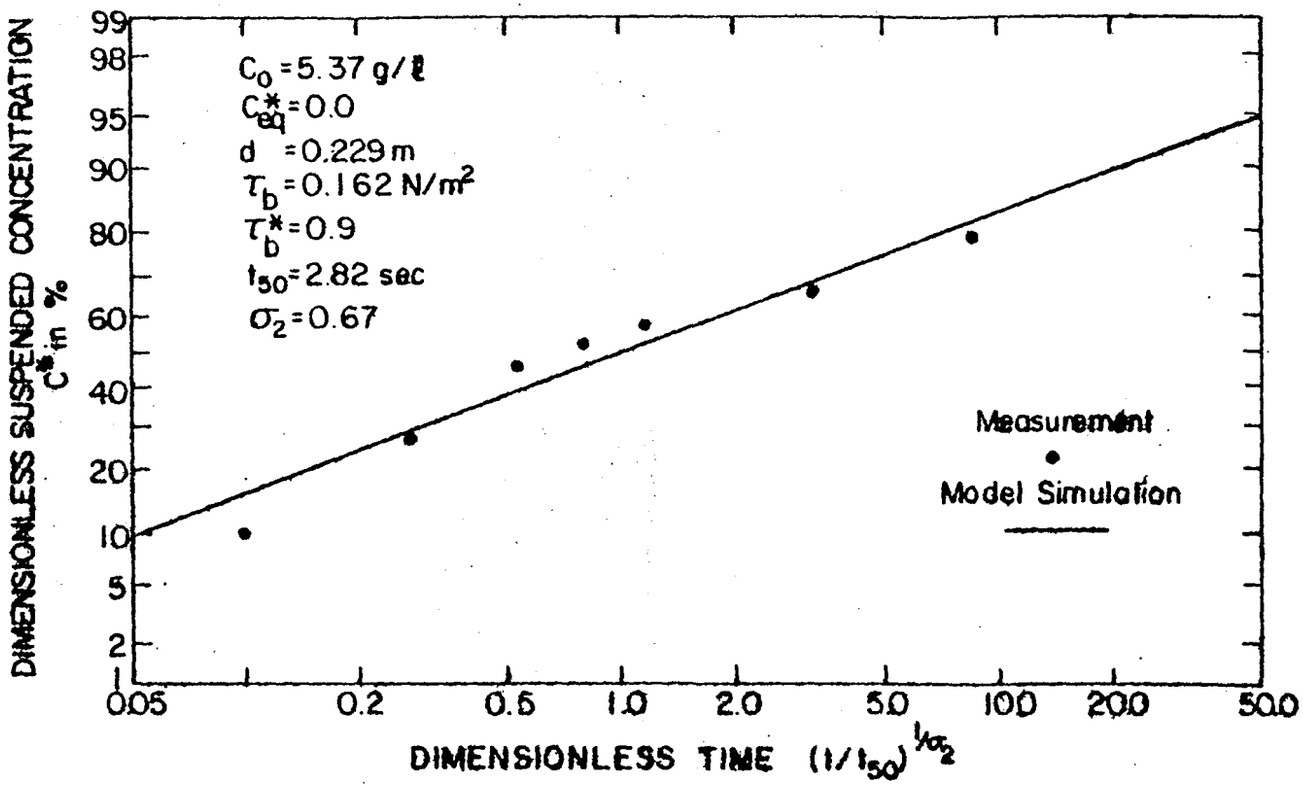

Fig. 3.4 Comparison of Predicted and Measured Variation of C^* versus $(t/t_{50})^{1/\sigma_2}$ for Kaolinite in Distilled Water with τ^*_b = 0.90.

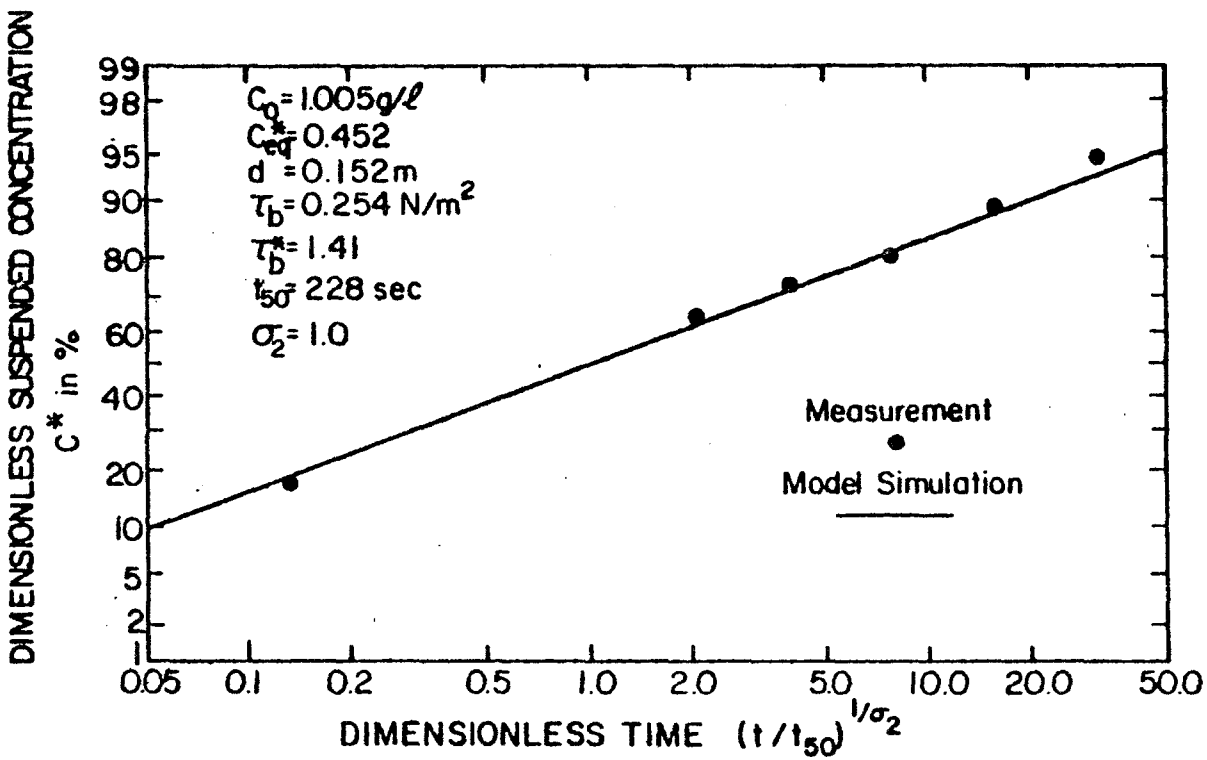

Fig. 3.5 Comparison of Predicted and Measured Variation of C^* versus $(t/t_{50})^{1/\sigma_2}$ for Kaolinite in Distilled Water with $\tau^*_b = 1.41$.

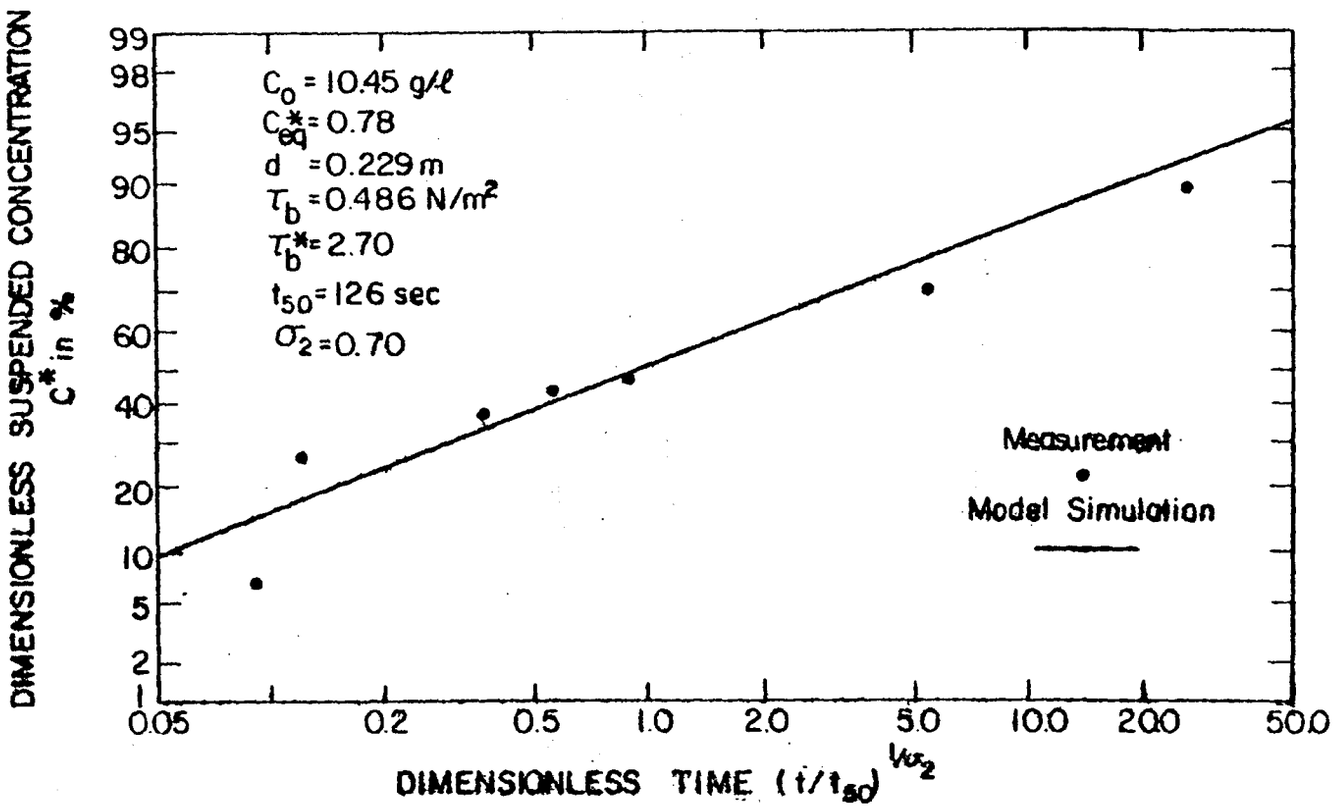

Fig. 3.6 Comparison of Predicted and Measured Variation of C^* versus $(t/t_{50})^{1/\sigma_2}$ for Kaolinite in Distilled Water with τ^*_b = 2.70.

aggregation of the sediment, and therefore on the rate of deposition, must not be ignored. This effect can often be the dominating factor controlling the rate of shoaling in a given reach of the estuary.

3.4. Simulation of Sedimentation Processes in a Prototype Canal

The dimensions of a 10 km long hypothetical canal are shown in Fig. 3.7. The canal was divided into nine elements and 48 nodes, with the length of elements 1 - 3 equal to 833 m and that of elements 4 - 9 equal to 1250 m. The canal was assumed to have a uniform bottom roughness, as quantified by a Manning's coefficient of 0.02, which is a reasonable value for a straight natural waterway with a muddy bottom. The depth and the mean velocity at nodes 1, 2 and 3 were taken to be 5.0 m and 0.5 m/s respectively. The velocities and water depths at nodes 4 - 48 were evaluated using the conservation of energy and mass equations for an open channel. The total drop in the water depth over the 10 km distance due to frictional resistance and the gradual enlargement in width at element 5 was determined to be 0.16 m. The initial suspension concentration in the canal was taken to be 0.0 g/l. The following boundary conditions were used: nodes 1, 2 and 3: $C(t) = 0$, and nodes 46, 47 and 48: $\partial C(t)/\partial x = 0$. The upstream (i.e. nodes 1, 2 and 3) boundary condition states that no suspended sediment was transported into the canal from upstream sources, while the downstream (i.e. nodes 46, 47 and 48) boundary condition stipulates that the longitudinal flux of suspended sediment across the downstream boundary was zero. In elements 1 - 4, an initial, partially consolidated sediment bed of 0.37 m in thickness was assumed to exist, while in elements 5 - 9, no initial bed was present.

Erosion of the initial sediment bed occurred in elements 1 - 4, while deposition of the sediment suspended in the first four elements occurred in elements 5 - 9. The suspension concentration-time record for elements 4 and 5 are shown in Figs. 3.8 and 3.9 for salinities of 0, 1, 20 and 35 ppt. As evidenced by the over three-fold decrease in concentration between Fig. 3.8 and 3.9, a high percentage of the suspended sediment deposited in element 5. Also observed in these two figures is a reduction in sediment suspended with increase in salinity. This observation follows from the previously described effect

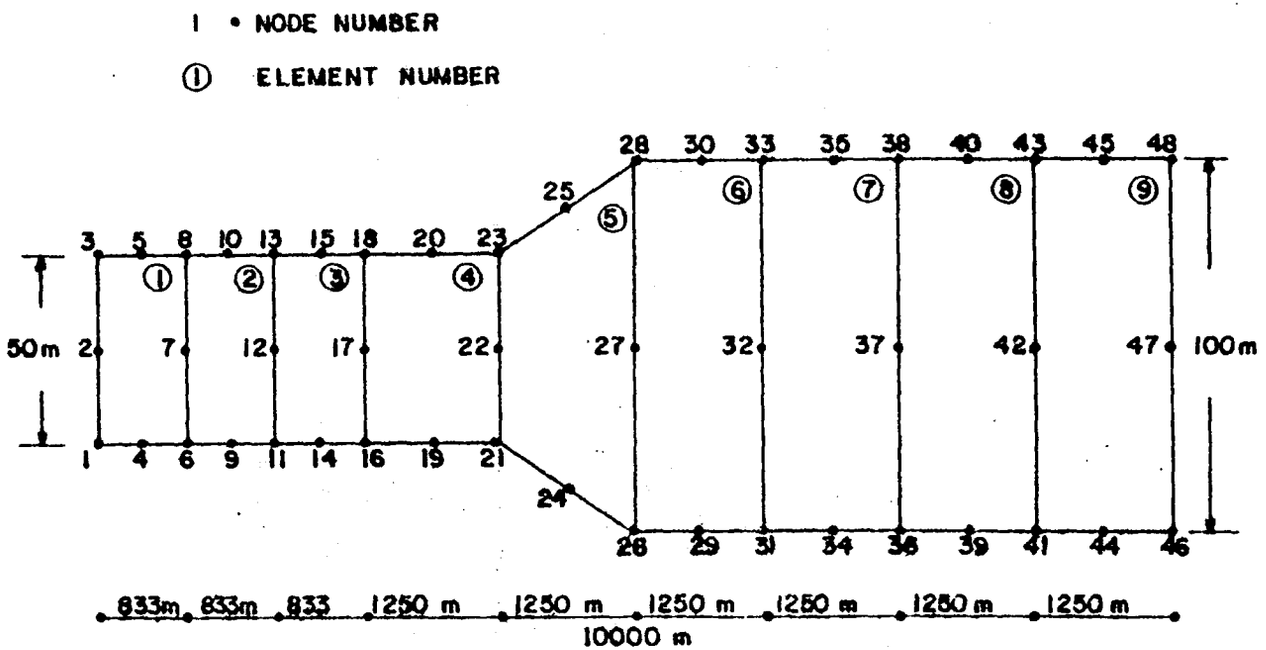

Fig. 3.7 Plan View of 10 km Hypothetical Canal.

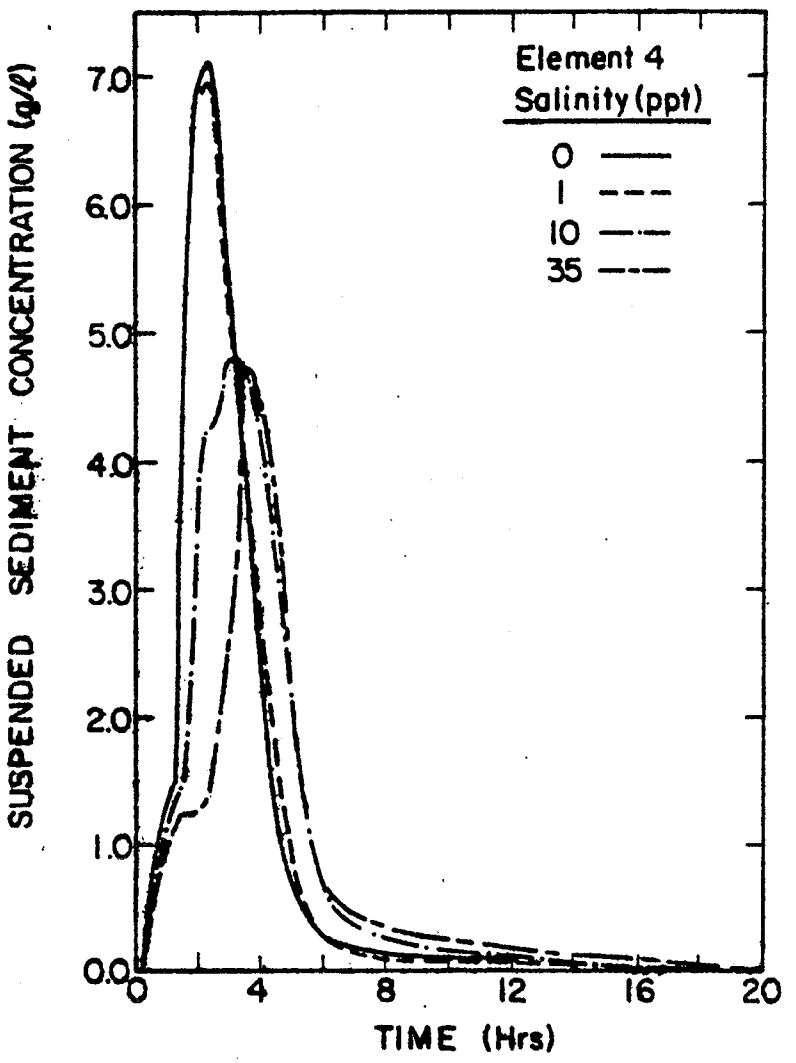

Fig. 3.8 Predicted Concentration-time Record for Element 4 in 10 km Canal.

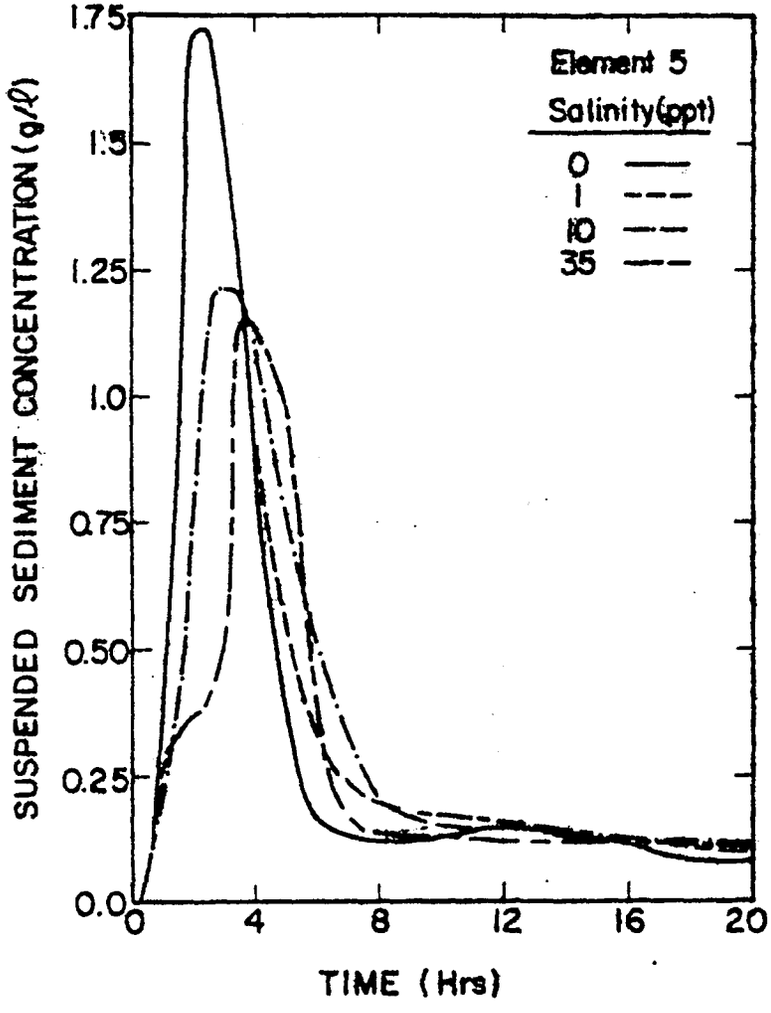

Fig. 3.9 Predicted Concentration-time Record for Element 5 in 10 km Canal.

of salinity on the rate of surface erosion. Also apparent is the small effect of salinity on the rates of deposition. This result is not surprising considering the fact that salinity was found from laboratory deposition tests to only slightly influence these rates.

IV. SUMMARY, CONCLUSIONS AND RECOMMENDATIONS

4.1. Summary and Conclusions

The following are the main observations from this study:

1. Modeling the movement of cohesive sediments in order to predict the fate of pollutants introduced into an estuary is important, because a significant fraction of many pollutants, e.g. heavy metals, radioactive elements, organic substances, is typically transported sorbed to these sediments rather than in the non-sorbed state.
2. Modeling the transport of cohesive sediments in an estuary requires a knowledge of its geometry, the flow and salinity fields, the coagulation, settling and depositional characteristics of the sediment, the structure (i.e. bed shear strength and bed density profiles) of the sediment bed at several different locations in the estuary, and the erosional characteristics of these beds when subjected to an excess bed shear stress.
3. SEDIMENT III, a two-dimensional, depth-averaged cohesive sediment transport mathematical model was upgraded by improving upon its capability of predicting the erosion and deposition of cohesive sediments in an estuarial environment, and by incorporating the effect of salinity on these two transport processes. The new model is referred to as SEDIMENT IIIA.
4. Deposited estuarial occur in three different stages of consolidation: unconsolidated, partially consolidated and settled (fully consolidated). Unconsolidated deposits, sometimes referred to as stationary suspensions, possess a very high water content and low shear strength and are redispersed, or mass eroded, when subjected to an excess bed shear stress (i.e. when the bed shear stress is greater than the shear strength of the exposed bed surface). Partially consolidated deposits have a somewhat lower water content and higher shear strength and are resuspended aggregate by aggregate, i.e. undergo surface erosion, when subjected to an excess shear stress. Settled, or fully consolidated beds possess a much lower water content, a much higher shear strength and as well are resuspended aggregate by aggregate when subjected to an excess shear. The shear strength and the density of partially

consolidated beds were shown by laboratory tests to increase with depth, z, below the water-bed interface, and as such are vertically stratified. Both stationary suspensions and partially consolidated beds undergo consolidation due to overburden pressure, with the bed shear strength increasing with time of consolidation. The bed density as well was found to increase with consolidation time up to 240 hours. In settled beds, the shear strength and the density profiles exhibit relatively uniform properties over the depth.

5. The sediment bed schematization incorporated into the model allows for the above-mentioned three bed sections, and divides each section into a characteristic number of layers. Within each layer, the bed shear strength and density are assumed to vary in a linear manner with depth. The number of layers as well as the shear strength and the density profiles in each section must be determined from laboratory resuspension tests.
6. Flow-deposited beds should be used in these laboratory tests. In forming such a bed in a flume the pre-erosion stress history (determined by the shear stress during mixing, the period of mixing, the shear stress during deposition and the periods of deposition and consolidation), has a significant effect on the resulting bed structure. The methodology depicted in Fig. 2.18 and described by Mehta et al. (1982a) may be used in investigating the resuspension potential of flow-deposited unconsolidated and partially consolidated beds. Resuspension tests performed during this study with beds of kaolinite and sediment from Lake Francis, Nebraska, showed that the rate of surface erosion of partially consolidated beds varied exponentially with the excess bed shear stress (Eq. 2.32). The empirical relationship given by Eq. 2.32 is analogous to the rate expression which results from a heuristic interpretation of rate process theory for chemical reactions. The rate of surface erosion of settled beds has been found to vary linearly with the excess shear stress (Eq. 2.31).
7. The erosion algorithm incorporated into the model simulates the mass erosion of unconsolidated stationary suspensions by instantly redispersing the thickness of bed above the level (i.e. depth below the bed surface) at which the bed shear stress is equal to the bed

shear strength. The average rate of surface erosion of the partially consolidated bed layers over one time-step Δt is given by Eqs. 2.34 and 2.35. The average rate of surface erosion of settled bed layers is given by Eqs. 2.34 and 2.40. In the latter two cases, the thickness of bed eroded per time-step is determined using an iteration routine. Erosion is simulated to occur only when the bed shear stress, τ_b, is greater than the shear strength of the bed surface and only when the flow is accelerating, i.e. $\tau_b(t+\Delta t) > \tau_b(t)$.

8. The settling velocity of the sediment is a function, among other parameters, of the suspension concentration, C. For concentrations less than $C_1 \approx 0.1 - 0.7$ g/l the sediment particles settle independently without much mutual interference, and therefore the settling velocity is independent of C. In the range $C1 < C < C2 \approx 10 - 15$ g/l, the settling rate is proportional to C^n with $n > 0$, due to mutual interference. In the range $C > C2$, the settling velocity decreases with increasing concentration due to hindered settling.

9. The deposition algorithm integrates the concepts proposed by various investigators and represents a unified model of this process. Deposition is predicted to occur only in decelerating flows, i.e. $\tau_b(t+\Delta t) < \tau_b(t)$, when the bed shear stress, τ_b, is less than the maximum value at which deposition can occur, $\tau_{b_{max}}$. For $\tau_b < \tau_{b,c}$ (Range I), where $\tau_{b,c}$ is the value of τ_b at which the deposition rate in Range I is equal to that in Range II (defined below), and for $C < C1$ for all values of $\tau_b < \tau_{b_{max}}$, the rate of deposition, dC/dt, is determined using the exponential law given by Eq. 2.54. For the intersection of $\tau_{b,c} < \tau_b < \tau_{b_{max}}$ (Range II) and for $C > C_I$, the deposition rate is given by the log-normal expression (Eq. 2.58). The mass of sediment deposited per time-step is evaluated by averaging dC/dt at times t and $t+\Delta t$ in Range I and for $C < C1$ in Range II, as given by Eq. 2.64, while in Range II, the log-normal relationship is integrated over this time period, as given by Eq. 2.65. The thickness of the bed formed by this deposited mass is determined using the properties of the unconsolidated and partially consolidated bed sections. As

deposition continues, first the unconsolidated layers are filled up, followed by the partially consolidated layers. This filling sequence has been used in order to account for consolidation of the bed due to overburden pressure by virtue of the increasing shear strength and density with bed thickness.

10. The salinity of the eroding fluid, S, had the following effect on the resuspension rates of partially consolidated beds using Lake Francis sediment. Between a salinity of ~0 and 2 ppt, the bed shear strength, as determined indirectly from analysis of resuspension tests conducted at salinities between ~0 and 10 ppt, was found to double in value, in a linear manner, between S = ≈0 and 2 ppt, and thereafter, i.e. for S > 2 ppt, was found to remain practically constant. Therefore, the erosion potential for a cohesive sediment bed with S = ~0 ppt is approximately twice that for the same bed with S >2 ppt.
11. Increasing the salinity of the suspending fluid increases slightly the settling velocities, and hence the rates of deposition of a natural mud. Deposition tests were performed with Lake Francis sediment at salinities of ~0, 1, 2, 5, 10, 20 and 35 ppt and for bed shear stress of 0.0, 0.015, 0.05, 0.10, 0.20 and 0.30 N/m^2. For the deposition tests in Range I, the settling velocity was found to increase at a rate proportional to $S^{0.13}$, and was practically invariant with respect to shear stress. For the tests in Range II, the effect of salinity on the deposition rate is given by Eqs. 2.75 and 2.77, and was approximately the same as that in Range I.
12. Simulation of various sediment problems using the model showed that the numerical scheme is stable for all conditions. The accuracy of the solution is affected when the Peclet number, which is the ratio of convection to diffusion, becomes too large (greater than 10^2) or to small (less than 10^{-3}).
13. The model was used to simulate a laboratory resuspension test and four laboratory deposition tests. Reasonably good agreement between the predicted and measured results was obtained in each of these cases. The effect of salinity on both the resuspension test and one of the deposition tests revealed that, as expected, the rates of resuspension and deposition decreased and increased, respectively,

with increasing salinity. Sedimentation processes in a 10 km hypothetical canal, in which both erosion and deposition of sediment occurred, were also simulated at three different salinities to show the effect of salinity under typical prototype conditions. The effect of salinity in this simulation was less apparent than in the case of the laboratory tests because of the simultaneous occurrence of erosion, convection, diffusion and deposition along the canal.

4.2. Recommendations for Future Research

The reported study was primarily concerned with improving the capability of an existing fine sediment transport model to simulate the erosion and deposition of fine, cohesive sediments in estuaries. The processes of turbulent diffusion of suspended sediment and the consolidation of a bed were not addressed. To further upgrade the model, an investigation of the latter two processes is recommended. Specific objectives of such a research could be the following:

1. Conduct a comprehensive review on the turbulent diffusion and dispersion of non-conservative suspended matter in estuarial flows.
2. Develop and incorporate a diffusion algorithm in order to account for the effect of local flow conditions and sediment properties on the diffusion processes. In this algorithm, the components of the turbulent dispersion coefficient in the horizontal dimensions, x and y, should be calculated as functions of the longitudinal (i.e. in the direction of the local flow) and transverse dispersion coefficients and the angle between the flow and the positive x-axis. Diffusion caused by the local velocity distribution and turbulent, Fickian diffusion processes should be combined and represented by these effective turbulent dispersion coefficients.
3. Conduct a comprehensive review on the consolidation of cohesive sediments.
4. Develop and incorporate a consolidation algorithm in order to account for the increase in the bed bulk density and shear strength and the decrease in bed thickness with time due to primary consolidation. Only consolidation, i.e. crushing, of underlying sediment material by new deposits during the bed formation process is currently considered. A complete consolidation algorithm is a useful component of an estuarial fine sediment transport model in

order to account for changes in the bed's structural properties, and hence its erosion potential, over relatively long periods of time (i.e. of the order of one month and longer).

V. REFERENCES

Aitchison, M. E., "The Nature, Extent and Engineering Significance of the Conditions of Unsaturation in Soils Within the Australian Environment," Ph.D. Dissertation, University of Melbourne, 1956.

Aitchison, J. and Brown, J. A. C., The Lognormal Distribution, University of Cambridge, Dept. of Applied Economics, Monograph No. 5, Cambridge, England, 1957.

Alizadeh, A., "Amount and Type of Clay and Pore Fluid Influences on the Critical Shear Stress and Swelling of Cohesive Soils," Ph.D. Dissertation, University of California, Davis, 1974.

Allison, L. E., Organic Carbon, Part II, American Society of Agronomy, Madison, Wisconsin, 1965.

April, G. C., and Brett, C. E., "Predicting Sediment Transport and Deposition Patterns in Mobile Bay, Alabama," Proc. First BHRA International Symposium Dredging Technology, Paper E3, University of Canterbury, England, August, 1975, pp. 359-372.

Ariathurai, R., "A Finite Element Model for Sediment Transport in Estuaries," Ph.D. Dissertation, University of California, Davis, 1974.

Ariathurai, R., and Krone R. B., "Finite Element Model for Cohesive Sediment Transport," Journal of the Hydraulics Division, Proc. ASCE, Vol. 102, No. HY3, March, 1976, pp. 323-338.

Ariathurai, R., MacArthur, R. C., and Krone, R. G., "Mathematical Model of Estuarial Sediment Transport," Technical Report D-77-12, U.S. Army Engineers Waterways Experiment Station, Vicksburg, Mississippi, October, 1977.

Ariathurai, R., and Arulanandan, K., "Erosion Rates of Cohesive Soils," Journal of the Hydraulics Division, ASCE, Vol. 104, No. HY2, February, 1978, pp. 279-283.

Aris, R., Vectors, Tensors, and the Basic Equations of Fluid Mechanics, Prentice-Hall, Englewood Cliffs, New Jersey, 1962.

Arulanandan, K., Sargunam, A., Loganathan, P., and Krone, R. B., "Application of Chemical and Electrical Parameters to Prediction of Erodibility," Special Report 135, Highway Research Board, Washington, D.C., 1973, pp. 42-51.

Arulanandan, K., "Fundamental Aspects of Erosion of Cohesive Soils," Journal of the Hydraulics Division, ASCE, Vol. 101, No. HY5, March, 1975, pp. 635-639.

Arulanandan, K., Loganathan, P., and Krone, R. B., "Pore and Eroding Fluid Influences on Surface Erosion of Soil," Journal of Geotechnical Engineering Division, ASCE, Vol. 101, No. GT1, January, 1975, pp. 51-66.

Bain, A. J., "Erosion of Cohesive Muds," M.S. Thesis, University of Manchester, England, 1981.

Baker, R. A., Editor, Contaminants and Sediments Volume I - Fate and Transport, Case Studies, Modeling, Toxicity, Ann Arbor Science, 1980.

Barnes, R. S. K., and Green, J., Editors, The Estuarine Environment, Applied Science Publishers, London, 1971.

Bauer, L., "Water Quality and Heavy Metals in Sediments of Thirty-Six Florida Marinas," M.S. Project Report, Dept. of Environmental Engineering Sciences, University of Florida, Gainesville, 1981.

Bellessort, B., "Movement of Suspended Sediments in Estuaries-Flocculation and Rate of Removal of Muddy Sediments," in Tracer Techniques in Sediment Transport, International Atomic Energy Agency, Technical Report Series No. 145, 1973, pp. 31-40.

Bennett, H. H., "Some Comparisons of the Properties of Humid-tropical and Humid-temperate American Soils: With Special Reference to the Indicated Relations Between Chemical Composition and Physical Properties," Soil Science, Vol. 21, 1926, pp. 349-375.

Berner, R. G., "Kinetic Models for the Early Diagenesis of Nitrogen, Sulfur, Phosphorus and Silicon in Anoxic Marine Sediments," in The Sea, V, Marine Chemistry, E. D. Goldberg Editor, Wiley-Interscience, 1974.

Berner, R. G., "Stoichiometric Models for Nutrient Regeneration in Anoxic Sediments," Limnology and Oceanography, Vol. 22, No. 5, September, 1977, pp. 781-786.

Bibeau, A. A., and Matijevic, E., "Stability of Polyvinyl Chloride Latex III-Effects of Simple Electrolytes," Journal of Colloid Interface Science, Vol. 44, 1973.

Bjerrum, L., "Geotechnical Properties of Norwegian Marine Clays," Publication No. 4, Norwegian Geotechnical Institute, Oslo, 1954.

Bolz, R. E., and Tuve, G. L., Editors, Handbook of Tables for Applied Engineering Science, Chemical Rubber Co., Cleveland, Ohio, 1976.

Bowles, F. A., "Microstructure of Unconsolidated and Consolidated Marine Sediments," Journal of Sedimentary Petrology, Vol. 39, No. 4, December, 1969, pp. 1546-1551.

Carlson, E. J., and Enger, P. F., "Tractive Force Studies of Cohesive Soils for Design of Earth Canals," Report No. HYD 504, Hydraulics Branch, U.S. Department of Interior, Bureau of Reclamation, Denver, 1962.

Casagrande, A., "The Structure of Clay and its Importance in Foundation Engineering," Journal of the British Society of Civil Engineers, April, 1932.

Christensen, B. A., Discussion of "Erosion and Deposition of Cohesive Soils," by Partheniades, E., Journal of the Hydraulics Division, Proc. ASCE, Vol. 91, No. HY5, September, 1965, p. 301.

Christensen, R. W. and Das, B. M., "Hydraulic Erosion of Remolded Cohesive Soils," Special Report 135, Highway Research Board, Washington, D.C., 1973, pp. 8-19.

Christenson, D. R., and Ferguson, H., "The Effects of Interaction of Salts and Clays on Unsaturated Water Flow," Journal of the Soil Science Society of America, Vol. 30, 1966, pp. 549-553.

Crickmore, M. J., and Aked, R. F., "Pump Samplers for Measuring Sand Transport in Tidal Waters," Instrumentation in Oceanography, Proc. of Institute of Electronic and Radio Engineers Conference, Bangor, September, 1975, pp. 311-326.

Dane, J. H., and Klute, A., "Salt Effects on the Hydraulic Properties of a Swelling Soil," Journal of the Soil Science Society of America, Vol. 41, 1977, pp. 1043-1049.

Das, M. M., "Study of Bingham Shear Strength of a Deep Marine Sediment by Capillary Viscometer," Report HEL-21-6, Hydraulics Engineering Laboratory, University of California, Berkeley, 1970.

Dash, U., "Erosive Behavior of Cohesive Soils," Ph.D. Dissertation, Purdue University, 1968.

Dixit, J. G., "Resuspension Potential of Deposited Kaolinite Beds," M.S. Thesis, University of Florida, 1982.

Dixit, J. G., Mehta, A. J., and Partheniades, E., "Redepositional Properties of Cohesive Sediments Deposited in a Long Flume," UFL/COEL-82/002, Coastal and Oceanographic Engineering Department, University of Florida, Gainesville, Florida, August, 1982.

Dyer, K. R., "Sedimentation in Estuaries," in The Estuarine Environment, Ch. 2, R. S. K. Barnes and J. Green Editors, Applied Science Publishers, London, 1971, pp. 10-32.

Dunn, I. S., "Tractive Resistance of Cohesive Channels," Journal of the Soil Mechanics and Foundation Division, Proc. ASCE, Vol. 85, No. SM3, March, 1959, pp. 1-24.

Dyer, K. R., "Sedimentation in Estuaries," in The Estuarine Environment, Ch. 2, R. S. K. Barnes and J. Green Editors, Applied Science Publishers, London, 1971, pp. 10-32.

Dyer, K. R., Estuaries: A Physical Introduction, John Wiley, London, 1973.

Dyer, K. R., Editor, Estuarine Hydrography and Sedimentation, Cambridge University Press, Cambridge, 1979.

Einstein, H. A., and Krone, R. B., "Experiments to Determine Modes of Cohesive Sediment Transport in Salt Water," Journal of Geophysical Research, Vol. 67, No. 4, April, 1962, pp. 1451-1464.

Edzwald, J. K., Upchurch, J. B., and O'Melia, C. R., "Coagulation in Estuaries," Environmental Science & Technology, Vol. 8, No. 1, January, 1974, pp. 58-63.

Espey, W. H., "A New Test to Measure the Scour of Cohesive Sediment," Technical Report HYD 01-6301, Hydraulics Engineering Laboratory, Dept. of Civil Engineering, University of Texas, Austin, 1963.

Fagerstrom, T., and Zernelov, I., "Formation of Methyl Mercury from Pore Mercuric Sulphide in Aerobic Organic Sediment," Water Research, Pergamon Press, Vol. 5, No. 121, 1971.

Finkelstein, K., and Prins, D., "An Inexpensive, Portable Vibracoring System for Shallow-Water and Land Application," Coastal Engineering Technical Aid No. 81-8, U.S. Army Corps of Engineers Coastal Engineering Research Center, Fort Belvoir, Virginia, July, 1981.

Fischer, H. B., Imberger, J., List, E. J., Koh, R. C. Y., and Brooks, N. H., Mixing in Inland and Coastal Waters, Academic Press, New York, 1979.

Flaxman, E. M., "Channel Stability in Undisturbed Cohesive Soils," Journal of the Hydraulics Division, Proc. ASCE, Vol. 89, No. HY2, March, 1963, pp. 87-96.

Fukuda, M. K., "The Entrainment of Cohesive Sediments in Freshwater," Ph.D. Dissertation, Case Western Reserve University, Cleveland, Ohio, 1978.

Gardner, W. H., Mayhugh, M. S., Goertzen, J. O., and Bower, C. A., "Effect of Electrolyte Concentration and Exchangeable Sodium Percentage on Diffusivity of Water in Soils," Journal of the Soil Science Society of America, Vol. 88, 1959, pp. 270-274.

Gibbs, R. J., "Clay Mineral Segregation in the Marine Environment," Journal of Sedimentary Petrology, Vol. 47, No. 1, March, 1977, pp. 237-243.

Ginsburg, R. N., and Lloyd, M. R., "A Manual Piston Coring Device for Use in Shallow Water," Journal of Sedimentary Petrology, Vol. 26, 1956, pp. 164-166.

Grim, R. E., Applied Clay Mineralogy, McGraw-Hill, New York, 1962.

Grim, R. E., Clay Mineralogy, McGraw-Hill, New York, 1968.

Grimshaw, R. W., The Chemistry and Physics of Clays, Wiley-Interscience, New York, 1971.

Grissinger, E. H., "Resistance of Clay Systems to Erosion by Water," Water Resources Research, Vol. 2, No. 1, 1966, pp. 131-138.

Gularte, R. C., Kelley, W. E., and Nacci, V. A., "The Threshold Erosional Velocities and Rates of Erosion for Redeposited Estuarine Dredge Materials," Proc. of the Second International Symposium on Dredging Technology, Texas A & M University, College Station, Texas, Paper H-3, November, 1977.

Gularte, R. C., "Erosion of Cohesive Sediment as a Rate Process," Ph.D. Thesis, University of Rhode Island, 1978.

Harris, H. S., Kaufman, W. J., and Krone, R. B., "Orthokinetic Flocculation in Water Purification," Journal of the Sanitary Engineering Division, Proc. ASCE, Vol. 92, No. SA6, December, 1966, pp. 95-111.

Harthmann, M., Muller, P., Suess, E. and Van Der Weijden, C. H., "Oxidation of Organic Matter in Recent Marine Sediments," Meteor Forschungsergeb. Reihe, Vol. C12, 1973, pp. 74-86.

Hauser, M. E., and Fauth, M., "Potomac River Sediment Study," Naval Ordinance Station, Indiana Head, Maryland, June, 1972.

Hirst, T. J., Perlow, M., Richards, A. F., Burton, B. S., and van Sciver, W. J., "Improved In Situ Gamma-Ray Transmission Densitometer for Marine Sediments," Ocean Engineering, Vol. 3, No. 1, 1975, pp. 17-27.

Huang, S., Han, N., and Zhang, X., "Analysis of Siltation at Mouth Bar of the Yangtze River Estuary," Proc. International Conference on River Sediment Transportation, Peking, China, March, 1980.

Hughes, P. A., "A Determination of the Relation Between Wind and Sea-Surface Drift," Quarterly Journal of the Royal Meteorological Society, London, Vol. 82, October, 1956, pp. 494-502.

Hunt, J. R., "Prediction of Oceanic Particle Size Distribution from Coagulation and Sedimentation Mechanisms," in Advances in Chemistry Series No. 189 - Particulates in Water, Ch. 11, M. C. Kavanaugh and J. O. Leckie Editors, American Chemical Society, 1980, pp. 243-257.

Hunt, S. D., "A Comparative Review of Laboratory Data on Erosion of Cohesive Sediment Beds," UFL/COEL/MP-81/7, M.E. Project Report, University of Florida, Gainesville, 1981.

Ingham, A. E., Editor, Sea Surveying, John Wiley & Sons, Chichester, U.K., 1975.

Ippen, A. T., Editor, Estuary and Coastline Hydrodynamics, McGraw-Hill, New York, 1966.

Jeffrey, D. J., and Acrives, A., "The Rheological Properties of Suspensions of Rigid Particles," Journal of the American Institute of Chemical Engineers, Vol. 22, No. 3, May, 1976.

Jones, A. S. G., "Partial Geochemical Study of Shallow Marine Sediments," Marine Geology, Vol. 12, 1972.

Kandiah, A., "Fundamental Aspects of Surface Erosion of Cohesive Soils," Ph.D. Dissertation, University of California, Davis, 1974.

Kelly, W. E., and Gularte, R. C., "Erosion Resistance of Cohesive Soils," Journal of the Hydraulics Division, ASCE, Vol. 107, No. HY10, October, 1981.

Keulegan, G. H., "The Mechanism of an Arrested Saline Wedge," in Estuary and Coastline Hydrodynamics, A. T. Ippen Editor, McGraw-Hill, New York, 1966, pp. 546-574.

King, I. P., Norton, W. R., and Orlob, G. T., A Finite Element Solution for Two-Dimensional Density Stratified Flow, U.S. Department of the Interior, Office of Water Resources Research, April, 1973.

Kirby, R., "The UCS Vibrocorer," Report No. UCS/10/1972, Unit of Coastal Sedimentation, Taunton, U. K., 1972.

Kirby, R., and Parker, W. R., "Fluid Mud in the Severn Estuary and the Bristol Channel and its Relevance to Pollution Studies," Proc. International Chemical Engineers Exeter Symposium, Exeter, England, Paper A-4, 1973, pp. 1-14.

Kirby, R., and Parker, W. R., "Seabed Density Measurements Related to Echo Sounder Records," Dock and Harbour Authority, Vol. 54, 1974, pp. 423-424.

Kirby, R., and Parker, W. R., "The Physical Characteristics and Environmental Significance of Fine Sediment Suspensions in Estuaries," in Estuaries, Geophysics and the Environment, National Academy of Sciences, Washington, 1977, pp. 110-120.

Kranck, K., "Sedimentation Processes in the Sea," in The Handbook of Environmental Chemistry, Vol. 2, Part A, O. Hutzinger Editor, Springer-Verlag, Berlin, 1980, pp. 61-75.

Kranck, K., "Particulate Matter Grain-Size Characteristics and Flocculation in a Partially Mixed Estuary, " Sedimentology, Vol. 28, No. 1, 1981, pp. 107-119.

Krom, M. D., and Berner, R. A., "The Diffusion Coefficients of Sulfate, Ammonium and Phosphate Ions in Anoxic Marine Sediments," Limnology and Oceanography, Vol. 25, No. 2, 1980, pp. 327-337.

Krone, R. B., "Flume Studies of the Transport of Sediment in Estuarial Shoaling Processes," Final Report, Hydarulic Engineering Laboratory and Sanitary Engineering Research Laboratory, University of California, Berkeley, June, 1962.

Krone, R. B., "A Study of Rheological Properties of Estuarial Sediments," Technical Bulletin No. 7, Committee on Tidal Hydraulics, U.S. Army Corps of Engineers, Vicksburg, Mississippi, September, 1963.

Krone, R. B., "A Field Study of Flocculation as a Factor in Estuarial Shoaling Processes," Technical Report 19, Committee on Tidal Hydraulics, U.S. Army Corps of Engineers, Vicksburg, Mississippi, June, 1972.

Krone, R. B., "Aggregation of Suspended Particles in Estuaries," in Estuarine Transport Processes, P. Kjerfve Editor, the Belle W. Baruch Library in Marine Science, No. 7, University of South Carolina Press, Columbia, 1978, pp. 177-190.

Kruyt, H. R., Editor, Colloid Science, Vol. I, Elsevier, New York, 1952.

Lambe, T. W., "The Structure of Inorganic Soil," ASCE, Vol. 79, No. 315, 1953.

Lambe, T. W., "The Structure of Compacted Clay," Journal of Soil Mechanics and Foundation Division, ASCE, Vol. 84, No. SM2, 1958.

Lambermont, J., and Lebon, G., "Erosion of Cohesive Soils," Journal of Hydraulic Research, Vol. 16, No. 1, 1978, pp. 27-44.

Lasage, A. C., and Holland, H. D., "Mathematical Aspects of Non-Steady-State Diagenesis," Geochimica et Cosmochimica Acta, Vol. 40, No. 3, March, 1976, pp. 257-266.

Lasater, J., "Chemical Oceanography," Unpublished Lecture Notes, Florida Institute of Technology, Melbourne, Florida, 1975.

Lee, D. Y., "Resuspension and Deposition of Lake Erie Sediments," M.S. Thesis, Case Western Reserve University, Cleveland, Ohio, 1979.

Lee, P. T., "Deposition and Scour of Clay Particles due to Currents," M.S. Thesis, Asian Institute of Technology, Bangkok, Thailand, 1974.

Leendertse, J. J., Alexander, R. C., and Liu, S. K., "Three-Dimensional Model for Estuaries and Coastal Seas: Vol. 1, Principles of Computation," Report R-1417-OWRR, Rand Corporation, Santa Monica, California, December, 1973.

Lerman, A., and Weiler, R. R., "Diffusion and Accumulation of Chloride and Sodium in Lake Ontario Sediment," Earth and Planetary Science Letters, Vol. 10, 1970, pp. 150-156.

Li, Y. H., and Gregory, S., "Diffusion of Ions in Sea Water and in Deep-Sea Sediments," Geochimica et Cosmochimica Acta, Vol. 38, 1974, pp. 703-714.

Liou, Y. D., "Hydraulic Erodibility of Two Pure Clay Systems," Ph.D. Dissertation, Colorado State University, Fort Collins, Colorado, 1970.

Liu, S. K., and Leendertse, J., "Multi-dimensional Numerical Modeling of Estuaries and Coastal Seas," Advances in Hydroscience, Vol. 11, Academic Press, 1978.

Lutz, J. F., "The Physico-chemical Properties of Soils Affecting Soil Erosion," Research Bulletin 212, University of Missouri, Agricultural Experiment Station, July, 1934.

MacArthur, R. C., "Turbulent Mixing Processes in a Partially Mixed Estuary," Ph.D. Dissertation, University of California, Davis, 1979.

Manheim, F. T., "The Diffusion of Ions in Unconsolidated Sediments," Earth and Planetary Science Letters, Vol. 9, 1970, pp. 307-309.

Martin, R. T., "Adsorbed Water on Clay: A Review," Proc. of Ninth National Conference on Clays and Clay Minerals, 1960, pp. 28-70.

Martin, R. T., "Quantitative Fabric of Consolidated Kaolinite," Research Report 65-47, Soils Publication No. 179, Department of Civil Engineering, M.I.T., 1965.

McConnachi, I., "Fabric Changes in Consolidated Kaolin," Geotechnique, Vol. 24, No. 2, 1974, pp. 207-222.

Mehta, A. J., "Depositional Behavior of Cohesive Sediments," Ph.D. Dissertation, University of Florida, Gainesville, 1973.

Mehta, A. J., and Partheniades, E., "Depositional Behavior of Cohesive Sediments," Technical Report No. 16, Coastal and Oceanographic Engineering Laboratory, University of Florida, Gainesville, March, 1973.

Mehta, A. J., and Partheniades, E., "An Investigation of the Depositional Properties of Flocculated Fine Sediments," Journal of Hydraulics Research, International Association for Hydraulics Research, Vol. 13, No. 14, 1975, pp. 361-381.

Mehta, A. J., and Partheniades, E., "Kaolinite Resuspension Properties," Journal of the Hydraulics Division, Proc. ASCE, Vol. 105, No. HY4, March, 1979, pp. 411-416.

Mehta, A. J., "Review of Erosion Function for Cohesive Sediment Beds," Proc. First Indian Conference on Ocean Engineering, Indian Institute of Technology, Madras, India, Vol. 1, February, 1981, pp. 122-130.

Mehta, A. J., and Hayter, E. J., "Preliminary Investigation of Fine Sediment Dynamics in Cumbarjua Canal, Goa, India," UFL/COEL-81-012, Coastal and Oceanographic Engineering Department, University of Florida, Gainesville, December, 1981.

Mehta, A. J., Parchure, T. M., Dixit, J. G., and Ariathurai, R., "Resuspension Potential of Deposited Cohesive Sediment Beds," in Estuarine Comparisons, V. S. Kennedy Editor, Academic Press, New York, 1982a, pp. 591-609.

Mehta, A. J., Partheniades, E., Dixit, J. and McAnally, W. H., "Properties of Deposited Kaolinite in a Long Flume," Proc. of Hydraulics Division Conference on: Applying Research to Hydraulic Practice, ASCE, Jackson, Mississippi, August, 1982b.

Michaels, A. S., "Mechanism of Deflocculation of Clays by Condensed Alkali Phosphates," Industrial Engineering Chemistry, 1957.

Middleton, H. E., "Properties of Soils which Influence Soil Erosion," U.S.D.A. Technical Bulletin 178, 1930.

Migniot, P. C., "A Study of the Physical Properties of Different Very Fine Sediments and Their Behavior Under Hydrodynamic Action," La Houille Blanche, No. 7, 1968, pp. 591-620. (In French, with English abstract)

Miller, C. R., "A Critique on Stable Channels in Cohesive Materials and a Research Proposal," Research Report 333, Agriculture Research Service, U.S.D.A., 1960.

Mitchell, J. K., "The Importance of Structure to the Engineering Behavior of Clay," D.Sc. Thesis, M.I.T., 1956.

Mitchell, J. K., "Fundamental Aspects of Thixotropy in Soils," Transactions of the ASCE, Vol. 126, Pt. 1, 1961, pp. 1586-1620.

Mitchell, J. K., Singh, A., and Campanella, R. G., "Bonding Effective Stresses and Strength of Soils," Journal of the Soil Mechanics and Foundation Division, ASCE, Vol. 95, No. SM5, September, 1969, pp. 1219-1246.

Mitchell, J. K., Fundamentals of Soil Behavior, John Wiley & Sons, New York, 1976.

Moore, W. L., and Masch, F. D., "Experiments on the Scour Resistance of Cohesive Sediments," Journal of the Geophysical Research, Vol. 67, No. 4, April, 1962, pp. 1437-1446.

Morgenstern, N. R., and Tchalenko, J. S., "The Optical Determination of Preferred Orientation in Clays and its Application to the Study of Microstructure in Consolidated Kaolin," Proc. Royal Society of London, Ser. A300, 1967, pp. 218-250.

Mortimer, C. H., "Chemical Exchanges between Sediments and Water in the Great Lakes - Speculations on Probable Regulatory Mechanisms," Limnology and Oceanography, Vol. 16, No. 2, March, 1971, pp. 387-404.

Murray, J. W., Grundmanis, V., and Smethie, Jr., W. M., "Interstitial Water Chemistry in the Sediments of Saanich Inlet," Geochimica et Cosmochimica Acta, Vol. 42, No. 7, July, 1978, pp. 1011-1026.

Nriagu, J. O., "Dissolved Silica in Pore Waters of Lakes Ontario, Erie, and Superior Sediments," Limnology and Oceanography, Vol. 23, No. 1, January, 1978, pp. 53-67.

O'Connor, B. A., "Mathematical Model for Sediment Distribution," Proc. Fourteenth Congress of the International Association of Hydraulic Research, Vol. 4, 1971, pp. 195-202.

Odd, N. V. M., and Owen, M. W., "A Two-layer Model for Mud Transport in the Thames Estuary," Proc. of the Institution of Civil Engineers, London, Supplement (ix), 1972, pp. 175-205.

Officer, C. B., Physical Oceanography of Estuaries, John Wiley, New York, 1976.

Officer, C. B., "Physical Dynamics of Estuarine Suspended Sediments," Marine Geology, Vol. 40, 1981, pp. 1-14.

O'Melia, C. R., in Physicochemical Processes for Water Quality Control, W. J. Weber Editor, Wiley-Interscience, New York, 1972, pp. 61-109.

Onishi, Y., and Wise, S. E., "Finite Element Model for Sediment and Toxic Contaminant Transport in Streams," Proc. Specialty Conference on Conservation and Utilization of Water and Energy Resources, ASCE, San Francisco, California, August, 1979, pp. 144-150.

Orlob, G. T., Shubinski, R. P., and Feigner, K. D., "Mathematical Modeling of Water Quality in Estuarial Systems," ASCE National Symposium on Estuarine Pollution, Stanford University, California, August, 1967.

Owen, M. W., "A Detailed Study of the Settling Velocities of an Estuary Mud," Report No. INT 78, Hydraulics Research Station, Wallingford, England, September, 1970.

Owen, M. W., "The Effect of Turbulence on the Settling Velocities of Silt Flocs," Proc. of Fourteenth Congress of I.A.H.R., Vol. 4, Paris, August, 1971, pp. 27-32.

Owen, M. W., "Erosion of Avonmouth Mud," Report No. INT 150, Hydraulics Research Station, Wallingford, England, September 1975.

Owen, M. W., "Problems in the Modeling of Transport, Erosion, and Deposition of Cohesive Sediments," in The Sea VI, Marine Modeling, E. D. Goldberg, I. N. McCave, J. J. O'Brien and J. H. Steele Editors, Wiley-Interscience, New York, 1977, pp. 515-537.

Paaswell, R. E., "Causes and Mechanisms of Cohesive Soil Erosion: The State of the Art," Special Report 135, Highway Research Board, Washington D.C., 1973, pp. 52-74.

Pacey, J. G., "The Structure of Compacted Soils," M.S. Thesis, M.I.T., 1956.

Parchure, T. M., "Effect of Bed Shear Stress on the Erosional Characteristics of Kaolinite," M.S. Thesis, University of Florida, Gainesville, December, 1980.

Parchure, T. M., Dixit, J. G., and Mehta, A. J., "Erosive Characteristics of Lake Francis Sediment," Special Report, Department of Coastal and Oceanographic Engineering, University of Florida, Gainesville, January, 1981.

Parker, W. R., and Kirby, R., "Fine Sediment Studies Relevant to Dredging Practice and Control," Proc. Second International Symposium on Dredging Technology, BHRA, Paper B2, Texas A & M University, College Station, November, 1977.

Parker, W. R., and Lee, K., "The Behavior of Fine Sediment Relevant to the Dispersal of Pollutants," ICES Workshop on Sediment and Pollutant Interchange in Shallow Seas, Texel, England, September, 1979.

Parker, W. R., "Sediment Dynamics," Unpublished Lecture Notes, University of Florida, Gainesville, February, 1980.

Partheniades, E., "A Study of Erosion and Deposition of Cohesive Soils in Salt Water," Ph.D. Dissertation, University of California, Berkeley, 1962.

Partheniades, E., "A Summary of the Present Knowledge on the Behavior of Fine Sediments in Estuaries," Technical Note No. 8, Hydrodynamics Lab, M.I.T., Cambridge, Mass., 1964.

Partheniades, E., "Erosion and Deposition of Cohesive Soils," Journal of the Hydraulic Division, Proc. ASCE, Vol. 91, No. HY1, January, 1965, pp. 105-138.

Partheniades, E., "Field Investigations to Determine Sediment Sources and Salinity Intrusion in the Maracaibo Estuary, Venezuela," Report No. 94, Hydrodynamics Lab., M.I.T., Cambridge, Mass., 1966.

Partheniades, E., Kennedy, J. F., Etter, R. J., and Hoyer, R. P., "Investigations of the Depositional Behavior of Fine Cohesive Sediments in an Annular Rotating Channel," Report No. 96, Hydrodynamics Lab., M.I.T., Cambridge, Mass., 1966.

Partheniades, E., Cross, R. H., and Ayora, A., "Further Results on the Deposition of Cohesive Sediments," Proc. Eleventh Conference on Coastal Engineering, Ch. 47, 1968, pp. 723-742.

Partheniades, E., "Erosion and Deposition of Cohesive Materials," in River Mechanics, Vol. II, H. W. Shen Editor, Fort Collins, Colorado, 1971.

Partheniades, E., "Unified View of Wash Load and Bed Material Load," Journal of the Hydraulics Division, ASCE, Vol. 103, No. HY9, 1977, pp. 1037-1057.

Patrick, W. H., Jr., and Khalid, R. A., "Phosphate Release and Sorption by Soils and Sediments: Effect of Aerobic and Anaerobic Conditions," Science, Vol. 186, October, 1974, pp. 53-55.

Postma, H., "Sediment Transport and Sedimentation in the Estuarine Environment," in Estuaries, G. H. Lauff Editor, American Association for Advancement of Science Publication 83, Washington D.C., 1967, pp. 158-179.

Preiss, K., "Non-destructive Laboratory Measurement of Marine Sediment Density in a Core Barrel using Gamma Radiation," Deep-Sea Research, Vol. 15, 1968, pp. 401-407.

Preiss, K., "In Situ Measurement of the Density of Sea Floor Sediment by Gamma Ray Transmission," Radiation Isotope Tech. in Latin American Dev., Proc. American Nuclear Society Topical Meeting, San Juan, Puerto Rico, 1969, pp. 483-493.

Quirk, J. P., and Schofield, R. K., "The Effect of Electrolyte Concentration on Soil Permeability," Journal of Soil Science, Vol. 6, No. 2, 1955.

Rao, L. V. G., Cherian, T., Varma, K. K., and Varadachari, V. V. R., "Hydrographic Conditions and Flow Pattern in Cumbarjua Canal, Goa," Indian Journal of Marine Sciences, Vol. 5, December, 1976, pp. 163-168.

Raudkivi, A. J., and Hutchison, D. L., "Erosion of Kaolinite Clay by Flowing Water," Proc. Royal Society, London, 1974, pp. 537-554.

Richards, A. F., Hirst, T. J., and Parks, J. M., "Bulk Density - Water Content Relationship in Marine Silts and Clays," Journal of Sedimentary Petrology, Vol. 44, No. 4, 1974, pp. 1004-1009.

Rose, V. C., and Roney, J. R., "A Nuclear Gage for In-place Measurement of Sediment Density," Offshore Tech. Conference Preprints, Vol. 1, 1971, pp. 43-52.

Rosillon, R., and Volkenborn, C., "Sedimentación de Material Cohesivo en Agua Salada," Thesis, University of Zulia, Maracaibo, Venezuela, November, 1964.

Salomons, W., and Mook, W. G., "Trace Metal Concentrations in Estuarine Sediments: Mobilization, Mixing or Precipitation," Journal of Sea Research, Netherlands, Vol. 11, No. 2, 1977, pp. 119-129.

Sargunam, A., Riley, P., Arulanandan, K., and Krone, R. B., "Effect of Physico-chemical Factors on the Erosion of Cohesive Soils," Journal of the Hydraulics Division, ASCE, Vol. 99, No. HY3, March, 1973, pp. 553-558.

Schindler, D. W., Hesslein, R. H., and Wagemann, R., "Effects of Acidification on Mobilization of Heavy Metals and Radionuclides from the Sediments of Freshwater Lakes," Canadian Journal of Fisheries and Aquatic Sciences, Vol. 37, 1980, pp. 373-377.

Sheng, Y. P., and Lick, W., "The Transport and Resuspension of Sediment in a Shallow Lake," Journal of Geophysical Research, Vol. 84, No. C4, 1979, pp. 1809-1826.

Sherard, J. L., Decker, R. S., and Ryka, N. L., "Piping in Earth Dams of Dispersive Clay," ASCE Soil Mechanics and Foundation Conference, Purdue University, Lafayette, Indiana, June, 1972.

Sholkovitz, E. R., "Interstitial Water Chemistry of Santa Barbara Basin Sediments," Geochimica et Cosmochimica Acta, Vol. 37, 1973, pp. 2043-2073.

Smerdon, E. T., and Beasley, R. P., "The Tractive Force Theory Applied to Stability of Open Channels in Cohesive Soils," Research Bulletin 715, Agricultural Experiment Station, University of Missouri, October, 1959.

Soule, D. F., and Oguri, M., Editors, "Marine Studies of San Pedro Bay, California," Sediment Investigations - Part VII, University of Southern California, Los Angeles, August, 1974.

Sugimoto, T., "Effects of Convection and Brownian Motion on Particle Growth Rate in Colloidal Dispersion," Journal of the American Institute of Chemical Engineering, Vol. 24, No. 6, November, 1978.

Sundborg, A., "The River Klaraven, A Study of Fluvial Processes," Bulletin No. 52, Institute of Hydraulics, Royal Institute of Technology, Stockholm, Sweden, 1956.

Terwindt, J. H. J., Brusers, H. N. C., and Svasek, J. N., "Experimental Investigation on the Erosion-Sensitivity of a Sand-Clay Lamination," Sedimentology, Vol. 11, 1968, pp. 105-144.

Terzaghi, K., and Peck, R. B., Soil Mechanics in Engineering Practice, John Wiley and Sons, New York, 1960.

Thorn, M. F. C., and Parsons, J. G., "Properties of Grangemouth Mud," Report No. EX781, Hydraulics Research Station, Wallingford, England, July, 1977.

Thorn, M. F. C., and Parsons, J. G., "Erosion of Cohesive Sediments in Estuaries: An Engineering Guide," Proc. Third International Symposium on Dredging Technology, Paper F1, March, 1980.

Thorn, M. F. C., "Physical Processes of Siltation in Tidal Channels," Proc. Hydraulic Modelling Applied to Maritime Engineering Problems, ICE, London, 1981, pp. 47-55.

Tubman, M. W., and Suhayda, J. N., "Wave Action and Bottom Movement in Fine Sediments," Proc. Fifteenth Coastal Engineering Conference, Honolulu, 1977, pp. 1168-1183.

Vanderborght, J. P., Wollast, R., and Billen, G., "Kinetic Models of Diagenesis in Disturbed Sediments, Part 2: Nitrogen Diagenesis," Limnology and Oceanography, Vol. 22, No. 5, September, 1977, pp. 794-803.

van Olphen, H., An Introduction to Clay Colloid Chemistry, Interscience Publishers, New York, 1963.

Veltman, M., "Disposal of Contaminated Estuarial Sediment," First International Conference on Cohesive Sediments, Churchill College, Cambridge, England, 1979.

Vincent, B., Bijsterbosch, B. H., and Lyklema, J., "Competitive Adsorption of Ions and Neutral Molecules in the Stern Layer on Silver Iodide and its Effect on Colloid Stability," Journal of Colloid Interface Science, Vol. 37, 1971.

Weckmann, J., "Sediment Management at a Coastal Marina," M.E. Thesis, University of Florida, Gainesville, 1979.

Whitehouse, U. G., Jeffrey, L. M., and Debbrecht, J. D., "Differential Settling Tendencies of Clay Minerals in Saline Waters," Proc. Seventh National Conference on Clays and Clay Minerals, 1960, pp. 1-79.

Whitmarsh, R. B., "Precise Sediment Density by Gamma-Ray Attenuation Alone," Journal of Sedimentary Petrology, Vol. 41, 1971, pp. 882-883.

Wilson, W., and Bradley, D., "Specific Volume of Sea Water as a Function of Temperature, Pressure and Salinity," Deep-Sea Research, Vol. 15, 1968, pp. 355-363.

Yeh, H. Y., "Resuspension Properties of Flow Deposited Cohesive Sediment Beds," M.S. Thesis, University of Florida, Gainesville, 1979.

Zeichner, G. R., and Schowalter, W. R., "Use of Trajectory Analysis to Study Stability of Colloidal Dispersion in Flow Fields," Journal of the American Institute of Chemical Engineering, Vol. 23, No. 3, 1977.

Zienkiewicz, O. C., The Finite Element Method in Engineering Science, McGraw-Hill, London, 1971.

APPENDIX A

Model Flow Chart of SEDIMENT IIIA

FLOW CHART OF SEDIMENT IIIA

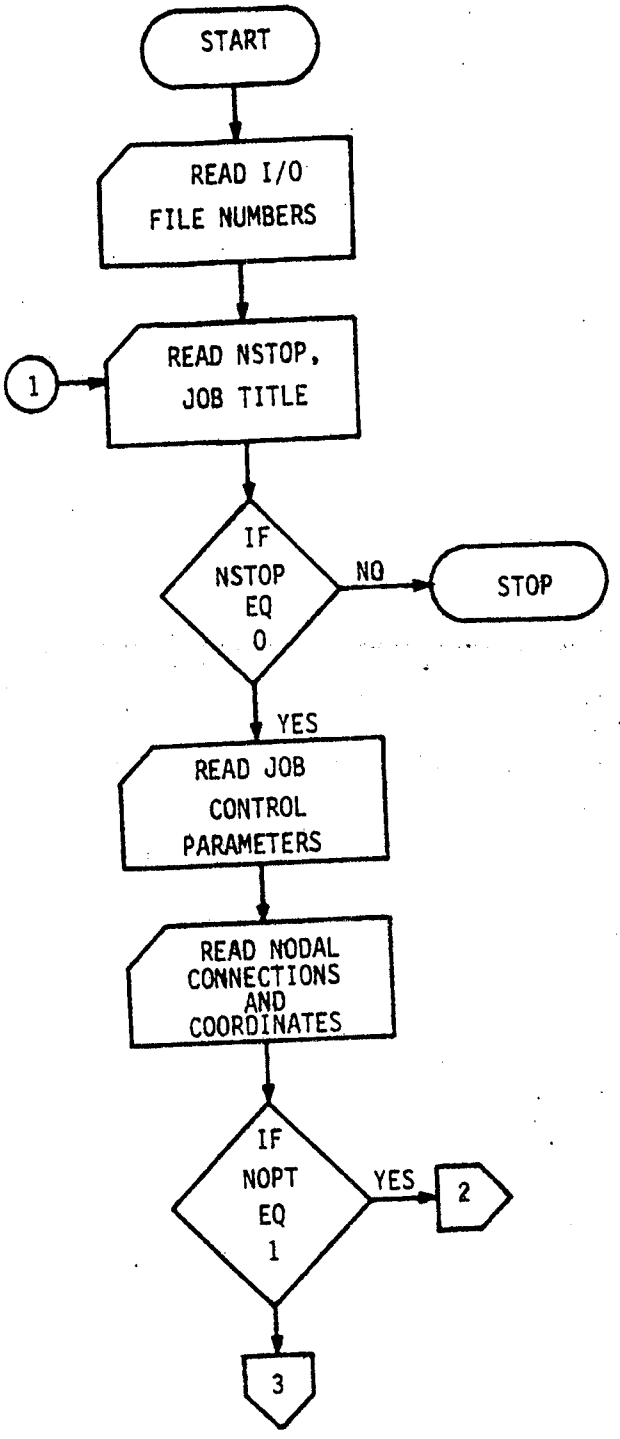

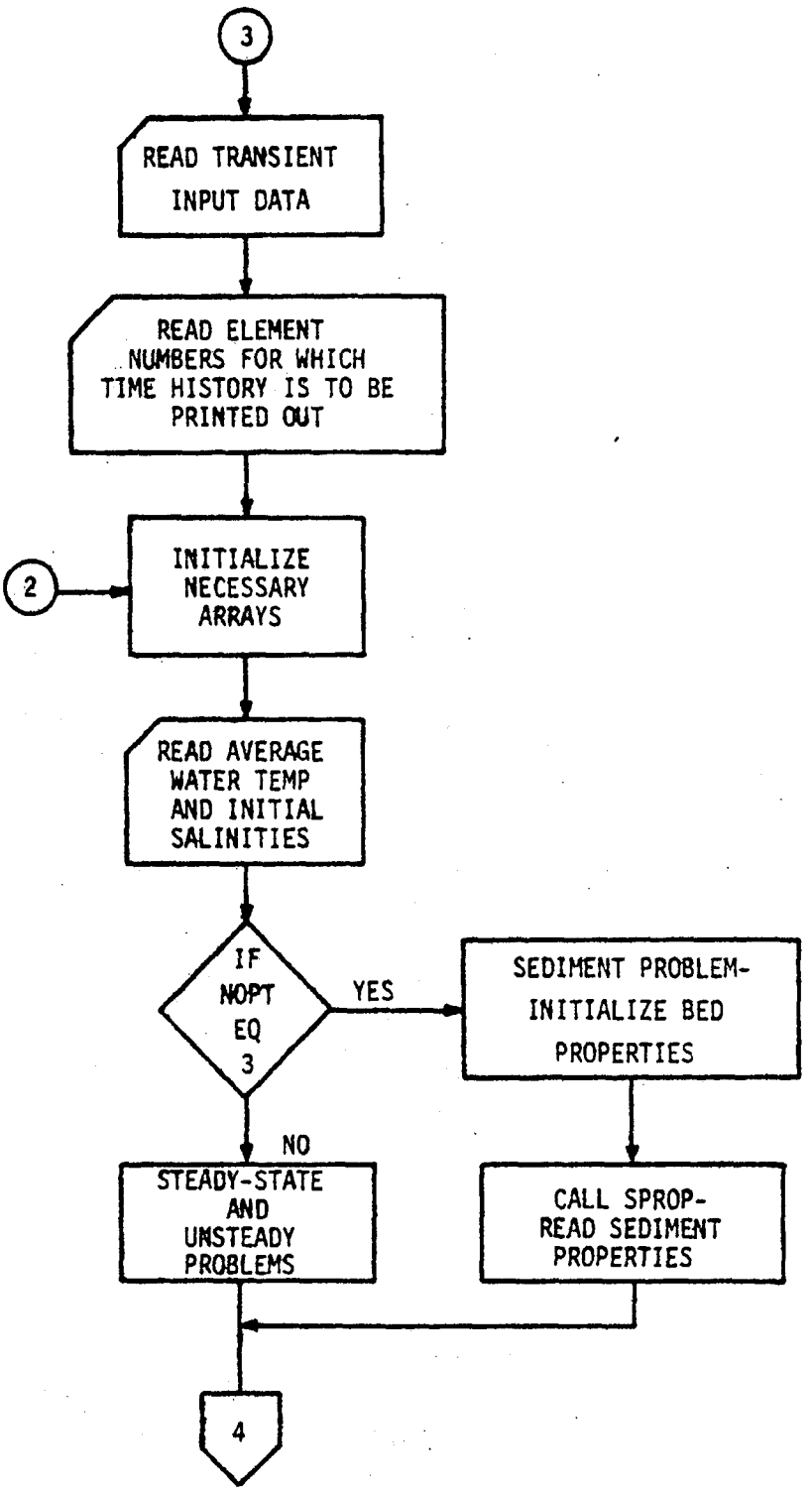
3
READ TRANSIENT INPUT DATA
READ ELEMENT NUMBERS FOR WHICH TIME HISTORY IS TO BE PRINTED OUT
2
INITIALIZE NECESSARY ARRAYS
READ AVERAGE WATER TEMP AND INITIAL SALINITIES
IF NOPT EQ 3
YES
SEDIMENT PROBLEM- INITIALIZE BED PROPERTIES
NO
STEADY-STATE AND UNSTEADY PROBLEMS
CALL SPROP- READ SEDIMENT PROPERTIES
4

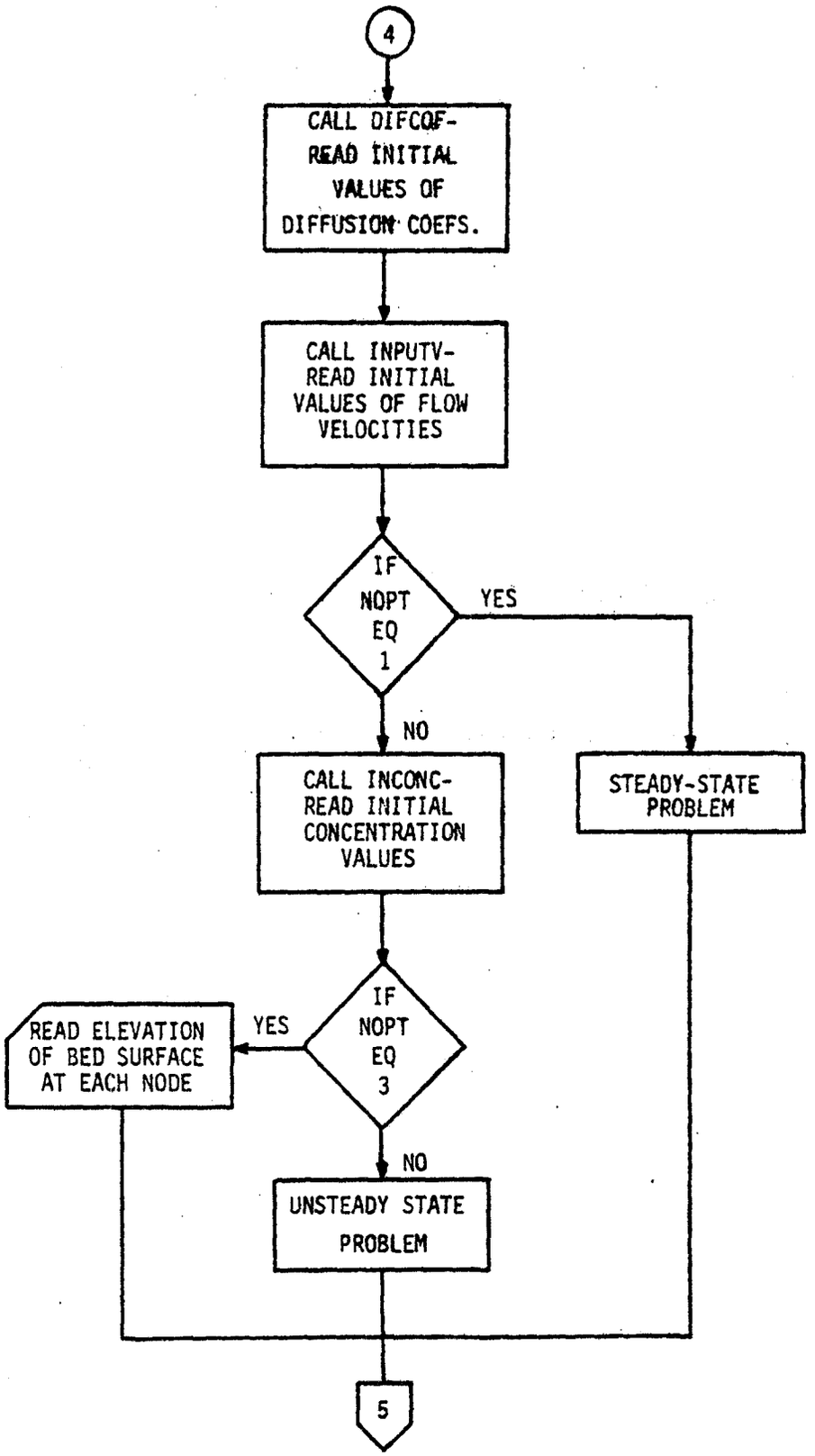
4
CALL DIFCOF-
READ INITIAL
VALUES OF
DIFFUSION COEFS.
CALL INPUTV-
READ INITIAL
VALUES OF FLOW
VELOCITIES
IF
NOPT
EQ
1
YES
NO
CALL INCONC-
READ INITIAL
CONCENTRATION
VALUES
STEADY-STATE
PROBLEM
IF
NOPT
EQ
3
YES
READ ELEVATION
OF BED SURFACE
AT EACH NODE
NO
UNSTEADY STATE
PROBLEM
5

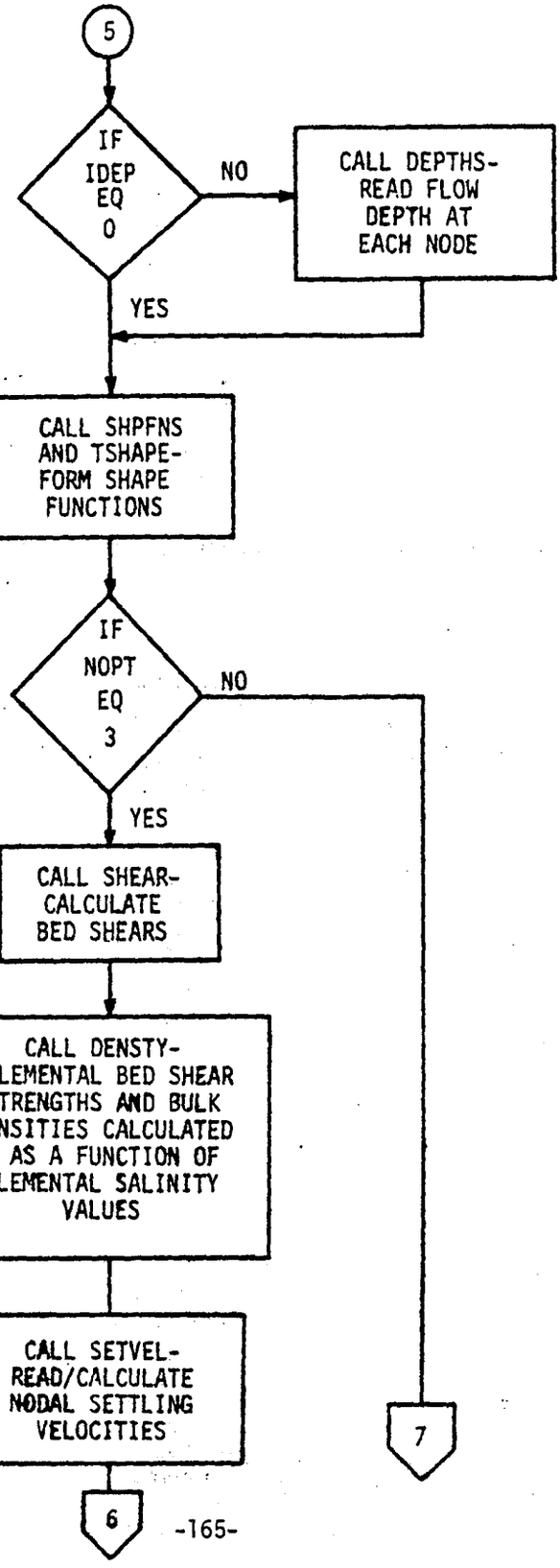
5
IF IDEP EQ 0
NO
CALL DEPTHS- READ FLOW DEPTH AT EACH NODE
YES
CALL SHPFNS AND TSHAPE- FORM SHAPE FUNCTIONS
IF NOPT EQ 3
NO
YES
CALL SHEAR- CALCULATE BED SHEARS
CALL DENSTY- ELEMENTAL BED SHEAR STRENGTHS AND BULK DENSITIES CALCULATED AS A FUNCTION OF ELEMENTAL SALINITY VALUES
CALL SETVEL- READ/CALCULATE NODAL SETTLING VELOCITIES
7
6

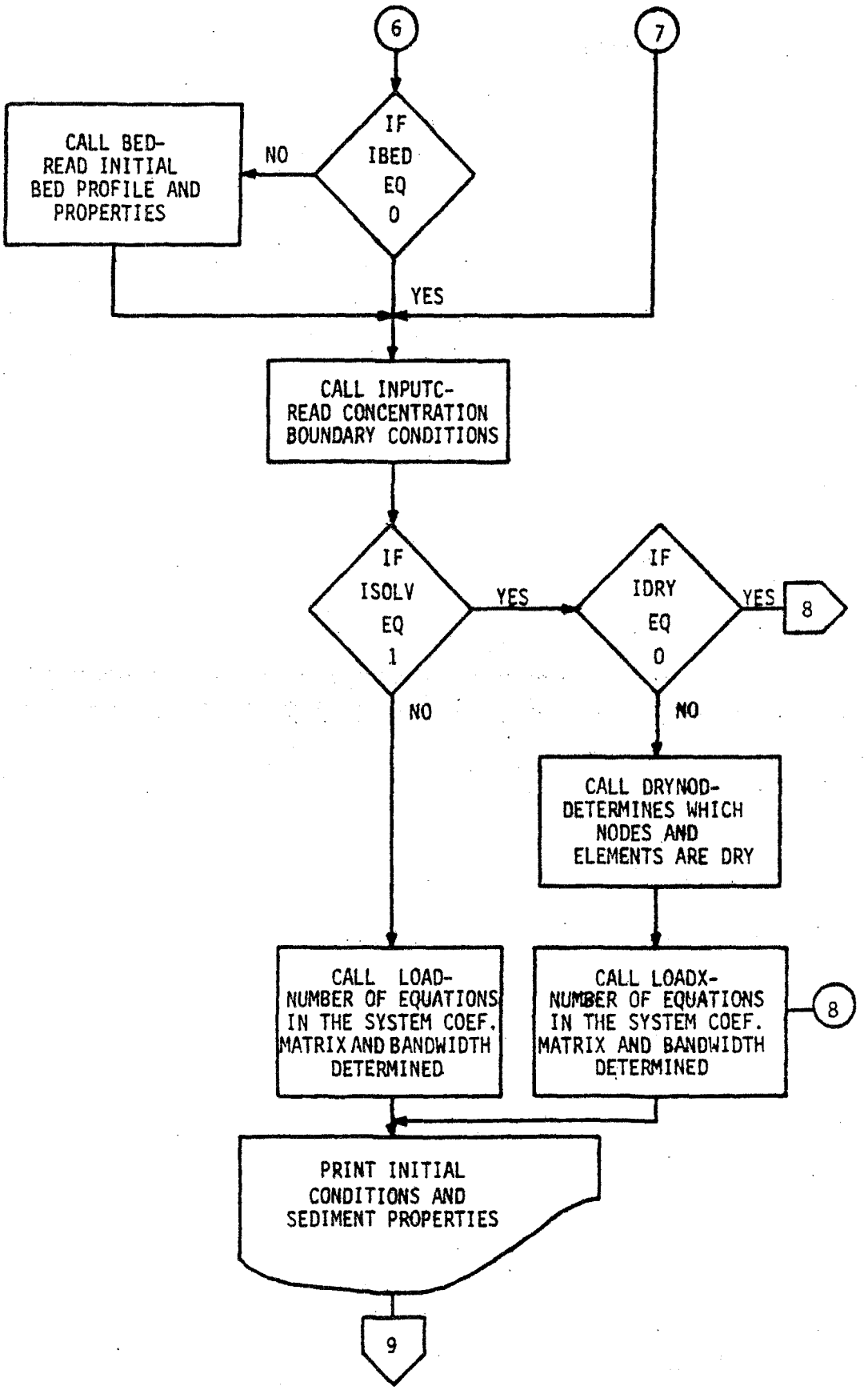
6
7
IF IBED EQ 0
NO
CALL BED- READ INITIAL BED PROFILE AND PROPERTIES
YES
CALL INPUTC- READ CONCENTRATION BOUNDARY CONDITIONS
IF ISOLV EQ 1
YES
IF IDRY EQ 0
YES
8
NO
NO
CALL DRYNOD- DETERMINES WHICH NODES AND ELEMENTS ARE DRY
CALL LOAD- NUMBER OF EQUATIONS IN THE SYSTEM COEF. MATRIX AND BANDWIDTH DETERMINED
CALL LOADX- NUMBER OF EQUATIONS IN THE SYSTEM COEF. MATRIX AND BANDWIDTH DETERMINED
8
PRINT INITIAL CONDITIONS AND SEDIMENT PROPERTIES
9

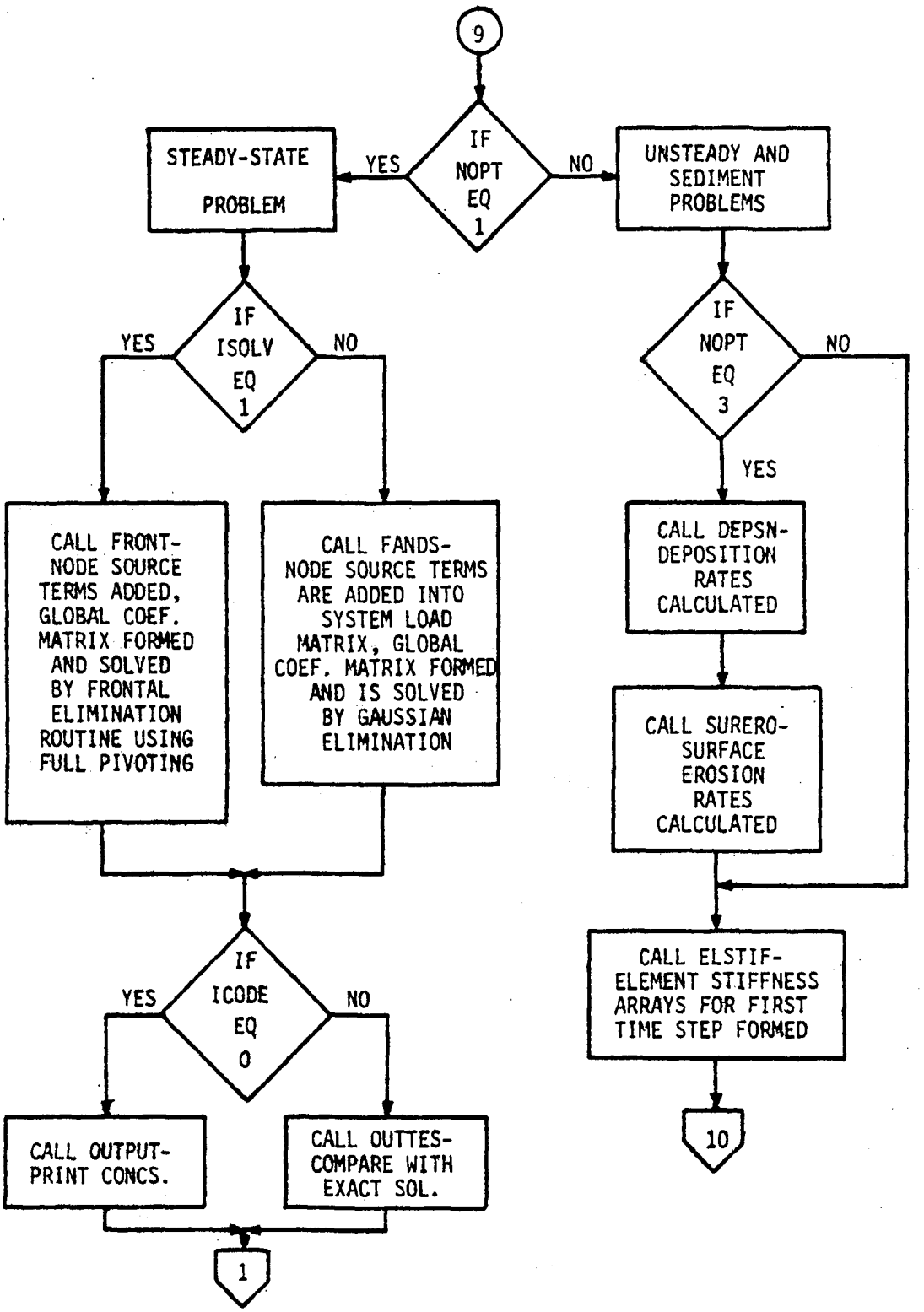
9
IF NOPT EQ 1
YES
NO
STEADY-STATE PROBLEM
UNSTEADY AND SEDIMENT PROBLEMS
IF ISOLV EQ 1
YES
NO
IF NOPT EQ 3
NO
YES
CALL FRONT-NODE SOURCE TERMS ADDED, GLOBAL COEF. MATRIX FORMED AND SOLVED BY FRONTAL ELIMINATION ROUTINE USING FULL PIVOTING
CALL FANDS-NODE SOURCE TERMS ARE ADDED INTO SYSTEM LOAD MATRIX, GLOBAL COEF. MATRIX FORMED AND IS SOLVED BY GAUSSIAN ELIMINATION
CALL DEPSN-DEPOSITION RATES CALCULATED
CALL SURERO-SURFACE EROSION RATES CALCULATED
IF ICODE EQ 0
YES
NO
CALL ELSTIF-ELEMENT STIFFNESS ARRAYS FOR FIRST TIME STEP FORMED
CALL OUTPUT-PRINT CONCS.
CALL OUTTES-COMPARE WITH EXACT SOL.
10
1

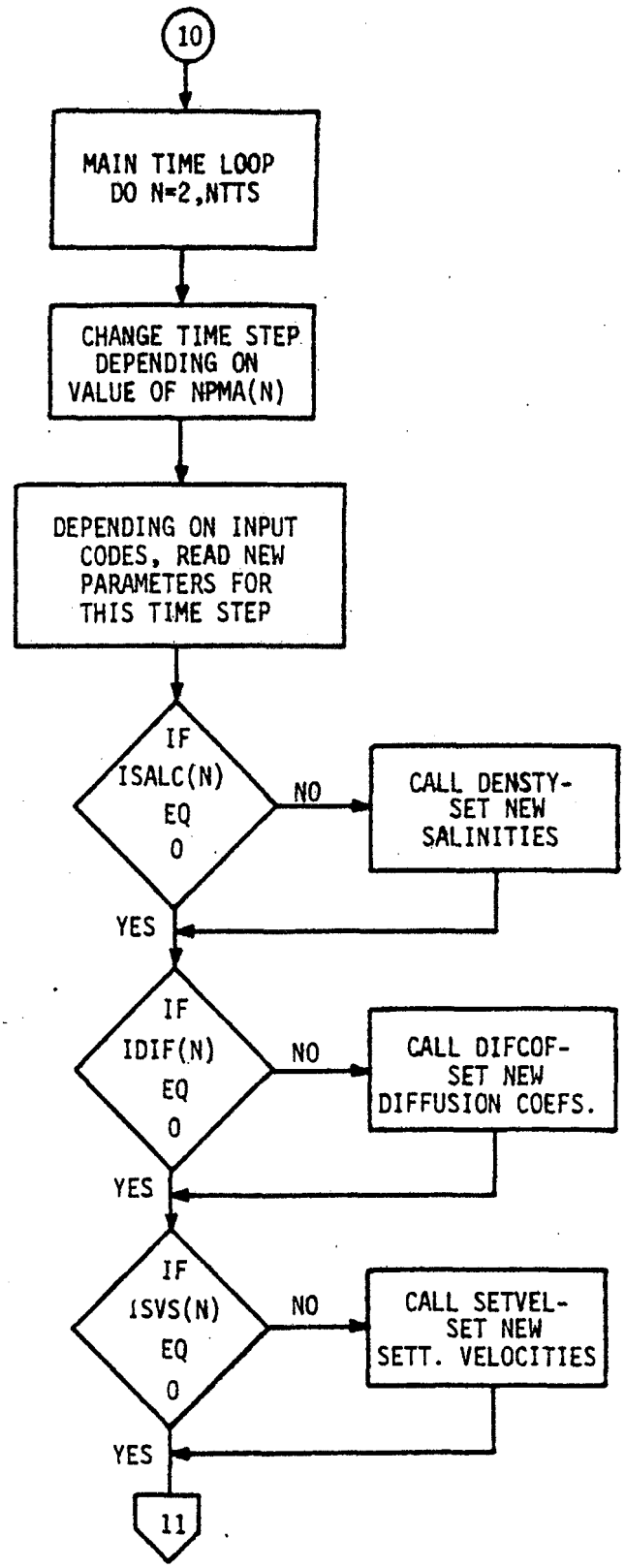
10
MAIN TIME LOOP
DO N=2,NTTS
CHANGE TIME STEP
DEPENDING ON
VALUE OF NPMA(N)
DEPENDING ON INPUT
CODES, READ NEW
PARAMETERS FOR
THIS TIME STEP
IF
ISALC(N)
EQ
0
NO
CALL DENSTY-
SET NEW
SALINITIES
YES
IF
IDIF(N)
EQ
0
NO
CALL DIFCOF-
SET NEW
DIFFUSION COEFS.
YES
IF
ISVS(N)
EQ
0
NO
CALL SETVEL-
SET NEW
SETT. VELOCITIES
YES
11

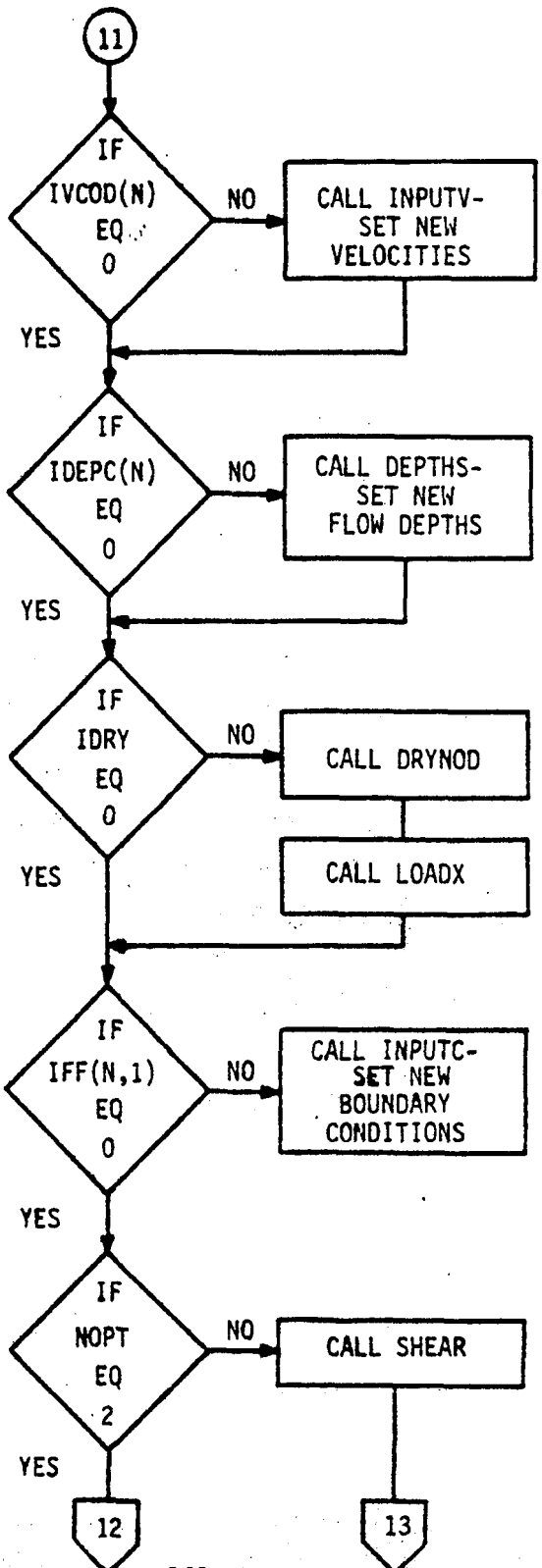
11
IF IVCOD(N) EQ 0
NO
CALL INPUTV- SET NEW VELOCITIES
YES
IF IDEPC(N) EQ 0
NO
CALL DEPTHS- SET NEW FLOW DEPTHS
YES
IF IDRY EQ 0
NO
CALL DRYNOD
CALL LOADX
YES
IF IFF(N,1) EQ 0
NO
CALL INPUTC- SET NEW BOUNDARY CONDITIONS
YES
IF NOPT EQ 2
NO
CALL SHEAR
YES
12
13

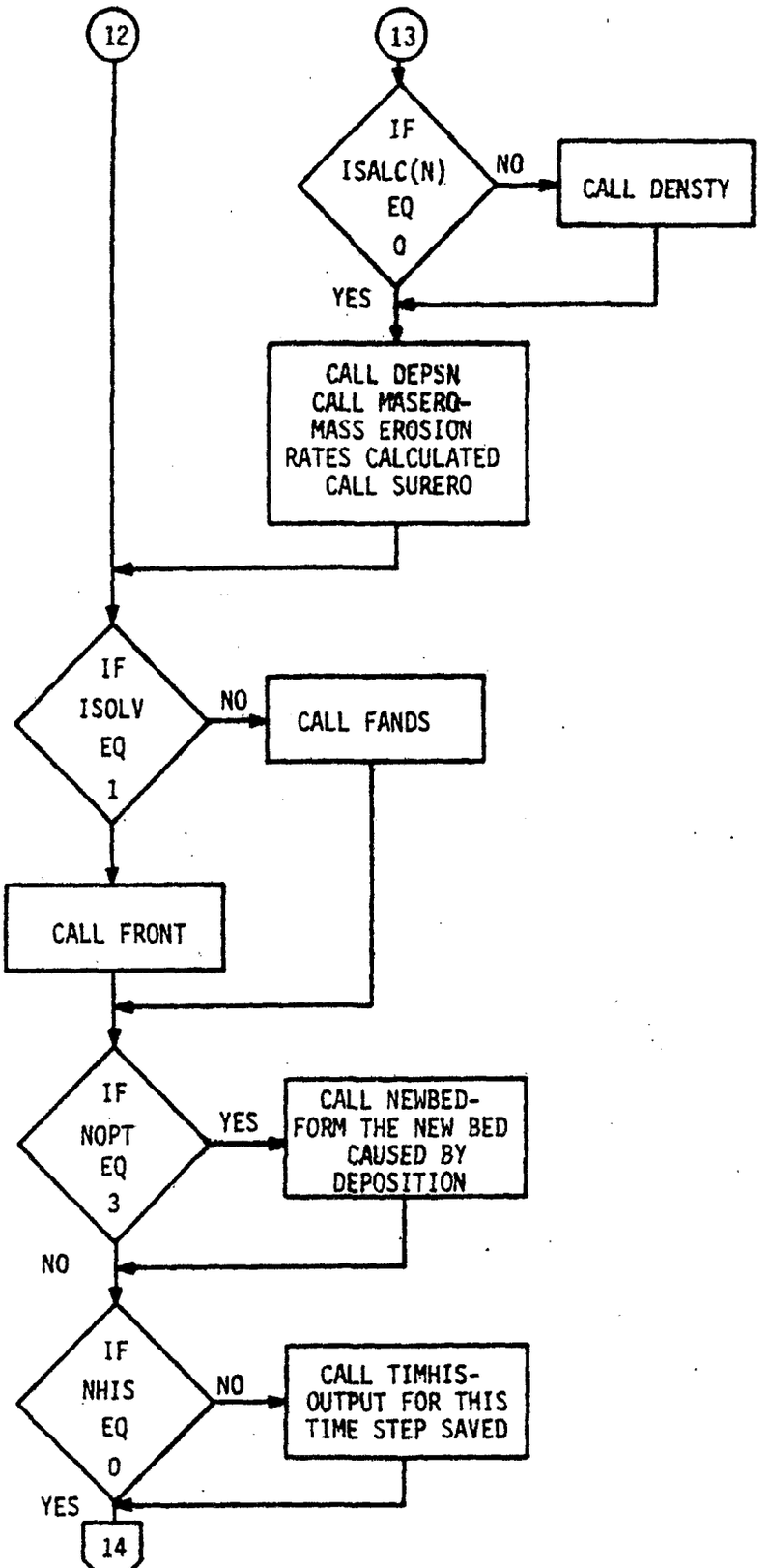
12
13
IF ISALC(N) EQ 0
NO
CALL DENSTY
YES
CALL DEPSN
CALL MASERO-
MASS EROSION RATES CALCULATED
CALL SURERO
IF ISOLV EQ 1
NO
CALL FANDS
CALL FRONT
IF NOPT EQ 3
YES
CALL NEWBED-
FORM THE NEW BED CAUSED BY DEPOSITION
NO
IF NHIS EQ 0
NO
CALL TIMHIS-
OUTPUT FOR THIS TIME STEP SAVED
YES
14

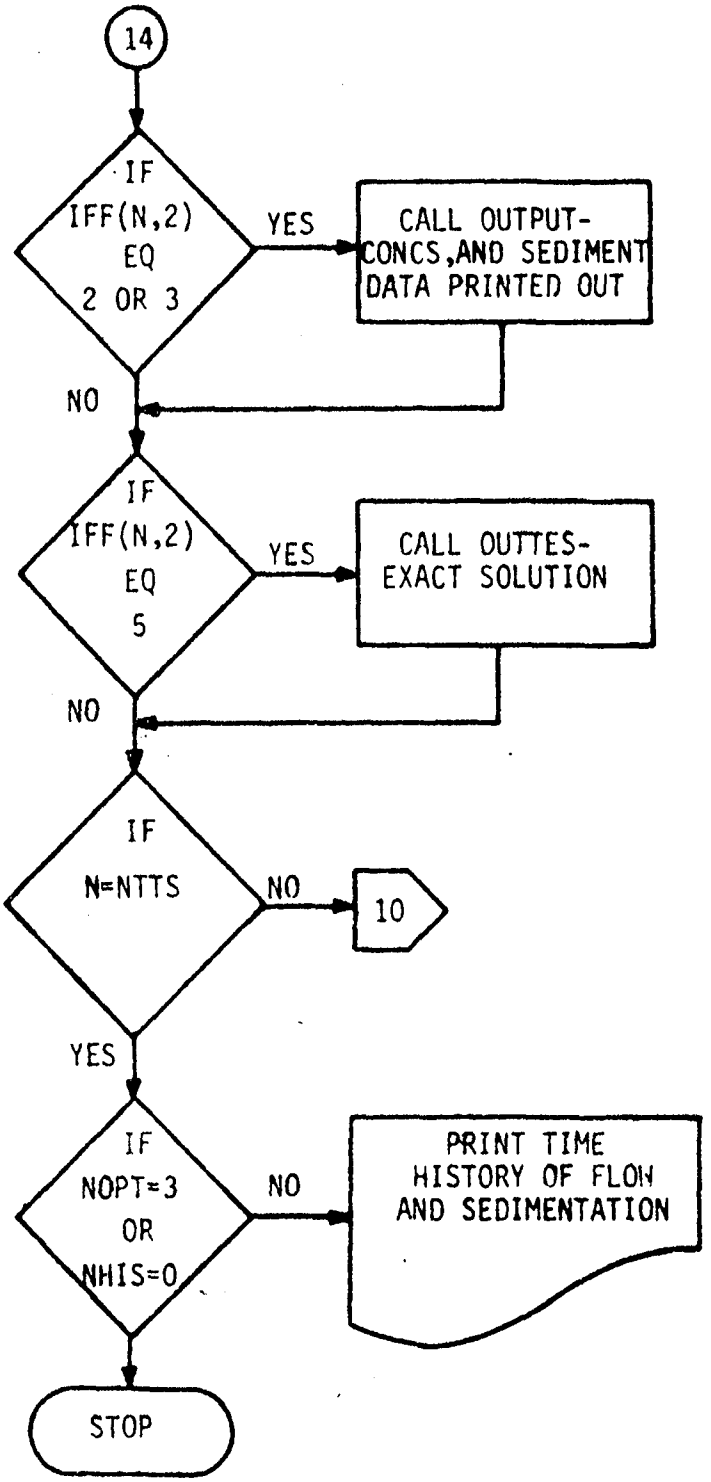
14
IF IFF(N,2) EQ 2 OR 3
YES
CALL OUTPUT-CONCS,AND SEDIMENT DATA PRINTED OUT
NO
IF IFF(N,2) EQ 5
YES
CALL OUTTES-EXACT SOLUTION
NO
IF N=NTTS
NO
10
YES
IF NOPT=3 OR NHIS=0
NO
PRINT TIME HISTORY OF FLOW AND SEDIMENTATION
STOP

APPENDIX B

User's Manual

B.1. Data Required for Model Use

SET A JOB CONTROL CARDS

CARD A.1		(13I5)	I/O file numbers and equation solver used
1-5	:	IN	General input file number (default 5)
6-10	:	LP	Output file number (default 6)
11-15	:	INC	Initial concentrations
16-20	:	IND	Diffusion coefficients
21-25	:	INE	Node point bottom elevations (initial)
26-30	:	INF	Node point flow velocities
31-35	:	ING	Settling velocities
36-40	:	INH	Flow depths
41-45	:	INI	Finite element grid geometry data
46-50	:	INB	Boundary conditions
51-55	:	INS	Salinities
56-60	:	INSS	New nodal salinities
61-65	:	ISOLV	0 - use band solver (Subroutine FANDS) 1 - use front solver (Subroutine FRONTS)
CARD A.2		(I1, 19A4)	Job stop and title
1	:	NSTOP	0 - continue 1 - end of job
2-78	:	TITLE	Job title
CARD A.3		(16I5)	Job Control Parameters, Input Codes, and Problem Options
1-5	:	NOPT	Type of Problem 1 - steady state transport problem 2 - unsteady transport problem 3 - sediment transport problem
6-10	:	ICODE	Output control for non-sediment problems 0 - standard output 1 - compares with analytic solution calculated in Subroutine EXACT
11-15	:	NTTS	Number of time steps
16-20	:	IVEL	Determines initial velocity field, i.e., at time step #1 (for unsteady problems only) 1 - X & Y velocities set equal to constants CONXV and CONYV read in Subroutine INPUTV 2 - each nodal velocity read in from input file INF 3 - velocity computed using user supplied routine in Subroutine INPUTV

21-25	:	IELEV	Elevation of bottom above a given datum at node points 0 - all elevations set equal to 0.0. 1 - read each value read in from file number INE
26-30	:	IDIF1	Initial diffusion coefficient values at each node. 1 - D_x and D_y are set equal to constants read in Subroutine DIFCOF 2 - Nodal diffusion coefficients are read in from file number IND 3 - Diffusion coefficients are calculated using user supplied procedure.
31-35	:	IBED	Initial bed profile 0 - no sediment present on bed 1 - bed profile read in Subroutine BED
36-40	:	ISET	Initial settling velocity at each node 1 - set to a constant read in Subroutine SETVEL 2 - each settling velocity is read in from file number ING 3 - settling velocities are computed from model in Subroutine SETVEL
41-45	:	IDEP	Initial depths of flow at each node 1 - set to constant read in Subroutine DEPTHS 2 - read in from file number INH 3 - computed according to user supplied procedure in Subroutine DEPTHS
46-50	:	ICONC	Initial suspended sediment concentrations 1 - set to constant 2 - read in from file number INC 3 - computed according to user supplied procedure in Subroutine INCONC
51-55	:	INBC	Boundary Conditions 1 - each value read in from file number INB 2 - computed in Subroutine INPUTC using user supplied routine
56-60	:	IDRY	Code to indicate dry node (i.e. negative flow depth) problem 0 - no dry nodes will occur 1 - possible dry nodes
61-65	:	IPL	Number of nodes where concentration-time plots are to be generated using plot routine in Subroutine PLOTR

SET B MESH DATA

These data are read from file unit INI

CARD B.1 (2I5)

1-5	:	NE	Number of elements in system
6-10	:	NP	Number of nodes in system

CARD B.2 et.seq.(8I5/)

1-5	:	NOP(I,K)	Nodal connections counterclockwise (8 per card for quadrilateral element)

CARD B.3 et.seq.(4(2F8.4/))

6-15	:	CORD(J,1)	X-coordinate (meters)
16-25	:	CORD(J,2)	Y-coordinate (meters)

SET C TRANSIENT PROBLEM INPUT

CARD C.1 (3F10.5)

1-10	:	TETA	"Implicitness factor" for Crank-Nicholson time-marching scheme 0. - explicit 1. - implicit
11-20	:	DT	Time step size - secs
21-30	:	TIM(1)	Starting time - secs

CARD C.2 et.seq.(80I1) Code to change time step

1,etc	:	NPMA(I)	The value of NPMA at each time determines if the time step will be changed 0 - no change 1 - double time step 2 - halve time step

for I=1,...,NTTS

CARD C.3 et.seq.(80I1) Code for new boundary conditions

1,etc	:	IFF(I,1)	Determines if there are new boundary conditions 0 - no change in boundary conditions 1 - each value read in from cards 2 - computed in Subroutine INPUTC using user supplied procedure 3 - each value read in from file number INB

CARD C.4 et.seq.(80I1) Output control

1,etc : IFF(I,2)

0 - no output
1 - sedimentation data only
2 - concentrations only
3 - concentrations and sediment transport data
5 - comparison with analytic solution in Subroutine EXACT

CARD C.5 et.seq.(80I1) New velocities

1,etc : IVCOD(I)

Same as IVEL but for each time step
0 - no new velocities
1 - X & Y velocities set equal to constants CONXV and CONYV read in Subroutine INPUTV
2 - each nodal velocity read in from input file INF
3 - velocity computed using user supplied routine in Subroutine INPUTV

CARD C.6 et.seq.(80I1) New diffusion coefficients

1,etc : IDIF(I)

Same as IDIF
0 - no new diffusion coefficients
1 - D_x and D_y are set equal to constants read in Subroutine DIFCOF
2 - nodal diffusion coefficients are read in from file number IND
3 - diffusion coefficients are calculated using user supplied procedure

CARD C.7 et.seq.(80I1) New depths of flow

1,etc : IDEPC(I)

Same as IDEP
0 - no new depths
1 - set to constant read in Subroutine DEPTHS
2 - read in from file number INH
3 - computed according to user supplied procedure in Subroutine DEPTHS

CARD C.8 et.seq.(80I1) New Salinities

1,etc : ISALC(I)

0 - no new salinities
1 - set to a constant read in Subroutine DENSTY
2 - new salinities at specified nodes are read in Subroutine DENSTY
3 - new salinities for all nodes are read in Subroutine DENSTY

CARD C.9 et.seq.(80I1) Only for sediment problems NOPT=3

1,etc	:	ISVS(I)	New settling velocities. Same as ISET 0 - no new settling velocities 1 - set to a constant read in Subroutine SETVEL 2 - each settling velocity is read in from file number JNG 3 - settling velocities are computed from model in Subroutine SETVEL

CARD C.10 (1615)

1-5	:	NHIS	number of elements that time history is required for (maximum 6)
6-10 etc	:	NELH	Element numbers

SET D WATER AND SEDIMENT PROPERTIES

Read in Subroutine DENSTY

CARD D.1 (F10.5,I10) Water Parameters

1-10	:	TMP	Average Water Temperature (°C)
11-20	:	IS	Determines how initial salinities are read in 0 - constant salinity for all nodes 1 - salinity for each node is read in

If IS = 0:

CARD D.2 (F10.5) Constant Salinity

1-10	:	SW	Value of constant salinity read in - ppt

If IS = 1:

CARD D.2 et.seq.(7F10.5) Nodal Salinity Values

1-10	:	SAL(I)	Salinity value for $I^{\underline{th}}$ node - ppt

Read in Subroutine SPROP for sediment problems (NOPT=3)

CARD D.3 (4F10.5) Settling Velocity Parameters

1-10	:	CRCN=C_1	See Equations for W_s below - kg/m^3
11-20	:	CRCN2=C_2	See Equations for W_s below - kg/m^3
21-30	:	CRCN3=C_3	See Equations for W_s below - kg/m^3
31-40	:	GAC	Density of sediment mineral - kg/m^3

CARD D.4 (6F10.5)

1-10	:	AA=A_1	See Equations for W_S below
11-20	:	AB=A_2	See Equations for W_S below
21-30	:	AC=A_3	See Equations for W_S below
31-40	:	B	See Equations for W_S below
41-50	:	F	See Equations for W_S below
51-60	:	AL	See Equations for W_S below

CARD D.5 (2E10.3)

1-10	:	WS1= W_{s1}	See Equations for W_S below - m/s
11-20	:	D	Equivalent Sediment Particle Diameter at t_{50} - m

CARD D.6 (2F10.5)

1-10	:	EXPN1=n_1	See Equations for W_S below
11-20	:	EXPN2=n_2	See Equations for W_S below

CARD D.7 (3F10.5)

1-10	:	EXPM1=m_1	See Equations for W_S below
11-20	:	EXPM2=m_2	See Equations for W_S below
21-30	:	EXPM3=m_3	See Equations for W_S below

CARD D.8 (2E10.3)

1-10	:	WSK1=K_1	See Equations for W_S below - m/s
11-20	:	WSK2=K_2	See Equations for W_S below - m/s

NOTE: For RANGE I ($0 \leq \tau_b^* < \tau_{b,c}^*$) and $C < C_1$ in Range II
($\tau_{b,c}^* \leq \tau_b^* < \tau_{b_{max}}^*$)

W_S = AA*WS1*(SAL)**EXPM1 for C ≤ CRCN1 where SAL = salinity
If (SAL < 0.1 ppt)SAL = 0.1 ppt

W_S = AA*WSK1*C**EXPN1*(SAL)**EXPM1 for CRCN1 < C ≤ CRCN2

W_S = AB*WSK2*C**EXPN2*(SAL)**EXPM2 for CRCN2 < C ≤ CRCN3

W_S = AC*G*D**2*(GAC/GAW-1)*250*(C/CRCN3-1)**AL*(SAL)**EXPM3/
(18*ν*D**1.8) for C > CRCN3

If there is only one $W_S = KC^n$ relationship between C = CRCN1 and the concentration at which hindered settling begins, set CRCN3 = CRCN2 in CARD D.3.

NOTE: For $C > C_1$ in Range II

T=ALOG10((TM/T_{50})*B*(SAL)**F)**(1./SIG2)

CARD D.9 (2I10, 2F10.5) Properties of new deposits

1-10	:	NLAYTM	Number of layers formed by unconsolidated new deposits (UND)
11-20	:	NLAYT	Number of layers formed by partially consolidated new deposits (CND)
21-30	:	TAUMIN	$\tau_{b_{min}}$ - N/m^2
31-40	:	TAUMAX	$\tau_{b_{max}}$ -N/m^2

Parameters characterizing functional relationship between τ_b^* and $\log_{10}(t_{50})$ and σ_2 at a salinity of 35 ppt.

CARD D.10 (5F10.5)

1-10	:	A1	See Equations for σ_2 below
11-20	:	S1	See Equations for σ_2 below
21-30	:	A2	See Equations for σ_2 below
31-40	:	S2	See Equations for σ_2 below
41-50	:	C1	See Equations for σ_2 below

CARD D.11 (5F10.5)

1-10	:	A3	See Equations for t_{50} below
11-20	:	S3	See Equations for t_{50} below
21-30	:	A4	See Equations for t_{50} below
31-40	:	S4	See Equations for t_{50} below
41-50	:	C2	See Equations for t_{50} below

Note: For

$$\tau_b^* < C1 \quad : \quad \sigma_2 = S1*\tau_b^* + A1$$

$$\tau_b^* > C1 \quad : \quad \sigma_2 = S2*\tau_b^* + A2$$

For

$$\tau_b^* < C2 \quad : \quad t_{50} = 60.*10^{(S4*\tau_b^* + A4)}$$

$$\tau_b^* > C2 \quad : \quad t_{50} = 60.*10^{(S3*\tau_b^* + A3)}$$

CARD D.12 et.seq.(4(2F10.5)) Shear strength and bulk density for unconsolidated new deposit layers. NLAYTM pairs of values are read in starting at the bed surface and proceeding down to the top of the bottom UND layer.

1-10	:	SSM(I)	Bed Shear Strength - N/m^2
11-20	:	GBM(I)	Bulk density - kg/m^3

for I = 1,...,NLAYTM

CARD D.13 et.seq.(8F10.5)

1-10 : TLAYM(I) Thickness of unconsolidated new deposit layers - m

for I = 1,...,NLAYTM

CARD D.14 et.seq.(4(2F10.5)) Shear strength and bulk density for partially consolidated new deposit layers. NLAYT+1 pairs of values are read in starting at top of these layers and proceeding downward.

1-10 : SS(I) Bed Shear Strength - N/m^2
11-20 : GB(I) Bulk density - kg/m^3

for I = i,...,NLAYT+1

CARD D.15 et.seq.(2(3F10.5)) Thickness, ε_o and α values for each partially consolidated new deposit layer.

1-10 : TLAY(I) Layer thickness - m
(Set TLAY(NLAYT) = 0.0)
11-20 : EPSLON(I) ε_o - $kg/m^2/s$
21-30 : ALFA(I) α - dimensionless

for I = 1,...,NLAYT

Note: The properties read in on CARDS D.12-D.15 are determined from laboratory experiments (see Section B.3 for a description of these experiments). These are the properties assigned to new deposits if/when deposition occurs during model simulation or initially if new deposits (i.e. fluid mud) are present on top of the consolidated original bed, as specified in SET K.

SET E INITIAL DIFFUSION COEFFICIENTS

The form of input is set by value of IDIF.

IDIF = 1 Diffusion coefficients are set to constant values.

CARD E.1 (2F10.5)

1-10 : CDIFX X-diffusion coefficient - m^2/sec
11-20 : CDIFY Y-diffusion coefficient - m^2/sec

IDIF = 2 Diffusion coefficients are read in node by node.

CARD E.2 et.seq.(3(I5,2F10.5)

1-5 : IT(J) Node number
6-15 : TEMP(1,J) X-diffusion coefficient - m^2/sec
16-25 : TEMP(2,J) Y-diffusion coefficient - m^2/sec

Reading stops for IT(J) < 0

IDIF = 3 Diffusion coefficients computed analytically using user supplied procedure.

SET F INITIAL VELOCITY FIELD

The velocity components at each node must be specified. The value of IVEL determines type of input. This input only for unsteady problems. All reads are from file number INF

IVEL = 1 Velocities are set to constant values.

Read from file unit INF

CARD F.1 (2F10.5)

1-10	:	CONXV	X-velocity - m/sec
11-20	:	CONYV	Y-velocity - m/sec

IVEL = 2 Each nodal velocity component read in.

CARD F.2 (4(2F10.5)) Must be read in order for all NP nodes.

1-10	:	XVEL(J,1)	X-velocity at node J - m/sec
11-20	:	XVEL(J,2)	Y-velocity at node J - m/sec

IVEL = 3 User supplied procedure in Subroutine INPUTV is used to calculate nodal velocities.

For NOPT = 2 or 3:

SET G INITIAL CONCENTRATION FIELD

The initial concentration at each node must be specified for all unsteady problems. The type of input is determined by the value of ICONC.
Read from file unit INC

ICONC = 1 Initial concentration set to a constant at all nodes.

CARD G.1 (F10.5)

1-10	:	CVSX	Concentration - kg/m^3

ICONC = 2 Read in for each node

CARD G.1 et.seq.(4(I10,F10.5))

1-10	:	IT(J)	Node number
11-20	:	TEMP(J)	Concentration - kg/m^3

Reading stops for IT(J) < 0

ICONC = 3 Compute concentrations at each node using user supplied model in Subroutine INCONC.

For NOPT = 3 (Sediment Problems):

SET H INITIAL BED ELEVATIONS

If IELEV≠0, the initial bed elevation, with respect to some datum, at each node is read in.

Read from file unit INE

CARD H.1 et.seq.(8F10.5)

1-10 : ELEV(I) Bed elevation for node I - m

I = 1,...,NP

SET I INITIAL DEPTHS OF FLOW

Depths of flow at each node are read in depending on the value of IDEP.

Read from file unit INH.

IDEP = 0 All depths set to 1. by default

IDEP = 1 All nodal depths set to constant

CARD I.1(F10.5) Constant value of depth

1-10 : CDEP Depth of flow - m

IDEP = 2 Read node point depths from file INH.

CARD I.2 (4(I10,F10.5))

1-10 : IT(J) Node Point Number
11-20 : TEMP(J) Depth of flow - m

Stops reading if IT(J) < 0.

IDEP = 3 Compute depths from user supplied procedure in Subroutine DEPTHS.

For NOPT = 3:

SET J INITIAL SETTLING VELOCITIES

The initial settling velocities at each node point must be read in. The form of input is determined by the value of ISET.

Read from file unit ING

ISET = 1 All settling velocities are set to constant

CARD J.1 (F10.5)

1-10 : CVSX Settling velocity - m/sec

ISET = 2

CARD J.2 et.seq.(4(I10, F10.5))

1-10 : IT(J) Node number
11-20 : TEMP(J) Settling velocity - m/sec

Stops reading if IT(J) < 0.

ISET = 3

Settling velocity model, for which parameters were read in in SET D, is used to compute each nodal settling velocity.

For NOPT = 3:

SET K ORIGINAL BED PROFILE

Read in only if IBED (Card A.3) is not zero. Otherwise the default bed condition will be a clean bed.

CARD K.1 et.seq.(3I5,F10.5) for each element

1-5 : NN Element number
6-10 : NLA Number of layers of consolidated original bed
11-15 : NM If NM = 0, bed properties are read in for each element. If NM≠0, constant values are read in and used for all elements.
16-25 : GWA Average density of pore water in original bed - kg/m^3

CARD K.2 et.seq.(2F10.5) Shear strength and bulk density for consolidated original bed layers. NLA+1 pairs of values are read in starting at the top layer and proceeding downward. The first values are for the top of the original bed.

1-10 : SSTO(NN,L) Bed shear strength - N/m^2
11-20 : GBO(NN,L) Bulk density - kg/m^3

For L = 1,...,NLA+1

CARD K.3 et.seq.(F10.5,E10.3) Thickness and value of M for each consolidated bed layer

1-10 : THICKO(NN,I) Thickness of Ith layer - m
11-20 : EPSLNO(NN,I) M value of Ith layer - $kg/m^2/s$

for I=1,...,NLA

Note: CARDS K.1, K.2 and K.3 are repeated for NN=1,...,NE when NM=0. When NM≠0, these cards are read in only once.

If stationary suspension is present on top of original bed, set NN=-10 at the end of the above set (i.e. CARDS K.1, K.2 and K.3). For NN=-10, read the following cards.

CARD K.4 et.seq. (3(I10,F10.5)) for each element

1-10	:	IT(J)	Element number
11-20	:	TEMP(J)	Dry mass per unit area of fluid mud (soft sediment) on top of consolidated original bed - kg/m^2.

Reading stops when IT(J) < 0.

SET L BOUNDARY CONDITIONS

For any problem, concentration boundary conditions must be specified at least at one node. At all external boundaries that have no cencentration specified, the normal diffusive flux is defaulted to zero. Type of input is determined by value of INBC. File number for input is INB.

INBC= 1 Read node number and specified boundary condition from cards

CARD L.1 (2(I10,F10.5))

1-10	:	IT(J)	Node number
11-20	:	TEMP(J)	Specified concentration - kg/m^3

for J=1,...,NP

INBC = 2 Concentration computed according to user supplied procedure in Subroutine INPUTC

INBC = 3 Read node number and specified boundary condition from file INB.

CARD L.2 (3(I10,F10.5))

1-10	:	IT(J)	Node Number
11-20	:	TEMP(J)	Specified concentration - kg/m^3

for J=1,...,NP

SET M New Salinities

Type of input is determined by value of ISALC(J), for J=2,...,NTTS.

ISALC(J)=1.

CARD M.1 (F10.5)

1-10 : SW Constant salinity value read in - ppt

ISALC(J)=2. File number for input is INSS

CARD M.2 (3(I10,F10.5)) Salinities for specified nodes

1-10 : IT(J) Node number
11-20 : TEMP(J) New salinity at node J - ppt

ISALC(J)=3. File number for input is INSS

Card M.3 (7F10.5) New salinities for all nodes.

1-10 : SAL(J) Salinity at Jth node.

DYNAMIC INPUT

The same subroutines that read initial values are used to read changes in these values during a dynamic run. The input code arrays in SET C tell the program if any new values should be read in at each time step. Note that the starting time is timestep 1. The order of reading each set of data is given below. If the code is zero no input of that parameter will be expected. If it is non-zero the value of the code will determine the type of input.

DESCRIPTION	CODE ARRAY	INPUT CARD SET
Salinities	ISALC(J)	SET M
Diffusion Coefficients	IDIF(J)	SET E
*Settling Velocities	ISVS(J)	SET J
Velocities	IVCOD(J)	SET F
Depths of Flow	IDEPC(J)	SET I
Concentration B.C.	IFF(J,1)	SET L

*only for sediment problems

B.2. Description of Field Data Collection Program

In this section a description of the field data collection program to obtain the data requirements of the model is summarized. The data collection program required for modeling the hydrodynamic regime in an estuary is rather well-known, and will not be discussed.

The first item that must be considered is the time period over which data will be collected for eventual use in the model. This will be contingent upon the desired results from the modeling effort. In tidal bodies of water, data should be collected over a minimum of 15 hours (assuming the tide is semi-diurnal) over a minimum of three

different tidal cycles: spring, mean and neap. It would be more desirable to have the data collection period span at least one week, starting, for example, on a spring tide and finishing at the subsequent neap tide. The next consideration is how many data sampling stations there should be and where they should be located in order to adequately monitor the spatial variations of the concentration of the suspended sediments. Stations should be located at all exterior water boundaries (cross-sections) of the estuarial system to be modeled. The width of the boundary cross-section and the lateral variability of the depth should be considered when deciding upon the minimum number of stations to be located laterally across such a boundary. For example, stations should definitely be located at predominant features such as navigation channels. Additional stations must be located at all interior confluences and bifurcations, and at as many other interior locations as possible. It is recognized that the length of the data collection period and the number of stations are often less than desired due to economic and logistical considerations.

A. Topographic and hydrographic surveys of the system to be modeled must be obtained at the outset. A sonar fathometer may be used to perform the latter survey in those areas which historically have not experienced any significant shoaling. However, in areas where shoaling has been a problem, a gamma-ray transmission densitometer may be used. This instrument obtains in situ measurements of the sediment bulk density profile, which, in high shoaling areas where stationary suspensions (i.e. new deposits) are typically present, can be used to determine the thickness of this suspension and the location (i.e. vertical elevation with respect to datum) of the top of the settled (consolidated) original bed. The location of the top of the settled bed is defined in Section B.3. Representative publications on gamma-ray densitometers and their use in obtaining in situ bulk density measurements include Preiss (1968, 1969), Rose and Roney (1971) and Hirst et al. (1975). A description of the methods available today to perform hydrographic surveying in estuaries is given by Ingham (1975) and Dyer (1979).

B. Before the data collection period begins, two or three 10-12 cm diameter cores should be collected at each sampling station. Each

core should have a minimum length of approximately 2 m. Fixed piston tube corers (Ginsburg and Lloyd, 1956) or vibracorers (Kirby, 1972; Finkelstein and Prins, 1981) may be used. The cores should contain both new deposits, if present, and consolidated bed sections. In addition, at least 200 liters of water should be collected during a peak flood flow.

C. At each station the location of the top of the consolidated bed with respect to a geodetic or tidal vertical datum must be determined using the method mentioned above. Then at the start of the data collection period the water temperature, electrical conductivity (or salinity) and concentration of suspended sediments should be measured at each of the sampling stations. These measurements should be made at a minimum of three depths over the vertical: one-half meter below the water surface, mid-depth and one-half meter above the bottom (i.e. top of consolidated bed). For locations where the water depth is greater than about 3.5 meters, measurements should be made at additional depths over the vertical. Both the measurement and analysis of water temperature and electrical conductivity data are discussed by Dyer (1979). The concentration of suspended sediments in a known volume of water can be determined gravimetrically. Several water sampling devices such as water bottles (NIO bottle), shipboard pump systems (Crickmore and Aked, 1975) and sediment traps (Delft Bottle) are available. A description of these and more water sampling devices, various filtration procedures, as well as other methods for determination of suspension concentrations (e.g. optical methods, remote sensing) is given by Dyer (1979).

D. The parameters listed in the previous paragraph should be measured at least once every one-half hour for the duration of the collection period at each of the sampling stations.

B.3. Description of Laboratory Sediment Testing

The following physico-chemical sediment and fluid properties need to be determined using the collected cores and water:

A. Properties of Undisturbed Sediment Cores

The gamma-ray densitometer may be used to determine the bulk sediment density profile in the undisturbed cores still in the liner tubes as soon after the cores are obtained as possible. A description of this procedure is given by Whitmarsh (1971) and Kirby and Parker (1974). If this instrument is not available, the freeze-drying procedure used by Parchure (1980) and Dixit (1982) or the pumping method used by Thorn and Parsons (1977) may be used to determine the bulk density profile. The pumping method consists of removing by suction a thin layer, e.g. 3 cm, from the top of the core. This procedure is repeated, layer, by layer and each layer is analyzed to determine the mean bulk density.

B. Properties of Consolidated (Original) Bed

The bulk density and bed shear strength profiles and the erosion rate constant for each layer need to be determined for one of the cores from each station. The number of layers and the thickness of each are determined from the nature of the bed shear strength profile (Section 2.6). The erosion rate constant for each layer and the shear strength profile can be determined, for example, in the rotating cylinder erodibility testing apparatus described by Sargunam et al. (1973). In order to use this apparatus, the core sample must be trimmed. The portion of each core that is sufficiently consolidated such that it can be trimmed and tested in the erosion apparatus is defined to be the consolidated bed. The thickness of this portion defines the location of the top of the settled bed. Soft, unconsolidated portions of each core are assumed to be new deposits.

C. Properties of Stationary Suspensions (New Deposits)

For cores with soft, unconsolidated sediment on top of the consolidated (settled) portion, the following method must be used to estimate the erodibility characteristics of such new deposits. The new deposit samples from the cores at all the stations should be mixed and subjected to laboratory erosion and deposition tests (described by Parchure (1980), Mehta and Partheniades (1973) and in Sections 2.6, 2.7 and 2.8) to determine: the settling velocity as a function of suspension concentration and salinity (see Section 2.8.5), minimum and maximum

depositional shear stresses, $\tau_{b_{min}}$ and $\tau_{b_{max}}$ (Section 2.7), variation of $t_{/0}$ and κ_2 with the bed shear stress, τ_b (Section 2.7), the number of characteristic unconsolidated new deposit layers and the thickness, bulk density and shear strength profile of each layer (Section 2.5), the number of characteristic partially consolidated new deposit layers and the thickness, bulk density, shear strength and the sediment parameters ϵ_0 and α of each layer (Sections 2.5 and 2.6). The variation of the bulk density and shear strength profiles with salinity should also be determined by performing the erosion tests at the following salinities: 0, 1, 2, 5, 10, 20 and 35 ppt.

D. Fluid Composition

Samples of the pore fluid in the consolidated bed portion of one core from each station should be collected. The pH, total salt concentration, and concentrations of ions such as Na^+, Ca^{+2}, Mg^{+2}, K^+, Fe^{+3} and Cl^- should be determined for both the pore fluid samples and a sample of the suspending fluid.

E. Composition and Cation Exchange Capacity of the Sediment

The sediment contained in the consolidated bed portion of one core from each collection station should be thoroughly mixed so that a spatially homogeneous sample is obtained. For each so-prepared sample a standard hydrometer analysis should be conducted to determine the sediment particle size distribution and thereby the percentage by weight of clay, silt and fine to coarse sand in each sample. In preparing the samples for this analysis, the sediment should not be initially air-dried (to obtain the dry weight of the material used in the test), as it has been found that dried, sediment will not completely redisperse when the dispersing agent is added (Krone, 1962). For this reason, the total dry weight of the sample should be obtained from another portion of the sample, and the corresponding value for the test sample calculated assuming that both portions have the same water content. The percentage by weight of organic matter should be determined through use of a method such as the Walkley-Black test (Allison, 1965). In addition, X-ray diffraction analysis of the bulk sample, and < 2 μm unglycolated and glycolated portions should be conducted in order to determine the predominant clay and non-clay mineral constituents. The cation exchange capacity must be determined for each sample.

APPENDIX C

Characterization of Factors Involved in the Study of Erosion of Fine Sediments

1. Introduction

The properties and behavior of cohesive sediments have been found to be quite different from those of non-cohesive sediments. Various researchers have attempted to understand these characteristics through laboratory experiments using a variety of apparatuses, techniques and measurements. This research revealed that conventional parameters from the field of soil mechanics, such as bulk density, vane shear strength, liquid limit, plastic limit, etc. are not adequate for a fundamental understanding. It has been shown that mineralogy of clays, chemistry of water, and structure of the bed are important factors in the study of erosion of cohesive sediment beds. In addition to obvious parameters such as particle size, water content, void ratio, etc., new parameters such as sodium adsorption ratio, dielectric constant and the cation exchange capacity have been added and their influence clearly demonstrated. However, due to the inadequate available knowledge on this subject during the early stages of the research effort, some of the parameters found to be important by one research worker were not measured by other researchers and vice versa. This has posed the following difficulties in comparing and evaluating the results of different research workers:

i) There is no consistency in the selection of parameters or indices used to characterize the sediment, the bed structure or the erosion process.

ii) Contradicting conclusions are offered, e.g. on the correlation of bed density to the bed shear strength.

iii) Different notions prevail in describing the "critical" shear stress.

iv) Size of the experimental apparatus, duration of tests and the range of magnitudes of parameters have a wide variation.

v) Different views exist on the interpretation of data, e.g. on the existence of a steady-state concentration and the exchange of material between the bed and the water column.

The purpose of this appendix is to reveal the diversity of physico-chemical parameters measured and experimental methods employed by researchers in investigating the erosive behavior of cohesive sediments. This diversity greatly enhances the complexity of this subject matter and makes the task of comparing the results of different studies a difficult one.

2. Procedure Followed for Laboratory Studies

The following procedure is generally adopted for laboratory studies:

i) A sediment of interest is selected. This may be a pure clay mineral, a mixture of clay minerals, or a mixture of clay and non-clay minerals. The sediment is described with the use of certain characterizing indices.

ii) Pore and eroding fluids of interest are selected and characterized.

iii) A sediment bed is formed in the laboratory apparatus and is characterized by suitable parameters. Several parameters/indices are used to determine the effect of the pore and eroding fluid on the structure of the bed. The bed formation/erosion processes which occur in the field are shown in Fig. 1.4 whereas the laboratory schematization of these processes is shown in Fig. 2.18.

iv) Erosion of bed is not directly measured. It is usually estimated from the analysis of relevant data, such as change in suspension concentration as a function of time, collected during the course of the experiment. This approach is schematically depicted in Fig. C.1.

3. Description of the Diversity in Laboratory Studies

Since there are few well-established parameters or indices to characterize cohesive sediments, the fluid, bed structure or the rate of erosion, a high degree of diversity exists in laboratory studies on each of these factors. However, these studies can, in general, be classified into one of the following seven categories:

1) Characterization of Sediment
2) Characterization of Pore Fluid and Eroding Fluid
3) Characterization of Bed Structure
4) Characterization of Coagulation and Settling
5) Characterization of Erodibility Index
6) Bed Shear Stress
7) Measure of Erosion

A list of parameters identified in each of the above seven areas is given under Tables A through G. Each table is followed by references to typical studies related to each parameter given in the table. These references are listed in the same order and denoted by the same serial number as the parameters, and are prefixed by the alphabet corresponding

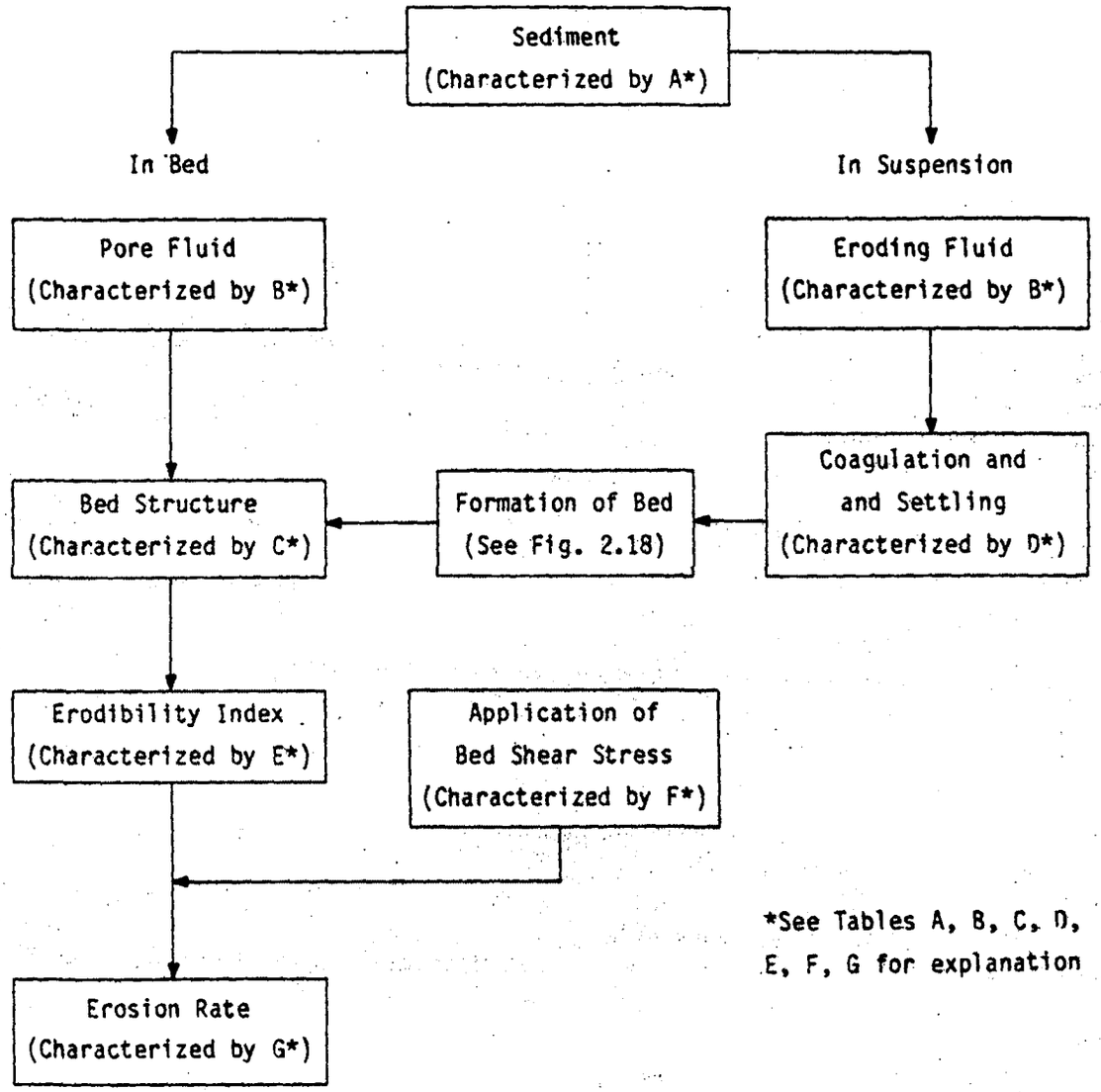

Fig. C.1: Diagramatic Representation of the Steps in the Study of Erosion Rates of Fine Sediments.

to the table. This tabulation has been carried out in order to organize the large number of research topics on the erosive behavior of cohesive sediments into a few relatively well-defined categories.

TABLE A: Characterization of Sediment

1. Type of Material
   - A. Clay Minerals
     - i) Clay mineral alone
     - ii) Mixture of clay minerals in varying proportions
     - iii) Mixture of clay-mineral and non-clay-mineral, both in the fine sediment range
   - B. Soils, Muds and Clay Material
     - i) Mixture of cohesive and non-cohesive (such as sand) sediments
     - ii) Mixture of clay material and organic matter or organic compounds
     - iii) Sediments from natural environment (unclassified)
     - iv) Sediments from natural environment (classified according to Soil Classification System)
   - C. Non-sediment Fine Materials
2. Nature of Clay Structure
   - A. Electrical forces acting between particles
     - i) Net Energy of Attraction
     - ii) Double Layer Thickness
   - B. Particle arrangement or fabric consisting of texture and particle orientation
3. Particle Size Distribution
   - A. Median Diameter
   - B. Effective Size
   - C. Uniformity Coefficient
   - D. Curvature Coefficient
4. Cation Exchange Capacity
5. Exchangeable Sodium Percentage
6. Sodium Adsorption Ratio of Clay
7. Dielectric Constant
8. Silica-sesquioxide Ratio
9. Chemical Composition
10. Specific Gravity
11. Hydration or Adsorbed Water
12. Antecedent Water
13. Aging

Illustrative References for TABLE A

A.1. Type of Material

A.1.A. Clay Minerals and Mixtures

1. Kaolinite	Christensen & Das (1973) Mehta & Partheniades (1973) Yeh (1979) Parchure (1980)
2. 40% Montmorillonite +60% Silica flour	Alizadeh (1974)
3. 40% Illite +60% Silica flour	Alizadeh (1974)
4. 40% Kaolinite +60% Silica flour	Alizadeh (1974)
5. Grundite: 50% Illite + 50% Silt	Christensen & Das (1973)
6. English Kaolinite (finer than 1μm) Georgia Kaolinite (between 2μm and 8μm)	Raudkivi & Hutchison (1974)
7. Sand-clay lamination	Terwindt et al. (1968)

A.1.B. Soils, Muds and Clay Material

1. Iredell Sandy Clay Loam Davidson Clay Putnam Soils Bentonite	Lutz (1934)
2. San Francisco Bay Mud (Predominently Montmorillonite and Illite)	Partheniades (1962) Krone (1962)
3. Fernandina Bay Mud	Yeh (1979)
4. Boston Blue Clay	Lambe (1958)
5. Lake Francis Sediment	Parchure et al. (1981)
6. Lake Erie Sediment	Fukuda (1978) Lee (1979)
7. Grangemouth Mud	Thorn & Parsons (1977)
8. Avonmouth Mud	Owen (1975)
9. Norwegian Marine Clays	Bjerrum (1954)
10. Soils within the Australian Environment	Aitchison (1956)
11. Taylor Marl	Espey (1963)
12. Yolo Loam (Montmorillonite, Kaolinite, Mica and Vermiculite)	Arulanandan (1975)
13. Mare Island Strait Sediment	Krone (1962)
14. Belawan Mud	Thorn & Parsons (1980)
15. Taunton River Spoil Thames River Spoil	Gularte et al. (1977)

A.1.C. Non-Sediment Fine Minerals	
1. Polyvinyl chloride	Bibeau & Matijevic (1973)
2. Silver iodide	Vincent et al. (1971)
A.2. Nature of Clay Structure	
A.2.A. Electrical Forces	
1. Bed shear strength as a function of net energy of attraction	Kandiah (1974)
A.2.B. Particle Arrangement	
1. Fabric of consolidated kaolinite	Martin (1965)
2. Particle orientation in clays	Morgenstern & Tchalenko (1967)
3. Fabric changes in kaolin	McConnachi (1974)
4. Structure of compacted clay	Lambe (1958)
5. Importance of structure to the engineering behavior of clay	Mitchell (1956)
6. Structure of compacted soils	Pacey (1956)
7. Structure of clay	Casagrande (1932)
A.3. Particle Size Distribution	Kranck (1981)
A.4. Cation Exchange Capacity	Kandiah (1974)
A.5. Exchangeable Sodium Percentage	Kandiah (1974) Gardner et al. (1959)
A.6. Sodium Adsorption Ratio	Kandiah (1974)
A.7. Dielectric Constant	Kandiah (1974) Alizadeh (1974)
A.8. Silica-sesquioxide Ratio	Middleton (1930) Bennett (1926)
A.9. Mineral Composition	Gibbs (1977)
A.10. Specific Gravity	Kranck (1981)
A.11. Adsorbed Water	Lambe (1958) Martin (1960)
A.12. Antecedent Water	Grissinger (1966)
A.13. Aging	Grissinger (1966)

TABLE B: Characterization of Pore Fluid

1. Type of Fluid
   - A. Distilled Water
   - B. Double Distilled/Redistilled/Conductivity Water
   - C. Deionized Water
   - D. Distilled Deionized Water
   - E. Reconstituted Water
   - F. Fresh Water

G. Salt Water
H. Fluid other than Water

2. Cations and/or Anions Constituting Electrolyte, as represented by:

A. Salinity of Fluid
B. Chlorinity of Fluid
C. Electrical Conductivity
D. Sodium Adsorption Ratio of the Fluid
E. Concentration of Electrolyte
F. Activity of Solute
G. Ion Valence
H. Anion Adsorption
I. Hydration Radius

3. pH

4. Temperature

5. Other chemicals

Illustrative References for TABLE B

B.1. Type of Fluid	
1. Salt Water	Partheniades (1962)
2. Distilled Water	Mehta (1973)
3. Fresh Water	Fukuda (1978) Sheng and Lick (1979)
4. Reconstituted Water	Parchure et al. (1981)
5. Distilled Deionized Water	Raudkivi & Hutchison (1974)
6. 0.1 M Solution of $NaNo_3$	Raudkivi & Hutchison (1974)
7. Carbon Tetrachloride	Liou (1970)
B.2. Electrolyte Ions	
1. Electrolyte Concentration	Lambe (1958) Gardner et al. (1959)
2. Ion Valence	Lambe (1958)
3. Dielectric Constant	Lambe (1958) Alizadeh (1974) Kandiah (1974)
4. Conductivity	Migniot (1968)
5. Sodium Adsorption Ratio	Kandiah (1974)
6. Hydration Radius	Lambe (1958)
7. Chlorinity	Whitehouse et al. (1958)
8. Salinity	Gularte (1978)
B.3. pH	Kandiah (1974)
B.4. Temperature	Lambe (1958) Gularte (1978) Christensen & Das (1973)

B.5. Other Chemicals

Alkali Phosphates — Michaels (1957)

TABLE C: Characterization of Bed Structure

Type of Bed: a) Placed (Remolded) Bed
b) Deposited Bed
c) Compacted Bed

	Physical Properties		Soil Indices	
1.	Water Content, also called Moisture Content	1.	Liquid Limit	
2.	Degree of Saturation	2.	Plastic Limit	
3.	Swelling	3.	Shrinkage Limit	
4.	Permeability, also called Hydraulic Conductivity	4.	Plasticity Index	
5.	Porosity	5.	Liquidity Index	
6.	Void Ratio	6.	Unconfined Compression Strength	
7.	Dry Density	7.	Consistency	
8.	Relative Density	8.	Relative Consistency	
9.	Unit Weight, also called Bulk Unit Weight	9.	Sensitivity	
10.	Dry Unit Weight which is the same as Dry Density	10.	Thixotropy	
11.	Saturated Unit Weight	11.	Activity of Clay	
12.	Submerged Unit Weight	12.	Compressibility Coefficient	
13.	Volumetric Soil Solution Content	13.	Compression Index	
14.	Solids Volume Fraction	14.	Group Index	
15.	Water Volume Fraction	15.	Diffusivity	
16.	Equilibration Time/Aging	16.	Rate of Wetting Front Advance	
		17.	Dilatancy	Used for field identification of soils
		18.	Dry Strength	
		19.	Toughness	

Illustrative References for TABLE C

Physical Properties

1. Water Content	Lee (1979)
2. Solids Volume Fraction	Kandiah (1974)
3. Water Volume Fraction	Kandiah (1974)
4. Hydraulic Conductivity	Dane & Klute (1977)
5. Volumetric Soil Solution Ratio	Dane & Klute (1977)
6. Bed Density	Thorn & Parsons (1980)
7. Swelling	Kandiah (1974)
8. Aging	Grissinger (1966)

Soil Indices

1. Density, Liquid Limit	Carlson & Enger (1962)
2. Vane Shear Strength, Plasticity Index	Dunn (1959)
3. Plasticity Index	Smerdon & Beasly (1959)

4. Shear Strength, Angle of Repose, Specific Weights of Fluid and Sediment, Particle Size	Sundborg (1956)
5. Unconfined Compression Strength	Flaxman (1963)
6. Diffusivity of Water in Soil	Gardner et al. (1959)
7. Rate of Wetting Front Advance	Christenson & Ferguson (1966)

TABLE D: Characterization of Coagulation and Settling

1. Settling Rate of sediment-water interface
2. Settling Velocity
3. Microscopic Observation
4. Change in the Order of Aggregation
5. Change in Permeability of Suspension
6. Degree of Coagulation

Illustrative References for TABLE D

D.1. Settling Rate of Interface	Thorn & Parsons (1977)
D.2. Settling Velocity	Whitehouse et al. (1960)
D.3. Microscopic Observations	Bowles (1969)
D.4. Order of Aggregation	Krone (1978)
D.5. Permeability of Suspension	Lutz (1934)
D.6. Degree of Coagulation	Harris et al. (1966)

TABLE E: Erodibility Index

1. For Sediment Bed
   - A. Critical Shear Stress for surface erosion
   - B. Bulk Shear Strength/Vane Shear Strength
   - C. Floc Shear Strength at surface
   - D. Critical Shear Stress at which the rate of erosion changes from "low" to "high"
   - E. Characteristic Shear Stress
   - F. Change in Concentraton of Suspension as a Function of Time
   - G. Dispersion Ratio
   - H. Erosion Ratio
   - I. Steady State Concentration
   - J. Limiting Flow Velocity
   - K. Erosion Factor
   - L. Erosion Index

2. For Sediment Suspension (Colloid): Rheologic Properties

   A. Bingham Shear Stress
   B. Dynamic Viscosity of Fluid
   C. Kinematic Viscosity of fluid
   D. Viscosity of sediment suspension
   E. Zeta Potential

Illustrative References for TABLE E

E.1. Erodibility Index for Sediment Beds

1.	Critical Shear Stress	Kandiah (1974)
2.	Bulk Shear Strentgh	Krone (1962) Partheniades (1962)
3.	Floc Shear Strength	Krone (1962)
4.	Critical Shear Stress for Erosion Rate	Espey (1963)
5.	Characteristic Shear Strength	Parchure (1980)
6.	Dispersion Ratio	Middleton (1930)
7.	Erosion Ratio	Middleton (1930)
8.	Limiting Flow Velocity	Miller (1960)
9.	Erosion Index/Erosion Factor	Dash (1968)

E.2. Rheological Properties of Colloids

1.	Rheological Properties of Estuarial Sediments	Krone (1963)
2.	Suspensions of Rigid Particles	Jeffrey and Acrives (1976)
3.	Measurement of Bingham Shear Strength of a Deep Marine Sediment	Das (1970)
4.	Viscosity	Krone (1962)
5.	Zeta Potential	Kandiah (1974)
6.	Particle Growth Rate	Sugimoto (1978)
7.	Colloidal Dispersion	Zeichner and Schowalter (1977)

TABLE F: Bed Shear Stress

1. Method

   A. Unidirectional flow in laboratory flume or in rotating cylinder apparatus
   B. Jet impinging on cohesive sediment bed.
   C. Wave induced bed shear stress

2. Measure

   A. Velocity of Flow
   B. Velocity of Jet
   C. Bed Shear Stress (τ_b)
   D. Series of Bed Shear Stresses ($\tau_{b_1}, \tau_{b_2}, \ldots \tau_{b_n}$)

E. Shear Stress Ratio: $\tau_r = \frac{\tau_{b_n} - \tau_{b_{n-1}}}{\tau_{b_{n-1}}}$

F. Excess Shear: $\tau_b - \tau_c$

G. Normalized Excess Bed Shear Stress $(\Delta\tau)_{ex} = \frac{\tau_b - \tau_c}{\tau_c}$

H. Equilibrium Bed Shear Stress, τ_{eq}

Illustrative References for TABLE F

F.1. Method

1. Unidirectional flow in straight flume	Krone (1962)
2. Unidirectional flow in rotating circular channel	Yeh (1979)
3. Unidirectional flow in rotating cylinder	Espey (1963)
4. Submerged vertical jet	Moore & Masch (1962)
5. Wave induced shear	Tubman & Suhayda (1977)

F.2. Measure

1. Velocity of flow	Krone (1962)
2. Velocity of jet	Dunn (1959)
3. Shear Stress Ratio	Parchure (1980)
4. Excess Shear	Thorn & Parsons (1977)
5. Equilibrium Bed Shear	Thorn & Parsons (1977)
6. Series of Bed Shear Stresses	Parchure (1980) Thorn & Parsons (1980)
7. Normalized Excess Bed Shear Stress	Parchure (1980)
8. Bed Shear Stress	Krone (1962) Partheniades (1962) Yeh (1979)

TABLE G: Measure of Erosion

1. Type of Erosion
   - A. Surface Erosion
     - i) Flocculated Particles
     - ii) Deflocculated Particles
   - B. Mass Erosion
     - i) Flocculated Particles
     - ii) Deflocculated Particles

2. Method Used to Determine Erosion Rate
   A. The rate of change of:
      i) Suspension concentration (dC/dt)
      ii) bed elevation (dz/dt)
      iii) weight of sediment in bed (dw/dt)
   B. Time required to reach Steady State Concentration (C_{eq})
   C. Equilibrium depth of scour

Illustrative References for TABLE G

G.1. Type of Erosion

Surface Erosion	Partheniades (1962)
Mass Erosion	Yeh (1979)

G.2. Method Used to Determine Erosion Rate

dC/dt	Partheniades (1962)
dz/dt	Thorn & Parsons (1977)
dw/dt	Espey (1963)

where, C = concentration of sediment in suspension
z = elevation of sediment bed
w = weight of sediment in the bed
t = time